Nuclear Quadrupole Relaxation in Liquid Metals and Alloys

A thesis submitted for the degree of

Doctor of Philosophy

JOHN MARSDEN

Department of Physics,
University of Sheffield,
Sheffield, S3 7RH.

September 1979

ACKNOWLEDGEMENTS

I would like to express my thanks to Professors W. Galbraith, T.R. Kaiser and G.E. Bacon for the use of laboratory facilities.

Special thanks are due to my supervisor Dr. J.M. Titman who offered guidance and encouragement throughout the course of this work.

I would also like to thank Dr. R.L. Havill for his assistance in electronics and the staff of the University Computing Services for help with computer programming.

Finally, I acknowledge the SRC for their maintenance grant and the University Scholarship Committee for the award of a Robert Styring Research Scholarship which I held during the final year of my studies.

ABSTRACT

Using continuous wave nmr the linewidths of the ^{199}Hg and ^{201}Hg resonances in liquid mercury have been measured over the temperature range 245°K to 413°K. From the linewidths the values of the longitudinal relaxation rate, R_1, were calculated for each isotope. R_1 for the ^{201}Hg isotope was found to consist of two significant contributions; R_{1m}, due to the hyperfine interactions and R_{1q}, due to the interaction between the nuclear electric quadrupole moment and the local time dependent field gradient. Using the ^{199}Hg rates, which were entirely due to the magnetic interaction, it was possible to isolate the two contributions to the ^{201}Hg rate and hence accurately determine the variation of R_{1q} with temperature.

The theories of nuclear quadrupole relaxation that were available predicted that R_{1q} should vary with temperature approximately as D^{-1}, where D is the diffusion coefficient. However, the variation of R_{1q} for the ^{201}Hg spins was found to be much slower than this with R_{1q} varying approximately as $T^{-\frac{1}{2}}$. A review of the reliable experimental data from both nmr and pac (perturbed angular correlation) experiments showed that R_{1q} followed a similar trend in a number of liquid metals. Therefore the theory of nuclear quadrupole relaxation in liquid metals was re-examined and a new version is presented together with detailed calculations of the variation of R_{1q} with temperature for liquid mercury.

Agreement between theory and experiment is obtained provided the range of the quadrupole interaction is small compared to the interatomic spacing.

The theory has been extended to cover the case of a liquid binary alloy in which it predicts a faster variation of R_{1q} with temperature than in the pure metal. Using pulsed nmr R_{1q} has been determined as a function of temperature for ^{85}Rb in Rb50at%Na and for ^{69}Ga in a number of Gallium alloys. The ^{85}Rb results were not accurate enough to determine the trend of R_{1q}. However, the ^{69}Ga results were found to agree qualitatively with the theory.

CONTENTS

CHAPTER ONE

Nuclear Magnetic Resonance in Liquid Metals

1.1. Nuclear Relaxation

Each nucleus in a metal with a non-zero spin angular momentum $\underline{I}$ has an associated magnetic moment $\underline{\mu}$ such that $\underline{\mu} = \gamma_n \underline{I} \hbar$, where γ_n is the nuclear gyromagnetic ratio.

The interaction between the nucleus and a steady magnetic field $\underline{H}$ is described by the Hamiltonian,

$$\mathcal{H} = -\underline{\mu}.\underline{H} = -\gamma_n \hbar \underline{I}.\underline{H} = -\gamma_n \hbar I_z H_z \qquad 1.1.$$

where z is the direction of H.

The nuclear Zeeman energies are determined by the eigenvalues of I_z and are given by $E = -\gamma_n \hbar m H_z$ where $m = I, I-1, \ldots, -I$. Transitions between these states are governed by the selection rule $\Delta m = \pm 1$ and may therefore be stimulated by an alternating magnetic field with an angular frequency given by $\omega = \gamma_n H_z$.

Following absorption of energy from the radio frequency field a return to thermal equilibrium is achieved by energy transfer between the nuclear spin system and its surroundings, usually termed the "lattice". This process is characterised by the spin-lattice relaxation time, T_1.

Besides interacting with their environment the spins may interact with each other and the spin-spin relaxation time, T_2, describes this interaction.

In thermal equilibrium the spin system has no nett magnetisation in the x-y plane but produces a steady magnetisation ,M_o, in the z direction owing to the presence of the applied field. In the absence of an exciting field and given that the relaxation along the x, y and z directions may be described by single characteristic times, the equations

$$\frac{dM_x}{dt} = \frac{-M_x}{T_2} \quad , \quad \frac{dM_y}{dt} = \frac{-M_y}{T_2} \qquad 1.2$$

and

$$\frac{dM_z}{dt} = \frac{M_o - M_z}{T_1} \ , \qquad 1.3$$

first suggested by Bloch (1), may be taken as operational definitions of the relaxation times T_1 and T_2. For this reason T_1 and T_2 are sometimes called the longitudinal and transverse relaxation times respectively.

For solids, where the magnetic dipole-dipole interaction between spins is important the resonance line shape is Gaussian rather than the Lorentz shape implied by 1.2. Usually the line width is greater than the intrinsic width governed by T_1. Bodily motion of the spins reduces the transverse effects of the dipole-dipole interactions and, when the correlation time of the molecular motion is small compared to the Larmor period, as it is in liquids, T_1 and T_2 become equal. This is the condition known as extreme narrowing.

In metals the contribution to the spin-lattice relaxation rate R_1 ($=1/T_1$) from the dipole-dipole interaction is usually so relatively small that it is obscured by the hyperfine contribution. Indeed, it has only been observed in Li(2).

1.2 The Hyperfine Interaction

The most important interaction in a metal is that between the nuclei and the surrounding conduction electrons. This interaction manifests itself in two ways, firstly, it produces a shift, termed the Knight shift, in the nuclear resonance frequency and secondly, it provides a mechanism for spin-lattice relaxation producing a contribution R_{1m} to R_1. In principle it is possible to determine R_{1m} from the measured Knight shift using the Korringa relationship.

The Hamiltonian for the hyperfine interaction may be expressed as follows (3),

$$\mathcal{H} = \gamma_e \gamma_n \hbar^2 \underline{I} \cdot \left[\frac{8\pi}{3} \underline{s}\, \delta(r) + \left(\frac{3\underline{r}(\underline{s}.\underline{r})}{r^5} - \frac{\underline{s}}{r^3} \right) + \frac{\underline{l}}{r^3} \right]$$

$$+ \text{ core polarisation terms} \qquad 1.4$$

where γ_e is the gyromagnetic ratio of the conduction electrons,

$\underline{I}$ is the spin of the nucleus at the origin,

$\underline{l}$ and $\underline{s}$ are the orbital and spin angular momentum of the electrons respectively,

$\underline{r}$ is the radius vector from the nucleus to the electron.

The first term inside the square brackets describes the effect of the electron spins at the nucleus and is called

the contact term. It is large for electrons which can be described by mainly s-type wave functions which peak sharply at the nucleus. The second term represents the dipole-dipole coupling between the nuclear and electronic magnetic moments and the final term represents the interaction between the nucleus and the orbital angular momentum of the electrons.

In addition to these direct interactions an indirect interaction between the conduction electrons and nucleus may occur. When the conduction electrons are polarised the spin up and spin down core electrons experience unequal forces causing their spatial wave functions to be altered in a different manner. This effect is termed core polarisation.

As mentioned above the hyperfine field produced by the conduction electrons makes the resonance frequency for a nucleus in a metal different from that of the same nucleus in a non-metallic substance. Quantitatively, the Knight shift, K, is defined by

$$K = \frac{\nu_m - \nu_r}{\nu_r} \qquad 1.5$$

where ν_m and ν_r are the resonance frequencies of the nuclei in the metal and the non-metallic reference respectively.

It is now well understood that the dominant contribution to the Knight shift and relaxation rate arises from the contact term in the hyperfine Hamiltonian. The contribution to the Knight shift can be written as (4,5)

$$K_\delta = \frac{8\pi}{3} \chi_p \langle |\psi(o)|^2 \rangle_F \qquad 1.6$$

where χ_p is the Pauli paramagnetic spin susceptibility and $\langle|\psi(o)|^2\rangle_F$ represents the average density of the conduction electrons at the Fermi surface on the nucleus.

Assuming that the conduction electrons behave independently it can be shown, (5), that the contribution to the relaxation rate from this term is

$$R_{1\delta} = \frac{64}{9}\pi^3\hbar^3\gamma_e^2\gamma_n^2\langle|\psi(o)|^2\rangle_F\left[g(E_F)\right]^2 k_B T \qquad 1.7$$

where k_B is Boltzmann's constant, T is the lattice temperature and $g(E_F)$ is the density of electron states at the Fermi level.

From 1.6 and 1.7 we obtain

$$TK_\delta^2 T_{1\delta} = \frac{1}{\pi k_B \gamma_n^2 \gamma_e^2 \hbar^3}\left[\frac{\chi_p}{g(E_F)}\right]^2 \qquad 1.8$$

and putting $\chi_p = \frac{(\gamma_e\hbar)^2}{2} g(E_F)$ we have

$$T_{1\delta}\, TK_\delta^2 = \frac{\hbar}{4\pi k_B}\left[\frac{\gamma_e}{\gamma_n}\right]^2 \qquad 1.9$$

which is the well known Korringa relationship (6).

It is generally accepted that the electrons in metals do not in fact act independently. Pines (7), Silverstein (8), Moriya (9) and Narath and Weaver (10) have investigated electron - electron interactions. The latter authors introduced the correction factor K(α) giving

$$T_{1\delta}\, TK_\delta^2 K(\alpha) = \frac{\hbar}{4\pi k_B}\left[\frac{\gamma_e}{\gamma_n}\right]^2 \qquad 1.10$$

where $a = 1 - \frac{X^o}{X}$, X being the real spin susceptibility compared to X^o which is for independent electrons.

Rearranging 1.10 we have

$$R_{1\delta} = \frac{4nk_B}{\hbar}\left[\frac{\gamma_n}{\gamma_e}\right]^2 K(a)\ T\ K_\delta{}^2 \qquad 1.11$$

Several authors have attempted to calculate R_{1m} using 1.11 and the measured Knight shifts. However, values obtained by this method are unlikely to be accurate for the following reasons. Firstly,there is the uncertainty in the value of K(a). It is difficult to calculate K(a) although several attempts have been made (11), (12), (13). Furthermore, the only experimental method of obtaining K(a) in liquid metals uses 1.11. Therefore values of K(a) used have been at best approximate guesses. Secondly, this method ignores the fact that, in addition to the contact term, both the orbital term and core polarisation may contribute to R_{1m} and K in a way that is not described by 1.11. The core polarisation contributions induced by the s-like part of the conduction electron density merely attach themselves to $R_{1\delta}$ and K_δ in 1.11 but the relationship has a different form for the p core polarisation and the orbital term (10). From presently available theoretical calculations (11) it seems likely that contributions from non-s terms could easily be of the order of 0.1 of the magnitude of those from other terms. It is therefore not justifiable to dismiss them and, as will become apparent in what follows, the quantitative relationship between the Knight shift and the magnetic relaxation rate is too approximate in many cases to be of value in the

analysis of the relaxation rates in heavy polyvalent liquid metals.

1.3 The Nuclear Quadrupole Interaction

If a nucleus has spin quantum number $I>\frac{1}{2}$ then it will possess a nuclear electric quadrupole moment. Spin lattice relaxation may then occur via the interaction between the nuclear electric quadrupole moment and the local time - dependent electric field gradient associated with the nuclear environment.

There are two types of quadrupolar relaxation possible in metals. In one process the time-dependent electric field gradient results from the translational motion of the charge of electrons having p or d character at the nucleus (14), (15). Relaxation results from a scattering process analagous to that encountered in the magnetic relaxation. However, estimates of the strength of the electronic scattering process have shown it to be too weak to account for the observed quadrupolar relaxation in liquid metals (14), (15), (16). The second process results from the motion of ions whose charge produces an electric field gradient at neighbouring nuclei. This process has been discussed by Sholl (17), Warren (18), and Yul'met'ev (19). Both Sholl and Warren use essentially the same model of free metallic ions interacting with each other by a screened potential. The conduction electrons are regarded as screening the ion cores and the electric field gradient at a given nuclear site is taken as the sum of the appropriate derivatives of the

screened potentials from all other ions. The positions of the ions and the way they move in time are described in terms of the van Hove correlation functions (20).

The basic expression for the quadrupolar relaxation rate, R_{1q}, is derived by perturbation theory where the quadrupole Hamiltonian is taken as a perturbation on the nuclear Zeeman states. The result is (3), (21),

$$R_{1q} = \frac{3(2I+3)(eQ)^2 \quad J(o)}{4I^2(2I-1)\hbar^2} \qquad 1.12$$

$$J(\omega) = \int_{-\infty}^{\infty} e^{-i\omega\tau} g_{mm'}(\tau)d\tau \qquad 1.13$$

$$g_{mm'}(\tau) = \overline{F^{(m)}(t-\tau)F^{(-m')}(t)} \qquad 1.14$$

$$F^{(m)} = \sum_{\lambda} u_m(\underline{r_\lambda}) = c\sum_{\lambda} v_2(r_\lambda)Y_{2m}(\Omega_\lambda) \qquad 1.15$$

$$c = (1-\gamma_\infty)\left(\frac{4\pi}{45}\right)^{\frac{1}{2}} \qquad 1.16$$

$$v_2(r) = r\frac{d}{dr}\left(\frac{1}{r}\frac{dv}{dr}\right) \qquad 1.17$$

where Q is the nuclear quadrupole moment, the bar in equation 1.14 denotes an ensemble average, and $u_m(\underline{r_\lambda})$ is the electric field gradient at a nucleus at the origin due to an ion at $\underline{r_\lambda}$. $u_m(\underline{r_\lambda})$ is expressed as the product of a spherical harmonic Y_{2m} (normalised to one) and a radial function, $v_2(r)$, which is determined by the ion-ion potential v(r). An important contribution to the field gradient is due to the distortion of the ion-ion charge distribution about the nucleus at the origin by the external

field gradient and the nuclear quadrupole moment. This contribution is taken into account by the inclusion of the factor $(1-\gamma_\infty)$ where γ_∞ is the Sternheimer antishielding factor. This is strictly only correct when the field gradient at the originarises from charges external to the core and since the conduction electrons in a metal contribute to $v_2(r)$ and do penetrate the core the correct treatment of antishielding may require a modification of the ion-core value.

Equation 1.12 is derived within the extreme narrowing approximation, i.e. that $J(2\omega_0) = J(\omega_0) = J(0)$, where ω_0 is the nuclear Larmor frequency. This is a necessary condition for an exponential approach to thermal equilibrium of the spin system (3).

The ion-ion potentials used by Sholl are those developed by Appapillai and Williams (22). The interionic potential is given by

$$v(r) = \frac{Z^*}{r}\left(1 - \frac{2}{\pi}\int_0^\infty F_N^*(q)\,\frac{\sin qr}{q}\,dq\right) \qquad 1.18$$

where q is the wave number, Z^* the effective charge and F_N^* the normalised energy wave number characteristic. This particular form of pseudopotential was chosen because it is thought to be quantitatively correct at near neighbour distances. Warren uses the potential given by Harrison (23) which is the same as that used in an earlier paper by Sholl (21) and which is thought to be strictly only correct for large r.

Having chosen the form of the interionic potential the calculation of R_{1q} is reduced to an evaluation of the correlation function of the electric field gradient given by equation 1.14. The ensemble average in 1.14 is formed using 1.15 from which we obtain

$$F^{m}(t-\tau)F^{(-m')}(t) = \sum_{\lambda\mu} u_m\left(\underline{r}_\lambda\ (t-\tau)\right) u_{m'}^{*}\left(\underline{r}_\mu(t)\right) \qquad 1.19$$

where $\underline{r}_\lambda\ (t-\tau)$ is the position of the λth. ion at time $t-\tau$ relative to the nucleus at the origin. The property $u_m^* = u_{-m}$ has been used.

Equation 1.19 may be divided into two parts. The first contains those terms where $\lambda = \mu$ and may be called the two-particle term. The second part or three-particle term contains the cross products, i.e. $\lambda \neq \mu$

Now equation 1.14 may be expressed as

$$g_{mm'}(\tau) = \iint u_m(\underline{r}_o)u_{m'}^{*}(\underline{r}_1)P(\underline{r}_o,t-\tau;\underline{r}_1,t)\underline{dr}_o\ \underline{dr}_1 \qquad 1.20$$

where $P(\underline{r}_o,t-\tau;\underline{r}_1,t)\ \underline{dr}_o\ \underline{dr}_1$ is the probability of finding an ion in $\underline{dr}_o$ at $\underline{r}_o$ at time $t-\tau$ and an ion in $\underline{dr}_1$ at $\underline{r}_1$ at time t given that there is one at the origin throughout. Obviously $P = P_s + P_d$ where the two-particle or self-term, P_s, is the probability of finding the same ion at $\underline{r}_o$ at time $t-\tau$ and at $\underline{r}_1$ at time t relative to an ion at the origin and the three-particle or different term, P_d, is the probability of finding an ion at $\underline{r}_o$ at time $t-\tau$ and a different ion at $\underline{r}_1$ at time t relative to an ion at the origin.

If the motion of ions at $\underline{r}_o$ and $\underline{r}_1$ were relative to a fixed origin in the liquid the function P could easily be written in terms of the van Hove functions G and G_s. These are defined as follows. $G(\underline{r},t)$ is the probability of finding ions at the origin at t = o and at $\underline{r}$ at time t and $G_s(\underline{r},t)$ is the probability of finding the same ion at the origin at time t = o and at r at time t. Because the origin in the definition of P is a moving nucleus some approximation is required in relating P to the van Hove functions. Further approximations are also necessary since P includes three body correlations while the van Hove functions are, by definition, two body correlation functions.

The correlation functions $G_s(\underline{r},t)$ and $G(\underline{r},t)$ are related to the dynamic structure factors $S_s(\underline{q},\omega)$ and $S(\underline{q},\omega)$ by the Fourier transforms,

$$S_s(\underline{q},\omega) = \frac{1}{2\pi}\int_{-\infty}^{\infty} dt \int G_s(\underline{r},t) e^{i(\underline{q}\cdot\underline{r}-\omega t)} \underline{dr} \qquad 1.21$$

and

$$S(\underline{q},\omega) = \frac{1}{2\pi}\int_{-\infty}^{\infty} dt \int [G(\underline{r},t)-\rho] e^{i(\underline{q}\cdot\underline{r}-\omega t)} \underline{dr} \qquad 1.22$$

where ρ is the number density of the liquid.

$S_s(\underline{q},\omega)$ determines the cross-section for incoherent scattering of thermal neutrons and $S(\underline{q},\omega)$ determines the cross-section for coherent scattering of neutrons or light. When a neutron is scattered the momentum transfer and energy transfer that occur are given by $\hbar q$ and $\hbar\omega$.

Using the relations 1.21 and 1.22 with suitable approximations for P_s and P_d the integrals required in evaluating J(o) in equation 1.12 can now be evaluated. Sholl finally obtains the following expressions for the relaxation rate,

$$R_{1q,self} = 2\beta \int_0^\infty q^2 I_{\frac{1}{2}}^2(q)dq \int_{-\infty}^\infty S_s^2(q,\omega)d\omega \qquad 1.23$$

for the self-term alone and

$$R_{1q} = 2\beta \int_0^\infty q^2 I_n^2(q)dq \int_{-\infty}^\infty S(q,\omega)S_s(q,\omega)d\omega \qquad 1.24$$

for the self and different terms.

$$\beta = \frac{2n\,(2I+3)}{15I^2(2I-1)} \left[\frac{eQ(1-\gamma_\infty)}{\hbar}\right]^2 \rho \qquad 1.25$$

and

$$I_n(q) = \int_0^\infty r^2 v_2(r) g^n(r) j_2(qr)dr \qquad 1.26$$

where g(r) is the radial distribution function and $j_2(qr)$ is a Bessel function.

Sholl suggests the following approximations for R_{1q}:

(A) expression 1.24 with n = $\frac{1}{2}$ or 1

(B) expression 1.24 with n = 1 and S_d in place of S plus expression 1.23.

In order to calculate R_{1q} the final integrals in 1.23 and 1.24 must be evaluated. Although $S_s(q,\omega)$ and $S(q,\omega)$ can, in principle, be measured by inelastic neutron scattering in prac tice there are experimental limitations on the range of q and ω that can be investigated and on the liquid metals that can be studied. Sholl uses a model for $S_s(q,\omega)$ given by Egelstaff and Schofield (23) which is

$$S_s(q,\omega) = \frac{e}{n} \frac{Dq^2/\gamma}{\left[\omega^2+(Dq^2)^2\right]^{\frac{1}{2}}} K_1\left\{\frac{\left[\omega^2+(Dq^2)^2\right]^{\frac{1}{2}}}{\gamma}\right\} \qquad 1.27$$

where D is the diffusion constant and K_1 is a modified Bessel function. γ is a parameter that can be determined by fitting $S_s(q,\omega)$ to the experimental data that exists for large q and is given by

$$\gamma = kT/M^*D \qquad 1.28$$

where T is the temperature and M^* is the effective mass of the ion. Barker et al. (24) have shown that the experimental data for Ga and Rb can be described by 1.27 and 1.28 with M^* equal to the actual mass of the ion.

Sholl uses several theoretical expressions for $S(q,\omega)$ the simplest of which is the Vineyard approximation (25)

$$S(q,\omega) = S(q)\, S_s(q,\omega) \qquad 1.29$$

where S(q) is the structure factor given by

$$S(q) = \int_{-\infty}^{\infty} S(q,\omega)d\omega \qquad 1.30$$

Sholl discusses the integral involving $S_s(q,\omega)$ in 1.23 as follows. If the motion of an ion were random in the sense that at time t it had no memory of its previous motion then

$$G_s(\underline{r},t) = \int G_s(\underline{r},t_1)G_s(\underline{r}-\underline{r_1},t-t_1)\underline{dr_1} \qquad 1.31$$

for all t such that $o \leqslant t_1 \leqslant t$. Putting $t_1 = \frac{1}{2}t$ the Fourier transform of 1.31 at $\omega = o$ gives

$$\int_{-\infty}^{\infty} S_s^{\,2}(q,\omega)d\omega = \tfrac{1}{2}\, S_s(q,o) \qquad 1.32$$

This can be verified by taking the classical diffusion limit, i.e. small q of 1.27 which is

$$S_{s,diff}(q,\omega) = \frac{1}{n}\left[\frac{Dq^2}{\omega^2+(Dq^2)^2}\right] \qquad 1.33$$

Expression 1.32 is not true for the general form of $S_s(q,\omega)$ but Sholl states that the most significant contribution to the integral occurs over a range of values of q that is sufficiently small for it to be a good approximation.

Using the Vineyard approximation the final integral in 1.24 can now be expressed as

$$\int_{-\infty}^{\infty} S(q,\omega)S_s(q,\omega)d\omega = S(q)\int_{-\infty}^{\infty} S_s^{\,2}(q,\omega)d\omega = \tfrac{1}{2}S(q,o) \qquad 1.34$$

Warren's final expression for R_{1q} is

$$R_{1q} = \beta\int_0^{\infty} q^2 S(q,0) I_1^{\,2} dq \qquad 1.35$$

which is the same as Sholl's result given by 1.24 and 1.34 with n=1. Warren arrives at his expression by assuming that $S_s(q,\omega)$ and $S(q,\omega)$ are Lorentzians of equal width. He quotes Skold et al. (26) who compared careful measurements of $S_s(q,\omega)$ for liquid Ar. They found that both were closely Lorentzian but the widths at half maximum differed by roughly 20 to 30%. However, Warren states that including a correction for such a difference in width only alters the final result for R_{1q} by about 2%.

As pointed out by Sholl the pseudopotential theory used to derive the ion-ion field gradient $v_2(r)$ while valid outside the ion cores does not accurately describe the conduction electrons within the core at the origin.

Furthermore, the field gradient due to these electrons should not be multiplied by the ionic $(1-\gamma_\infty)$ since this is only valid for field gradients arising from charges external to the core. Sholl estimates that the values of $(1-\gamma_\infty)\, v_2(r)$ he uses could lead to an error in the absolute value of R_{1q} of at least an order of magnitude. Therefore there seems little point in discussing in detail the calculated values of R_{1q} and we shall consider the variation of R_{1q} with temperature predicted by the theory.

The product $v_2(r)g^n(r)$ in the integral 1.26 for $I_n(q)$ is a highly peaked function and because of this the predominant contribution to R_{1q} comes from ions that are "nearest neighbours" to the relaxing nucleus. If, as suggested by Sholl, $v_2(r)g^n(r)$ is approximated by a δ function then $I_n(q) \simeq A_n j_2(q\sigma)$ where $\sigma \sim r_o$, the cutoff of $g(r)$ at small r. The integrands in 1.23 and 1.24 are then products of the damped oscillatory functions $I_n^2(q)$ and either the monotonically decreasing function $S_s(q,o)$ or the damped oscillatory function $S(q,o)$.

Now the parameters that can influence the variation of R_{1q} with temperature are the density, the potential, the van Hove functions $S_s(q,o)$ and $S(q,o)$ and the radial distribution function. The effects of temperature variations in the density and potential should be small and can be neglected. According to Sholl, over the important region of integration $S_s(q,o)$ is well approximated by the diffusion limit and its temperature variation will therefore be determined by that of D^{-1}. Furthermore, the theoretical models chosen by Sholl

for $S(q,o)$ suggest that it also has a D^{-1} dependence on temperature. This is easily seen for the Vineyard approximation given that the structure factor, $S(q)$, is independent of temperature. Warren, however, chooses a theoretical model for $S(q,o)$ given by Cocking and Egelstaff (27) which predicts a quite different temperature variation. According to this model $S(q,o)$ is given by

$$S(q,o) = \frac{N_{12}}{n} \left[\frac{M}{k_B T}\right]^{\frac{1}{2}} \left[\frac{S(q)}{q}\right]^{3/2} \qquad 1.36$$

where M is the atomic mass and N_{12} is a parameter determined by fitting the expression to neutron diffraction data. Now if $S(q)$ is independent of temperature 1.36 predicts that $S(q,o)$ will have a temperature dependence of the form $T^{-\frac{1}{2}}$.

Now the experimental data of Page et al (28) shows that for liquid Gallium, over the relevant range of q, $S(q)$ is indeed almost independent of temperature and that the frequency width of the Lorentzian quasi-elastic peak increases approximately as $T^{3/2}$ so that $S(q,o)$ decreases at about that rate. This is slightly slower than D^{-1} since for liquid Ga D is approximately proportional to T^2. It certainly is not as slow as the variation predicted by Cocking and Egelstaff's model and for this reason their model is thought to be a poor representation of $S(q,o)$.

The important effect on $g(r)$ of increasing the temperature is the decrease in r_o. Because of the steepness of $v_2(r)$ for small r even a small decrease in r_o could cause a significant increase in $I_n(q)$ and hence R_{1q}. Using

the model of the hard sphere temperature variation of Protopapas et al (29) Sholl calculates for the case of Sb a 20% increase in R_{1q} when the temperature is increased by about 300°K. Diffusion constants typically increase by a factor of two or three over this range. Therefore the theory predicts that the overall dependence of R_{1q} on temperature should be that R_{1q} will decrease with increasing temperature but not quite as fast as D^{-1}. This is a similar result to that obtained by Sholl in his original paper (21) where the motion of the ions was assumed to be adequately described by the diffusion approximation.

Sholl's original theory has been extended to cover the case of a liquid binary alloy by Titman (30) and Claridge et al (31). These authors point out that, if three particle terms are important, then the magnitude of R_{1q} for either ionic species of an alloy will be a non-linear function of its fractional concentration. They also predict that R_{1q} will have a similar temperature dependence in alloys as in pure metals.

At the time the present studies were undertaken experimental data on the variation of R_{1q} with temperature in liquid metals and alloys was available from both conventional nuclear magnetic resonance measurements and also from measurements using the more recently developed perturbed angular correlation (pac) methods. In the pac experiments nuclear reactions with a pulsed particle beam are used to produce and align isomeric nuclear states leading to an anisotropic distribution of emitted radiation. Using the

spin rotation method the longitudinal relaxation time is determined from the envelope of the γ-ray intensity modulation caused by an external magnetic field perpendicular to the beam detector plane. An alternative method depends on the measurement of the time-dependent γ-ray anisotropy in successive time windows with respect to the beam pulse. The pure metal data obtained using nmr and pac methods was as follows.

Measurements of R_1 for the ^{69}Ga and ^{71}Ga spins in liquid gallium made by Cartledge et al (32) and Kerlin and Clark (33) using nuclear magnetic resonance indicated a variation of R_{1q} with temperature that was much slower than that given by the inverse of the self-diffusion coefficient. However, measurements of the relaxation rate of trace amounts of ^{71}Ge in liquid gallium made by Riegel et al (34) using the perturbed angular correlation method showed a relatively rapid decrease proportional to D^{-1}.

Similar contrasting results existed for liquid mercury. Using nmr Cornell (35) had shown that R_{1q} for the ^{201}Hg spins decreased slowly with increasing temperature. However, using the pac method on trace amounts of ^{206}Pb nuclei in mercury Bräuer et al (36) reported that R_{1q} decreased as D^{-1}.

Measurements of R_1 for ^{121}Sb and ^{123}Sb using nmr had been reported by Warren and Clark (16). Their measurements showed (37) that R_{1q} decreased with temperature but not as fast as D^{-1}.

Nmr measurements of R_1 in ^{209}Bi had been reported by several groups (37), (38), (39). The most recent measurements, which agreed well with the earlier ones, were those of Heighway and Seymour (39) who found from their analysis that R_{1q} decreased with temperature at a rate given approximately by D^{-1}. However, their interpretation of their results involved the use of the Korringa relationship to estimate R_{1m}.

The temperature dependence of R_1 in ^{115}In had been measured by many different groups using nmr (40),(41), (42), (16), (43). Again extraction of R_{1q} from the measured R_1 involved the use of the Korringa relationship and mainly due to errors inherent in this method of interpretation no general agreement had been reached on the temperature variation of R_{1q}.

It can therefore be seen that there was a great deal of ambiguity in the pure metal data and no clear indication of a general trend in the variation of R_{1q} with temperature.

As with pure metals the temperature dependence of R_{1q} in liquid alloys was also not well established. Although many attempts had been made to measure the temperature dependence of R_{1q} in alloy systems (31), (16), (38), (39), (43), (44), (45) most of these used the Korringa relationship. This method is particularly unreliable if the results are to be compared to the pure metal case since, although the Knight shift can be measured in the alloys, changes in the core polarisation and orbital terms and $K(\alpha)$ are difficult to estimate. The only data that did not depend on the

Korringa relationship for its interpretation was that of Warren and Clark (16) on ^{121}Sb and ^{123}Sb in InSb and that of Cartledge et al (45) on ^{69}Ga in Ga-In alloys. In both of these systems alloying produced a marked increase in the rate of variation of R_{1q} with temperature compared with the relatively slow variation in the pure metal.

In consideration of the experimental data outlined above it was felt that further work would be useful in the following areas. Firstly, in order to obtain reliable data on the variation of R_{1q} with temperature in a pure metal it was decided to re-examine the variation of R_1 with temperature for the ^{199}Hg and ^{201}Hg spins in liquid mercury. In principle, mercury offers an experimental situation for the very accurate determination of R_{1q} using the nmr technique. Furthermore, the work of Cornell (35) had been limited to a small number of data points. Secondly, an attempt was made to obtain further accurate data on the variation of R_{1q} with temperature in liquid alloys in order to check whether the rate of variation of R_{1q} is faster in an alloy than in the pure metal.

In the course of this work further pac results were published which removed much of the ambiguity in the earlier data. Pac measurements in liquid In (46), Pb (47), Sn(48), Bi (48) and Hg (49) all showed a slow variation of R_{1q} with temperature. An examination of this work together with our Hg results and the other reliable nmr data revealed that in a number of liquid metals R_{1q} varied with temperature approximately as $T^{-\frac{1}{2}}$. Further, the new pac data on InSb (46)

showed that the variation of R_{1q} with temperature for In was much faster in the alloy than in the pure metal. It therefore seemed appropriate at this stage to re-examine the theory of quadrupole relaxation to see if a new version could be produced which predicted the now well established slow variation of R_{1q} with temperature in pure metals and the relatively faster variation in alloys.

1.4 References

1) F. Bloch, Phys. Rev., 70, 460 (1946)

2) D.F. Holcomb and R.E. Norberg, Phys. Rev., 98, 1074 (1955)

3) A. Abragam, Principles of Nuclear Magnetism (Oxford Press, Oxford 1961)

4) W.D. Knight, Solid State Physics, (Academic Press, New York, 1956) vol. 2, 93.

5) C.P. Slichter, Principles of Magnetic Resonance, (Harper and Row, New York, 1963)

6) J. Korringa, Physica, 16, 601 (1950)

7) D. Pines, Solid State Physics, (Academic Press, New York, 1955) vol. 1, 367

8) S.D. Silverstein, Phys. Rev., 130, 912 (1963)

9) T.J. Moriya, Phys. Soc. Japan, 18, 516 (1963)

10) A. Narath and H.T. Weaver, Phys. Rev., 175, 373 (1968)

11) S.D. Mahanti and T.P. Das, Phys. Rev., B3, 1599 (1971)

12) R.W. Shaw Jr. and W.W. Warren Jr. , Phys. Rev., B3, 1562 (1971)

13) P. Bhattacharyya, K.N. Pathak and K.S. Singwi, Phys. Rev., B3, 1568 (1971)

14) A.H. Mitchell, J. Chem. Phys., 26, 1714 (1957)

15) Y. Obata, J. Phys. Soc. Japan, 18, 1020 (1963)

16) W.W. Warren Jr. and W.G. Clark, Phys. Rev., 177, 600 (1969)

17) C.A. Sholl, J. Phys. F: Metal Phys., 4, 1556 (1974)

18) W.W. Warren Jr., Phys. Rev., A10, 657 (1974)

19) R.M. Yul'met'ev, Izv. Vuz. Fiz. U.S.S.R., 8, 28 (1968)

20) L. van Hove, Phys. Rev., 95, 249 (1954)

21) C.A. Sholl, Proc, Phys. Soc., 91, 130 (1967)

22) M. Appapillai and A.R. Williams, J. Phys. F: Metal Phys., 3, 759 (1973)

23) P.A. Egelstaff and P. Schofield, Nucl. Sci, Engng., 12, 260 (1962)

24) M.I. Barker, M.W. Johnson, N.H. March and D.I. Page, The Properties of Liquid Metals ed S. Takeuchi (London: Taylor and Francis, 1973)

25) G.H. Vineyard, Phys. Rev., 110, 999 (1958)

26) K. Skold, Phys. Rev. Lett., 19, 1023 (1967)

27) S.J. Cocking and P.A. Egelstaff, J. Phys. C., 1, 507 (1968)

28) D.I. Page, D.H. Saunderson and C.G. Windsor, J. Phys.C., 6, 212 (1973)

29) P. Protopapas, H.C. Anderson and N.A.D. Parlee, J. Chem. Phys., 59, 15 (1973)

30) J.M. Titman, Proc. 17th Ampere Colloque (Amsterdam: North Holland, 1973), p 301

31) E. Claridge, D.S. Moore, E.F.W. Seymour and C.A. Sholl, J. Phys. F., 2, 1162 (1972)

32) G. Cartledge, R.L. Havill and J.M. Titman, J. Phys. F: Metal. Phys., 6, 639 (1976)

33) A.L. Kerlin and W.G. Clark, Phys. Rev., B12, 3533 (1975)

34) D. Riegel, N. Bräuer, B. Focke, B. Lehmann and K. Nishiyama, Phys. Lett., 41A, 459 (1972)

35) D.A. Cornell, Phys. Rev., 153, 208 (1967)

36) N. Bräuer, F. Dimmling, B. Focke, A. Goldmann, M. von Hartrott, Th. Kornrumpf, K. Nishiyama, D. Quitmann and D. Riegel, Proc. Int. Conf. Hyperfine Interactions, Uppsala p. 254, (1974)

37) F.A. Rossini and W.D. Knight, Phys. Rev., 178, 641 (1969)

38) G.A. Styles, Advan. Phys., 16, 275 (1967)

39) J. Heighway and E.F.W. Seymour, J. Phys. F., 1, 138 (1971)

40) E.F.W. Seymour and G.A. Styles, Proc. Phys. Soc., 87, 473 (1966)

41) F.A. Rossini, E. Geissler, E.M. Dickson and W.D. Knight, Adv. Phys., 16, 287 (1967)

42) G. Bonera, F. Borsa and A.Rigamonti, Proc. 15th. Colloque Ampere (Amsterdam North Holland 1969) p 359.

43) R.I. Jolly and J.M. Titman, J. Phys. C: Solid State Phys., 5, 1284 (1972)

44) R.I. Jolly and J.M. Titman, J. Phys. F., 3, 1071 (1973)

45) G. Carledge, R.L. Havill and J.M. Titman, J. Phys. C: Solid State Phys., 6, L23, (1973)

46) M. von Hartrott, K. Nishiyama, J. Rossbach, E. Weihreter and D. Quitmann, J. Phys. F: Metal Phys., 7, 713, (1977)

47) D. Riegel, Phys. Scr., 11, 228 (1975)

48) F. Dimmling, M. von Hartrott, Th. Kornrumpf, K. Nishiyama and D. Riegel, Proc. 4th Int. Conf. on Hyperfine Interactions, U.S.A., (1977)

49) N. Bräuer, F. Dimmling, Th. Kornrumpf, M. von Hartrott, K. Nishiyama and D. Riegel, Hyperfine Interactions 2 (Amsterdam: North Holland) p. 248 (1976)

CHAPTER TWO

Nuclear Quadrupole Relaxation in Liquid Mercury

2.1 Introduction

In order to observe the behaviour of nuclear quadrupolar relaxation in liquid metals it is necessary to reduce the observed relaxation rate, R_1, into its components R_{1m} due to the magnetic hyperfine interaction and R_{1q} due to the electric quadrupole interaction. There are two methods of doing this. One is to use the modified Korringa relationship to estimate R_{1m}. As shown in Chapter 1 this method is unreliable and leads to uncertainty in the interpretation of experimental data. In the case of a nuclear species which has two isotopes with observable resonances another method exists whereby it is possible to unambiguously separate the magnetic and quadrupolar contributions.

For the two isotopes A and B the total relaxation rates are given by (1)

$$R_{1A} = R_{1m}^{A} + R_{1q}^{A} \qquad 2.1$$

$$R_{1B} = R_{1m}^{B} + R_{1q}^{B} \qquad 2.2$$

Now

$$\frac{R_{1q}^{A}}{R_{1q}^{B}} = \frac{F(I_A)}{F(I_B)} \left[\frac{Q_A}{Q_B} \right]^2 \qquad 2.3$$

$$\text{where } F(I) = \frac{2I+3}{I^2(2I-1)}$$

and

$$\frac{R_{1m}^{A}}{R_{1m}^{B}} = \left[\frac{\gamma_n^{A}}{\gamma_n^{B}}\right]^2 \qquad 2.4$$

Equations 2.1, 2.2, 2.3, and 2.4 can be solved for R_{1m}^{A}, R_{1m}^{B}, R_{1q}^{A} and R_{1q}^{B} in terms of the observed values of R_1, F(I) and the ratios $(\gamma_n^{A} / \gamma_n^{B})$ and (Q_A/Q_B). Obviously this method is most accurate when the two isotopes have widely differing gyromagnetic ratios or quadrupole moments and when the two contributions are of similar magnitude. Table 2.1 shows the metals to which the two isotope method can be applied. From this it will be seen that mercury has a particularly fortunate combination of nuclear parameters. The ^{199}Hg isotope has spin $I = \frac{1}{2}$ so that its relaxation is entirely magnetic and there is no quadrupole contribution. The other isotope, ^{201}Hg, has a relatively small gyromagnetic ratio but an appreciable electric quadrupole moment. This combination of parameters is likely to lead to $R_{1q} > R_{1m}$ and, in fact, Cornell (2) showed that ~ 90% of the observed rate of this isotope is quadrupolar in origin.

Thus mercury appears to offer a particularly advantageous set of experimental criteria from which to determine R_{1m} and, more importantly, R_{1q}. Unfortunately the ^{201}Hg resonance is very weak and because of the large quadrupolar contribution its relaxation rate is rather rapid. These factors make the actual experimental measurement of R_1 difficult and this is discussed in the next section.

Table 2.1 Metals to which the two isotope method is applicable.

Metal	Isotope	Spin I	γ_n ($s^{-1}g^{-1}$ x10^3)	Q (x10^{-24} cm^2)	γ_n^A/γ_n^B	Q_A/Q_B
Rubidium	^{85}Rb	5/2	2.583	0.31	0.295	2.067
	^{87}Rb	3/2	8.754	0.15		
Copper	^{63}Cu	3/2	7.091	-0.15	0.933	1.071
	^{65}Cu	3/2	7.596	-0.14		
Mercury	^{199}Hg	1/2	4.783	0.0	2.708	∞
	^{201}Hg	3/2	1.766	0.5		
Gallium	^{69}Ga	3/2	6.421	0.2318	0.787	1.586
	^{71}Ga	3/2	8.158	0.1461		
Antimony	^{121}Sb	5/2	6.402	-0.8	1.847	0.8
	^{123}Sb	7/2	3.467	-1.0		

2.2 Experimental Method

2.2.1 The Continuous Wave and Pulsed n.m.r. Techniques

Nuclear magnetic resonance can be observed using either continuous wave or pulsed methods. In both of these the radio frequency field for exciting the resonance is supplied by surrounding the specimen by a coil whose axis is perpendicular to the main field.

In continuous wave n.m.r. the r.f. field is continuously applied to the sample while the external magnetic field is swept linearly through the resonance condition. The effect of the resonance on the coil is to produce a change in its impedence related to the complex nuclear magnetic susceptibility,

$$\chi = \chi' - i\chi'' \qquad 2.5$$

The change in inductance of the coil is proportional to χ' and its effective series resistance varies as χ'' (3). Basically, two types of circuit are used to detect these changes. In bridge circuits the coil is made part of a balanced bridge network so that small changes in the impedence of the coil upset the delicate balance. In practice the bridge is adjusted to leave a residual unbalance in either amplitude or phase. In the former case the change in χ'' is detected and an absorption curve is obtained. For liquids this has a Lorentzian form, the normalised line shape function being given by

$$g(H) = n^{-1} \frac{T_2}{1+ (H-H_o)^2 \gamma^2 T_2^2} \qquad 2.6$$

This is the usual way in which a bridge circuit is operated. A residual unbalance in phase detects X' giving the dispersion curve. The other type of circuit used is the marginal oscillator. Here the coil containing the sample is made part of a self-oscillating circuit, just sufficient feed-back being provided to sustain the oscillations. Under these conditions the amplitude of oscillation is critically dependent on the resistance of the coil and hence is very sensitive to the effective change in resistance associated with a nuclear magnetic resonance. Marginal oscillators therefore give a pure absorption signal proportional to X''. The dispersive component of the susceptibility produces a frequency modulation of the oscillator which is not detected.

In order to improve the sensitivity of continuous wave spectrometers the technique of audio-frequency modulation of the external magnetic field is used. On the slow sweep by which the resonance is traced there is superimposed a sinusoidal variation in the audio range. This gives an a.f. output from the r.f. receiver and detector suitable for selective amplification. The a.f. signal is finally rectified in a phase sensitive detector and amplifier.

The output of the phase sensitive detector is proportional to the coefficient of the first harmonic term in the Fourier expansion of the resonance line shape. If the amplitude of the magnetic field modulation is small compared to the

width of the line then this output will be proportional to the derivative of the resonance curve (4). The distance between the peaks of the derivative curve is then equal to the width, δH, between the points of maximum and minimum slope on the absorption curve. For the Lorentzian curve given by 2.6 this is

$$\delta H = \frac{2}{\sqrt{3}\ \gamma T_2} \qquad 2.7$$

One can therefore, in principle, determine the spin-spin relaxation time, T_2, from such a measurement of the linewidth. In practice, however, the natural linewidth is broadened owing to the inhomogeneity of the external magnetic field. T_2 in 2.7 must then be replaced by an effective spin-spin relaxation time T_2^* given by

$$\frac{1}{T_2^*} = \frac{1}{T_2} + \frac{1}{T_2'} \qquad 2.8$$

where T_2' is determined by magnetic field inhomogeneity.

In pulsed n.m.r. the external magnetic field is kept constant and r.f. power at the Larmor frequency is applied to the sample in very short pulses.

If, as in section 1.1., we let the external magnetic field lie along the z-direction then the exciting field, H_1, lies in the x-y plane. In the steady state the spin system will have a nett magnetic moment, M_o, directed along z. When a pulse of duration Δt is applied this has the effect of tipping M_o away from the z axis such that α, the angle between M_o and the axis, is given by

$$\alpha = \gamma_n H_1 \Delta t \qquad 2.9$$

Thus for a $\pi/2$ pulse, M_o is turned into the x-y plane and for a π pulse into the negative z direction. It is assumed here that H_1 is sufficiently large for the condition $\Delta t \ll$, T_1, T_2 to be satisfied otherwise relaxation effects will occur within the duration of the pulse.

Following a $\pi/2$ pulse, M_o rotates in the x-y plane inducing a signal in the coil which, in a single coil apparatus , acts as both transmitter and receiver coils. The signal is observed to decay exponentially and is termed a free induction decay. The time constant of the decay is T_2^* as defined in 2.8. This experiment is, in fact, analagous to the continuous wave method outlined above, an exponential in the time domain being related to a Lorentzian in the frequency domain by the Fourier transform.

The spin-lattice relaxation time, T_1, can be measured by using two pulses in succession. For liquids, where $T_1 = T_2$, a $\pi - \pi/2$ pulse sequence is used. The first pulse tips M_o into the negative z direction. After a time t the second pulse rotates the magnetisation into the x-y plane where it produces a free induction decay the height of which will be proportional to the magnitude of the longitudinal magnetisation, M(t), at time t. By varying t the growth of M(t) can be observed and T_1 can be found from the equation

$$M(t) = M_o \left[1 - 2 \exp(-t/T_1) \right] \qquad 2.10$$

The direct method of measuring T_1 using pulse techniques as outlined above is the most straight-forward method available and therefore to be preferred provided it can be applied to the particular spin system in which one is interested. Unfortunately we could not use this method for measuring T_1 for the ^{201}Hg spins in liquid mercury for the following reasons. Firstly, the magnitude of the exciting field, H_1, of our existing pulse spectrometer was of the order of 15g. Using 2.9 the length of a $\pi/2$ pulse for this isotope is calculated to be about 60 μs. Because of the large quadrupole contribution T_1 for ^{201}Hg is about 25 μs. Thus the condition $\Delta t \ll T_1$ was not satisfied. Secondly, the recovery time of the receiver of the spectrometer was about 50 μs. which was again not negligable compared to T_1. Thirdly, our spectrometer was, overall, not sensitive enough to be able to display the ^{201}Hg resonance on an oscilloscope thus making it difficult to set up experimental parameters such as the external magnetic field and the r.f. pulse lengths. It was therefore decided that the most straight-forward approach would be to measure the linewidth of the ^{201}Hg resonance in a continuous wave experiment. Since in a liquid $T_1 = T_2$, T_1 may be obtained from the line-width corrected for broadening by the inhomogeneity of the external field.

2.2.2. Experimental Arrangement

It was decided to use a bridge system for the continuous wave experiments rather than a marginal oscillator. This choice was made since, because of the weakness of the ^{201}Hg

resonance signal, we required a high r.f. power level in order to increase the signal size and also a high frequency stability as we proposed to average the signal over long periods of time. Both of these are more easily achieved with a bridge. A block diagram of the complete spectrometer is shown in figure 2.1. Its components were as follows.

2.2.2.1. The r.f. Transmitter, Bridge and Receiver

A crystal controlled oscillator was employed as a high stability frequency generator the output frequency of which was 6.0 MHz with a stability of 1 part in 10^6. This was built using a 12 MHz crystal oscillator from Meon Electronics Ltd. The design included a Schmitt trigger circuit which clipped the output of the crystal oscillator before frequency division, thus removing a certain amount of noise from the signal. The output from the oscillator was 2v. peak to peak. This was amplified in a power amplifier consisting of two stages, a C class stage employing an EL360 valve driven by an A class stage which used an E180F valve. The maximum output from this transmitter was 20v peak to peak.

The bridge used was of the form first employed by Anderson (5). The bridge circuit and component values are shown in figure 2.2. This type of bridge was chosen for two reasons. Firstly, the phase and amplitude controls are completely orthogonal. Resistive balance is obtained by adjusting the capacitors C and the reactive balance is controlled by the capacitors C'. Secondly, because it does

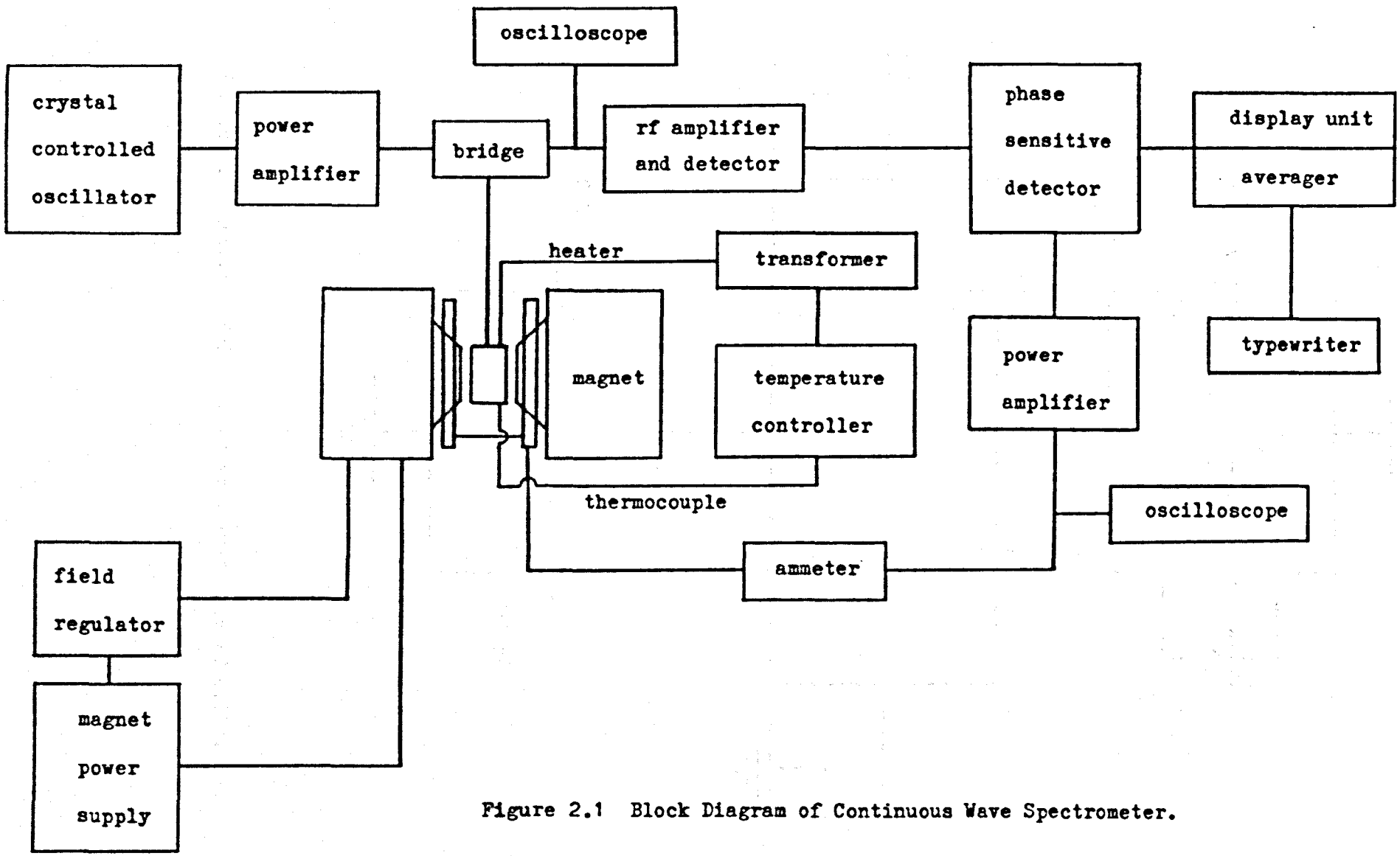

Figure 2.1 Block Diagram of Continuous Wave Spectrometer.

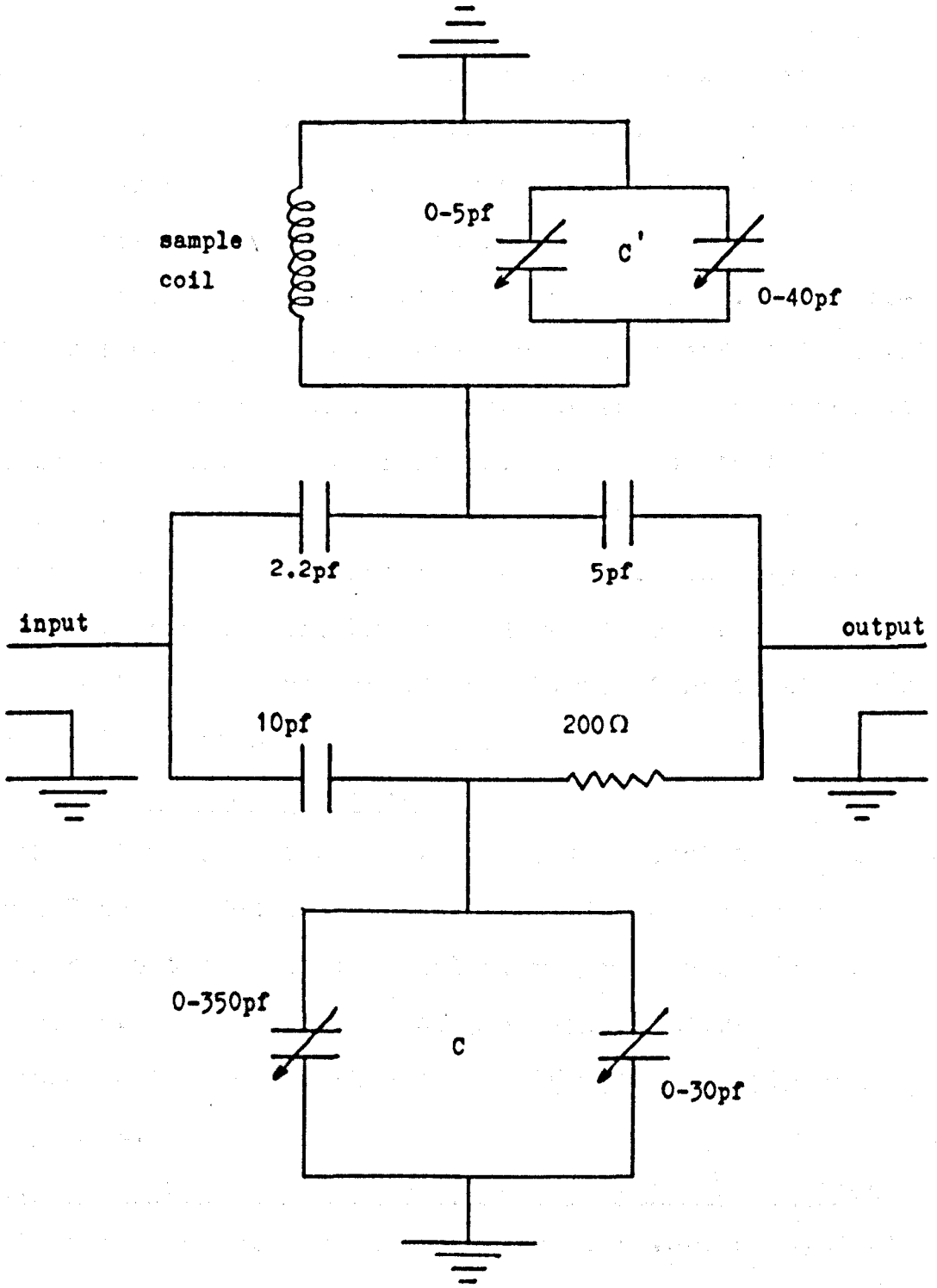

Figure 2.2 Anderson Bridge Used at a Frequency of 6.0MHz.

not employ a dummy circuit its long term stability is better than many other bridge arrangements. The residual unbalance was set to 200mv. using a Hewlett Packard Model 175A high frequency oscilloscope.

The receiver consisted of three stages of r.f. amplification followed by a diode detector. Field effect transistors type 3N201 obtained from Texas Instruments were used because of their low noise characteristics. The input to the amplifier was tuned as was the drain of the first stage. The overall gain of the amplifier was $\sim 10^4$. The crystal oscillator, transmitter, bridge and receiver were all made in the electronics workshop of the Physics Department under the supervision of Dr. R.L. Havill.

2.2.2.2. The PSD and Averager

The output from the receiver was fed first to a Princeton Applied Research Model JB4 phase sensitive detector and from there to the digital signal averager made by Tracor. The averager consisted of an NS-544 digital memory oscilloscope together with a series 500 power supply and display unit.

2.2.2.3. The Magnet System and Magnetic Field Modulation

The magnet system used consisted of a Varian V-7300 12 inch electromagnet with V7800 basic power unit and a Fieldial Mark II field regulator which uses a Hall effect probe attached to one of the pole caps to detect and regulate the magnetic field. Using pole caps with a face diameter of 4½" and an air gap of 1.5" the magnetic field was continuously variable up to a maximum of about 25kg. The maximum set

field used in these experiments was 20.8465 kg. which is the resonant field for the ^{201}Hg isotope at a frequency of 6.0 MHz. At this field the performance specifications of the system indicate field regulation within 20 mg. for a $\pm$ 10% line voltage or load resistance change and long term field stability to within 200mg. for a $\pm$ 5°C temperature variation. The specifications also give the magnetic field resetability as within 20mg. The field regulator was used to provide automatic sweeping of the field with a variety of sweep ranges and sweep times.

Magnetic field modulation was provided by two coils of 26 swg copper wire connected in series. Each coil was 22.5 cm in diameter and had 135 turns giving a resistance of 40 Ω. The wire was wound onto strong brass formers which were securely fastened onto the pole tips. In order to minimise vibration and so reduce modulation pick-up the coils were potted in glue to form a solid unit. The modulation frequency was derived from the phase sensitive detector and was set at a nominal 127 Hz. to avoid mains pickup. An H & H 50 watt power amplifier was used to provide the modulation current. The current was measured using an avometer and the voltage across the coils monitored on an oscilloscope.

2.2.2.4. The n.m.r. Probe and Temperature Controller

The n.m.r. probe used is shown in figure 2.3. Because of the weakness of the ^{201}Hg resonance a sample tube with a large internal diameter of 12 m.m. was used. This fitted snugly into the r.f. coil which was 22 m.m. long and

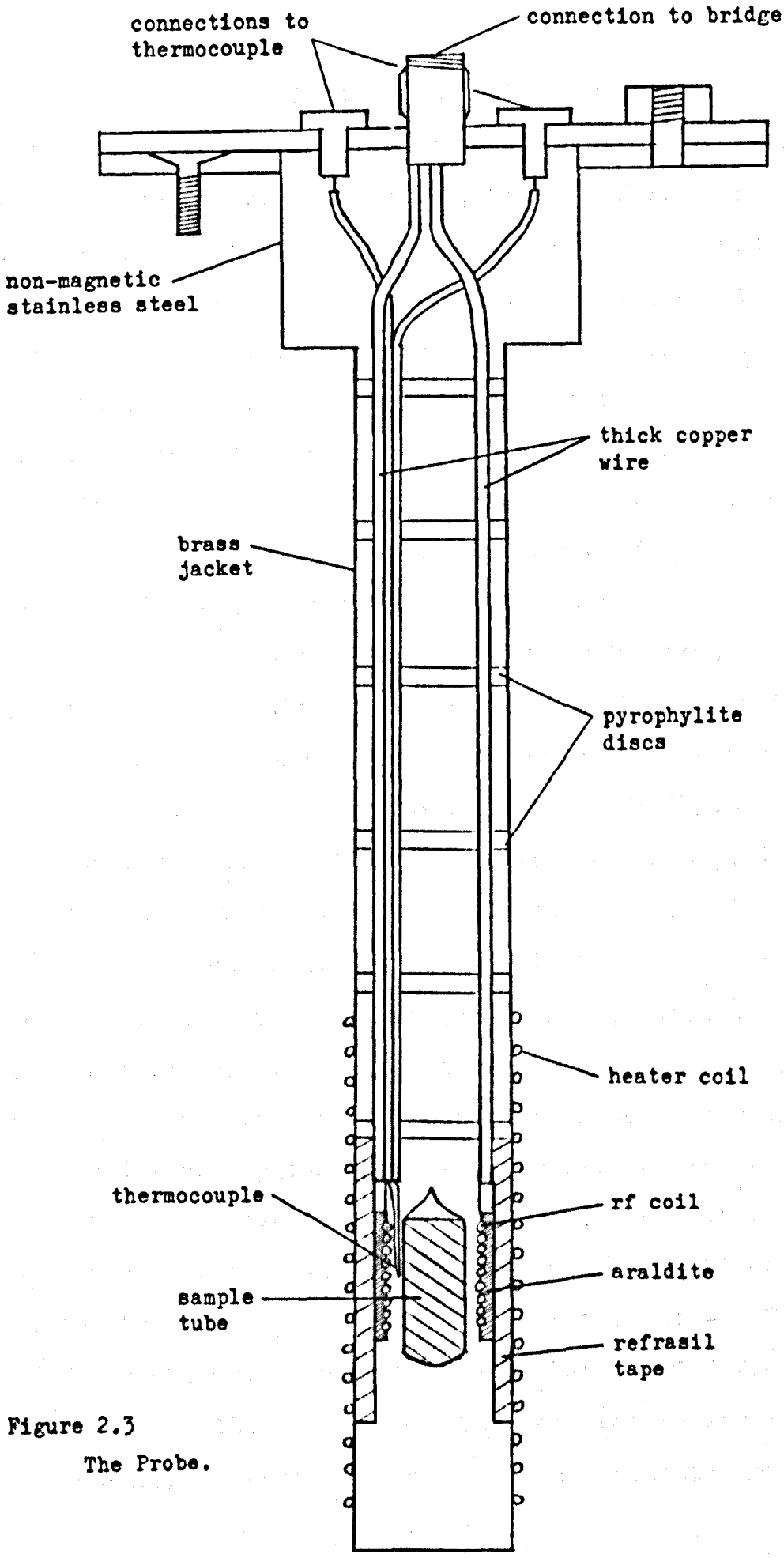

Figure 2.3

The Probe.

consisted of 32 turns of 28 swg enamelled copper wire. The coil was potted in araldite cement and held firmly in position in the outer, cylindrical, brass jacket by refrasil tape. The probe itself was securely bolted to a rigid platform located above the magnet gap. In this way the long term stability of the bridge was improved and effects due to modulation pick up minimised. Temperatures above room temperature were obtained using a heater coil wound non-inductively around the brass jacket. The coil was made from 3.5m of Eureka wire with a total resistance of about 30 ohms and was insulated with refrasil sleeving. The temperature of the sample was measured using a platinum/platinum - 13% rhodium thermocouple with its junction placed between the r.f. coil and the sample tube. The thermocouple acted as a sensing element for a "Eurotherm" model DHS/PID/SCR temperature controller. The heater current was supplied by a variac which was set between 10v and 50v depending on the temperature required. By using this temperature controlling equipment the sample temperature was kept within $1^{o}C$ of the required value. For temperatures below room temperature the heater was removed and the outer brass tube surrounded by a glass dewar. By filling the dewar with a mixture of ice and water a sample temperature of $7^{o}C$, constant to $1^{o}C$, was obtained. Similarly, filling the dewar with liquid freon maintained the sample at a steady temperature of $-28.2^{o}C$. Liquid freon was obtained from cans of "Arcton 12" from ICI Limited. In the latter case the temperature was measured using a copper/constanton thermocouple and potentiometer.

2.2.3. Sample Preparation

Because of the r.f. skin effect it was necessary to have the sample in the form of small particles dispersed in an insulating medium, the diameter of the particles being smaller than the skin depth of the r.f. field. Using a value of 98.4. 10^{-8} ohms metres for the resistivity of liquid mercury at 50°C the skin depth was calculated to be about 200 μm. The sample was made by rapidly shaking 99.9999% pure mercury obtained from the Koch Light Company with liquid paraffin in a conical flask and decanting the resulting suspension into several large tubes. After a short time the tiny mercury particles settled at the bottom of the tubes and the clear liquid paraffin was returned to the conical flask. This was repeated until the required amount of sample was obtained. Microscopic analysis showed that the sample consisted of particles with diameters of the order of 50μm. The sample was finally transferred to the sample tube which was sealed off under argon at 1/3 atmospheric pressure. Samples prepared in this way were found to be sufficiently stable for prolonged experiments below about 150°C.

2.2.4. Calibration of Magnetic Field Modulation

As stated earlier, if the magnitude of the magnetic field modulation is small compared to the resonance linewidth then the output of the phase sensitive detector will be proportional to the derivative of the resonance line shape. If the modulation is large compared to the linewidth this is no longer true. In particular the linewidth obtained from the experimental derivative is larger than the true linewidth.

Modulation effects in magnetic resonance have been discussed by several authors (6), (7), (8), (4). Smith (4) points out that if the modulation amplitude is much greater than the true linewidth then the measured linewidth is approximately equal to the peak to peak modulation amplitude and suggests that this may be used as a basis for modulation calibration. In fact an analytical treatment based on the work of Wahlquist (see Appendix I) shows that, if δH_{meas} represents the measured linewidth, H_ω the modulation amplitude, and δH the true linewidth then

$$\delta H_{meas} = 2H_\omega - \delta H \qquad 2.11$$

provided $H_\omega \gg \delta H$.

Expression 2.11 was used to calibrate the 'modulation in these experiments. The two set fields were 7.6953 kg. for the ^{199}Hg isotope and 20.8465kg. for the ^{201}Hg isotope. A sample of Li metal was used to calibrate the modulation at the lower field and the deuterium resonance in deuterium oxide doped with ferric chloride was used at the higher field. The resonances were observed using a variable frequency marginal oscillator the output of which was fed to the phase sensitive detector and from there to a pen recorder. The frequency of oscillation was measured using a timer counter TC8 made by Advance Instruments. Care was taken to ensure that each sample occupied a central position in the magnet gap. The procedure used was as follows. First the various magnet sweep widths to be used were calibrated by obtaining three narrow resonance lines on the pen recorder.

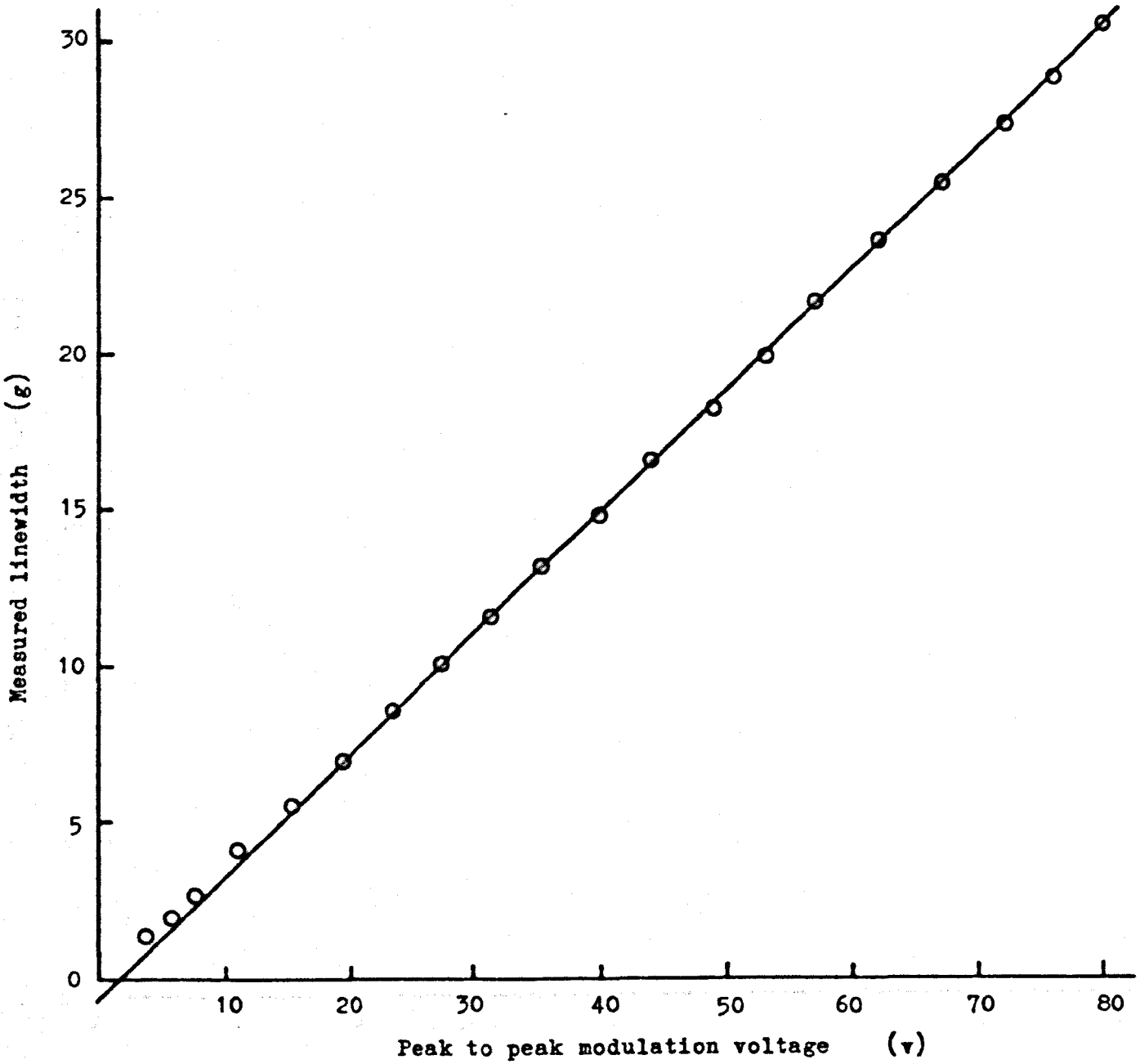

Figure 2.4 Graph of measured linewidth against modulation voltage at a set field of 7.6953 kg.

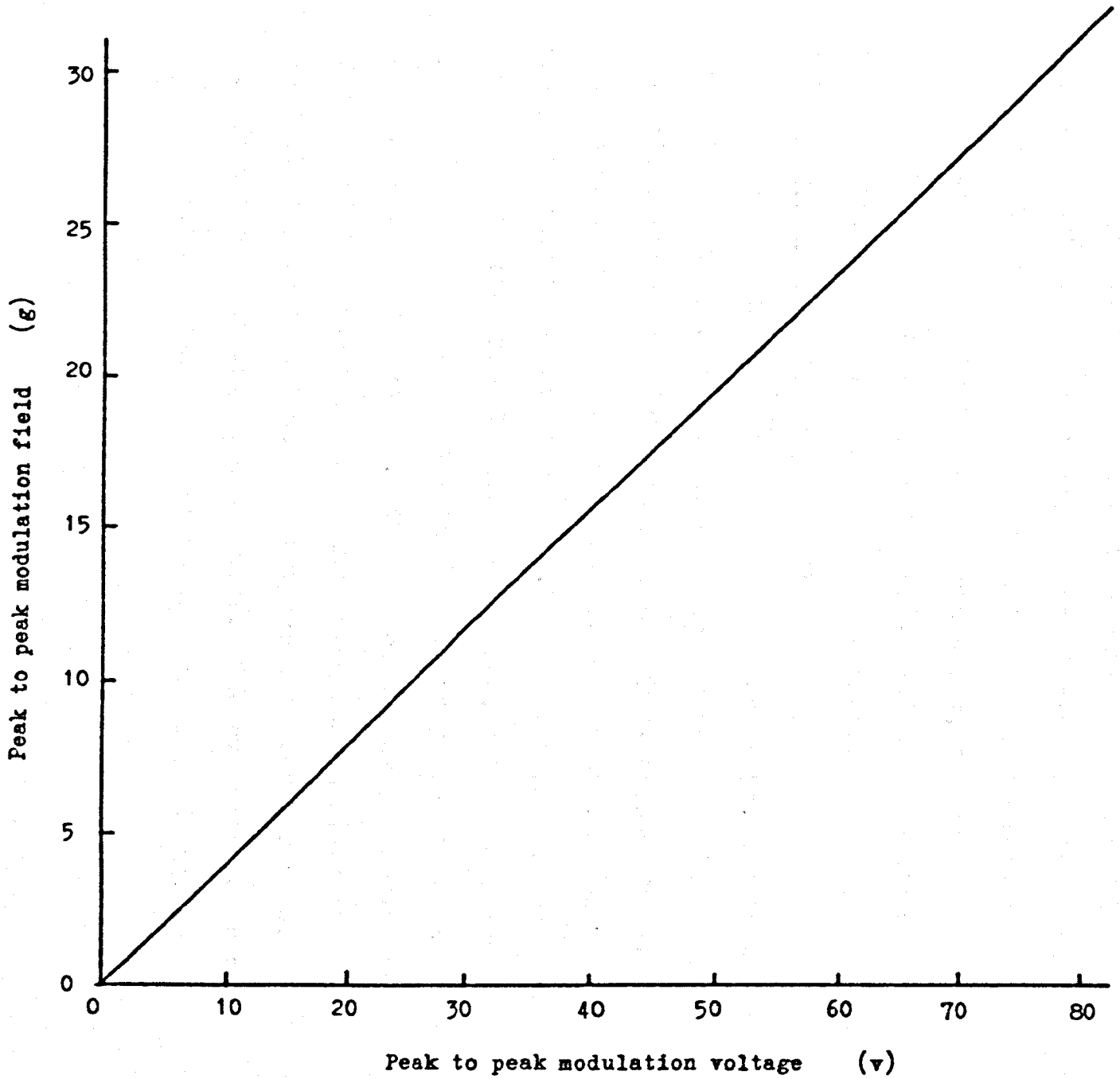

Figure 2.5 Graph of amplitude of modulation field against modulation voltage at a set field of 7.6953 kg.

Then the linewidth of the sample was measured as a function of peak to peak modulation voltage. The corresponding modulation current was also recorded. Figure 2.4 shows the results obtained at the low field. The straight line is a least squares fit to the top 13 points. The negative intercept gives a linewidth of 0.67g for the Li sample. By shifting the line up by this amount the graph of modulation amplitude against modulation voltage shown in Figure 2.5 was constructed. In practice, the modulation amplitude was set using the modulation current as this could be read more accurately than the voltage. Unfortunately, the current could not be used directly in the calibration procedure as the avometer scale was found to be non-linear.

2.2.5 Measurement of the Linewidths

The linewidth of ^{199}Hg resonance is about 5g. and that of ^{201}Hg about 25g. The resonances were observed using magnetic field sweep widths of 50g. and 250g. respectively. Each sweep took 30s. and the output time constant, τ, of the phase sensitive detector was 0.3s. If T represents the time taken to traverse the linewidth, then, for both isotopes, $T/\tau \sim 10$ and hence asymmetry in the lineshape due to a time constant effect was avoided. The magnet was swept continuouly in the sawtooth mode and a negative going ramp derived from the field regulator was used to trigger the averager about 2s. after the beginning of each sweep. The averager was run in the internal advance mode at a sweep speed of 50 ms. per

channel. Since only half of the available memory of 1024 channels was used each averager sweep lasted 25.6s. There was thus a delay of about 4s. between averager sweeps during which the magnetic field fell back to its initial value. Averaging times were about 4 hr. for the ^{201}Hg line and 1 hr. for the stronger ^{199}Hg line. The bridge was balanced to detect the absorption mode. Because of a slow drift off balance it was necessary to rebalance the bridge after every 8 scans with the averager temporarily halted. In this way the dispersion signal never exceeded 10% of the absorption signal in any one sweep and the average over many sweeps was not large enough to give any detectable asymmetry to the lineshape.

The linewidth was obtained using a computer program to fit the expression given by Wahlquist (6) to the observed derivative curve. The program automatically corrected for modulation broadening. However, this was never more than 0.5g. in ~ 25g. for the ^{201}Hg line although we did allow it to rise to 1.5g. in ~ 5g. for the ^{199}Hg line in order to save averaging time. A small amount of field dependent modulation pick up was observed at the high field which was taken into account in the program by adding a sloping base-line to the Wahlquist formula. An outline of Wahlquist's theory together with details of the computer program are given in Appendix I.

2.2.6 Measurement of the Knight Shift and its Variation with Temperature

The program was also designed to give the position of

the centre of the resonance lines and using this information relative changes in the Knight shifts of the isotopes could be calculated. The absolute values of the Knight shifts were determined as follows. First, an averaged mercury signal was obtained on the first half of the averager memory. Then, using the marginal oscillator, three narrow signals from a sample of doped D_2O accurately placed in the central position in the magnet gap previously occupied by the mercury sample were obtained on the second half of the memory. During this procedure the magnetic field was kept on in order to avoid errors in resetting. The position of the centre of the mercury line was found using the program and the value of the magnetic field at this position calculated using the deuterium signals. Deuterium oxide was used to provide markers for both mercury isotopes. On comparing the positions of resonances from the D_2O sample relative to signals from a Li metal sample a small paramagnetic shift in the deuterium resonance was found. The shift was equivalent to an error in gyromagnetic ratio of 0.008%. This was taken into account in the calculation of the mercury Knight shifts.

Finally, the inhomogeneity of the external magnetic field over the region occupied by the mercury sample was determined by placing the same size of sample of doped D_2O at the same position in the magnet gap and obtaining resonances at the high and low fields. The sample was doped to give a natural linewidth of about 0.1g. The linewidths at the two

fields were obtained using the computer program. It was found that the magnetic field contributed 0.7g. to the ^{201}Hg line and 0.5g. to the ^{199}Hg line.

2.3 Experimental Data

The variation with temperature of the linewidths of the ^{201}Hg and ^{199}Hg isotopes of liquid mercury is shown in Figure 2.6. The linewidths are corrected for modulation broadening and broadening by the inhomogeneity of the magnetic field.

The total longitudinal relaxation rates for the two isotopes were derived from the linewidths using equation 2.7 which may be written as

$$R_1 = \frac{\sqrt{3}}{2} \gamma_n \delta H \qquad 2.12$$

since $T_1 = T_2$. The value of the gyromagnetic ratio for the ^{199}Hg isotope, $\gamma_n^{199} = 4.7830. 10^3 s^{-1}. g^{-1}.$, was taken from the n.m.r. measurements of Proctor and Yu (9). The gyromagnetic ratio of the ^{201}Hg isotope was calculated using the magnetic moment given by Cagnac and Brossel (10) which gives $\gamma_n^{201} = 1.7658. 10^3 s^{-1}. g^{-1}.$ Figure 2.7 shows the variation with temperature of the relaxation rates of the two isotopes.

The magnetic contribution, R_{1m}, to the relaxation rate of the ^{201}Hg isotope was calculated from the relaxation rate of the ^{199}Hg isotope using equation 2.4. which is

$$\frac{R_{1m}^{201}}{R_{1m}^{199}} = \left[\frac{\gamma_n^{201}}{\gamma_n^{199}}\right]^2 = 0.136 \qquad 2.13$$

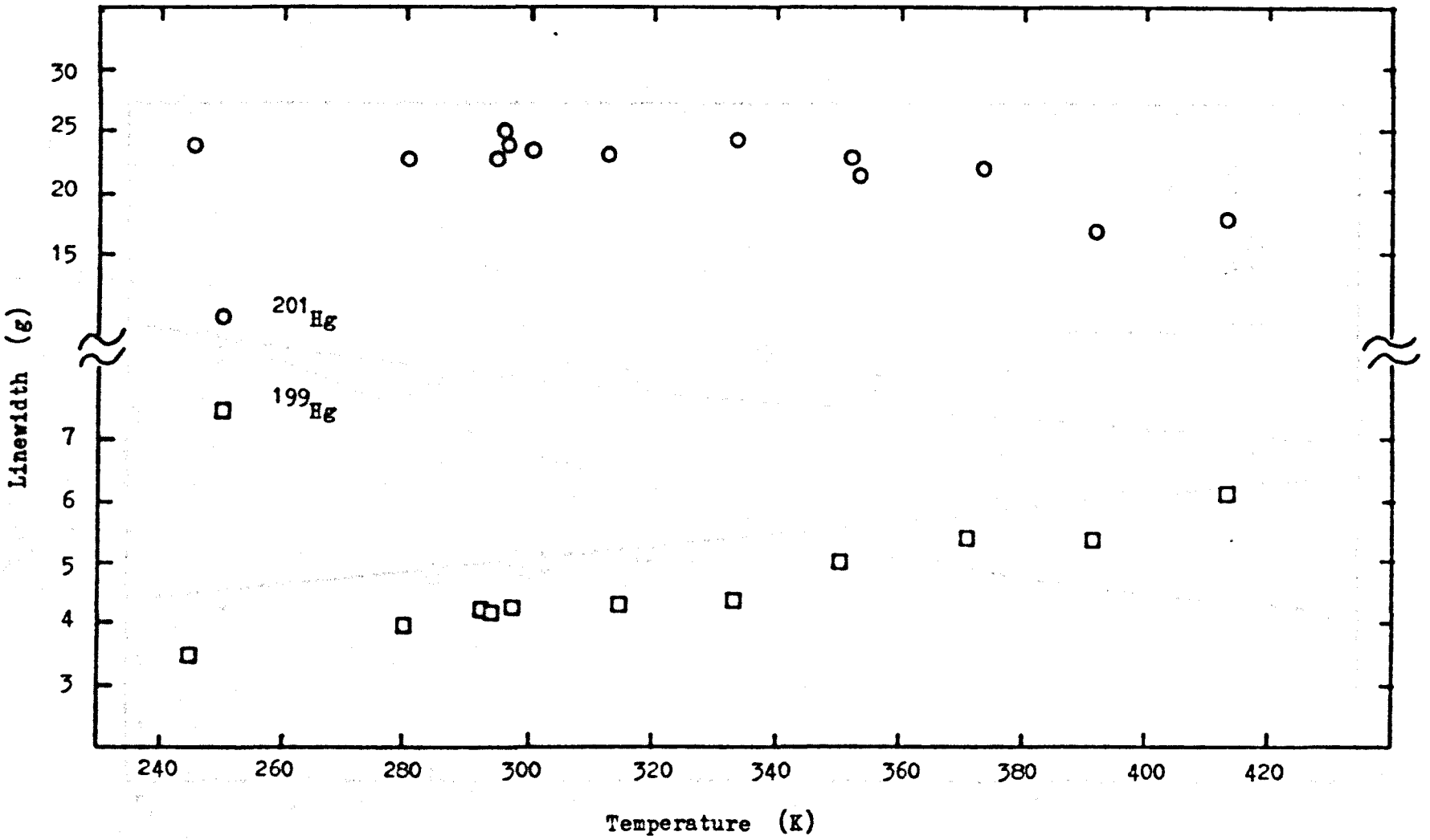

Figure 2.6 Variation of the linewidths with temperature.

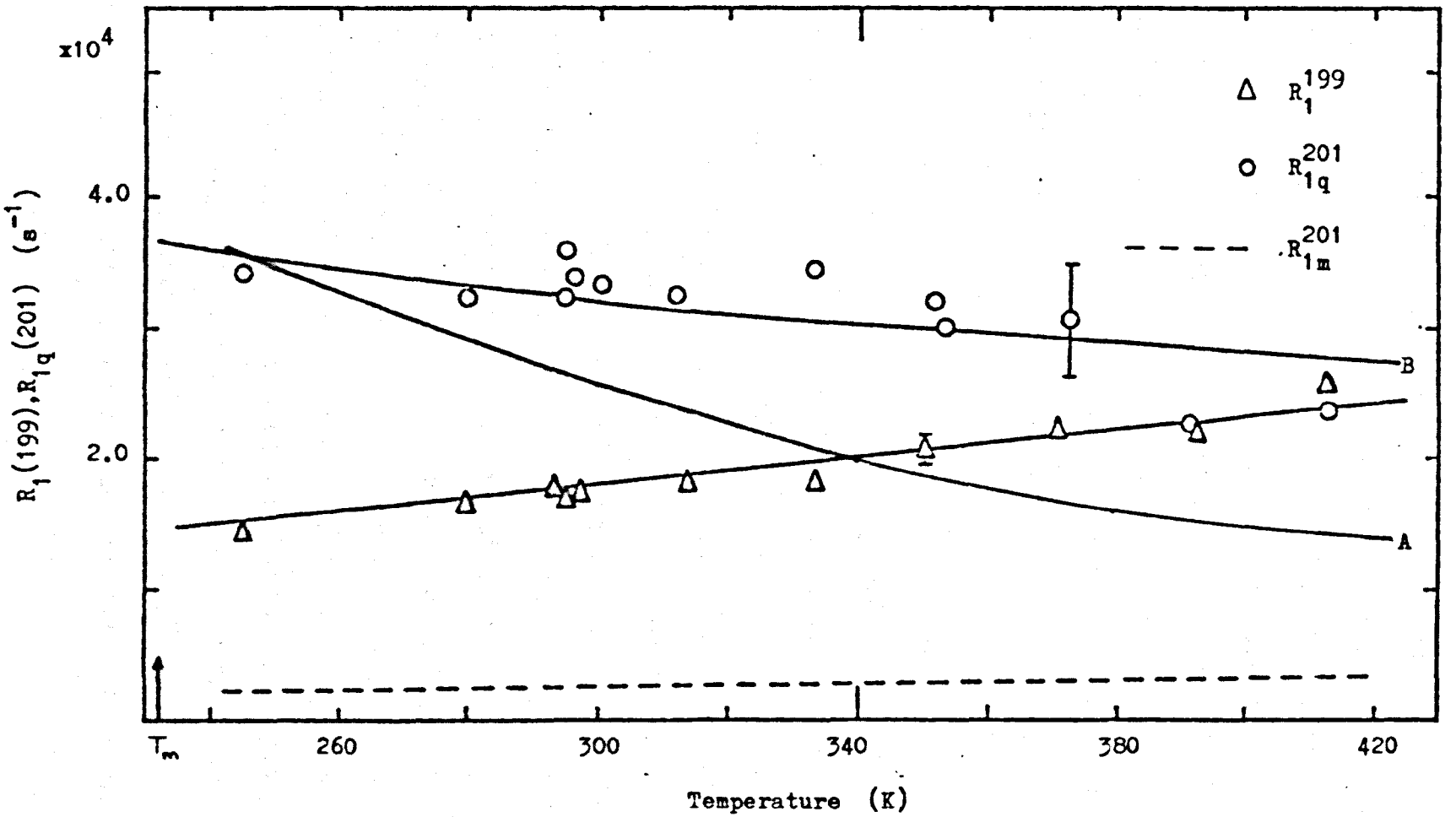

Figure 2.7 Variation with temperature of the longitudinal relaxation rates.

This was then subtracted from the total relaxation rate of the ^{201}Hg isotope to give the quadrupole contribution, R_{1q}^{201}. It is easily seen that relaxation via the quadrupole interaction is the dominant relaxation process for this isotope. Also the quite different dependence on temperature shows up the different origin of the relaxation in the two isotopes. The quadrupolar contribution is seen to decrease slowly with temperature whereas the magnetic oontribution has the characteristic linear variation with temperature associated with the Korringa relation.

The Knight shifts of the ^{199}Hg and ^{201}Hg resonances were found to be 2.424 $\pm$ 0.002% and 2.43 $\pm$ 0.01% respectively at a temperature of 20°C. The gyromagnetic ratios given above were used in the calculation of the Knight shifts. The poorer error in the value given for the ^{201}Hg isotope is due to the lower signal to noise ratio and wider line.

The variation of the Knight shift with temperature is shown in Figure 2.8. The figure was constructed by calculating the shift of the metal resonance relative to its position at 20°C. The experimental error for each point here is greater than that in the absolute shifts given above. This is because the magnet was switched off between runs and we relied on the resetting action of the Fieldial to give the same value of magnetic field at the start of the sweep for each run. Unfortunately, the magnet's behaviour at the time of these experiments was well below specification in

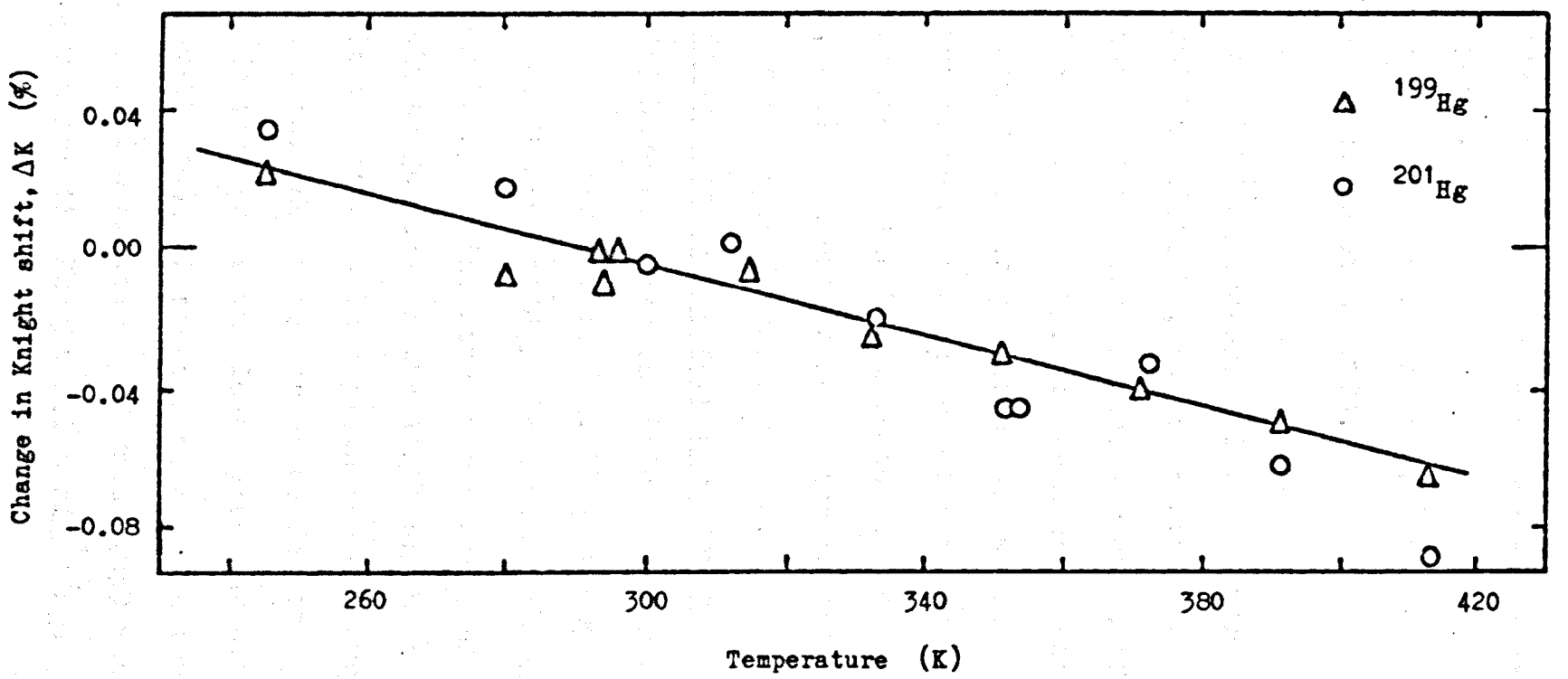

Figure 2.8 Variation with temperature of the Knight shift relative to the shift at 20 C.

this respect. The straight line represents $K^{-1}\ dK/dT = -\ 20.10^{-5}\ K^{-1}$ with respect to an estimated Knight shift of 2.453% at the melting point.

These results have been reported in the publications by Havill et al (11) and Marsden et al (12).

2.4 Discussion

For both the ^{199}Hg and ^{201}Hg isotopes of liquid mercury we have measured the Knight shift, K , together with its dependence on temperature and the temperature variation of the spin - lattice relaxation rate, R_1. These measurements have been made in the course of our principal aim which was to determine the variation of the quadrupolar relaxation rate, R_{1q}, with temperature for the ^{201}Hg isotope. Therefore, in what follows, while concentrating on the interpretation of R_{1q}, we attempt a simple discussion of K.

2.4.1 The Knight Shift and its Temperature Dependence

Blumberg et al (13) have measured the Knight shifts of the ^{199}Hg and ^{201}Hg isotopes and obtained 2.724 $\pm$ 0.005% for ^{199}Hg and 2.722 $\pm$ 0.005% for ^{201}Hg. From these measurements they deduced a small hyperfine structure anomaly although this is difficult to justify in the light of their experimental error. It is not easy to explain the difference between their data and ours. However, our value for the Knight shift of the ^{199}Hg isotope is in close agreement with the 2.418% found by Havill (14). Further agreement is found in the data quoted in a review article by Seymour (15) where a value of 2.42% is given for the Knight shift of ^{199}Hg,

together with a temperature dependence $K^{-1} \frac{dK}{dT}$ of -15. 10^{-5} $^{o}C^{-1}$.

The theory of the Knight shift in liquid metals is very complicated and for details the reader is referred to the review articles by Seymour (15) and Titman (16).

From Chapter 1 it will be remembered that the direct Fermi contact interaction leads to a Knight shift given by eq. 1.6 which is

$$K_\delta = \frac{8\pi}{3} \chi_p \langle |\psi(o)|^2 \rangle_F \qquad 2.14$$

This may be more conveniently written as

$$K_\delta = \frac{8\pi}{3} \chi \Omega P_F \qquad 2.15$$

where Ω is the atomic volume and ΩP_F is the probability density of the conduction electrons at a nuclear site averaged over the states at the top of the Fermi distribution. The Pauli susceptibility for independent electron spins χ_p is replaced in 2.15 by χ which takes into account the enhancement of the Pauli value by the presence of many body electron-electron interactions in the Fermi gas (17). Although the Knight shift has been measured with fair accuracy for most metals in both the liquid and solid states it has proved difficult to test 2.15 in a general way. The important quantities P_F and χ appearing on the righthand side of 2.15 have been measured independently only in a few cases, notably the alkali metals, and then only in the solid state. Good agreement between theory and experiment has

been obtained in the cases of Li and Na (18), (19).

For other metals the direct term of P_F must be obtained from pseudopotential theory and combined with a value of X determined from some independent calculation.

As a first step in the evaluation of P_F the single orthogonalised plane wave calculations of Mahanti et al (20) and Heighway and Seymour (21) have met with some success. A further refinement may be introduced by allowing for the effect of scattering of the conduction electrons by the ion-cores. This principle has been adopted in a number of papers concerned with the evaluation of P_F (22), (23) (24).

The Knight shifts of most liquid metals are weakly dependent on temperature. Almost all measurements have been made at constant pressure so that the temperature coefficient reflects the effect of the volume expansion of the liquid. The effect of the variation of X and P_F may be found from

$$\frac{1}{K}\left(\frac{\partial K}{\partial T}\right)_p = \frac{1}{X}\left(\frac{\partial X}{\partial T}\right)_p + \frac{1}{P_F}\left(\frac{\partial P_F}{\partial T}\right)_p \qquad 2.16$$

The intrinsic dependence of X on temperature is very small and the main change occurs through the effect of the volume expansion on the density of states and the electron-electron enhancement. Ford and Styles (25) have found that $(1/X)(\partial X/\partial T)_p$ lies between $-2.\ 10^{-5}$ and $-3.\ 10^{-5}\ K^{-1}$ for a number of liquid metals. The temperature coefficient of P_F must be calculated from the appropriate pseudopotential theory.

As observed with liquid mercury the temperature coefficient is often negative for polyvalent metals. The

calculations of Ford and Styles (25) for Ga, Cd, In, Sn, Pb and Bi and Halder (26) for Cd, Sb, and In give values for $(1/K)\ (\partial K/\partial T)_p$ close to the experimental magnitudes. As far as the author is aware only a simple calculation of the temperature variation of the Knight shift in liquid mercury based on the single orthogonalised plane wave method has been carried out (15) giving a theoretical value of $-7.\ 10^{-5}\ ^{o}C^{-1}$ for $\frac{1}{K}\left(\frac{dK}{dT}\right)$.

2.4.2. The Magnetic Relaxation Rate

The linewidth of the ^{199}Hg resonance has been measured by Cornell (2) and Blumberg et al (13). Cornell's measurements were made at three temperatures ranging from $233^{o}K$ to $363^{o}K$ but Blumberg's measurement was restricted to room temperature. Our linewidths agree with Cornell's within the experimental error but our room temperature linewidth is considerably smaller than that given by Blumberg et al. This could possibly be explained by overmodulation of the resonance line by these authors.

Our data may be analysed using the modified Korringa relationship introduced in Chapter 1. Equation 1.11 relating the contributions to the Knight shift and relaxation rate produced by the s- like part of the conduction electron density may be written as

$$R_{1s} = 4\pi k_B\ \gamma_n^{\,2}\ K_s^{\,2}\ TK(a)\ \ (\hbar\gamma_e^{\,2})^{-1} \qquad 2.17$$

It was pointed out that 2.17 describes the contributions from the contact term in the hyperfine Hamiltonian and the

core polarisation induced by the s-like conduction electrons. It is not, however, valid for contributions from the p-core polarisation and the orbital term. Equation 2.17 contains the correction factor K(α) which, as stated previously, is difficult to calculate. Accurate calculations have only been made using an interacting electron gas model for the alkali's where K(α) is found to lie between 0.6 and 0.7.

The solid line in figure 2.7 shows a fit to the relaxation rates of the ^{199}Hg isotope using 2.17 with our measured value of K, including its variation with temperature, and assuming K(α) = 0.81. Thus a possible conclusion is that the Knight shift and relaxation rate are simply produced by the s-terms. However, 0.81 is perhaps a rather large value for K(α) which lies in the range 0.67-0.75 for most liquid metals. Our value of K(α) may be brought into line with these values by allowing quite small contributions from non-s terms. For example, if these are taken to be of the order of 1/10 of the magnitude of the observed shift and of the opposite sign K(α) is reduced to 0.7. Non-s terms of this magnitude seem reasonable in the light of the presently available theoretical calculations (27). Until some way can be found to separate the non-s terms the true value of K(α) will remain a matter of conjecture.

2.4.3 The Quadrupole Relaxation Rate

Cornell (2) also measured the linewidth of the ^{201}Hg resonance at three different temperatures 265°K, 317°K and

356°K and Blumberg et al (13) measured the linewidth at room temperature. Our linewidths are about 20% smaller than Cornell's but much closer to Blumberg's result. It is not possible, from the published material, to discover the reason for these differences. However, Cornell's analysis of his results taken in conjunction with his measurements on the linewidth of the ^{199}Hg isotope lead to a temperature variation of R_{1q} which is in agreement with our own.

Further information on the variation of R_{1q} with temperature in liquid Hg has been obtained using pac techniques. A direct comparison of absolute values of quadrupolar relaxation rates obtained using nmr and pac methods is not possible because of a lack of precise values for the nuclear quadrupole moments of the excited nuclear states.

The earlier measurements of Bräuer et al (28) on trace amounts of ^{206}Pb nuclei in liquid mercury were interpreted as representing a variation in R_{1q} with temperature proportional to the reciprocal of the diffusion coefficient. This is a much faster trend than that observed in our experiment. However, there is considerable scatter in their data, the observed relaxation rate varying by as much as a factor of two between different measurements at the same temperature. Greater weight should be attached to their recent, more accurate, measurements on ^{202}Tl nuclei in liquid mercury (29). In this data the decreasing trend in R_{1q} is much slower and generally in agreement with our own.

As pointed out in Chapter 1 the major problem in calculating the absolute value of R_{1q} lies in the calculation of the electric field gradient and antishielding. In particular Sholl (30) points out that, in his theory, the effects of the conduction electrons inside the core at the origin are inaccurately described. These problems have been discussed separately by Lodge (31) and Schirmacher (32).

Now there are essentially two approaches to the interaction of an ion core in a metal with all other charge. One is to take the point charge interaction of the ion cores and add separately to this the interaction with the conduction electrons. This is basically the approach used by Lodge. The other approach, as used by Sholl, is to regard the electrons as screening the ion cores and to describe the potential at a given site as a sum of screened potentials from all other ion-core positions.

In the introduction to his paper Lodge states that the efg in a metal may be calculated from the equation (33)

$$q = \int_0^\infty \left[1+ \gamma(r)\right] q(r)dr \qquad 2.18$$

where $q(r)dr$ is the contribution to the efg from charge, other than that of the local ion core, lying between r and $r + dr$ and $\gamma(r)$ is the radial dependent antishielding factor (34)

Equation 2.18 may be simplified to give (35)

$$q = q_{latt} (1-\gamma_\infty) + q_{loc} (1-R) \qquad 2.19$$

where q_{latt} is the efg at a nucleus from conduction electrons

and ions outside the ion core surrounding the nucleus, the lattice region, and q_{loc} is the efg from conduction electrons within that ion core, the local region. The factors γ_∞ and R are the Sternheimer antishielding factor and the core-correction factor respectively and take into account the distortions induced in the ion-core surrounding the nucleus in question.

The very involved theory of Lodge eventually produces an expression for q that is considerably more complicated than 2.19. However, when approximations are allowed in order to make calculations using model orthogonalised wavefunctions, it is found that for Be and Mg metal the values of q given by Lodge's expression differ from those given by 2.19 by only 10%. Thus, while being a valuable theoretical paper this treatment goes little way in helping to accurately calculate efg's in liquid metals. Furthermore, it is difficult to see how Lodge's treatment may be incorporated into the pseudo-potential approach used by Sholl.

Schirmacher (32) has calculated the efg in Ga and In using a pseudopotential theory that attempts to accurately describe the effects of the conduction electrons inside the core at the origin. The results of his calculations differ significantly from those of Sholl (30) especially in the degree of overlap between the efg function and the radial distribution function. This will be discussed in detail in Chapter 3.

Since the magnitude of R_{1q} depends on the strength of the electric field gradient, the effective antishielding of the quadrupole moment and also critically on the degree of overlap between the efg function and g(r) it is obvious that a comparison between theory and experiment in absolute terms is not possible at this stage. We therefore turn to a discussion of the variation of R_{1q} with temperature.

It was shown in Chapter 1 that Sholl's theory predicts that R_{1q} will vary with temperature in a way which is slightly slower than D^{-1}. Line A on figure 2.7 represents a variation proportional to D^{-1} for liquid mercury. The self diffusion data of Meyer (36) was used to construct this line. It will be seen that the temperature variation of R_{1q} is much slower than that predicted by the theory. A much better fit to the data is obtained with line B which represents a variation with temperature proportional to $T^{-\frac{1}{2}}$.

As shown in figure 2.9 the variations of R_{1q} with temperature in liquid mercury and a number of other liquid metals are directly comparable. The results illustrated in the figure, taken from nmr and pac measurements, were chosen because they were thought to be particularly reliable. As shown in the introduction to this chapter the most accurate values of R_{1q} are obtained when measurements can be made on two isotopes with very different gyromagnetic ratios or quadrupole moments, one of the isotopes having a relatively large quadrupole contribution. These criteria were satisfied

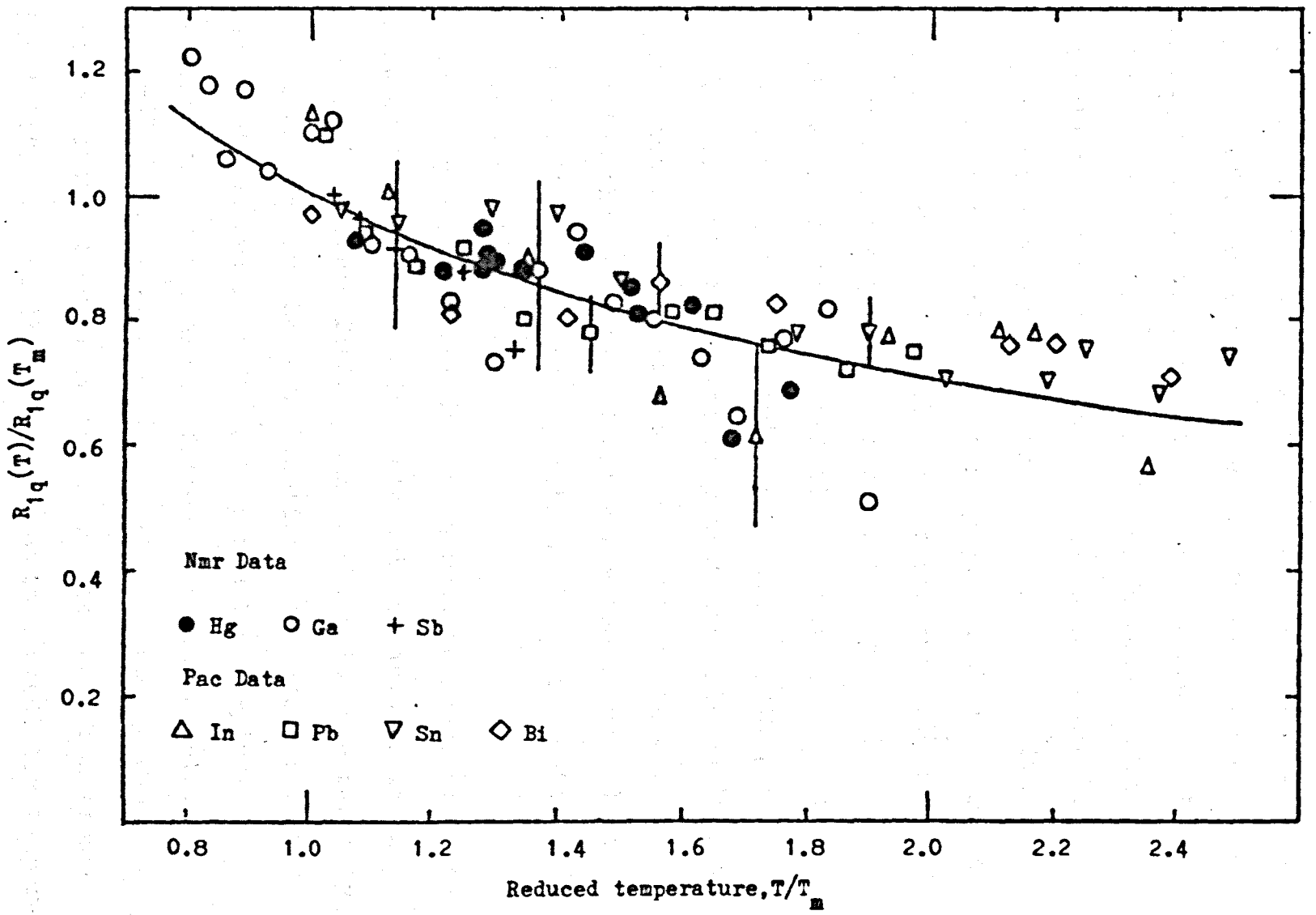

Figure 2.9 R_{1q} for various liquids normalised to unity at their melting points, T_m.

for the nmr measurements on Ga(37), Sb(38), our own Hg(12) and the pac measurements in liquid Sn(39) which were made on excited states of the two isotopes ^{114}Sb and ^{122}Sb. Reliable measurements of R_{1q} using a single isotope can only be made if $R_{1q} \gg R_{1m}$. This condition was satisfied in the case of the pac data on ^{117}Sb in liquid In (40) and is particularly true for the pac measurements in liquid Pb(41) and Bi (39) which were made on trace amounts of ^{207}Po, the relaxation of which is almost entirely quadrupolar in origin.

The line drawn through the data represents $T^{-\frac{1}{2}}$ and it can be seen that the quadrupolar relaxation rates in all seven metals appear to fit a relation of this form up to temperatures equal to about twice the melting point, T_m. It is believed that the controversy that has entered into the interpretation of R_{1q} in liquid metals has arisen because in some cases the experimental error was too large and in others the criteria for the separation of R_{1q} indicated above were not satisfied.

Nuclear quadrupole relaxation is brought about via the interaction between the nuclear electric quadrupole moment and the local electric field gradient which is made randomly dependent on time by the thermal motion. The nuclear Larmor period is of the order of 10^{-8}s. compared to a typical correlation time for ionic diffusion in a liquid metal of about 10^{-14}s. It is therefore easy to see why one would expect the dominant contribution to R_{1q} to come from translational diffusion of the ions leading to a predicted temperature dependence of 1/D.

However, the experimental data is obviously at variance with this prediction. The theories given by Sholl (30) and Warren (43) relate R_{1q} to the ionic motion through the van Hove function S(q,o). At small q, corresponding to movements over large distances, i.e., translational diffusion, this has a Lorentzian form and varies with temperatures as 1/D (30). However, at high q, that is for movement over relatively small distances, it has the ideal gas form varying with temperature as $T^{-\frac{1}{2}}$.

Since the experimental data demonstrates that R_{1q} varies with temperature as $T^{-\frac{1}{2}}$ this suggests that the main contribution to S(q,o) comes from the region of k space where q is relatively large. We have therefore re-examined the theory of quadrupolar relaxation in liquid metals and in the next chapter a new version of the theory is presented which goes some way in explaining the experimental data.

2.5 References

1) W.W. Warren Jr., and W.G. Clark, Phys. Rev., 177, 600, (1969)

2) D.A. Cornell, Phys. Rev., 153, 208 (1967)

3) E.R. Andrew, Nuclear Magnetic Resonance (Cambridge University Press, Cambridge, England, 1955)

4) G.W. Smith, J. Appl. Phys., 35, 1217 (1964)

5) H.L. Anderson, Phys. Rev., 76, 1460 (1949)

6) H Wahlquist, J. Chem. Phys., 35, 1708 (1961)

7) C.P. Flynn and E.F.W. Seymour, J. Sci. Instru., 39, 352 (1962)

8) G.V.H. Wilson, J. Appl. Phys., 34, 3276 (1963)

9) W.G. Proctor and F.C. Yu, Phys. Rev., 81, 20 (1951)

10) B Cagnac and J. Brossel, Compt. Rend., 249, 77 (1959)

11) R.L. Havill, J. Marsden and J.M. Titman, Phys. Stat. Solidi (b), 80, K141 (1977)

12) J. Marsden, R.L. Havill and J.M. Titman, J. Phys.F: Metal Phys., 8, 1321 (1978)

13) W.E. Blumberg, J. Eisinger and R.G. Shulman, J. Phys. Chem. Solids, 26, 1187 (1965)

14) R.L. Havill,Proc. Phys. Soc., 92, 945 (1967)

15) E.F.W. Seymour, NMR Studies of Liquid Metals and Alloys, 5th International Symposium on Magnetic Resonance, Bombay,(1974)

16) J.M. Titman, Nuclear Magnetic Resonance in Liquid Metals and Alloys, Phys. Reports, Vol. 33C, No. 1, p.1(1977)

17) D. Pines, Phys. Rev., 92, 626 (1954); Solid State Physics 1,367 (1955)

18) Ch. Ryter, Phys. Rev. Letters, 5, 10 (1960)

19) Ch. Ryter, Phys. Letters, 4, 69 (1963)

20) D. Mahanti, L. Tterlikkis and T.P. Das, in Magnetic Resonance, ed. Crogan (Plenum Press, N.Y., 1970) p.91

21) J. Heighway and E.F.W. Seymour, Phys. Konders. Materie, 13, 1 (1971)

22) J.P. Perdew and J.W. Wilkins , Phys. Rev., B7, 2461 (1973), Solid State Commun. 8, 2041 (1970)

23) T.E. Faber, Adv. in Phys., 16, 637 (1967)

24) P. Jena, T.P. Das, G.D. Gaspari and N.C. Halder, Phys. Rev., B3, 2158 (1971)

25) C.J. Ford and G.A. Styles in: Properties of Liquid Metals, ed. Takeuchi (Taylor and Francis, 1973) p. 189

26) N. C. Halder, in: Properties of Liquid Metals, ed. Takeuchi (Taylor and Francis, 1973) p.337

27) S.D. Mahanti and T.P. Das, Phys. Rev., B3, 1599 (1971)

28) N. Brauer, F. Dimmling, B. Focke, A. Goldmann, M. von Hartrott, Th Kornrumpf, K. Nishiyama, D. Quitman and D. Riegel, Proc. Int. Conf. Hyperfine Interactions, Uppsala, p.254 (1974)

29) N. Brauer, F. Dimmling, Th. Kornrumpf, M. von Hartrott, K. Nishiyama and D. Riegel, Hyperfine Interactions 2 (Amsterdam: North Holland) p.248 (1976)

30) C. A. Shol l, J. Phys. F: Metal Phys., 4, 1556, (1974)

31) K.W. Lodge, J. Phys. F: Metal Phys., 6, 1989 (1976)

32) W. Schirmacher, Inst. Phys. Conf. Ser. No. 30 p.610 (1977)

33) M.H. Cohen and F. Reif, Solid State Physics vol. 5. ed. F. Seitz and D. Turnbull (Academic Press: New York, 1957) p.321

34) H.M. Foley, R.M. Sternheimer and D. Tycko, Phys. Rev., 93, 734 (1954)

35) R.E. Watson, A.C. Gossard and Y. Yafet, Phys. Rev., 140, A375 (1965)

36) R.E. Meyer, J. Phys. Chem., 65, 567 (1961)

37) G. Cartledge, R.L. Havill and J.M. Titman, J. Phys.F: Metal Phys., 6, 639 (1976)

38) F.A. Rossini and W.D. Knight, Phys. Rev., 178, 641 (1969)

39) F. Dimmling, M. von Hartrott, Th. Kornrumpf, K. Nishiyama and D. Riegel, Proc. 4th Int. Conf. on Hyperfine Interactions, U.S.A. (1977)

40) M. von Hartrott, K. Nishiyama, J. Rossbach, E. Weihreter and D. Quitman, J. Phys. F: Metal Phys., 7, 713 (1977)

41) D. Riegel, Phys. Scr., 11, 228 (1975)

42) W.W. Warren Jr., Phys. Rev., A10, 657 (1974)

CHAPTER THREE

Theory of Nuclear Quadrupole Relaxation in Liquid Metals

3.1 Introduction

It was shown in Chapter 1 that Sholl's theory (1), which treats the liquid metal as a collection of N mobile screened ions, leads to a quadrupolar relaxation rate given by

$$R_{1q} = \frac{3(2I+3)(eQ)^2}{4I^2(2I-1)\hbar^2} J(o) \qquad 3.1$$

with

$$J(m\omega_o) = \int_{-\infty}^{\infty} \langle F_m(t) F_m^*,(o)\rangle e^{-im\omega_o t} dt \qquad 3.2$$

$$F_m(t) = \sum_{i=1}^{N-1} u_m\left(\underline{r_i}(t)\right) \qquad 3.3$$

$$u_m(\underline{r_i}) = c v_2(r_i) Y_{2m}(\vartheta_i \varphi_i) \qquad 3.4$$

$$c = (1-\gamma_\infty)\left(\frac{4\pi}{45}\right)^{\frac{1}{2}} \qquad 3.5$$

and

$$v_2(r) = r\frac{d}{dr}\left(\frac{1}{r}\frac{dv(r)}{dr}\right) \qquad 3.6$$

The angular brackets denote an ensemble average, γ_∞ is the Sternheimer antishielding factor, Y_{2m} is a spherical harmonic normalised to unity and $v_2(r_i)$ is the radial electric field gradient function derived from the electric potential, $v(r)$, at the nucleus at the origin due to an ion at the position r_i, ϑ_i, φ_i.

It was also pointed out in Chapter 1 that the ensemble average contains two types of terms, i.e.,

$$\langle F_m(t)F_m^*,(o)\rangle = \left\langle \sum_{i=1}^{N-1} u_m\left(\underline{r}_i(t)\right) u_m^*,\left(\underline{r}_i(o)\right)\right\rangle + \left\langle \sum_{i,j(i\neq j)}^{N-1} u_m\left(\underline{r}_i(t)\right) u_m^*,\left(\underline{r}_j(o)\right)\right\rangle \qquad 3.7$$

The first term on the right-hand side of 3.7, called the pair term, describes the correlations of the electric field gradient at the nucleus at the origin due to the same ion at two different times. In the second term, the triplet term, the gradients at the two times are from different ions. These ionic configurations are shown in Figure 3.1.

The ensemble average may also be written as

$$\langle F_m(t)F_m^*,(o)\rangle = \iint u_m(\underline{r}_o)u_m^*,(\underline{r}_1)P(\underline{r}_o,0;\underline{r}_1,t)\underline{dr}_o\ \underline{dr}_1 \qquad 3.8$$

where P is the probability of finding a pair of ions within $\underline{r}_o + \underline{dr}_o$ of each other and the same pair or another pair within $\underline{r}_1 + \underline{dr}_1$ of each other at a time t later. The origin of $\underline{r}_o$ and $\underline{r}_1$ is fixed on the same ion throughout the motion (figure 3.2)

If, for the moment, the screened ion model is assumed to be correct, the problem becomes one of evaluating the joint probability function, P, and the radial electric field gradient $v_2(r)$. An exact expression for P has yet to be discovered and consequently an approximate form must be used. The simplest approximation for the pair terms, i.e. for the self-part, P_s, of the joint probability function, is to write P_s as the convolution of two van Hove functions, i.e.

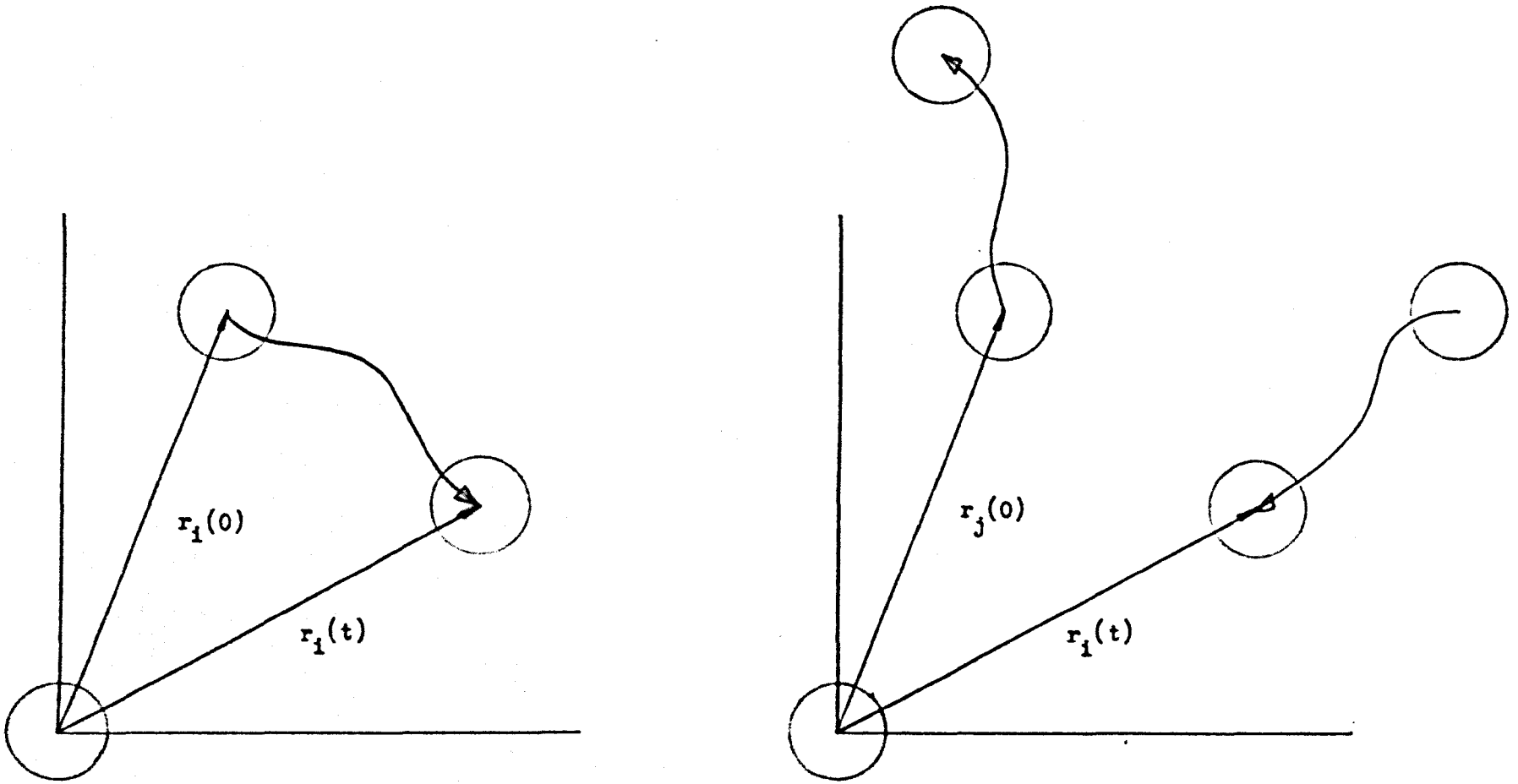

Figure 3.1 Schematic Representation of the Self and Triplet Terms in Equation 3.7.

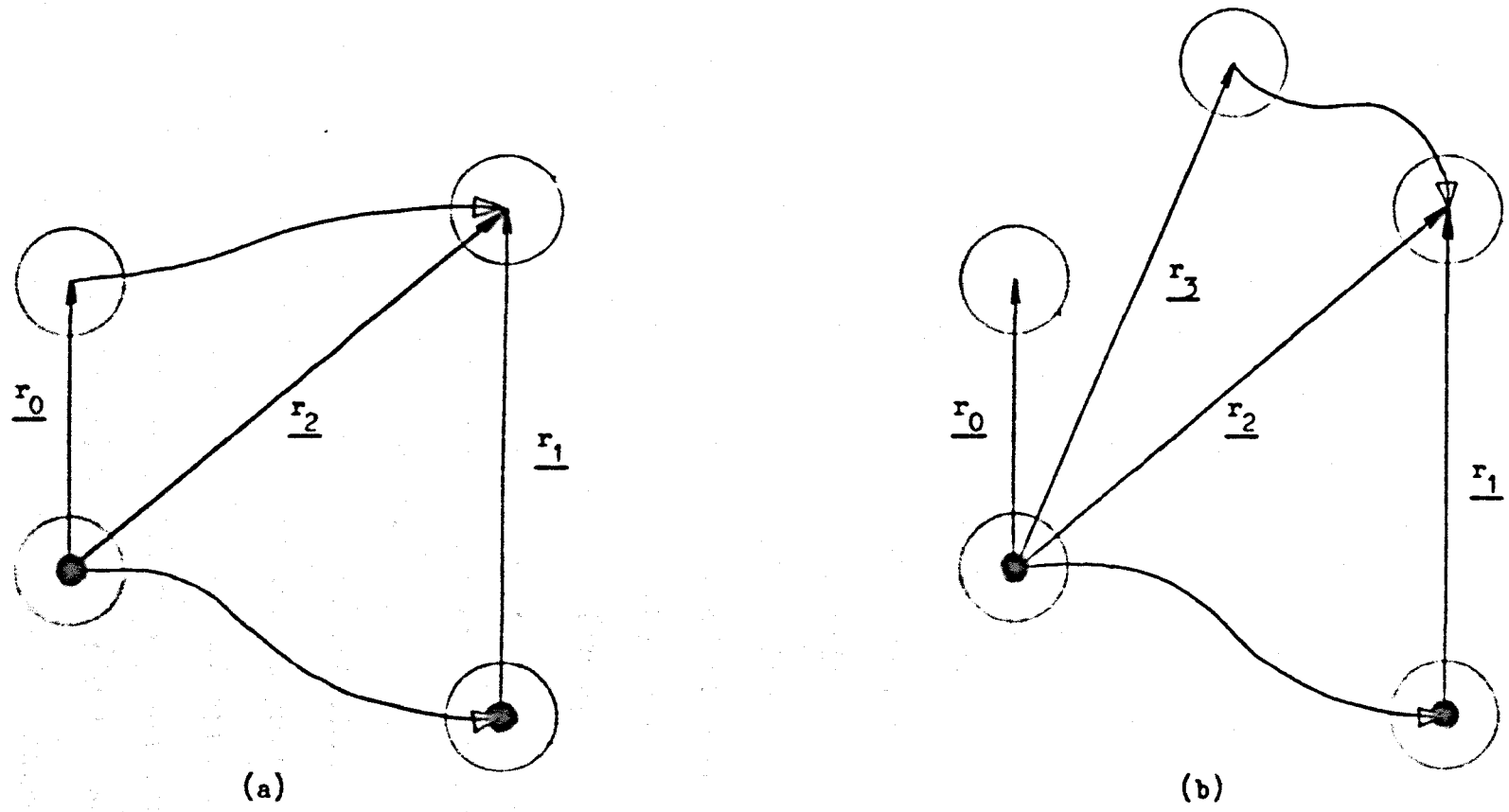

Figure 3.2 Schematic representation of the relative motions of ions described by the probability function P. The ion at the origin has a solid circle at the centre. (a) represents the pair term and (b) the triplet term.

$$P_s = \rho g(r_o) \int G_s(\underline{r_2}-\underline{r_o},t) G_s(\underline{r_2}-\underline{r_1},t) d\underline{r_2} \qquad 3.9$$

where the initial probability of finding the pair $\underline{r_o}$ apart is given by the pair distribution function $g(r_o)$ and the atomic density ρ. The subsequent motion of each ion is represented by the self-part, $G_s(\underline{r},t)$, of a van Hove correlation function, $G(\underline{r},t)$, defined by

$$G(\underline{r},t) = G_d(\underline{r},t) + G_s(\underline{r},t) \qquad 3.10$$

The trouble with this approximation is that it does not have the correct symmetry with respect to the interchange of $\underline{r_o}$ and $\underline{r_1}$ (2). Furthermore, it does not take into account any correlation in the motion of the two particles during the interval t, i.e. the convolution implies independent motion of the ions. From a computational point of view the latter difficulty results in the integral in the expression 3.8 over the variable r_1 having no cut off for $r_1 = o$ and, consequently, an infinitely large value. This result is equivalent to the physical condition that the two particles occupy the same position at time t.

Torrey (3) sought to overcome both difficulties by arbitrarily restricting r_o and r_1 to have magnitudes greater than a where a was some nearest distance of approach of the ions and $g(r_o)$ was taken as unity for $r_o > a$ and zero for $r_o < a$. Oppenheim and Bloom (4) working from the equations of motion of particles in a classical liquid arrived, with certain plausible approximations, at the result

$$P_s = \rho g^{\frac{1}{2}}(r_o) g^{\frac{1}{2}}(r_1) \int G_s(\underline{r_2}-\underline{r_o},t) G_s(\underline{r_2}-\underline{r_1},t) d\underline{r_2} \qquad 3.11$$

which satisfactorily disposes of the symmetry problem and also overcomes the difficulty associated with the zero value of r_1. However, the original equations of motion from which they worked are only valid in the hydrodynamic limit of $G_s(\underline{r},t)$ where it is a solution of the diffusion equation. Since this approach gives R_{1q} proportional to D^{-1} (5) the Oppenheim and Bloom solution does not appear to be a suitable starting point from which to explain the present data. Neither Torrey, nor Oppenheim and Bloom give the triplet term.

Warren (6) and Sholl (5) have suggested that both the pair and triplet terms may be contained in the expression

$$P = \rho g(r_o) g(r_1) \int_0^\infty G_s(\underline{r_2}-\underline{r_1},t) G(\underline{r_2}-\underline{r_o},t) d\underline{r_2} \qquad 3.12$$

Here the pair term is given by the self part, $G_s(\underline{r_2}-\underline{r_o},t)$ of the van Hove function $G(\underline{r_2}-\underline{r_o},t)$ and the triplet term by its distinct part, $G_d(\underline{r_2}-\underline{r_o},t)$. The correlations in the motion, neglected in the convolution, are supposed to be taken into account in the static term, $g(r_1)$.

Unfortunately equation 3.12 does not encompass the correct balance of pair and triplet components at time $t = o$ (5). At $t = o$, 3.12 gives

$$P = \rho g(r_o) g(r_1)\, \delta(\underline{r_o}-\underline{r_1}) + \rho^2 g(r_o) g(r_1) g(|\underline{r_o}-\underline{r_1}|) \qquad 3.13$$

whereas the exact form of P at t = o is,

$$P = \rho g(r_o)\delta(\underline{r_o}-\underline{r_1})+\rho^{(3)}(\underline{r_o},\underline{r_1}) \qquad 3.14$$

Thus the triplet term is satisfied in the superposition approximation, where the static three particle distribution function, $\rho^{(3)}$, is given by

$$\rho^{(3)}(\underline{r_o},\underline{r_1}) = \rho^2 g(r_o)g(r_1)g(|\underline{r_o}-\underline{r_1}|) \qquad 3.15$$

but the pair term is clearly overestimated by a factor g(r). Sholl (5) attempted to correct for this discrepancy by using the Oppenheim and Bloom expression for the pair term and equation 3.12 with G_d instead of G for the triplet term but this resulted in a negative value for R_{1q}.

Equation 3.12 for P leads to the result

$$R_{1q} = 2\beta\int_0^\infty q^2 I^2(q)dq\int_{-\infty}^{\infty}S(q,\omega)S_s(q,\omega)d\omega \qquad 3.16$$

where $$\beta = \frac{2n(2I+3)}{15I^2(2I-1)}\left[\frac{eQ(1-\gamma_\infty)}{\hbar}\right]^2\rho \qquad 3.17$$

and $$I(q) = \int_0^\infty v_2(r)r^2 g(r)j_2(qr)dr \qquad 3.18$$

which has been used in a number of calculations. The essential features of equation 3.16 are, firstly, the integral over I(q) is a series of positive peaks in k space, their spacing being determined by the small r cut off in g(r) and, secondly, the integral over the dynamic structure factors is very approximately equal to $\frac{1}{2}S(q,o)$.

Since S(q,o) is zero at small q the first peak of $I^2(q)$ does not enter the final computation (5). According to Sholl (5) and Warren (6) the main contribution to the integral comes from q values near the principal peak in S(q). Thus the variation of R_{1q} with temperature appears to be primarily dependent on the behaviour of S(q,o) near the principal peak and this is not well known.

As outlined in Chapter 1, Warren (6) chose to use the theoretical model for S(q,o) given by Cocking and Egelstaff (7). According to this model S(q,o) is given by

$$S(q,o) = \frac{N_{12}}{\pi}\left[\frac{M}{k_B T}\right]^{\frac{1}{2}}\left[\frac{S(q)}{q}\right]^{3/2} \qquad 3.19$$

where M is the atomic mass and N_{12} is a parameter determined by fitting the expression to neutron diffraction data. The term $T^{-\frac{1}{2}}$ appears explicitly in this expression and, since this is the principal temperature dependent term, Warren obtained essentially the correct variation of R_{1q} with temperature in his calculations on liquid Ga. Similar calculations by Halder (8) which included a more recent form of $v_2(r)$ (9) adopted the same model for S(q,o) and arrived at somewhat similar dependences on temperature for In, Hg and Ga.

In contrast Sholl (5) has argued, on the basis of the empirical expression for $S_s(q,\omega)$ given by Egelstaff and Schofield (10) (and given in equations 1.27 and 1.28 in Chapter 1), that S(q,o) near the principal peak is approximately proportional to D^{-1} and consequently the predicted

variation of R_{1q} with temperature is as T^{-2}.

The temperature dependence of $S(q,\omega)$ is generally not well known. However, a few measurements have been made at various temperatures for Ga. (11) (12) (13) (14). The results from the various investigations are not entirely consistent. Gläser et al (12) (see also Copley and Lovesay (15)) have measured $S(q,\omega)$ at 305°K and 1253°K. They find that, near the principal peak of $S(q)$, $S(q,o)$ is reduced by a factor of more than 10 between the lower and higher temperatures, while the width in ω increases by about 5. Thus the integral

$$\int_{-\infty}^{\infty} S^2(q,\omega)d\omega$$

decreases by a factor of about 20. This is approximately proportional to T^{-2}.

Now in the same region of k-space the data of Page et al (14), taken over a much smaller range of temperature, may be interpreted as follows. The static structure factor, $S(q)$, given by

$$S(q) = \int_{-\infty}^{\infty} S(q,\omega)d\omega \qquad 3.20$$

is found to be almost independent of temperature and the frequency width of the Lorentzian quasi-elastic peak increases approximately as $T^{3/2}$. Thus $S(q,o)$ must be approximately proportional to $T^{-3/2}$. Since, for a Lorentzian,

$$\int_{-\infty}^{\infty} S^2(q,\omega)d\omega = \tfrac{1}{2}S(q,o) \qquad 3.21$$

this integral must decrease at the rate $T^{-3/2}$ also. This is a rather weaker dependence on temperature than that given by the data of Gläser et al but it appears to confirm that the rate of decrease of $S(q,o)$ is likely to be much faster near the principal peak than is implied by the expression used by Warren and Halder.

$S_s(q,\omega)$ cannot be measured for Ga but the theoretical work of Barker et al (13) points to a function with a Lorentzian dependence on ω with a width slightly greater than that of $S(q,\omega)$ and a dependence on temperature (over a very narrow range) of approximately T^{-2} for $S_s(q,o)$. Barker et al also observed that the Egelstaff and Schofield form for $S_s(q,\omega)$ could be used to interpret the experimental data for $S(q,\omega)$ through the Vineyard approximation (16),

$$S(q,\omega) = S(q)S_s(q,\omega) \qquad 3.22$$

For the remaining liquid metals of Figure 2.9 one must use the Egelstaff and Schofield expression for $S_s(q,\omega)$. As Sholl (5) has pointed out the straightforward application of this expression coupled with the Vineyard approximation is likely to lead to the prediction that R_{1q} varies with temperature as D^{-1}. The Egelstaff and Schofield expression gives the correct form for $S_s(q,\omega)$ at small and large q, i.e.,

$$S_s(q,\omega) \rightarrow \frac{1}{\pi} \frac{Dq^2}{\omega^2+(Dq^2)^2}, q^2 \ll \frac{1}{m\beta D^2} \qquad 3.23$$

and

$$S_s(q,\omega) \rightarrow \left(\frac{m\beta}{2nq^2}\right)^{\frac{1}{2}} \exp\left(\frac{-m\beta\omega^2}{2q^2}\right), \quad q^2 \gg \frac{1}{m\beta D^2} \qquad 3.24$$

where $\beta = k_B T$. How reliably the model describes the transition between these limits is difficult to assess. Some aspects of the dynamics of liquids have been interpreted successfully by it.

In particular the self-part of the intermediate scattering function

$$F_s(q,t) = \int_{-\infty}^{\infty} d\omega e^{i\omega t} S(q,\omega) \qquad 3.25$$

for liquid argon near the principal peak in S(q) as obtained from molecular dynamics calculations and the Egelstaff - Schofield model have been found to be consistent with each other (15).

To sum up, the failings of the Sholl and Warren calculations are

(i) R_{1q} is predicted to vary with temperature approximately as D^{-1}. This is very different from the $T^{-\frac{1}{2}}$ variation shown by the experimental data.

(ii) The correct balance between the pair and triplet contributions is not maintained and, when this is corrected for, negative values of R_{1q} are obtained.

It is arguable that (i) and (ii) are related. The pair term contains a considerable contribution from small q values below the principal peak as well as contributions at higher q. The main contribution to the triplet term comes almost

entirely from below the principal peak and is negative. Thus, if the pair term is overestimated, as it is in expression 3.12., then there will be a substantial spurious contribution to the predicted R_{1q} which comes from that region of k space where the D^{-1} temperature variation is to be found.

With these points in mind it was argued that a modified form of the theory should be sought which would better preserve the balance of the pair and triplet terms and would therefore give an improved prediction of the temperature variation of R_{1q}.

3.2 Derivation of the Theoretical Expression for R_{1q}

We note first that the quantity which determines the rate of change of the z-magnetisation of the spins under the condition of extreme narrowing depends only on the perturbing Hamiltonian at time t = o.(17). Indeed we can write

$$R_1 \sim \left\langle |\mathcal{H}_1(o)|^2 \right\rangle \tau_c \qquad 3.26$$

where τ_c is some "correlation time" in which the correlation function of the random Hamiltonian has become small with respect to $1/\omega_o$. We do not follow this method of calculation here but merely make the point that the correct initial value of the field gradient is important.

In the manner of Sholl and Warren we write

$$P_s = \rho g(r_o) f(r_o, r_1) \int_0^\infty G_s(\underline{r_2}-\underline{r_1}, t) G_s(\underline{r_2}-\underline{r_o}, t) \underline{dr_2} \qquad 3.27$$

where the initial value is given by $\rho g(r_o)\delta(r_o-r_1)$ and the

assumption has been made that the interdependence of the motion of the two particles between t = o and t = t can be represented by some static function dependent only on the initial and final relative positions. The only certain knowledge we have of $f(r_o,r_1)$ is that it must be zero for r_1 less than the nearest distance of approach of the ions. Thus the simplest possible form of $f(r_o,r_1)$ which gives the correct initial value is that it takes the value unity when r_1 is greater than the cut-off in g(r) and is zero for r_1 less than this. Thus we write for the pair terms,

$$\langle F_m(t)F_m^*,(o)\rangle_{pair} = \iint \underline{dr_o}\ \underline{dr_1}\ u_m(\underline{r_o})u_m^*,(\underline{r_1})\rho g(r_o)f(r_1)$$

$$x \int \underline{dr_2} G_s(\underline{r_2}-\underline{r_1},t)G_s(\underline{r_2}-\underline{r_o},t) \qquad 3.28$$

and the pair component of $J(m\omega_o)$ becomes,

$$J_p(m\omega_o) = \rho\int dt \iint u_m(\underline{r_o})u_m^*,(\underline{r_1})g(r_o)f(r_1)\underline{dr_o}\ \underline{dr_1}$$

$$x \int G_s(\underline{r_2}-\underline{r_1},t)G_s(\underline{r_2}-\underline{r_o},t)\underline{dr_2} \qquad 3.29$$

As Sholl (5) has pointed out the integrals may be partially performed by substituting the Fourier transforms of the van Hove functions. These are

$$G_s(\underline{r_2}-\underline{r_o},t) = \left(\frac{1}{2\pi}\right)^3 \int d\omega_1 \int \underline{dq_1} S_s(\underline{q_1},\omega_1)e^{-i\left[\underline{q_1}.(\underline{r_2}-\underline{r_o})-\omega_1 t\right]}$$

3.30

and a similar expression for $G_s(\underline{r}_2-\underline{r}_1,t)$. The substitution gives

$$J_p(m\omega_o) = \rho\int e^{i(\omega_1+\omega_2-m\omega_o)t}dt$$

$$x \iint u_m(\underline{r}_o)u_m^*,(\underline{r}_1)g(r_o)f(r_o)d\underline{r}_o\ d\underline{r}_1$$

$$x \iint d\omega_1 d\omega_2 \iint d\underline{q}_1\ d\underline{q}_2 S_s(\underline{q}_1,\omega_1)S_s(\underline{q}_2,\omega_2)$$

$$x\ e^{i(\underline{q}_1\cdot\underline{r}_1+\underline{q}_2\cdot\underline{r}_o)} \int e^{-i(\underline{q}_1\cdot\underline{r}_2+\underline{q}_2\cdot\underline{r}_2)}d\underline{r}_2 \qquad 3.31$$

The integrals over t and r_2 give δ functions from which it is possible to reduce the double integrals in $\omega_1\omega_2$ and $q_1\ q_2$ to single integrals in ω and q with the result that

$$J_p(m\omega_o) = \left(\frac{1}{2\pi}\right)^2 \rho \iint u_m(\underline{r}_o)u_m^*,(\underline{r}_1)d\underline{r}_o\ d\underline{r}_1 g(r_o)f(r_o)$$

$$x \int d\omega \int d\underline{q} S_s(\underline{q},\omega)S_s(\underline{q},\omega-m\omega_o)e^{i\underline{q}\cdot(\underline{r}_o-\underline{r}_1)} \qquad 3.32$$

The assumption that the relaxation may be described by a single rate as implied by equation 1.3 in Chapter 1 requires $J(o) = J(\omega_o) = J(2\omega_o)$. This extreme narrowing condition is satisfield if $m\omega_o$ is much smaller than the frequency width of the dynamic stucture factor. This width is typically $10^{12}s^{-1}$ in liquid metals compared to $\omega_o \sim 10^8 s^{-1}$ so we may make the approximation that $S_s(q,\omega)$ and $S_s(q,\omega-m\omega_o)$ are coincident and $J_p(m\omega_o)$ is independent of the index m.

Also $e^{i\underline{q}.\underline{r}_o}$ and $e^{-i\underline{q}.\underline{r}_1}$ may be expanded in the form

$$e^{iqr} = 4\pi\sum_{lm}(i)^l Y^*_{lm}(\theta_r\varphi_r)Y_{lm}(\theta_q\varphi_q)j_l(qr) \qquad 3.33$$

and the angular integrals performed. Since $u(\underline{r}_o)$ and $u(\underline{r}_1)$ may be written in terms of spherical harmonics with $l = 2$ the orthogonality leads to a reduction in the number of terms in the summation. The final result is

$$J_p(m\omega_o) = 4\pi c^2\rho\int_0^\infty g(r_o)v_2(r_o)r_o^2 j_2(qr_o)dr_o$$
$$\times \int_0^\infty f(r_1)v_2(r_1)r_1^2 j_2(qr_1)dr_1 \int_0^\infty q^2 dq \int_{-\infty}^{\infty} S_s^2(q,\omega)d\omega \qquad 3.34$$

The triplet terms may be treated in a similar fashion. They may be written,

$$\langle F_m(t)F^*_m,(o)\rangle_{\text{triplet}} = \iint \underline{dr}_o\ \underline{dr}_1 u_m(\underline{r}_o)u^*_m,(\underline{r}_1)P_d(\underline{r}_o,o;\underline{r}_1,t) \qquad 3.35$$

where P_d is the probability that there is an atom within $\underline{dr}_o$ at $\underline{r}_o$ from the relaxing nucleus at $t = o$ and that there will be a different atom within $\underline{dr}_1$ at $\underline{r}_1$ at $t = t$. In Figure 3.2(b) there are atoms at $\underline{r}_o$ and $\underline{r}_3$ with respect to the atom at the origin. Thus the average over the initial positions is given by the triplet distribution $\rho^{(3)}(r_o,r_3)$. In the subsequent motion the atom at $\underline{r}_o$ moves to some other point in the liquid while the atom at $\underline{r}_3$ moves to position

$\underline{r_1}$ with respect to the atom which was at the origin at t = o and is now also in a different position. All of these motions are taken to be independent of each other and the final position of the atom originally at $\underline{r_o}$ is assumed not to influence the motion. Only the correlation of the atom originally at $\underline{r_3}$ and finally at $\underline{r_1}$ and the atom at the origin is taken into account through the term $f(r_1)$ as in the pair term. Thus,

$$P_d = f(r_1) \iint \rho^{(3)}(\underline{r_o},\underline{r_3})G_s(\underline{r_2}-\underline{r_3},t)G_s(\underline{r_2}-\underline{r_1},t)\underline{dr_3}\ \underline{dr_2} \qquad 3.36$$

From this the triplet part of J(o) is given by

$$J_t(o) = \int dt \int \underline{dr_1} f(r_1)u_m^*,(\underline{r_1}) \int \underline{dr_o} u_m(\underline{r_o})$$

$$\times \iint \rho^{(3)}(\underline{r_o},\underline{r_3})G_s(\underline{r_2}-\underline{r_3},t)G_s(\underline{r_2}-\underline{r_o},t)\underline{dr_2}\ \underline{dr_3} \qquad 3.37$$

As in the case of the pair terms the angular integrals may be performed if the van Hove functions are replaced by their Fourier transforms.

The angular part of $\rho^{(3)}(\underline{r_o},\underline{r_3})$ may be explicitly displayed by means of the exact relation (18)

$$\rho^{(3)}(\underline{r_o},\underline{r_3}) = \rho^2 \sum_l g_l(r_o,r_3)P_l(\cos\theta) \qquad 3.38$$

where ϑ is the angle between $\underline{r_o}$ and $\underline{r_3}$, $P_1(\cos\vartheta)$ is the Legendre function and $g_1(r_o,r_3)$ is a function of the radial magnitudes of the position vectors. As will be shown later the $l = 2$ symmetry of the quadrupole interaction picks out the $l = 2$ term in equation 3.38 and the measurement of the quadrupole relaxation rate appears to be the only experiment which depends on this term. Thus this expression is of no immediate use in calculating R_{1q} since the form of $g_2(r_o,r_3)$ is not known. The alternative, but approximate form, is the superposition approximation i.e.,

$$\rho^{(3)}(r_o,r_3) = \rho^2 g(r_o)g(r_3)g(r_{o3}) \qquad 3.39$$

where $g(r_{o3}) = g(|r_o-r_3|)$ and $r_{o3} = r_o^2+r_3^2-2r_or_3\cos\vartheta$

Within the superposition approximation $J_t(o)$ may be written

$$J_t(o) = \rho^2 \int dt \int \underline{dr_1} f(r_1)u^*(\underline{r_1}) \int \underline{dr_o} g(r_o)u(\underline{r_o})$$

$$\times \iint g(r_3)g(r_{o3})G_s(\underline{r_2}-\underline{r_3},t)G_s(\underline{r_2}-\underline{r_o},t)\underline{dr_2}\ \underline{dr_3}$$

The integration then proceeds as for the pair terms after substitution of the Fourier transforms of the van Hove functions. The expansion of the resulting exponential is then made and the integration over the angular parts of q performed. The result is

$$J_t(o) = \frac{16\pi^2\rho^2c^2}{(2\pi)^2} \int dr_1 r_1^2 f(r_1)v_2(r_1)j_2(qr_1)$$

$$\times \int q^2dq \int d\omega S_s^2(q,\omega) \int v_2(r_o)g(r_o)g(r_3)g(r_{o3})$$

$$\times Y_{2m}(\vartheta_o\varphi_o)Y^*_{2m}(\vartheta_3\varphi_3)j_2(qr_3)\underline{dr_o}\ \underline{dr_3} \qquad 3.40$$

Now the angular part of the final integral is

$$\int Y_{2m}(\theta_o\varphi_o)\sin\theta_o d\varphi_o d\theta_o \int g(r_{o3})Y^*_{2m}(\theta_3\varphi_3)\sin\theta_3 d\theta_3 d\varphi_3 \qquad 3.41$$

This angular integral may be solved by the use of well-known relationships between the spherical harmonics (19) and, according to Sholl (5) the result is

$$2\pi\int_0^{\pi} g(r_{o3})P_2(\cos\theta)\sin\theta d\theta$$

Thus finally,

$$J_t(o) = 8\pi\rho^2c^2\int_0^{\infty} dr_1 r_1^2 v_2(r_1)f(r_1)j_2(qr_1)$$

$$\times \int_{-\infty}^{\infty} q^2dq \int_0^{\infty} d\omega S_s^2(q,\omega)\int_0^{\infty} dr_o v_2(r_o)g(r_o)r_o^2$$

$$\times \int_0^{\infty} dr_3 g(r_3)r_3^2 j_2(qr_3)\int_{-1}^{1} g(r_{o3})P_2(z)dz \qquad 3.42$$

where $z = \cos\theta$.

Since the only significant angular term in $\rho^{(3)}(\underline{r_o},\underline{r_3})$ is $P_2(\cos\theta)$ then $J_t(o)$ may be re-written to include the exact form of $\rho^{(3)}(\underline{r_o},\underline{r_3})$ in the following way.

Firstly the superposition approximation is replaced by the exact form by putting

$$g(r_o)g(r_3)g(r_{o3}) = \sum_1 g_1(r_o r_3)P_1(\cos\theta) \qquad 3.43$$

Thus $g(r_{o3})$ is no longer the pair distribution function but is now defined by the equation

$$g(r_{o3}) = \frac{1}{g(r_o)g(r_3)} \sum_1 g_1(r_o r_3) P_1(\cos\theta) \qquad 3.44$$

The right-hand side of equation 3.44 is then substituted into the last integral in the expression 3.42 for $J_t(o)$ i.e.

$$\int_0^\pi g(r_{o3}) P_2(\cos\theta)\sin\theta d\theta = \frac{1}{g(r_o)g(r_3)} \int_0^\pi \sum_1 g_1(r_o r_3)$$

$$x \quad P_1(\cos\theta)\ P_2(\cos\theta)\sin\theta d\theta \qquad 3.45$$

Because of the orthogonality of the Legendre function the only non-zero integral is

$$\int P_2(\cos\theta) P_2(\cos\theta)\sin\theta d\theta = \frac{2}{5} \qquad 3.46$$

Thus $J_t(o)$ becomes for the exact $\rho^{(3)}(r_o r_3)$

$$J_t(o) = \frac{16\pi\rho^2 c^2}{5} \int_0^\infty dr_1 v_2(r_1) r_1^2 f(r_1) j_2(qr_1) \int_{-\infty}^\infty q^2 dq$$

$$x \int_0^\infty d\omega S_s^2(q,\omega) \int_0^\infty dr_o v_2(r_o) r_o^2 \int_0^\infty dr_3 g_2(r_o r_3) r_3^2 j_2(qr_3)$$

3.47

The same result may be obtained directly by substituting 3.38 into 3.37 and integrating.

The quadrupole relaxation rate may therefore be written in the superposition approximation as

$$R_{1q} = 2\delta \int_0^\infty q^2 \left[I_p(q) + 2\pi\rho I_t(q) \right] dq \int_{-\infty}^\infty S_s^2(q,\omega) d\omega \qquad 3.48$$

where

$$I_p(q) = \int_0^\infty f(r_1)v_2(r_1)r_1^2 j_2(qr_1)dr_1 \int_0^\infty g(r_o)v_2(r_o)r_o^2 j_2(qr_o)dr_o \qquad 3.49$$

$$I_t(q) = \int_0^\infty f(r_1)v_2(r_1)r_1^2 j_2(qr_1)dr_1 \int_0^\infty g(r_o)v_2(r_o)r_o^2 dr_o$$

$$\times \int_0^\infty g(r_3)r_3^2 j_2(qr_3)dr_3 \int_{-1}^{1} g(r_{o3})P_2(z)dz \qquad 3.50$$

and

$$\beta = \frac{2n(2I+3)\rho}{15I^2(2I-1)} \left[\frac{eQ(1-\gamma_{eff})}{\hbar}\right]^2 \qquad 3.51$$

When the exact form of $\rho^{(3)}(r_o r_3)$ is used $I_t(q)$ must be replaced by

$$I_t(q) = \frac{2}{5}\int_0^\infty dr_1 v_2(r_1)r_1^2 f(r_1) j_2(qr_1) \int_0^\infty dr_o r_o^2 v_2(r_o)$$

$$\times \int_0^\infty dr_3 g_2(r_o r_3)r_3^2 j_2(qr_3) \qquad 3.52$$

Equation 3.52 cannot, of course, be used in computation as the form of $g_2(r_o r_3)$ is not known.

3.3. Calculation of the Temperature Dependence of R_{1q}

The calculation may proceed only in the superposition approximation. The three basic quantities required are $v_2(r)$, $g(r)$, and $S_s(q,\omega)$. As we have already pointed out the last of these is most significantly dependent on temperature. Also since, for the metals of interest here,

very few measurements have been made which give the variation of $S_s(q,\omega)$ with temperature over the wide range of q-values required, we must use either the Egelstaff and Schofield empirical expression or a theoretical model.

Of the latter, the most promising are based on the Mori technique, as explained by Copely and Lovesay (15). However, although an expression for $S_s(q,\omega)$ may be arrived at (15) it contains parameters which are not readily quantified. In contrast, the Egelstaff and Schofield formula is a closed expression for $S_s(q,\omega)$ which depends only on the atomic mass and self-diffusion coefficient apart from q, ω and the temperature. This expression, therefore, appears to be the only viable form of $S_s(q,\omega)$ for our purposes.

The Egelstaff and Schofield expression may be written as

$$nS_s(q,\omega) = ck^2D\left[\omega^2+(q^2D)^2\right]^{-\frac{1}{2}} \exp\,(cq^2D)K_1\left\{ c\left[\omega^2+(q^2D)^2\right]^{\frac{1}{2}}\right\} \qquad 3.53$$

where $c = mD/k_BT$ and K_1 is a modified Bessel function of the first kind whose asymptotic behaviour is such that, as indicated in equations 3.23 and 3.24, $S_s(q,\omega)$ has the correct limits at large and small q.

The integral that appears in the expression for R_{1q} is $\int S_s^{\,2}(q,\omega)d\omega$ and with $S_s(q,\omega)$ given by 3.53 this has been evaluated numerically by Sholl (5) to give, to within 1%,

$$\int S_s^2(q,\omega)d\omega = \frac{Ce^x K_1(x)}{2n}\left[\frac{0.582+x\sqrt{2}}{0.582+x}\right] \qquad 3.54$$

where $x = cDK^2$ is a dimensionless parameter and $Ce^x K_1(x)$ is $nS_s(q,o)$. Thus our expression for R_{1q} may be written as

$$R_{1q} = \beta\int_0^\infty dq\ q^2\left[I_p(q)+2n\rho I_t(q)\right]S_s(q,o)\left[\frac{0.582+cDq^2\sqrt{2}}{0.582+cDq^2}\right] \qquad 3.55$$

The final term varies from 1 to $\sqrt{2}$ as q goes from zero to infinity and is not very sensitive to temperature. It indicates the departure of the Egelstaff and Schofield expression from the Lorentzian form of $S_s(q,\omega)$ for which

$$\int_{-\infty}^{\infty} S_s^2(q,\omega)d\omega = \tfrac{1}{2}S_s(q,o) \qquad 3.56$$

In the ideal gas limit $S_s(q,\omega)$ is Gaussian and then

$$\int_{-\infty}^{\infty} S_s^2(q,\omega)d\omega = \frac{1}{\sqrt{2}}S_s(q,o) \qquad 3.57$$

It is clear that R_{1q} as given by equation 3.55 will have the $T^{-\frac{1}{2}}$ variation characteristic of the ideal gas limit if $\left[I_p(q)+2n\rho I_t(q)\right]$ are such as to drive the significant part of the integral to large q values. An examination of $I_p(q)$, for example, immediately shows that this can only be the case if the spatial extent of the products $v_2(r_1)f(r_1)r_1^2$ and $v_2(r_o)g(r_o)r_o^2$ are small compared to the interatomic spacing a; the principal peak of the static

structure factor occuring near the wave vector $2\pi/a$.

According to Schirmacher (9) the electric field gradient around an ion in a liquid metal may be written as

$$u(r) = u_{ion}(r)+u_{cond}(r) \qquad 3.58$$

In his calculations the contribution from the ionic charges, u_{ion}, was assumed to derive from point charges at the ionic sites and the conduction electron contribution, u_{cond}, was calculated from pseudopotential theory. Using a local pseudopotential of the Ashcroft (20) empty core type the result for $v_2(r)$ is, in atomic units,

$$v_2(r) = 3Z\left[\frac{1}{r^3}+\frac{2}{3\pi}\int_0^\infty dq\ q^2 j_2(qr)\cos(qR_c)\left(\frac{1}{\varepsilon(q)}-1\right)\right] \qquad 3.59$$

where the dielectric constant, in the absence of exchange, is given by

$$\varepsilon(q) = 1+\frac{2k_F}{\pi q^2}\left[1+\left(\frac{1-\eta^2}{2\eta}\right)\ln\left|\frac{1+\eta}{1-\eta}\right|\right] \qquad 3.60$$

where $\eta = q/2k_F$, k_F being the value of the wave vector at the Fermi surface. R_c is an adjustable parameter.

The significant feature, of expression 3.59 is that the second term peaks in the neighbourhood of $r = a$ and is negative. At larger r it is of the order of $1/r^3$, but oscillates slightly. Thus, near to $r = a$, $v_2(r)$ falls very rapidly below $1/r^3$ and then executes small amplitude oscillations about zero. These general features are

illustrated in Figures 3.3 to 3.5 for Hg and Ga which were obtained using numerical integration to evaluate the second term.

In earlier calculations Schirmacher (9) and Halder (8) obtained similar results for Ga and In but found that the rapidly decreasing part of $v_2(r)$ came at $r < a$ and consequently only the slowly decaying oscillatory part of the field gradient was assumed to have any significance. However, the position and strength of the peak in $v_2(r)$ depends, albeit slightly, on the choice of R_c. Now R_c, and for that matter, the equivalent parameters of other model single ion potentials, are often chosen to fit the experimental values of the electron transport properties, for example, the resistivity. They are not related directly to the ion-core as measured by the interatomic spacing. It might be argued, therefore, that the appropriate value of R_c for the resistivity is not necessarily the best choice to give the electric field gradient. Halder and Schirmacher obtained their values of R_c from Cohen and Heine (21) and the resistivity was the principal experimental data used to determine R_c.

We have therefore investigated the effect of adjusting R_c and the results are shown Figures 3.3 to 3.5. Figure 3.3 shows the results obtained for Hg with $R_c = 0.91$ and 1.62. The lower value is considered to give the best fit to the resistivity data, but clearly the larger R_c gives a better

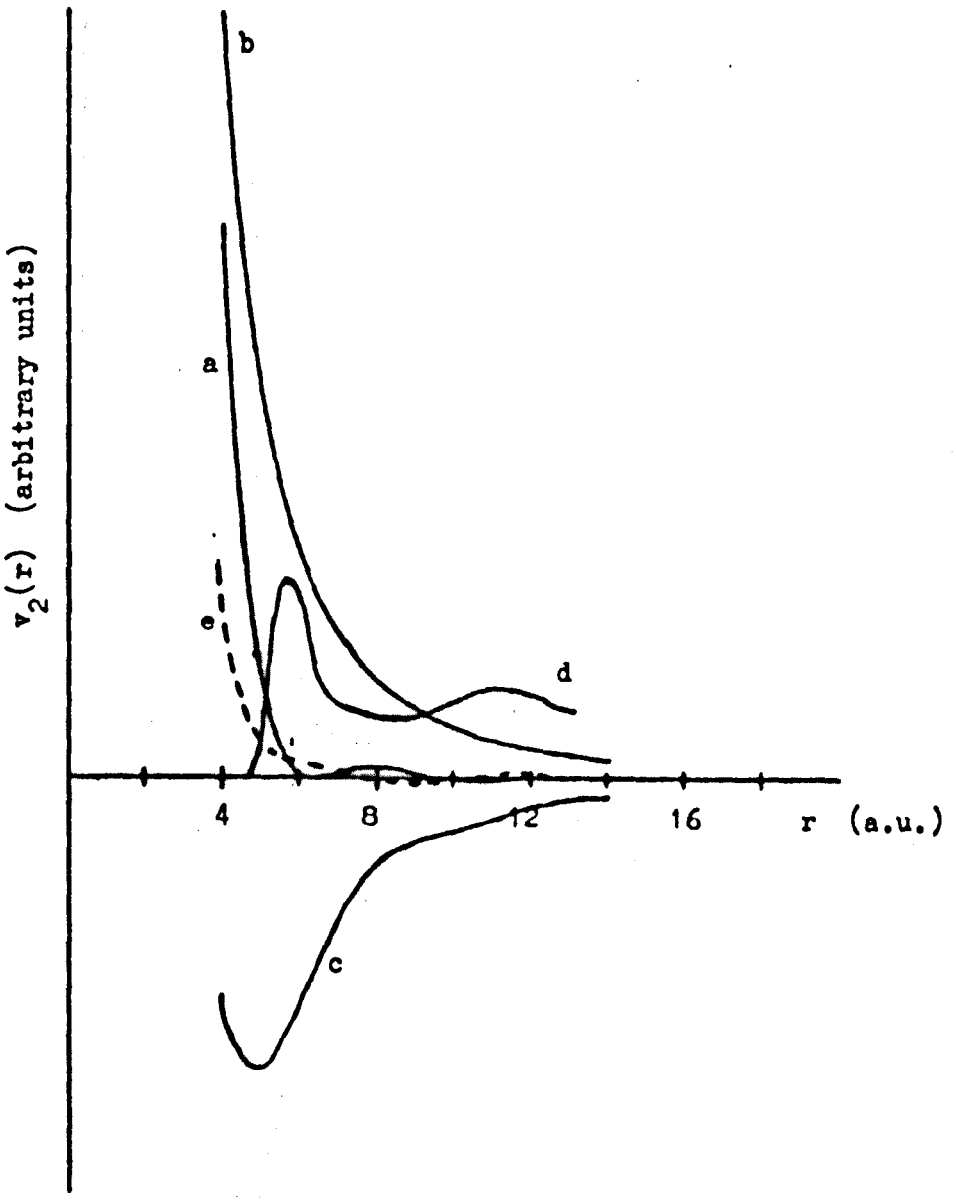

Figure 3.3 Plot of $v_2(r)$ against r for liquid mercury using the parameters k_F = 0.7231 a.u.$^{-1}$ and R_c = 1.62 a.u. Curve a represents $v_2(r)$, b represents $1/r^3$ and c represents the second term in the square brackets in expression 3.59. Curve d represents g(r) for liquid mercury. The dotted curve, e, represents $v_2(r)$ obtained with R_c = 0.91.

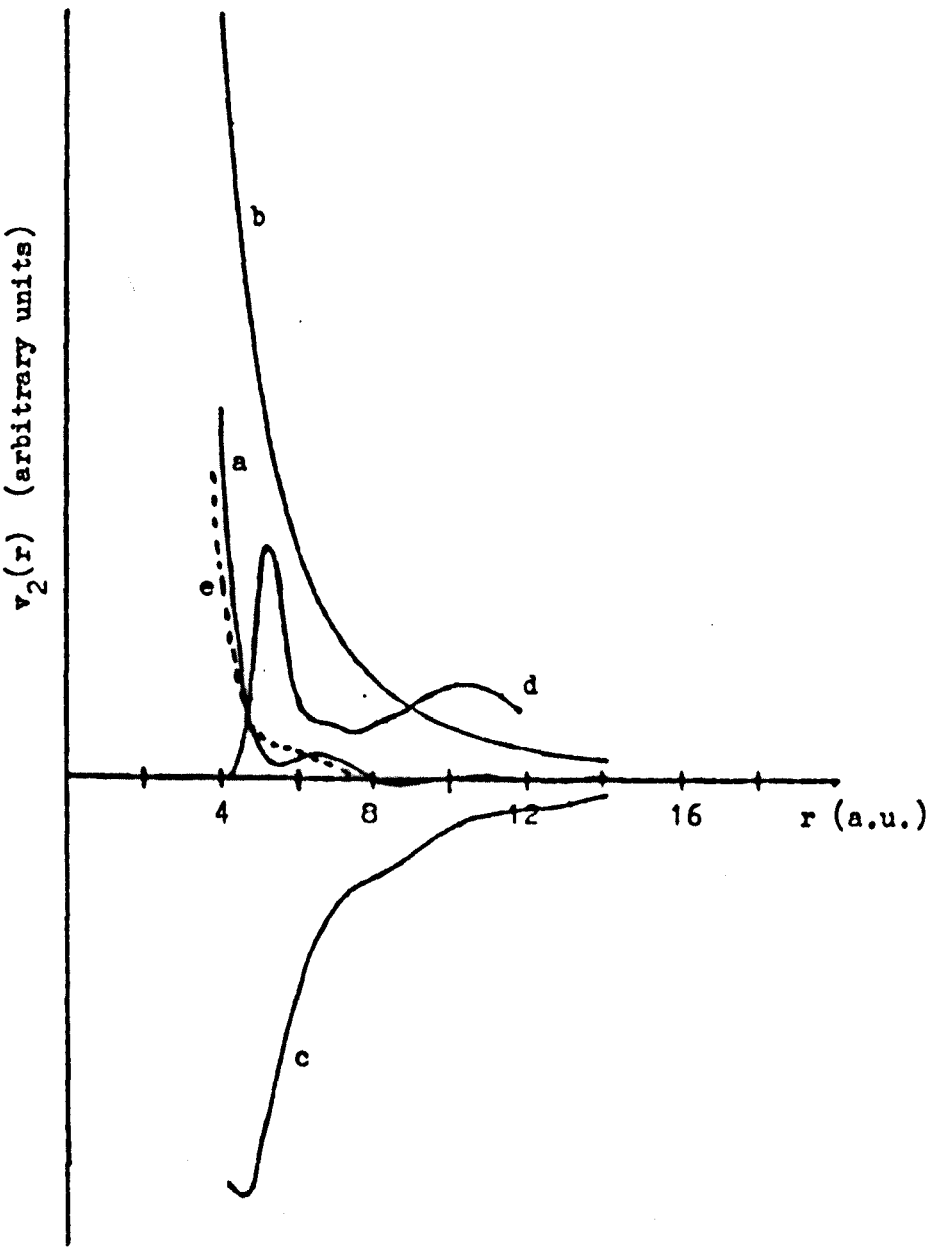

Figure 3.4 Plot of $v_2(r)$ against r for liquid mercury using $k_F = 0.7231$ a.u.$^{-1}$. Curve a represents $v_2(r)$ with $R_c = 1.5$, the dotted curve,e,represents $v_2(r)$ with $R_c = 1.05$. The rest of the notation is the same as in Figure 3.3.

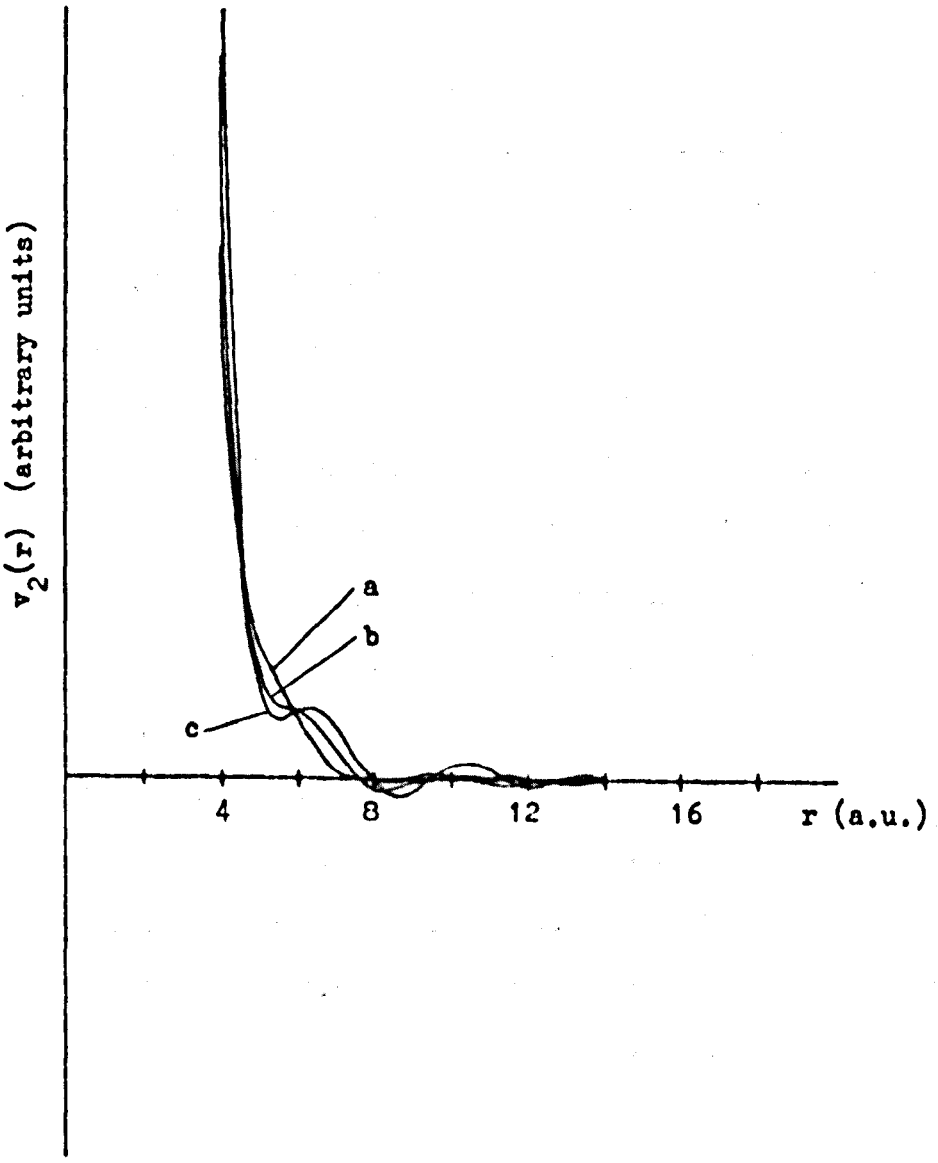

Figure 3.5 Plots of $v_2(r)$ against r for liquid Ga with $k_F = 0.8776$ a.u.$^{-1}$ and various values of R_c. For curve a $R_c = 0.84$, curve b, $R_c = 1.05$, curve c, $R_c = 1.26$.

overlap with g(r) for our purpose. In Figure 3.4 are shown the results obtained for Ga with R_c = 1.05 and 1.5. The former value fits the resistivity. It will be seen that for both values overlap occurs but this is not as marked as in the Hg case with R_c = 1.62.

Figure 3.5 shows how $v_2(r)$ changes for Ga when R_c takes the values 0.84, 1.05 and 1.26. The steep part of $v_2(r)$ does not change a great deal but rather the long range part diminishes as R_c increases. According to Schirmacher's calculations the inclusion of exchange terms in $\varepsilon(q)$ produces a further diminution.

It is found that the values of the ratio R_c/r_o for the metals of interest are found to lie between 0.23, the value corresponding to Ga with R_c = 1.05, and 0.33 which corresponds to Hg with R_c = 1.62. Therefore we expect the results for these metals to lie between the two limits illustrated.

Now the field gradient obtained in this way does not include the enhancement from the Sternheimer antishielding. Schirmacher has included this effect in his calculations. The deformation of the ion core by the electric field gradient which produces the antishielding was obtained by a variational method. The general effect was to increase $v_2(r)$ by an order of magnitude and to bring the steeply varying part to slightly larger values of r. However, the calculation of the Sternheimer enhancement by Lodge (22)

seems to indicate that the calculations may not be quite as straight-forward as Schirmacher suggests.

Furthermore, it is well known that for heavy metals the pseudopotential is non-local. It would, however, be a major undertaking to attempt calculations of $v_2(r)$ using a full non-local pseudopotential.

Bearing these problems in mind we shall proceed by considering $v_2(r)$ to be essentially of the form given by the local theory described above and assume that it falls rapidly to zero just beyond the cut-off in $g(r)$. The product $v_2(r)$ $g(r)$ r^2 will then be a sharply peaked function whose width is much less than the interatomic spacing. This product will then, in fact, be similar to that obtained by Sholl (5) from the ion-ion potential although, of course, as Schirmacher has pointed out, the ion-ion potential should not be used to calculate the field gradient. Since we do not have a definitive form for this product, we suppose that the interaction can be represented by a delta function, i.e.,

$$v_2(r)g(r)r^2 = \delta(b) \qquad 3.61$$

where $b \geq a$. We then integrate over all delta functions between $b = a$ and $1+\Delta a$, taking the profile of our integration to be a right-angled triangle of base Δa. The parameter Δ we will call the range of the interaction and the triangle profile represents an attempt to recreate the profile of $v_2(r)g(r)r^2$ as given by Sholl (5). We regard the range as

an adjustable parameter. The corresponding product $f(r_1)$ $v_2(r_1)r_1^2$ may be treated in the same way. If we formulate the problem in this way g(r) does not enter into the two particle terms directly but merely helps to determine the strength of the δ functions.

Details of the calculations are given in Appendix II. However, the general procedure adopted is given below together with the significant features of the results.

The calculation proceeds first with the evaluation of $I_p(q)$ and $I_t(q)$. For a δ function interaction at a the pair term is just

$$q^2 I_p(q) = q^2 j_2^2(qa) \qquad 3.62$$

which does not converge. The convergence is introduced by the allowed range of Δ. Typical results for two different ranges are shown in Figures 3.6 and 3.7. where also it can be seen that $I_p(q)$ is a series of positive peaks in k-space.

In order to evaluate $I_t(q)$ it is first necessary to calculate the final integral in equation 3.50. The form of this integral multiplied by $2\pi\rho g(r)r^2$ is shown in Figure 3.8. Calculations were made for Hg and for a hard sphere liquid with a packing fraction $\eta = 0.455$. Computing time was reduced by using simulated forms of the appropriate pair distribution functions as indicated in the Appendix. The significant features of this integral are the large negative contribution and the extent in real space which is of the order of the

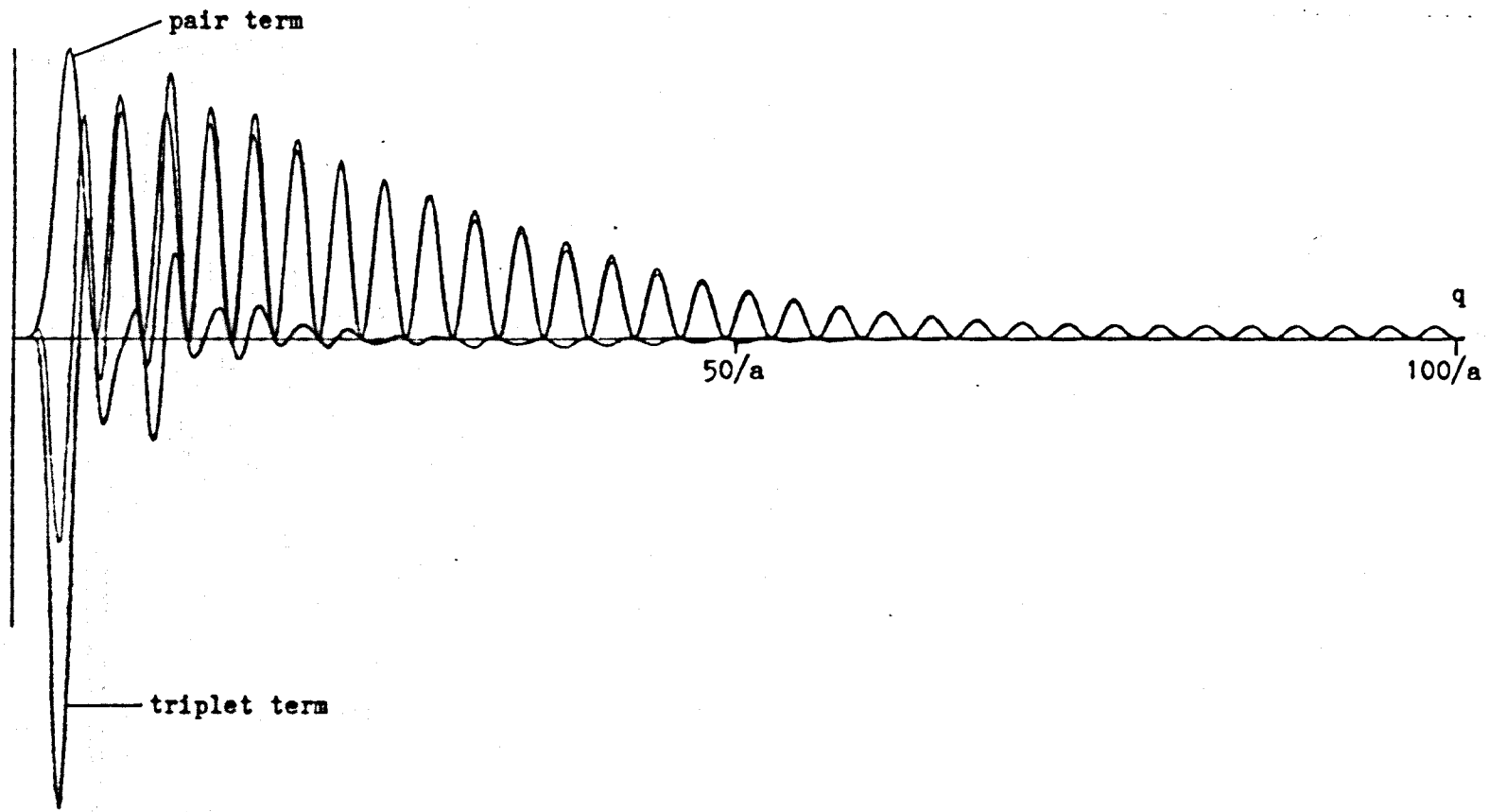

Figure 3.6 Plot of $q^2[I_p(q) + 2n\rho I_t(q)]$ as a function of q for liquid mercury with a range $\Delta = 0.1a$. Also shown separately are the pair and triplet terms.

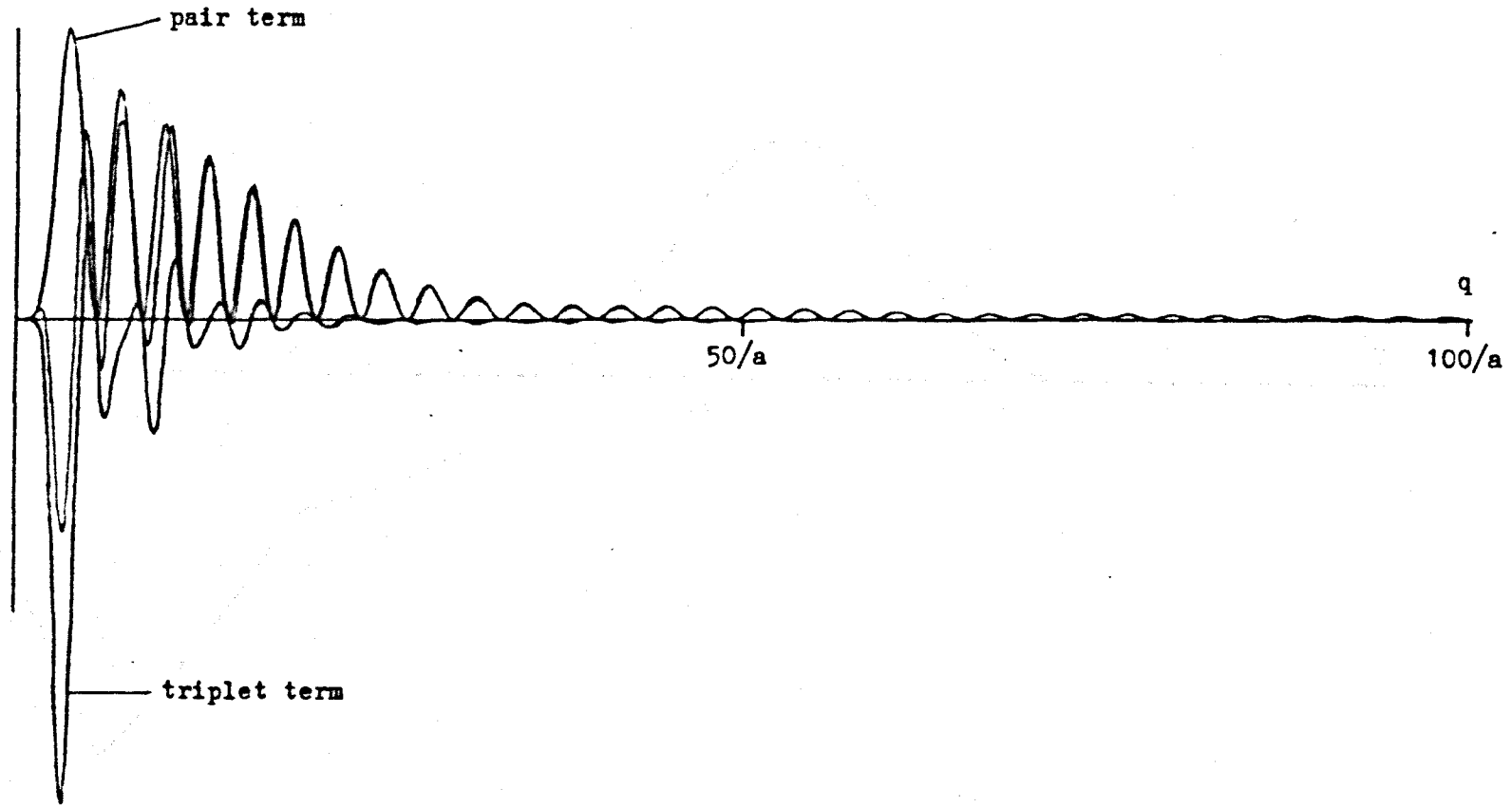

Figure 3.7 Plot of $q^2[I_p(q) + 2n\rho I_t(q)]$ as a function of q for liquid mercury with a range $\Delta = 0.2a$.

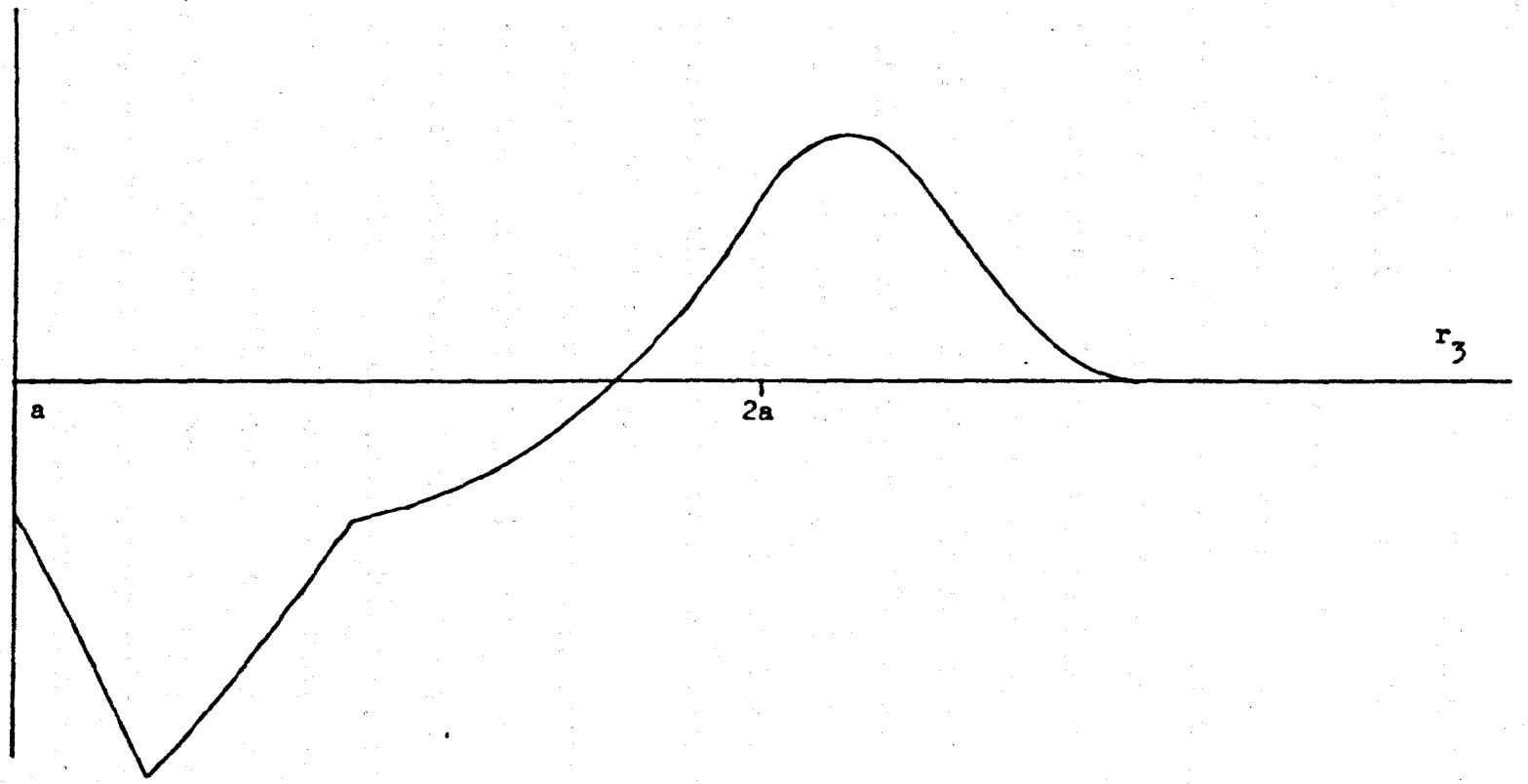

Figure 3.8 Plot of the function $2\pi\rho g(r_3)r_3^2\int_{-1}^{1} g(r_{03})P_2(z)dz$ against r_3 for liquid mercury with a range $\Delta = 0.1a$.

interatomic spacing. Consequently the convolution with the spherical Bessel function results in a series of negative going peaks which decay rapidly towards high q values. The general features of $I_t(q)$ can be seen from Figures 3.6 and 3.7. The sum $I_p(q) + 2n\rho I_t(q)$ is also shown and generally this consists of a large negative peak at low q values which gives way to a series of positive peaks at high q.

The final integration was carried out in accordance with equation 3.55 with $S_s(q,o)$ given by the Egelstaff and Schofield expression with parameters appropriate to liquid Hg. It is clear that the final result for the temperature variation of R_{1q} will not simply be a $T^{-\frac{1}{2}}$ dependence but is some complicated balance of a negative triplet contribution whose dependence on temperature is principally D^{-1} and the positive pair terms which change from a D^{-1} variation at low q to a $T^{-\frac{1}{2}}$ variation at high q.

The results obtained using the Hg pair distribution function are shown in figure 3.9. It can be seen that if the range of the interaction, Δ, is 0.1a then a slow variation of R_{1q} with temperature is obtained. However, as the range is increased to 0.2a a negative result for R_{1q} is obtained. This can be understood with reference to figures 3.6 and 3.7 where it will be seen that as the range increases I_p tends to lower q values but I_t remains hardly changed. This result tends to imply that we have overestimated the triplet contribution in our calculations which could be due to our use of the superposition approximation. We have

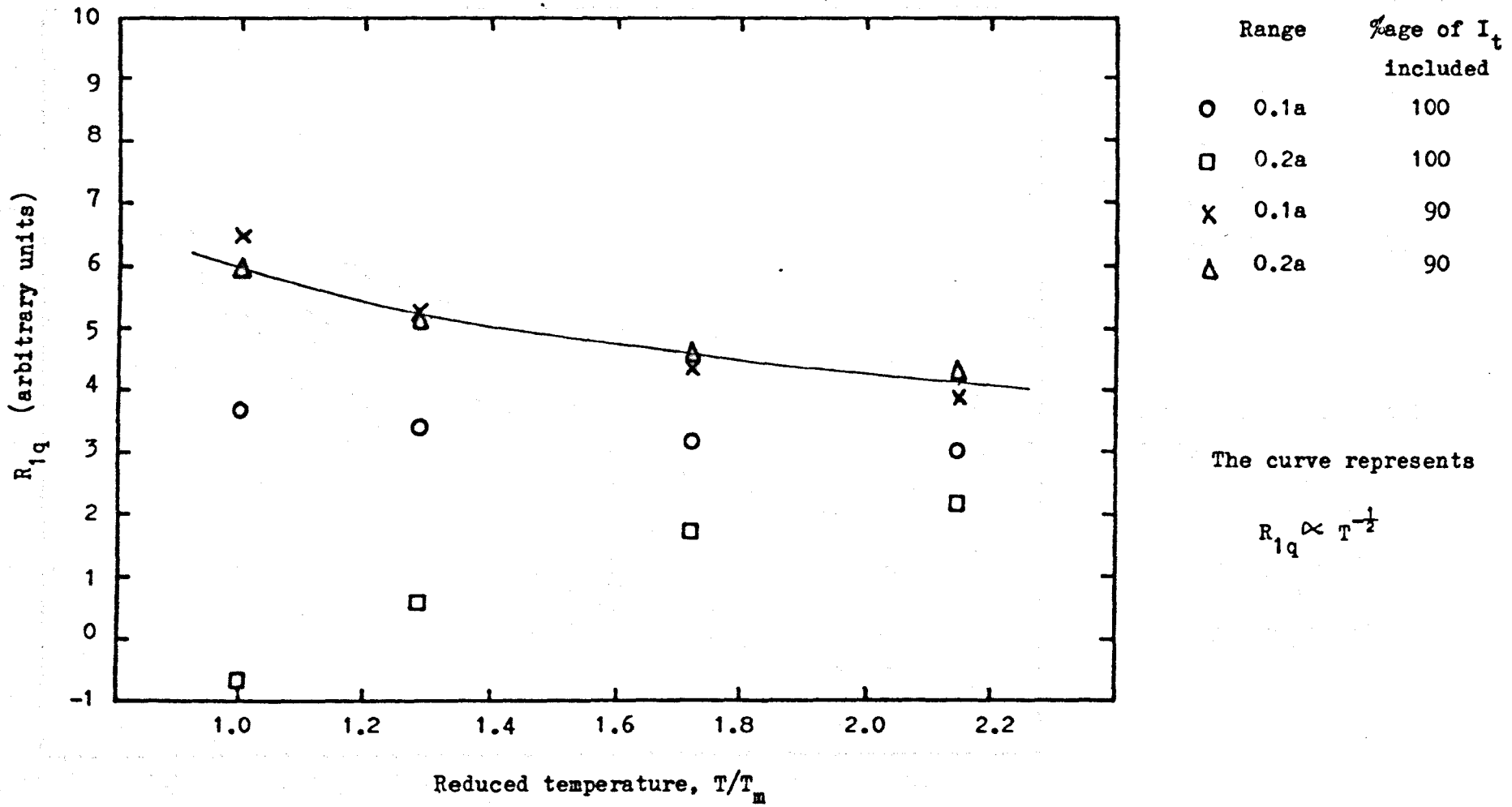

Figure 3.9 Graphs of R_{1q} against temperature obtained using the mercury g(r)

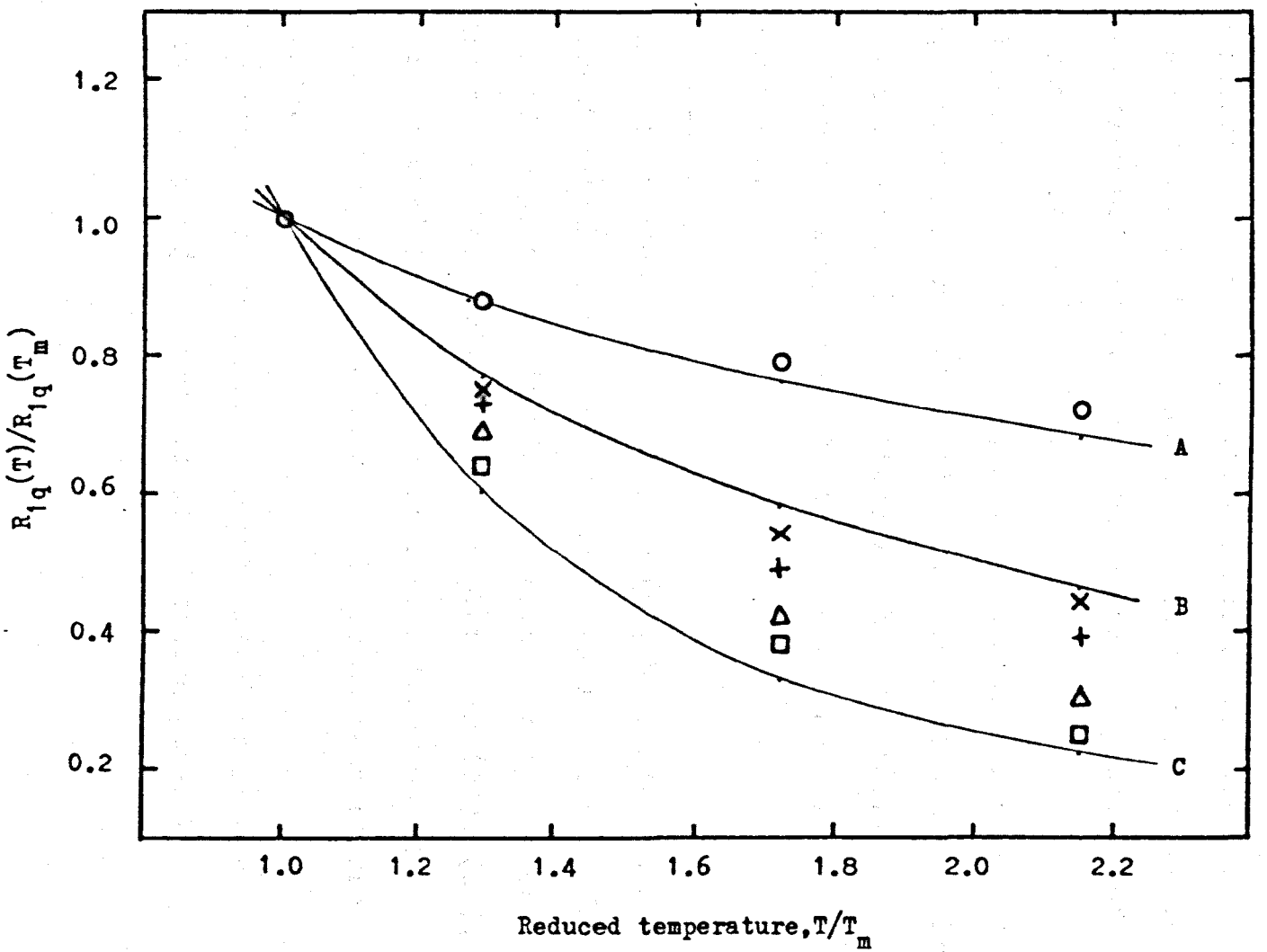

	Range	%age of I_t included
O	0.1a	100
×	0.1a	75
+	0.2a	75
Δ	0.5a	75
□	2.0a	75

The curves represent the following,

A $R_{1q} \propto T^{-\frac{1}{2}}$

B $R_{1q} \propto T^{-1}$

C $R_{1q} \propto T^{-2}$

Figure 3.10 Graphs of R_{1q} against temperature obtained using the hard sphere g(r).

studied the effect of reducing I_t and find that for the 0.1a and 0.2a range a reduction of I_t by about 5% to 10% leads to a predicted variation of R_{1q} which is very close to $T^{-\frac{1}{2}}$.

Similar results were obtained using the hard sphere g(r). These are shown in Figure 3.10. With a range of 0.1a and including all the triplet term the variation of R_{1q} was found to be close to $T^{-\frac{1}{2}}$ but if the range was increased we had to reduce I_t to get a positive result. If only 75% of I_t is included in the calculations then as the range is increased from 0.1a to 1.0a the temperature dependence of R_{1q} increases from T^{-1} to T^{-2}.

Although we did not carry out calculations for any other metals, since the pair distribution functions of most metals are similar, as are the parameters in the Egelstaff-Schofield expression, we would only expect minor differences in the results.

3.4 Discussion

The differences between Sholl's (5), Warren's (6) and the present calculations have already been described. For the sake of completeness it might be pointed out that earlier calculations either neglected the triplet term (23), (24), or used a restricted form of the correlation function (1) which was not capable of giving the observed temperature dependence.

A possible criticism which may be levelled at our model is that the joint probability function given by

equation 3.27 which is

$$P_s = \rho g(r_o) f(r_o, r_1) \int_0^\infty G_s(\underline{r_2}-\underline{r_1}, t) G_s(\underline{r_2}-\underline{r_o}, t) \underline{dr_2} \qquad 3.63$$

is not symmetric under the reversal of r_o and r_1(2). An alternative may have been to have used the joint probability function of Oppenheim and Bloom which is explicitly symmetric in r_o and r_1. However, the apparent non-reversal is probably not significant in the approximation used here for the following reason. Since the motion of the two particles is taken to be independent r_2, r_o, and r_1 are then independent variables which may be integrated over all directions. Consequently, as an examination of equation 3.49 shows, the final result for the pair term contribution to R_{1q} is devoid of angular terms and is merely proportional to the product of two quite separate integrals over the radial magnitudes r_o and r_1. Interchange of r_o and r_1 does not alter this product. In fact, actual calculations using the Oppenheim and Bloom joint probability function gave similar values of the pair and triplet terms to those using equations 3.49 and 3.50.

The physical process involved in our model may be described in the following way. Consider the relaxing nucleus surrounded by a shell of atoms. Generally the atoms will be distributed over most of the surface of the shell and the resultant efg could be calculated from the pair and triplet distributions. The fluctuations of the efg are

caused by the flexing of the shell as the atoms change their radial positions. If the potential is short range, movements of the atoms over distances both large and small compared with the atomic spacing will contribute to R_{1q} through the pair terms. However, if an atom makes a diffusive step of the order of the interatomic spacing, a, then the void it leaves behind is filled by the movement of other atoms. The effect of the replacement of one atom by another is contained in the triplet term which is spread over a range of a in real space. It thus tends to cancel the diffusive motion, leaving mainly the high q part of the pair term i.e. the small distance motion of the atoms to be the principal contribution to R_{1q}. Clearly, as the range of the potential is increased the strength of the high q terms will fall and our model will thus lead to an approximately $T^{-\frac{1}{2}}$ temperature dependence when the range is small compared to a and to a D^{-1} dependence when it is of the order of a.

Unfortunately, as we have already indicated, our calculations give a triplet term which is too large except when the range of interaction is of the order of 0.1a. This negative result for R_{1q} may be caused by overestimation of the triplet term due to calculation error or the use of the superposition approximation. Calculation error certainly exists since the integrals involve functions of complicated shape and in order to reduce the computing requirements we

have made fairly drastic simplifications of these shapes. However, we feel that the 25% reduction required to give R_{1q} positive when the range of interaction, $\Delta \sim a$ is too large to be explained in this way. As evidence we point to the fact that a similar result is obtained for both the mercury and the hard sphere $g(r)^s$ which, in our approximations, have quite different shapes. Remember g(r) only enters the triplet term, whereas in the pair term it has been reduced to a δ function. The error caused by the superposition approximation is unknown, but is, in general, thought to be substantial at near neighbour distances. However, our calculations show that the reduction factor for the triplet term required to keep R_{1q} positive is smaller for the short ranges than for the long range interactions.

During the course of our work Gaskell (25) has suggested an approximate method of formulating the pair correlation function. He divides the efg into a short range part lying within the atomic core, whose radius is only slightly larger than the interatomic spacing, and a long range part which is zero inside this core but may be non-zero outside. For the long range part the core thus plays the role of f(r) in our model. Within the core he restricts the position vectors of the particles to certain angles thus keeping the interaction within finite bounds. More importantly, he argues that, because of the short range, the joint probability appearing in Equation 3.9 may be replaced by its short time approximation. This is equivalent to taking the ideal gas approximation

for $S_s(q,\omega)$, which, as has been pointed out, has a $T^{-\frac{1}{2}}$ dependence. Gaskell further treats the triplet term according to the Sholl-Warren formula but with the total van Hove function replaced by its distinct part. Thus his R_{1q} consists of a pair term with a $T^{-\frac{1}{2}}$ dependence plus another pair term from the long range part of the field gradient and a triplet term. In order to obtain agreement with experiment he therefore suggests that the contribution from the long range component of the field gradient and that from the three particle terms are either small or show a marked degree of cancellation. However, if the long and short range field gradients are taken to be the long and short range parts of the Schirmacher field gradient then the triplet term is likely to be large and negative at small q and the long range pair term will be small and positive. Thus the final result of Gaskell's model would seem to be the sum of two terms, one positive with a $T^{-\frac{1}{2}}$ dependence, the other negative with a D^{-1} dependence. The fault in his theory lies in his assumption that the short range pair term involves only particle motions over short distances. In fact, as pointed out above, the change in position of a particle may be of any length and consequently there is no need to make the distinction between short and long range terms. The Fourier transform of his joint probabilty function would then cover the range of q values to be found in our calculations with a similar cancellation occuring at low q through the

distinct part in the triplet term.

There are two physical phenomena that contribute to the temperature dependence of R_{1q} that we have yet to describe. Both of these involve the changes in g(r) with increasing temperature.

As pointed out in Chapter 1 the principal effect is a decrease in the cut-off at small r. In our model we assume that $v_2(r)\ g(r)\ r^2$ is a sharply peaked function thus implying that $v_2(r)$ falls sharply to zero just beyond the cut-off in g(r). Since $v_2(r)$ is a rapidly varying function, the amplitude of the peak is sensitive to the compression of the ion cores. As the temperature increases, the kinetic energy of the particles will further compress the cores during collisions. Thus $I_p(q)$ and $I_t(q)$ will both increase and, although cancellation is maintained, the result will be an increase in R_{1q}. Sholl has estimated the increase in R_{1q} from this effect with the aid of the semi-empirical calculations of the hard-sphere diameters in liquid metals by Protopapas et al (26). The calculations have been extended by Cartledge et al (27) who find a predicted increase in R_{1q} of between 20 to 30% for the range T_m to $2T_m$ for the liquid metals of interest.

The other effect on g(r) of increasing the temperature is that the peak of g(r) flattens. This leads to a reduction in the amplitude of the δ functions used to calculate R_{1q} in our approximate method. Hence this effect would produce a decrease in R_{1q} with temperature. Although we have not

made detailed calculations of the extent of this effect it would obviously tend to cancel the increase in R_{1q} caused by the "squashyness" of the ion cores described above.

The overall temperature dependence of R_{1q} therefore depends on a large number of parameters which include the form of the interionic potential, the relative sizes and extent in k space of the pair and triplet contributions and the radial distribution function. It is therefore not surprising that a definitive form of the theory of R_{1q} in liquid metals which agrees with the experimental data has yet to be produced.

The important feature of the model proposed here is that, owing to the cancellation occuring between the pair and triplet contributions at low q, it predicts an approximately $T^{-\frac{1}{2}}$ dependence of R_{1q} on temperature provided that the range of the quadrupolar interaction is small compared to the interatomic spacing. Furthermore, it is shown in the next chapter that our model is reasonably successful in predicting the temperature dependence of R_{1q} in liquid binary alloys. Hence, further effort on this difficult theoretical problem would seem worthwhile in view of the information that may be deduced about the ion-ion potentials and molecular dynamics in liquid metals and alloys.

The work described in this chapter is contained in the publications by Havill et al (28) and Titman et al (29).

3.5 References

1) C.A. Sholl, Proc. Phys. Soc., 91, 130 (1967)

2) A. Abragam, Principles of Nuclear Magnetism (Oxford Press, Oxford, 1961)

3) H.C. Torrey, Phys. Rev., 92, 962 (1953)

4) I. Oppenheim and M. Bloom, Canad. J. Phys., 39, 845 (1961)

5) C.A. Sholl, J. Phys. F: Metal Phys., 4, 1556 (1974)

6) W.W. Warren Jn., Phys. Rev., A10, 657 (1974)

7) S.J. Cocking and P.A. Egelstaff, J. Phys. C., 1, 507 (1968)

8) N. C. Halder, Phys. Stat. Sol. (b), 80, 273 (1977)

9) W. Schirmacher, Proc. 3rd. Int. Conf. Liquid Metals, Bristol 1977: Inst. Phys. Conf. Ser. No. 30, 610 (1976)

10) P.A. Egelstaff and P. Schofield, Nucl. Sci. Engng., 12, 260 (1962)

11) S.H. Chen, Y. Lefevre and S. Yip, Properties of Liquid Metals, ed. S. Takeuchi (Taylor and Francis, 1973) p. 119

12) W. Gläser, S. Hagen, U. Löffler, J.B. Suck and W. Schommers, Properties of Liquid Metals, ed. S. Takeuchi (Taylor and Francis, 1973) p. 111

13) M.I. Barker, M.W. Johnson, N.H. March and D.I. Page, Properties of Liquid Metals, ed. S. Takeuchi (Taylor and Francis, 1973)

14) D.I. Page, D.H. Saunderson and C.G. Windsor, J. Phys. C: Solid St. Phys., 6, 212 (1973)

15) J.R.D. Copley and S.W. Lovesay, Rep. Prog. Phys., 38, 461 (1975)

16) G.H. Vineyard, Phys. Rev., 110, 999 (1958)

17) A. Abragam, Principles of Nuclear Magnetism (Oxford Press, Oxford, 1961) p. 292

18) R. Hutchinson, Proc. Phys. Soc., 91, 506 (1967)

19) A. Messiah, Quantum Mechanics (Wiley, New York, 1962) p.1074

20) N.W. Ashcroft, Phys. Letts., 23, 48 (1966)

21) M.L. Cohen and V. Heine, Solid St. Phys., 24, 37 (1970)

22) K.W. Lodge, J. Phys. F: Metal Phys., 6, 1989 (1976)

23) F. Borsa and A. Rigamonti, A. Nuovo Cimento, 48, 194 (1967)

24) R.M. Yul' met' ev, Izv. Vuz.Fiz. U.S.S.R., 8, 28 (1968)

25) T. Gaskell, Phys. Chem.Liq., 8,23 (1978)

26) P. Protopapas, H.C. Anderson and N.A.D. Parlee, J. Chem. Phys., 59, 15 (1973)

27) G. Cartledge, R.L. Havill and J.M. Titman, J. Phys. F: Metal Phys., 6, 639 (1976)

28) R.L. Havill, J. Marsden and J.M. Titman, J. Phys. F: Metal Phys., 7, 2357 (1977)

29) J.M. Titman, J. Marsden and R.L. Havill (to be published)

CHAPTER FOUR

Nuclear Quadrupole Relaxation in Liquid Metal Alloys

4.1 Introduction

The theory of nuclear quadrupole relaxation in pure metals presented in chapter three can be easily extended to cover the case of a binary alloy. For a pure liquid metal the ensemble average required to calculate J(o) is given by equation 3.8 which is

$$\langle F_m(t)F_m^{*},(o)\rangle = \iint u_m(\underline{r}_o)u_m^{*},(\underline{r}_1)P(\underline{r}_o,o;\underline{r}_1,t)d\underline{r}_o\ d\underline{r}_1 \qquad 4.1$$

In a liquid binary alloy consisting of A and B type ions this becomes the sum of four terms as below.

$$\begin{aligned}\langle F_m(t)F_m^{*},(o)\rangle = &\iint u_m^A(\underline{r}_o)u_m^{A*},(\underline{r}_1)P_{AA}(\underline{r}_o,o;\underline{r}_1,t)d\underline{r}_o\ d\underline{r}_1 \\ &+ \iint u_m^B(\underline{r}_o)u_m^{B*},(\underline{r}_1)P_{BB}(\underline{r}_o,o;\underline{r}_1,t)d\underline{r}_o\ d\underline{r}_1 \\ &+ \iint u_m^A(\underline{r}_o)u_m^{B*},(\underline{r}_1)P_{AB}(\underline{r}_o,o;\underline{r}_1,t)d\underline{r}_o\ d\underline{r}_1 \\ &+ \iint u_m^B(\underline{r}_o)u_m^{A*},(\underline{r}_1)P_{BA}(\underline{r}_o,o;\underline{r}_1,t)d\underline{r}_o\ d\underline{r}_1 \qquad 4.2\end{aligned}$$

where $P_{AB}(\underline{r}_o,o;\underline{r}_1,t)d\underline{r}_o\ d\underline{r}_1$ is the probability of finding

an ion of type A in $\underline{dr_o}$ at $\underline{r_o}$ at time zero and an ion of type B in $\underline{dr_1}$ at $\underline{r_1}$ at time t given that there is an ion of type A at the origin. The first two terms in equation 4.2 give rise to pair and triplet contributions to R_{1QA} whereas the latter terms can give rise only to triplet contributions.

Following the same method as in chapter three we can write

$$P_{AAp} = \rho c g_{AA}(r_o) f_{AA}(r_1) \int_0^\infty G_{SA}(\underline{r_2}-\underline{r_1},t) G_{SA}(\underline{r_2}-\underline{r_o},t) \underline{dr_2} \qquad 4.3$$

$$P_{BBp} = \rho(1-c) g_{AB}(r_o) f_{AB}(r_1) \int_0^\infty G_{SA}(\underline{r_2}-\underline{r_1},t) G_{SB}(\underline{r_2}-\underline{r_o},t) \underline{dr_2} \qquad 4.4$$

for the pair terms and

$$P_{AAt} = f_{AA}(r_1) \iint \rho^{(3)}_{AAA}(r_o,r_3) G_{SA}(\underline{r_2}-\underline{r_3},t) G_{SA}(\underline{r_2}-\underline{r_1},t) \underline{dr_2}\ \underline{dr_3} \qquad 4.5$$

$$P_{BBt} = f_{AB}(r_1) \iint \rho^{(3)}_{ABB}(r_o,r_3) G_{SB}(\underline{r_2}-\underline{r_3},t) G_{SA}(\underline{r_2}-\underline{r_1},t) \underline{dr_2}\ \underline{dr_3} \qquad 4.6$$

$$P_{ABt} = f_{AB}(r_1) \iint \rho^{(3)}_{AAB}(r_o,r_3) G_{SB}(\underline{r_2}-\underline{r_3},t) G_{SA}(\underline{r_2}-\underline{r_1},t) \underline{dr_2}\ \underline{dr_3} \qquad 4.7$$

$$P_{BAt} = f_{AA}(r_1) \iint \rho^{(3)}_{ABA}(r_o,r_3) G_{SA}(\underline{r_2}-\underline{r_3},t) G_{SA}(\underline{r_2}-\underline{r_3},t) \underline{dr_2}\ \underline{dr_3} \qquad 4.8$$

for the triplet terms, where ρ is the number density, c the fractional concentration of A, g_{AA}, g_{AB} partial radial distribution functions, f_{AA} is the partial equivalent of the

function f in the pure metal theory, G_{SA} is the self-part of the van Hove correlation function describing the motion of an A type ion and $\rho^{(3)}_{AAA}(r_o,r_3)$ the three particle correlation function i.e. the probability of finding ions of type A at $\underline{r_o}$ and $\underline{r_3}$ given an ion of type A at the origin.

Using the superposition approximation we have

$$\rho^{(3)}_{AAA}(r_o,r_3) = c^2\rho^2 g_{AA}(r_o)g_{AA}(r_3)g_{AA}(r_{03}) \qquad 4.9$$

$$\rho^{(3)}_{ABB}(r_o,r_3) = (1-c)^2\rho^2 g_{AB}(r_o)g_{AB}(r_3)g_{BB}(r_{03}) \qquad 4.10$$

$$\rho^{(3)}_{AAB}(r_o,r_3) = c(1-c)\rho^2 g_{AA}(r_o)g_{AB}(r_3)g_{AB}(r_{03}) \qquad 4.11$$

$$\rho^{(3)}_{ABA}(r_o,r_3) = c(1-c)\rho^2 g_{AB}(r_o)g_{AA}(r_3)g_{AB}(r_{03}) \qquad 4.12$$

Substitution of equations 4.3 to 4.12 into 4.2 then gives for the pair term contribution

$$\begin{aligned}\langle F_m(t)F^*_{m'}(o)\rangle_{pair} = {} & \iint u^A_m(\underline{r_o})u^{A*}_{m'}(\underline{r_1})\rho c g_{AA}(r_o)f_{AA}(r_1) \\ & \times \int_0^\infty G_{SA}(\underline{r_2}-\underline{r_1},t)G_{SA}(\underline{r_2}-\underline{r_o},t)\underline{dr_o}\underline{dr_1}\underline{dr_2} \\ & + \iint u^B_m(\underline{r_o})u^{B*}_{m'}(\underline{r_1})\rho(1-c)g_{AB}(r_o)f_{AB}(r_1) \\ & \times \int_0^\infty G_{SA}(\underline{r_2}-\underline{r_1},t)G_{SB}(\underline{r_2}-\underline{r_o},t)\underline{dr_o}\underline{dr_1}\underline{dr_2}\end{aligned} \qquad 4.13$$

and the triplet term oontribution

$$\langle F_m(t)F_{m'}^*(o)\rangle_{\text{triplet}} = \iint u_m^A(\underline{r}_o)u_{m'}^{A*}(\underline{r}_1)f_{AA}(r_1)\underline{dr}_o\underline{dr}_1$$

$$\times \iint c^2\rho^2 g_{AA}(r_o)g_{AA}(r_3)g_{AA}(r_{o3})$$

$$\times G_{SA}(\underline{r}_2-\underline{r}_3,t)G_{SA}(\underline{r}_2-\underline{r}_1,t)\underline{dr}_2\underline{dr}_3$$

$$+ \iint u_m^B(\underline{r}_o)u_{m'}^{B*}(\underline{r}_1)f_{AB}(r_1)\underline{dr}_o\underline{dr}_1$$

$$\times \iint (1-c)^2\rho^2 g_{AB}(r_o)g_{AB}(r_3)g_{BB}(r_{o3})$$

$$\times G_{SB}(\underline{r}_2-\underline{r}_3,t)G_{SA}(\underline{r}_2-\underline{r}_1,t)\underline{dr}_2\underline{dr}_3$$

$$+ \iint u_m^A(\underline{r}_o)u_{m'}^{B*}(\underline{r}_1)f_{AB}(r_1)\underline{dr}_o\underline{dr}_1$$

$$\times \iint c(1-c)\rho^2 g_{AA}(r_o)g_{AB}(r_3)g_{AB}(r_{o3})$$

$$\times G_{SB}(\underline{r}_2-\underline{r}_3,t)G_{SA}(\underline{r}_2-\underline{r}_1,t)\underline{dr}_2\underline{dr}_3$$

$$+ \iint u_m^B(\underline{r}_o)u_{m'}^{A*}(\underline{r}_1)f_{AA}(\underline{r}_1)\underline{dr}_o\underline{dr}_1$$

$$\times \iint c(1-c)\rho^2 g_{AB}(r_o)g_{AA}(r_3)g_{AB}(r_{o3})$$

$$\times G_{SA}(\underline{r}_2-\underline{r}_3,t)G_{SA}(\underline{r}_2-\underline{r}_3,t)\underline{dr}_2\underline{dr}_3$$

4.14

If we assume that $G_{SA} = G_{SB}$, independent of composition, then J(o) and hence R_{1QA} can be written down by analogy with the pure metal case;

$$R_{1QA} = 2\beta\int_{-\infty}^{\infty} S_s^{\,2}(q,\omega)d\omega \int_0^{\infty} q^2 dq \Big[cI_p(f_{AA},g_{AA},v_2^A)+(1-c)I_p(f_{AB},g_{AB},v_2^B)$$

$$+ 2n\rho c^2 I_t(v_2^A,v_2^A,f_{AA},g_{AA},g_{AA},g_{AA})$$

$$+ 2n\rho(1-c)^2 I_t(v_2^B,v_2^B,f_{AB},g_{AB},g_{AB},g_{BB})$$

$$+ 2n\rho c(1-c) I_t(v_2^A,v_2^B,f_{AB},g_{AA},g_{AB},g_{AB})$$

$$+ 2n\rho c(1-c) I_t(v_2^B,v_2^A,f_{AA},g_{AB},g_{AA},g_{AB})\Big] \qquad 4.15$$

where $I_p(f_{AA},g_{AA},v_2^A) = \int_0^{\infty} f_{AA}(r_1)v_2^A(r_1)r_1^{\,2}j_2(qr_1)dr_1$

$$\times \int_0^{\infty} g_{AA}(r_o)v_2^A(r_o)r_o^{\,2}j_2(qr_o)dr_o \qquad 4.16$$

and

$$I_t(v_2^A,v_2^B,f_{AB},g_{AA},g_{AB},g_{AB}) = \int_0^{\infty} f_{AB}(r_1)v_2^B(r_1)r_1^{\,2}j_2(qr_1)dr_1$$

$$\times \int_0^{\infty} g_{AA}(r_o)v_2^A(r_o)r_o^{\,2}dr_o$$

$$\times \int_0^{\infty} g_{AB}(r_3)r_3^{\,2}j_2(qr_3)dr_3$$

$$\times \int_{-1}^{1} g_{AB}(r_{o3})P_2(z)dz \qquad 4.17$$

Equation 4.15 may be written

$$R_{1QA} \propto cI_p(aa)+(1-c)I_p(ab)+2n\rho\left[c^2I_t(aaa)+(1-c)^2I_t(abb)\right.$$

$$\left.+\ 2c(1-c)I_t(aba)\right] \qquad 4.18$$

where $I_p(aa)$ and $I_t(aba)$ are given by (4.16) and (4.17).

Rearranging terms,

$$R_{1QA} \propto c\left[I_p(aa)+2n\rho I_t(aaa)\right]+(1-c)\left[I_p(ab)+2n\rho I_t(abb)\right]$$

$$+\ 2n\rho c(1-c)\left[2I_t(aba)-I_t(aaa)-I_t(abb)\right] \qquad 4.19$$

Now, if we assume that the field gradient due to an A ion and a B ion are identical apart from a constant factor a i.e. $v_2^B = a\,v_2^A$ then

$$\frac{I_p(ab)}{I_p(aa)} = a^2, \quad \frac{I_t(abb)}{I_t(aaa)} = a^2 \quad \text{and} \quad \frac{I_t(aba)}{I_t(aaa)} = a \qquad 4.20$$

This assumption is not an unreasonable one if the Schirmacher pseudopotential approach is used to calculate the field gradient.

Substituting 4.20 into 4.19 we obtain

$$R_{1QA} \propto c\left[I_p(aa)+2n\rho I_t(aaa)\right]+(1-c)a^2\left[I_p(aa)+2n\rho I_t(aaa)\right]$$

$$-\ c(1-c)(1-a)^2 2n\rho I_t(aaa) \qquad 4.21$$

which may be written as

$$R_{1QA} \propto \left[c+(1-c)a^2\right]A-c(1-c)(1-a)^2B \qquad 4.22$$

where $$A = I_p(aa)+2n\rho I_t(aaa) \qquad 4.23$$

and $$B = 2n\rho I_t(aaa) \qquad 4.24$$

It will be seen that equation 4.22 predicts that the quadrupolar relaxation rate in a binary alloy can be thought of as being proportional to the sum of two separate terms. The first term, containing both pair and triplet terms, is similar to that obtained for the pure metal case. It was shown in chapter 3 that, provided the range of the quadrupolar interaction is small compared to the interatomic spacing, this term leads to a variation of R_{1q} with temperature that is approximately proportional to $T^{-\frac{1}{2}}$. The second term, however, contains only the triplet terms which contribute a temperature variation proportional to D^{-1}. It will be appreciated that this contribution to the relaxation rate is a positive one since the triplet terms themselves are predominantly negative.

The first term in equation 4.22 is linear in c but the second term has a quadratic dependence on c. Therefore, the theory predicts that the rate of variation of R_{1QA} with temperature will increase as the concentration of A increases up to a fractional concentration of 0.5.

A review of the reliable experimental data indicates that the predicted increase in the rate of change of R_{1q}

has been observed in the following work. Using nmr Warren and Clark (1) found a slow variation of R_{1q} with temperature for the ^{121}Sb spins in pure liquid Sb. This contrasted with the much faster variation found in liquid InSb. The latter result has recently been confirmed by von Hartrott et al (2) who, using pac measurements on the ^{117m}Sb isomer, found R_{1q} approximately proportional to 1/D in InSb.

Cartledge et al have examined the variation of R_{1q} with temperature for the ^{69}Ga spins in a number of Ga alloys. Their data for Ga/In alloys (3) agrees closely with the theoretical variation predicted by the new alloy theory. As the amount of In is increased the rate of change of R_{1q} for the ^{69}Ga spins gradually increases. However, a similar effect was not observed in other Ga alloys containing Al, Zn and Sn (4). In these the temperature variation of R_{1q} remained the same as in the pure metal. This may be explained by the fact that most of the alloys were of low concentration. However a similar result was obtained with a Ga30at%Sn alloy where one might expect a faster variation to be observed. In this case the fact that it was not may be due to the small temperature range that was covered.

We decided to investigate more alloy systems as described below in order to obtain further reliable data.

Holcomb and Norberg (5) have measured the variation of R_1 for the ^{85}Rb and ^{87}Rb spins in liquid Rubidium. Their data has been analysed by Rossini and Knight (6) who found

that the ^{87}Rb relaxation is almost entirely magnetic in origin but that approximately 10% of the relaxation of the ^{85}Rb isotope is quadrupolar. However, this small quadrupolar contribution taken together with the large error in the measurements makes it difficult to estimate the variation of R_{1q} with temperature. We therefore decided to attempt to obtain more accurate data on the variation of R_{1q} with temperature in liquid Rb. Having done this we would then observe the variation of R_{1q} with temperature for ^{85}Rb in a Rb50at%Na alloy where one would expect to see a relatively larger quadrupole contribution which has a faster variation with temperature. Kaeck (7) has observed a small quadrupolar contribution to R_1 for ^{85}Rb in a number of Rb/Cs alloys but did not determine the dependence of R_{1q} on temperature.

We also decided to extend the work of Cartledge et al by looking at further Ga alloys. Now the theory really relates only to substitutional alloys. However, perfectly substitutional alloys do not exist so a strict test of the theory is impossible. On the other hand Cartledge et al (4) have shown the existence of a "size effect" i.e. they observe an increase in the magnitude of R_{1q} which is proportional to the difference in size between the solvent and solute ions. We decided to investigate alloys where one would expect a large "size effect" even though these show the maximum departure from the substitutional case

because these alloys are likely to contain a large 1/D like contribution to R_{1q}. The alloys chosen were Ga10at%Mg, Ga20at%Mg, Ga20at%Al and Ga61.5at%Bi.

4.2 Experimental Method

In chapter 2, section 2.2.1 continuous wave and pulsed nmr techniques were introduced and compared. It was shown that the most direct method of measuring T_1 is to use pulse techniques but that this can only be done when the lengths of the pulses, $\Delta t \ll T_1, T_2$ otherwise relaxation effects will occur during the duration of the pulses. Using the pulse spectrometer described below this condition was satisfied for all the metals studied in this chapter and therefore pulse techniques were used throughout. Since we were investigating liquids where $T_1 = T_2$ the $\pi - \pi/2$ pulse sequence was used.

4.2.1 The Spectrometer

A block diagram of the pulse spectrometer used in these experiments is shown in figure 4.1. It was similar to the one used by Jolly (8) and Cartledge (9) and a fuller account can be found in these references. The spectrometer had, however, been modified to operate with a single coil and with phase sensitive detection. A swept pulse delay had also been added. These alterations will be described in the text.

4.2.1.1 The Magnet

The magnet was the same Varian system that was used for the continuous wave experiments described in chapter 2.

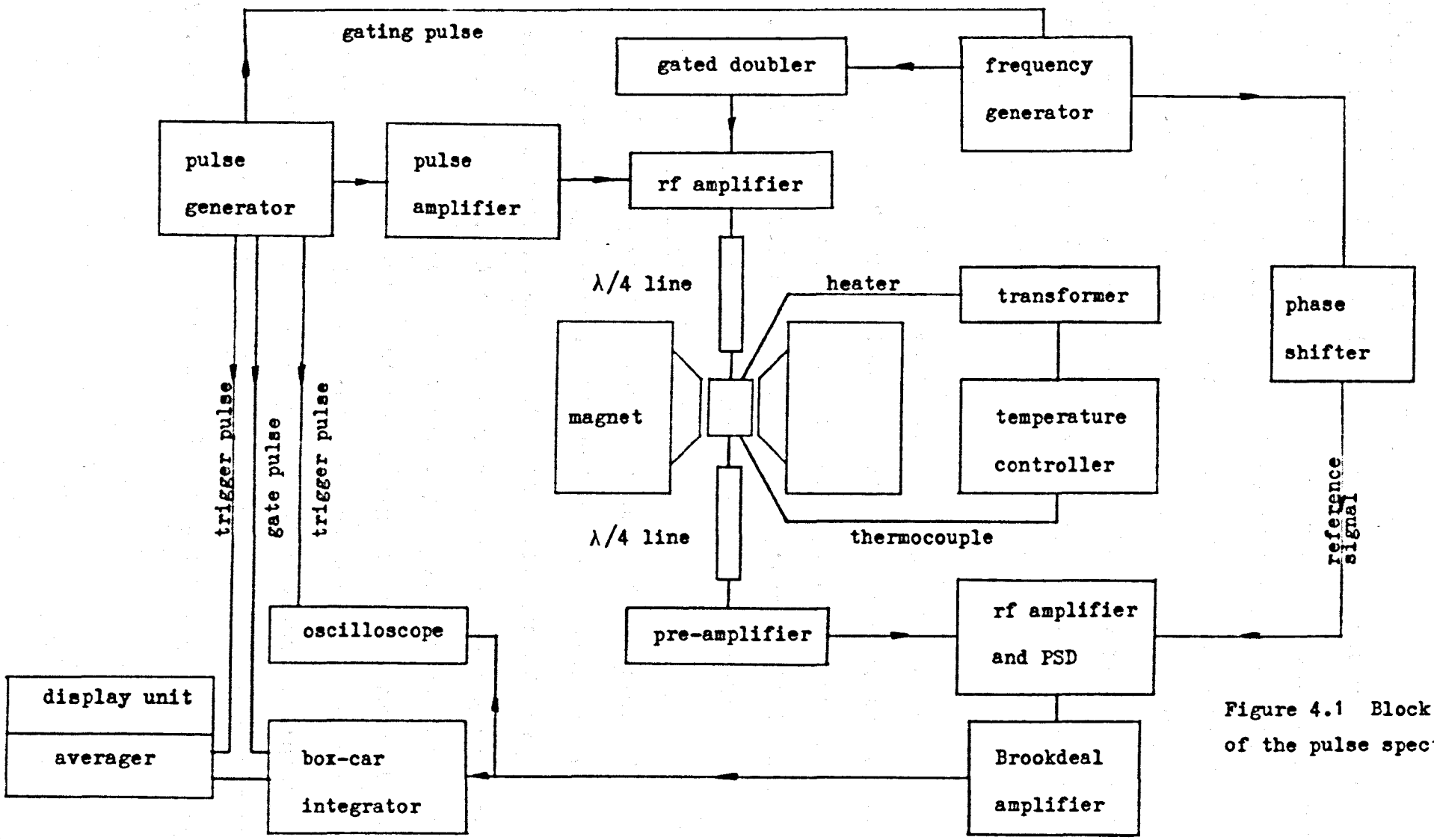

Figure 4.1 Block diagram of the pulse spectrometer.

4.2.1.2 The Frequency Generator System

The first component of the frequency generator system was a high stability frequency generator the output frequency of which was 4.4 MHz with a stability of 1 part in 10^7.

A gated frequency doubler was used to minimise break through of the resonance frequency between pulses. The output from the frequency generator of about 8v peak to peak was fed into a class A amplification stage followed by the gated pentode frequency doubler and finally a gated pentode class C stage.

The output was then fed to the main power amplifier which consisted of three class C amplifier stages, the first being gated. The output of the power amplifier consisted of r.f. pulses at 8.8 MHz which were fed tothe coil in the probe via a $\lambda/4$ length of low capacity co-axial cable.

4.2.1.3 The Pulse Generator System

The pulse generator system consisted of a series of modules supplied by Farnell Ltd. and a swept pulse delay unit which was made in the electronics workshop of the Physics Department. A block diagram is shown in figure 4.2.

The pulse repetition unit had repetition rates from 0.1 Hz to 10 MHz. Throughout these experiments a repetition rate of 50 Hz was used. The pulse width unit had ranges of 0.1μs. to 1s. The swept pulse delay unit produced a linear ramp of variable length from 1μs. to 100ms. with sweep times of 5s. to 250s. and adjustable delay between sweeps.

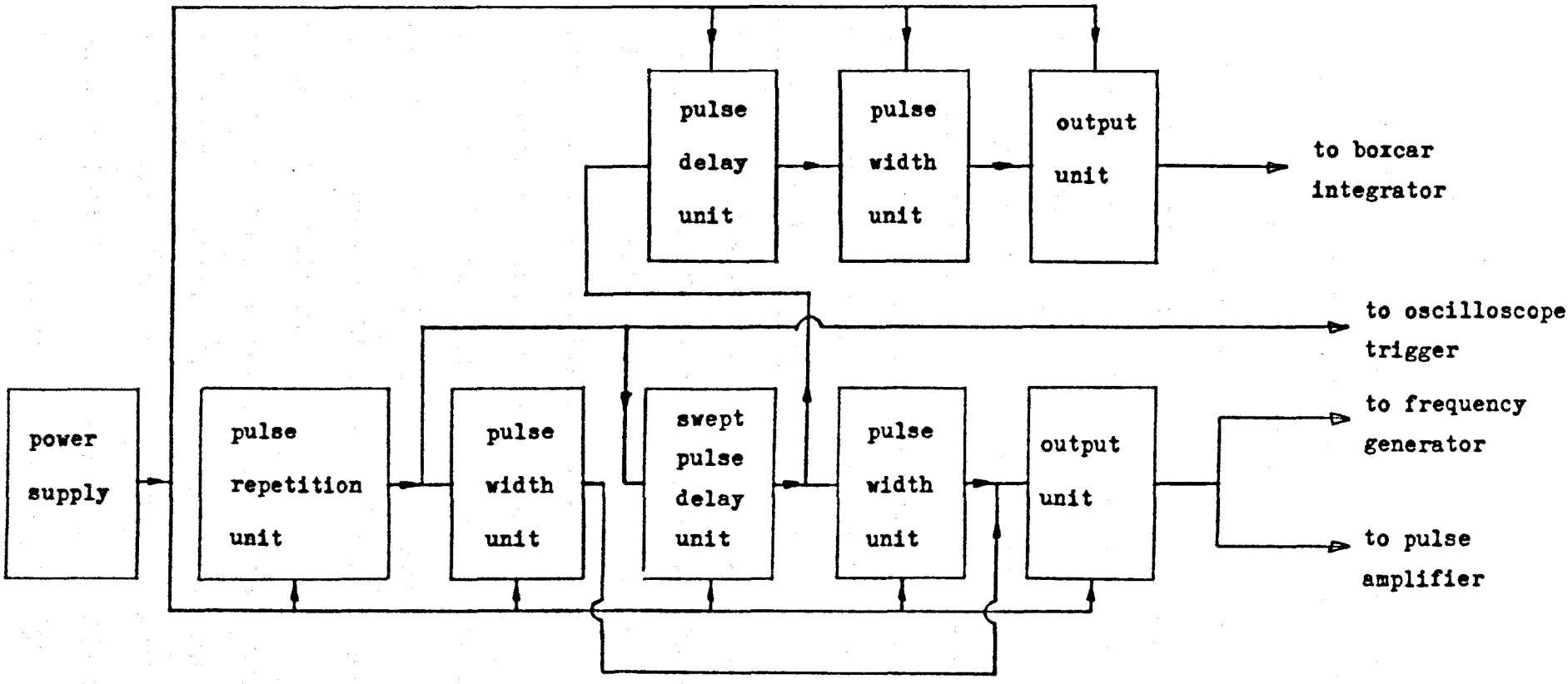

Figure 4.2 The Pulse Generator System.

Both of the pulse output units had variable outputs up to 20v. One output unit fed 20v pulses into the pulse amplifier which consisted of three amplification stages giving 250 volt positive going pulses on a 150 volt negative line. These pulses were used to gate the screen grids of the frequency doubler and other stages in the frequency generator system described above.

The other output unit provided the reference pulse for the box car integrator. The pulse was of variable width, the sampling gate width of the integrator, and was adjusted so that it was delayed a certain time after the second pulse.

4.2.1.4 The Receiver, Detector and Averager

The resonance signal induced in the coil of the probe was fed via a $\lambda/4$ length of co-axial cable to a tuned pre-amplifier. The arrangement of the transmitter, sample coil and pre-amplifier is shown in figure 4.3.

The output from the pre-amplifier was fed to the main receiver which consisted of a number of amplifying stages followed by the phase sensitive detector. The reference signal for the detector was obtained from the frequency generator via a phase shifter.

The output from the detector was fed into a Brookdeal broadband, low noise, amplifier, type 450. The output from this amplifier was then fed into a Brookdeal boxcar integrator type 415, and a Hewlett Packard oscilloscope. The reference pulse for the boxcar integrator, taken from the pulse

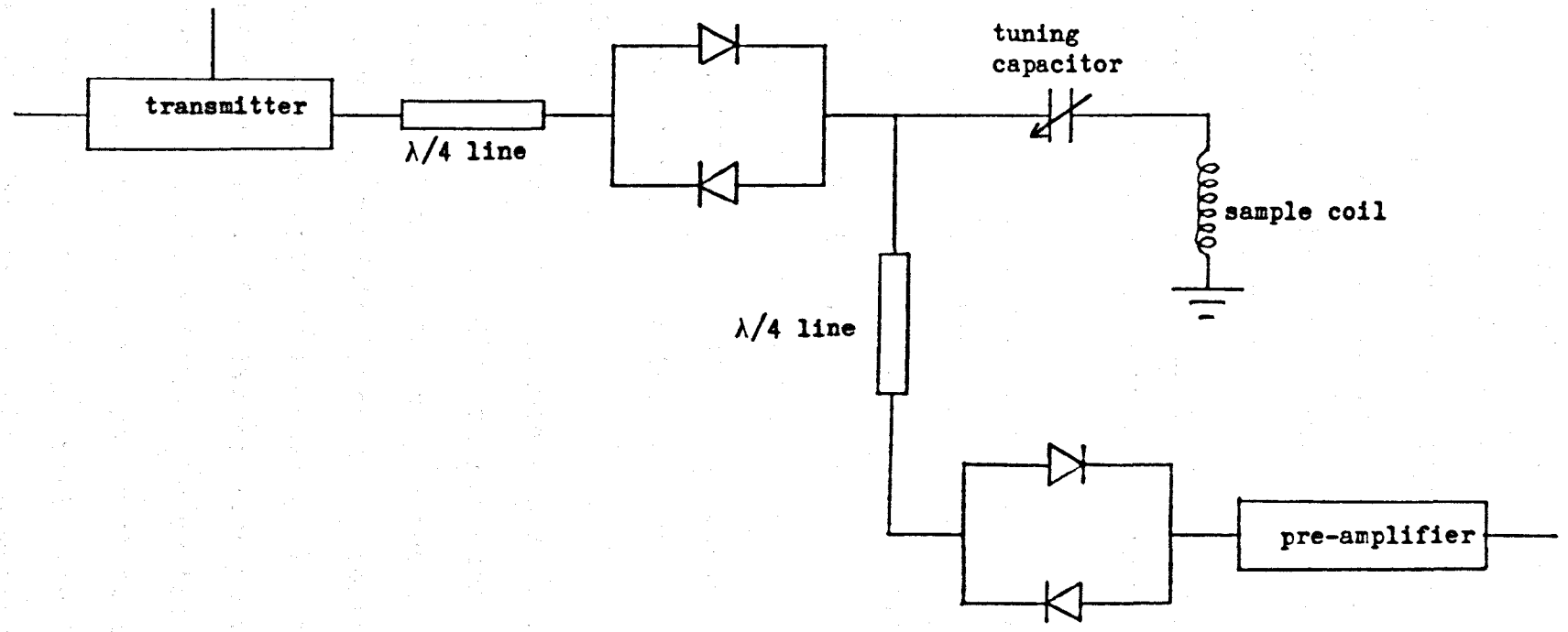

Figure 4.3 Detailed arrangement of the transmitter,sample coil and pre-amplifier

generator system as described above, had a magnitude of 1v. and a width of 5μs. The delay between the second r.f. pulse and the reference pulse was generally about 80μs. so as to make the signal to noise ratio as large as possible.

The output from the boxcar integrator was taken to the Tracor digital signal averager.

4.2.1.5 The Sample Probe and Temperature Controller

The sample probe used in these experiments is shown in figure 4.4.

The r.f. coil was 20 mm. long and consisted of 14 turns of 32 swg copper wire insulated by refrasil sleeving wound on silica tubing. The coil was potted in high temperature cement to hold it in place.

Heat was provided by a 128 turn coil of resistance wire insulated in refrasil sleeving wound non-inductively around the outer pyrex tube. The total resistance of the wire was about 40 ohms.

The temperature of the sample was measured using a platinum/platinum - 13% rhodium thermocouple with its junction placed immediately beneath the sample tube. As in the continuous wave experiments temperature control was obtained by using the thermocouple as a sensing element for a Eurotherm temperature controller. The heater current was supplied by a Variac set between 20v and 70v. Using this system the temperature of the sample was kept constant to within 0.5 ^{o}C of the required temperature. The probe was insulated from the magnet pole pieces by passing cold water through the brass jacket as shown in the figure.

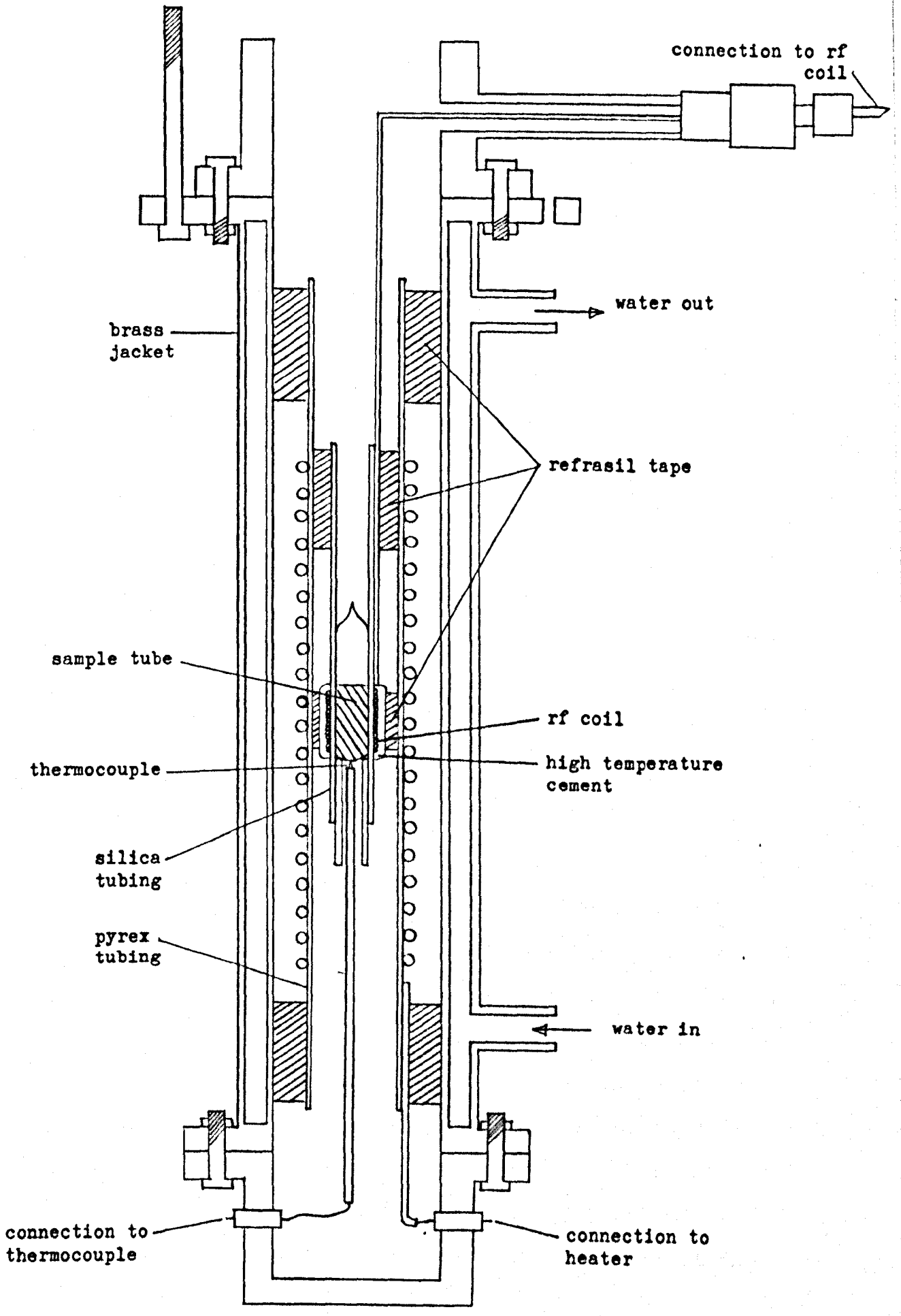

Figure 4.4 The Probe.

4.2.2 Sample Preparation

4.2.2.1 Preparation of the Rb sample and the Rb/Na alloy

Since Rubidium is highly reactive almost all the preparation of the Rb sample and the Rb/Na alloy sample was carried out in a glove box under an inert atmosphere of Argon gas.

The pure Rb sample was prepared in the following way. 99.9% pure Rb was obtained from the Koch Light Co. in the form of a 1g. sample sealed under argon in a glass ampoule. This was placed in the glove box together with the other apparatus required. The glove box was then sealed and 99.999% pure argon allowed to flow through the box for about 15 mins. thus ensuring that all the air in the box had been replaced.

About 30 ml of degassed heavy liquid paraffin together with about 2ml of oleic acid were placed in a large pyrex tube and heated to a temperature of about 60 ^{o}C by a small heating coil. The ampoule containing the Rb was then lowered into the oil and the Rb, m.p. 39.0 ^{o}C, allowed to melt. The ampoule was then quickly removed from the oil, its seal was broken, and the liquid Rb was poured into the oil. A high speed stirrer was then lowered into the oil and the mixture of oil and metal was whisked for about 10 min. During this time it was ensured that the temperature of the mixture did not fall below 39 ^{o}C. Following this the sample was transferred to a large sample tube and since it now consisted of tiny particles of Rb dispersed in oil it could

safely be removed from the glove box.

Finally, the sample was poured into a 1 cm diameter pyrex test tube and centrifuged so that most of the excess oil could be removed. The tube was then sealed off under argon at approximately ½ atmospheric pressure.

The Rb/Na alloy sample was prepared in a similar way except that, following the melting of the Rb in the ampoule, it was poured into a pre-weighed sample tube containing degassed oil. As the Rb solidified in the oil it sank to the bottom of the tube so that the tube could safely be removed from the glove box and re-weighed. The appropriate amount of Na was then added to the tube and it was returned to the glove box and the glove box sealed. After allowing about 10 min. for the atmosphere in the glove box to become inert again the oil was decanted from the sample tube. The remaining oil was then washed off several times with ether. The sample tube was then lowered into degassed oil plus a little oleic acid in a large pyrex tube and the oil was heated to about 20 ^{o}C above the liquidus temperature of the alloy. The metals were stirred with a glass rod for about 15 min. to allow them to form an alloy. During this time it was ensured that the temperature of the oil was kept well above the liquidus temperature of the alloy. The sample tube was then quickly removed from the pyrex tube and the alloy poured into the oil. The rest of the preparation then followed the same procedure as for the pure Rb sample.

4.2.2.2 Preparation of the Ga Alloys

All the metals used to prepare the Ga alloys were obtained from the Koch Light Company and were at least 99.999% pure.

The alloys were prepared and dispersed in liquid paraffin using the method described by Cartledge (9) however, since it was required to heat the alloys to temperatures well above the boiling point of liquid paraffin, about 220 ^{o}C, it was necessary to use an alternative method of insulating the alloy particles from each other. The particles were thus dispersed in silica as follows.

The alloy particles in oil were poured into a large sample tube and the particles allowed to settle to the bottom of the tube. The excess oil was then poured off and the alloy was washed several times with ether to remove the rest of the oil. An equal volume of silica powder was then added to the alloy and the mixture was vigorously shaken in ether. In this way a homogeneous mixture of alloy and silica particles was obtained. This was then transferred to a 1 cm. diameter test tube and centrifuged. Finally, the tube was sealed off under argon at about $\frac{1}{3}$ atmospheric pressure.

4.2.3 Measurement of Relaxation Rates

As stated previously measurements were made using the $\pi-\pi/2$ pulse sequence. Typical pulse lengths were as follows. For the ^{85}Rb isotope a $\pi/2$ pulse took 20μs and a π pulse 40 μs and for the ^{69}Ga isotope the corresponding pulse lengths were 8 μs and 16 μs. These will be seen to be much

shorter than the relaxation times which were of the order of 2.5 ms for ^{85}Rb and 450 μs for ^{69}Ga.

In order to achieve a reasonable signal to noise ratio all the signals were averaged. Typical averaging times were 10 min. for ^{85}Rb and 30 min. for ^{87}Rb, ^{69}Ga and ^{71}Ga.

Averaging was carried out as follows. A signal derived from the swept pulse delay was used to trigger the averager which was run in the internal advance mode at a sweep speed of 12.5 ms per point. Since only the first half of the averager memory was being used, i.e. 510 channels, each averager sweep took 6.4s. The sweep time for the linear ramp was 5s but, by adjusting the delay between sweeps to about 2s., the total cycle time was approximately 7 seconds.

Now using the $\pi-\pi/2$ pulse sequence the growth of the nuclear magnetisation is described by equation 2.10 which is

$$M(t) = M(o)\left[1-2\exp(-t/T_1)\right] \qquad 4.25$$

where M(t) represents the magnitude of the longitudinal magnetisation at time t and M(o) is the equilibrium magnetisation. Obviously in order to analyse a recovery curve one requires a baseline. This was aohieved in our experiments by blanking out the first pulse at the end of each ramp using a signal derived from the swept pulse delay unit. This left the $\pi/2$ pulse which simply gave a signal representing M(o). This signal was therefore recorded for the last 1.4s. of each averager sweep providing a convenient baseline for the preceeding curve.

A ramp of length 10 ms. was used for the ^{85}Rb spins. For the ^{87}Rb, ^{69}Ga and ^{71}Ga spins a 1 ms. ramp was used owing to their relatively shorter relaxation times. The ramps were calibrated using the circuit shown in figure 4.5. The circuit used two separate pulse generators made by Intercontinental Instruments In corporated and worked as follows. The π pulse from the Farnell pulse generator was used to trigger the first pulse generator which itself triggered the second pulse generator producing another pulse after a fixed delay. The delay was measured on the timer, an Advance Instruments Timer Counter TC8. This pulse, about 10 μs long, was fed together with the π/2 pulse, also about 10 μs long, to a coincidence circuit made from a 7408 i.c. The output from the coincidence circuit triggered a monostable multivibrator made using a 74121 i.c. which acted as a "pulse stretcher" producing an output pulse of about 400μs. This pulse was fed to the second half of the signal averager memory. By using various fixed delays several markers were obtained on the averager sweep from which the sweep could be calibrated. The sweeps used were calibrated at the beginning of the experiments and the calibrations periodically checked.

The spectrometer produced an inverted magnetisation recovery curve. Also the baseline was shifted by an amount M(ò)relative to the usual baseline representing zero magnetisation. Therefore the equation of the curve with respect to the baseline was, from 4.25

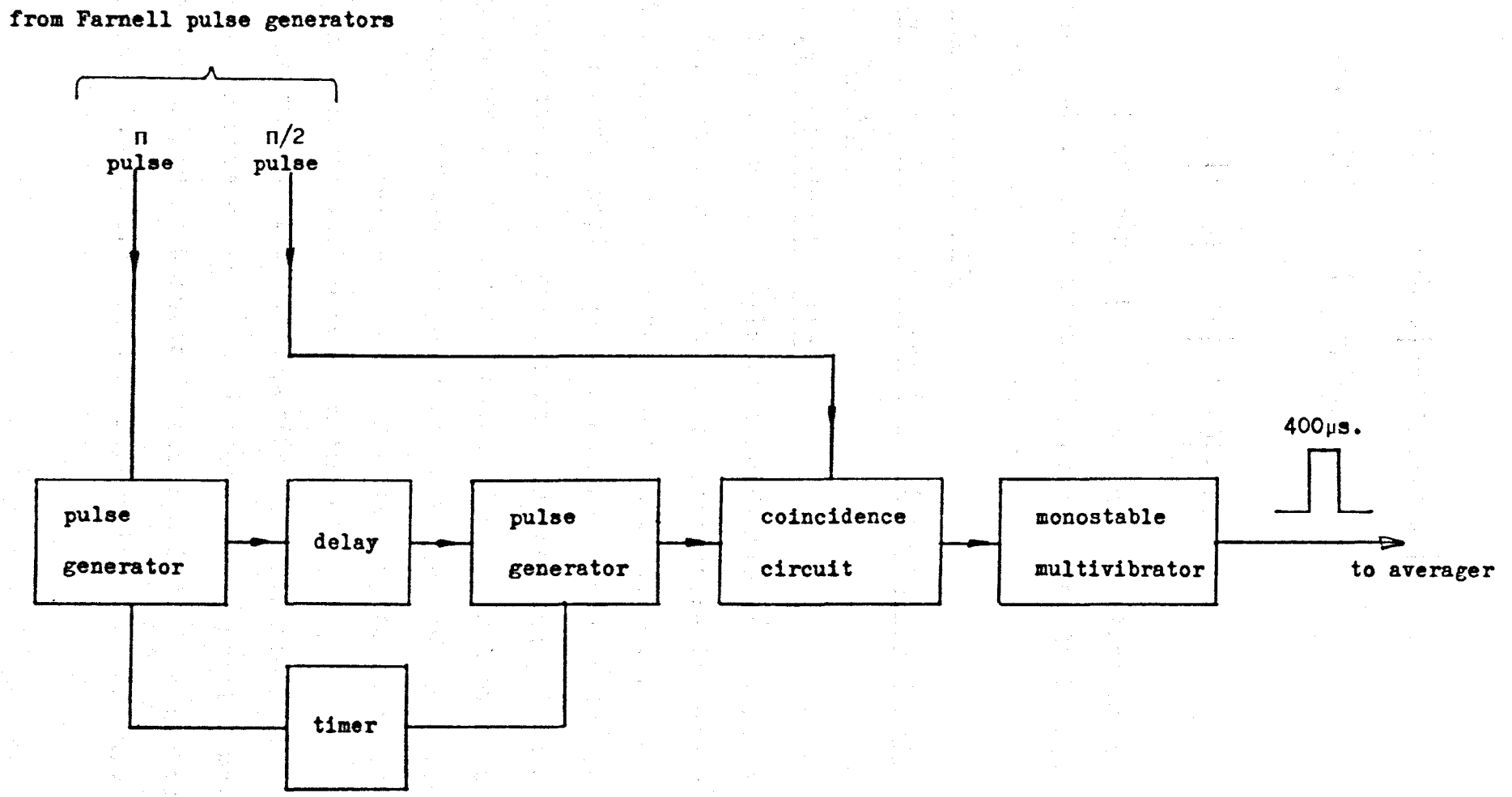

Figure 4.5 Circuit used to calibrate the ramps produced by the swept pulse delay unit.

$$M(t) = -M(o)\left[1-2\exp(-t/T_1)\right]+M(o)$$

$$\text{i.e.}\quad M(t) = 2M(o)\exp(-t/T_1) \qquad 4.26$$

Hence

$$\ln\left[M(t)\right] = \ln\left[2\,M(o)\right]-t/T_1 \qquad 4.27$$

and a graph of $\ln[M(t)]$ against t gave a straight line with gradient $-R_1$. Throughout this work the best straight line fit to the data was estimated by eye.

4.3 Experimental Data

4.3.1 Relaxation Measurements in Pure Rubidium and in the Rb50at%Na Alloy

4.3.1.1 Rubidium Results

The observed spin-lattice relaxation rates for the ^{85}Rb and ^{87}Rb spins as a function of temperature in pure Rb and in the Rb50at%Na alloy are shown in figure 4.6.

For each sample measurements were made at 10^{o} intervals starting from room temperature. The melting points of the samples are shown on the figure. The upper limits to the temperature ranges were determined by the decomposition of the samples. This was probably caused by reaction of the metals with residual oxygen in the oil.

The quadrupolar and hyperfine contributions to the total relaxation rate of the ^{85}Rb isotope were separated using the method outlined in Chapter 2, section 2.1. The method uses equations 2.1 to 2.4 which we repeat here for convenience.

For two isotopes A and B we have

$$R_{1A} = R_{1m}^{A} + R_{1q}^{A} \qquad 4.28$$

$$R_{1B} = R_{1m}^{B} + R_{1q}^{B} \qquad 4.29$$

also
$$\frac{R_{1q}^{A}}{R_{1q}^{B}} = \frac{F(I_A)}{F(I_B)} \left[\frac{Q_A}{Q_B}\right]^2 = \Theta \qquad 4.30$$

where $F(I) = \dfrac{2I+3}{I^2(2I-1)}$

and
$$\frac{R_{1m}^{A}}{R_{1m}^{B}} = \left[\frac{\gamma_n^{A}}{\gamma_n^{B}}\right]^2 = \Phi \qquad 4.31$$

Solving these equations for R_{1m}^{A}, R_{1q}^{A}, R_{1m}^{B} and R_{1q}^{B} we have

$$R_{1m}^{A} = \frac{R_{1A} - \Theta R_{1B}}{1 - \Theta/\Phi} \qquad 4.32$$

$$R_{1q}^{A} = \frac{R_{1A} - \Phi R_{1B}}{1 - \Phi/\Theta} \qquad 4.33$$

$$R_{1m}^{B} = R_{1m}^{A}/\Phi \qquad 4.34$$

$$R_{1q}^{B} = R_{1q}^{A}/\Theta \qquad 4.35$$

Equations 4.32 and 4.33 were used to reduce the total relaxation rate of ^{85}Rb into its component parts. The value of $\dfrac{\gamma_n^{85}}{\gamma_n^{87}}$ used was 0.295 and $\dfrac{Q_{85}}{Q_{87}}$ was taken as 2.067. The

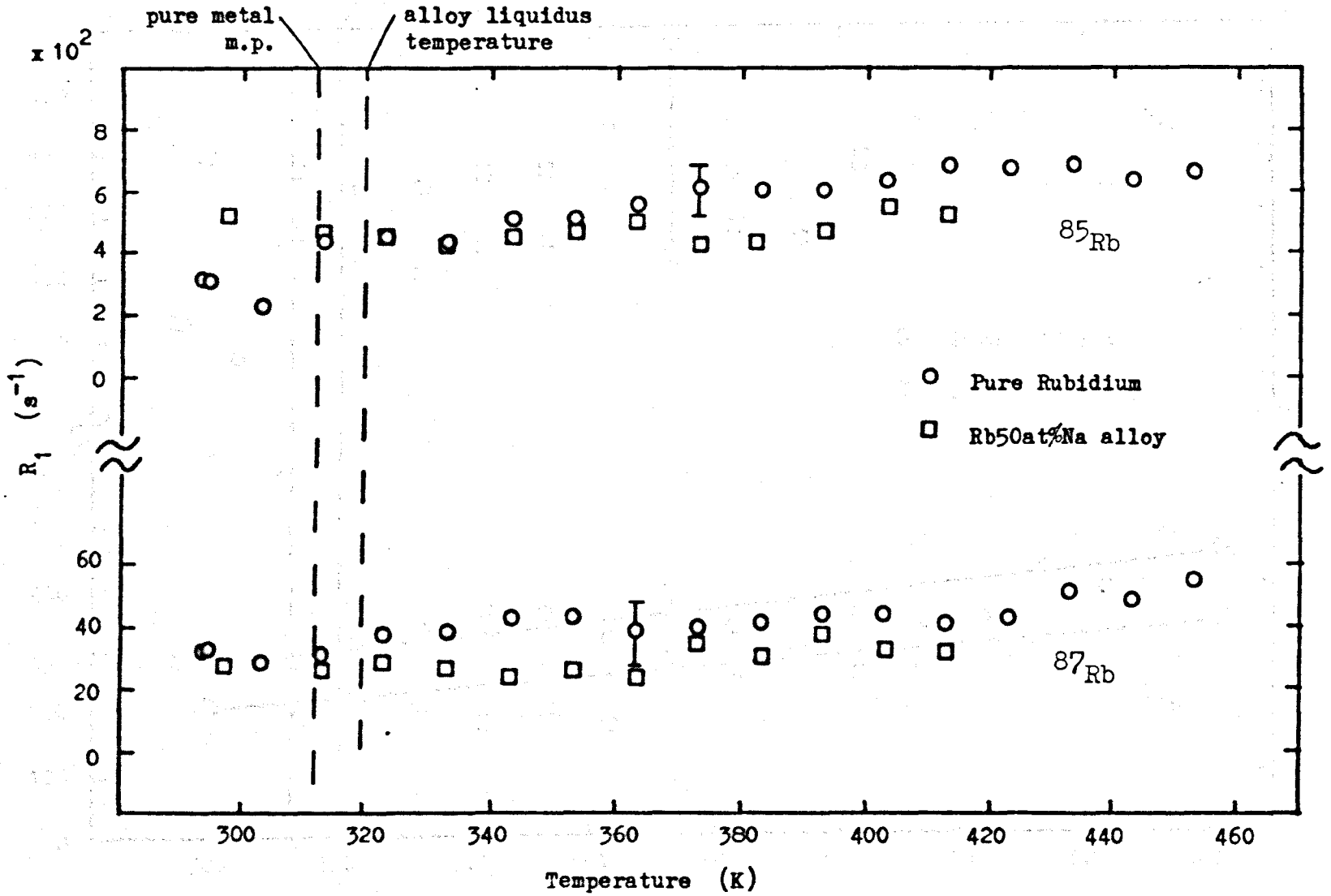

Figure 4.6 Variation of R_1 with temperature for the ^{85}Rb and ^{87}Rb spins in pure Rb and in the Rb50at%Na alloy.

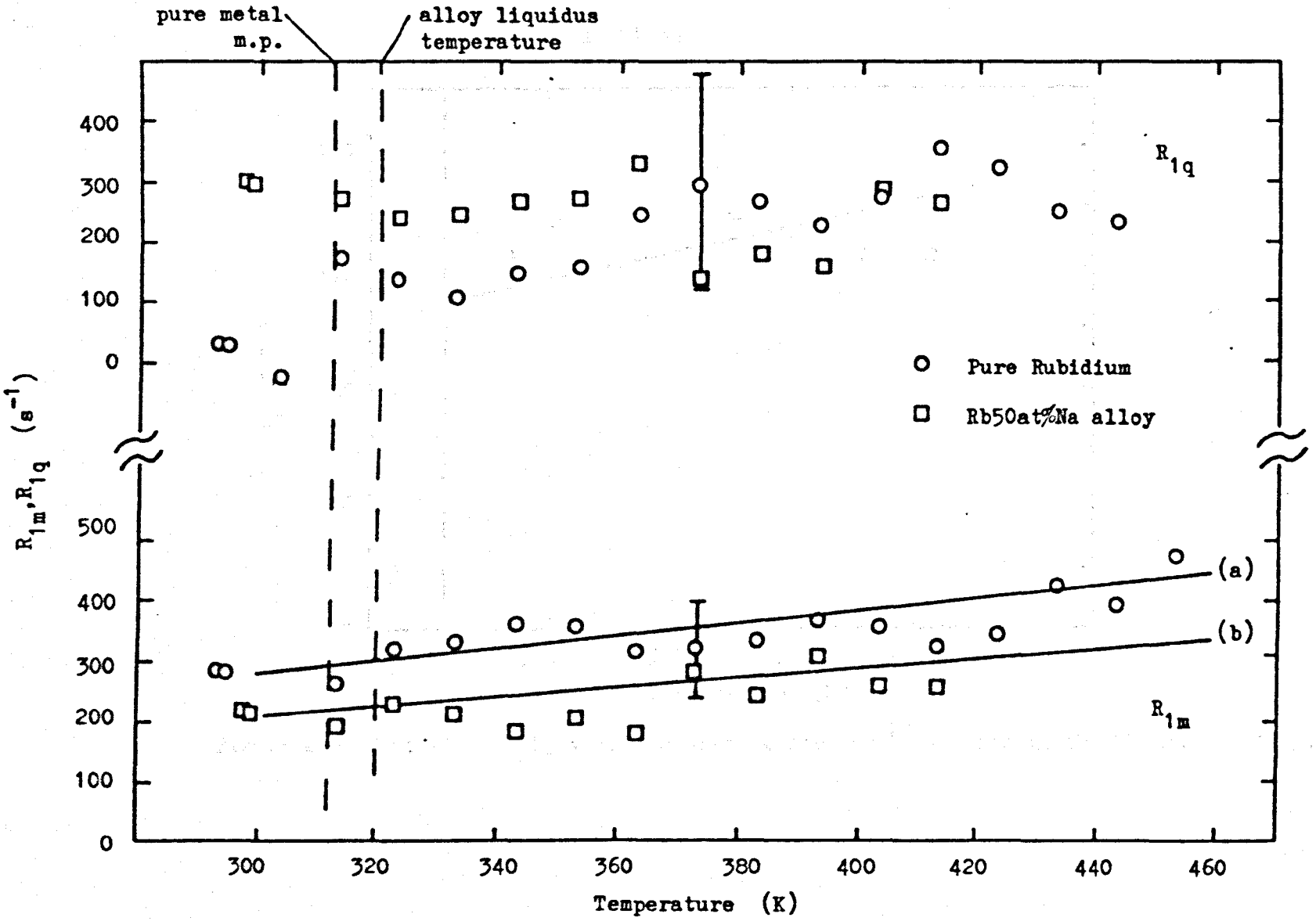

Figure 4.7 Variation of R_{1m} and R_{1q} with temperature for the ^{85}Rb spins in pure Rb and the Rb50at%Na alloy.

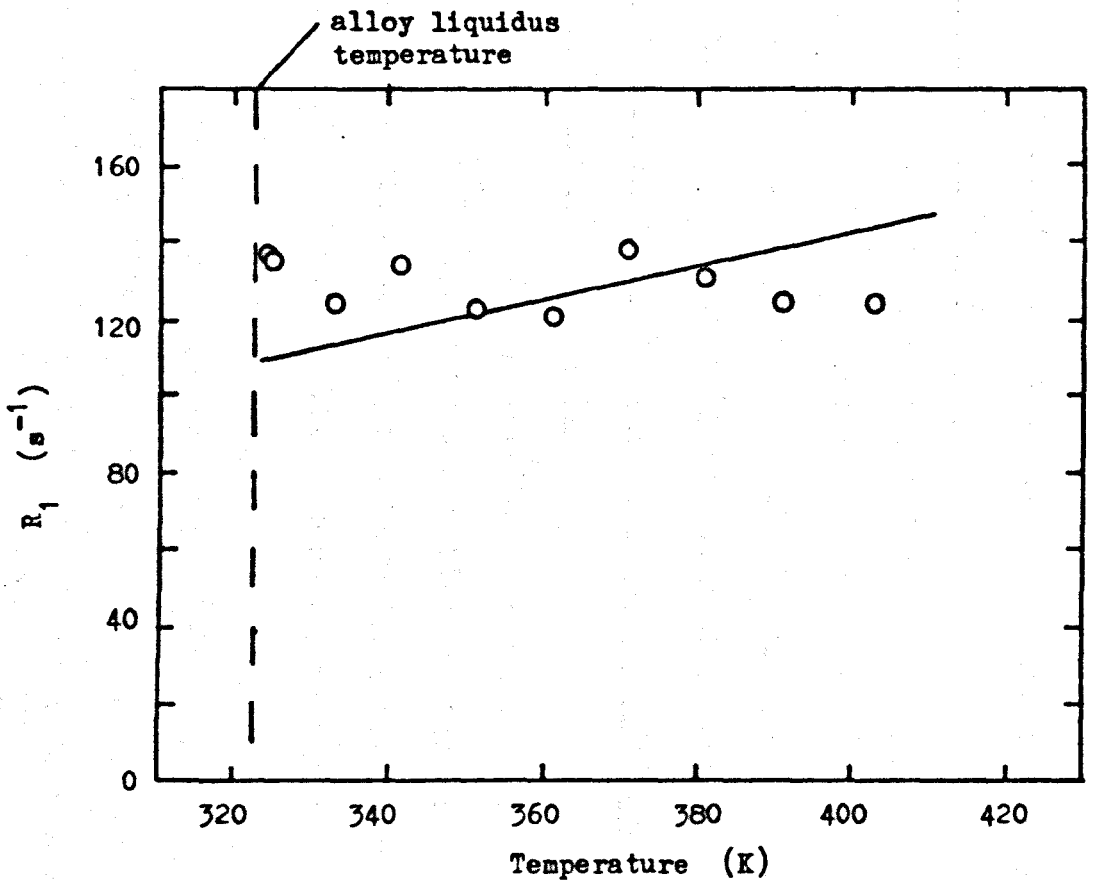

Figure 4.8 Variation of R_1 with temperature for the ^{23}Na spins in the Rb50at%Na alloy.

values of R_{1q}^{85} and R_{1m}^{85} derived in this way are shown as a function of temperature in pure Rb and in the Rb50at%Na alloy in figure 4.7. The corresponding values for the ^{87}Rb isotope can be calculated using equations 4.34 and 4.35.

The errors in the derived values of R_{1q} and R_{1m} depend upon the accuracy of the values of R_1 for ^{85}Rb and ^{87}Rb. Typical limits of error are indicated in the figures.

4.3.1.2 Sodium Results

The observed spin lattice relaxation rate for the ^{23}Na spins as a function of temperature in the Rb50at%Na sample are shown in figure 4.8. The lower end of the temperature range was determined by the liquidus temperature of the alloy.

4.3.2 Relaxation Measurements in the Gallium Alloys

4.3.2.1 Gallium Results

The observed spin-lattice relaxation rates for the ^{69}Ga and ^{71}Ga spins as a function of temperature in Ga20at%Al, Ga61.5at%Bi, Ga10at%Mg and Ga20at%Mg are shown in Figures 4.9, 4.10 and 4.11. The lower end of the temperature range was determined by the liquidus temperature of each alloy.

Isotopic separation of the ^{69}Ga rates into the quadrupolar and hyperfine contributions was achieved in the manner described above. The value used for $\frac{\gamma_n^{69}}{\gamma_n^{71}}$ was 0.787 and for $\frac{Q_{69}}{Q_{71}}$ the value 1.586 was used.

The temperature dependence of the derived values of R_{1q} and R_{1m} for ^{69}Ga in the alloys studied is shown in Figures 4.12, 4.13 and 4.14.

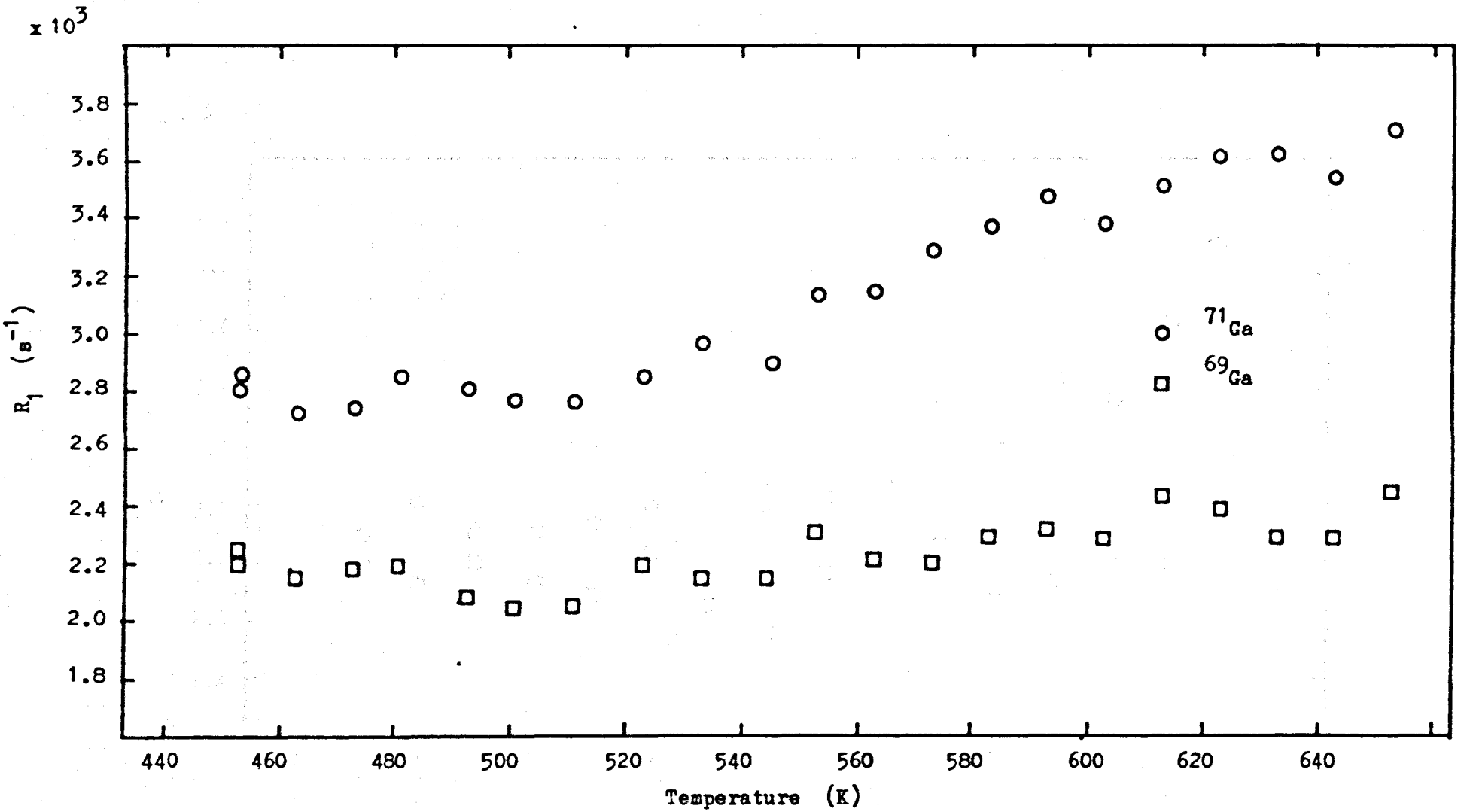

Figure 4.9 Variation of R_1 with temperature for the ^{69}Ga and ^{71}Ga spins in Ga20at%Al.

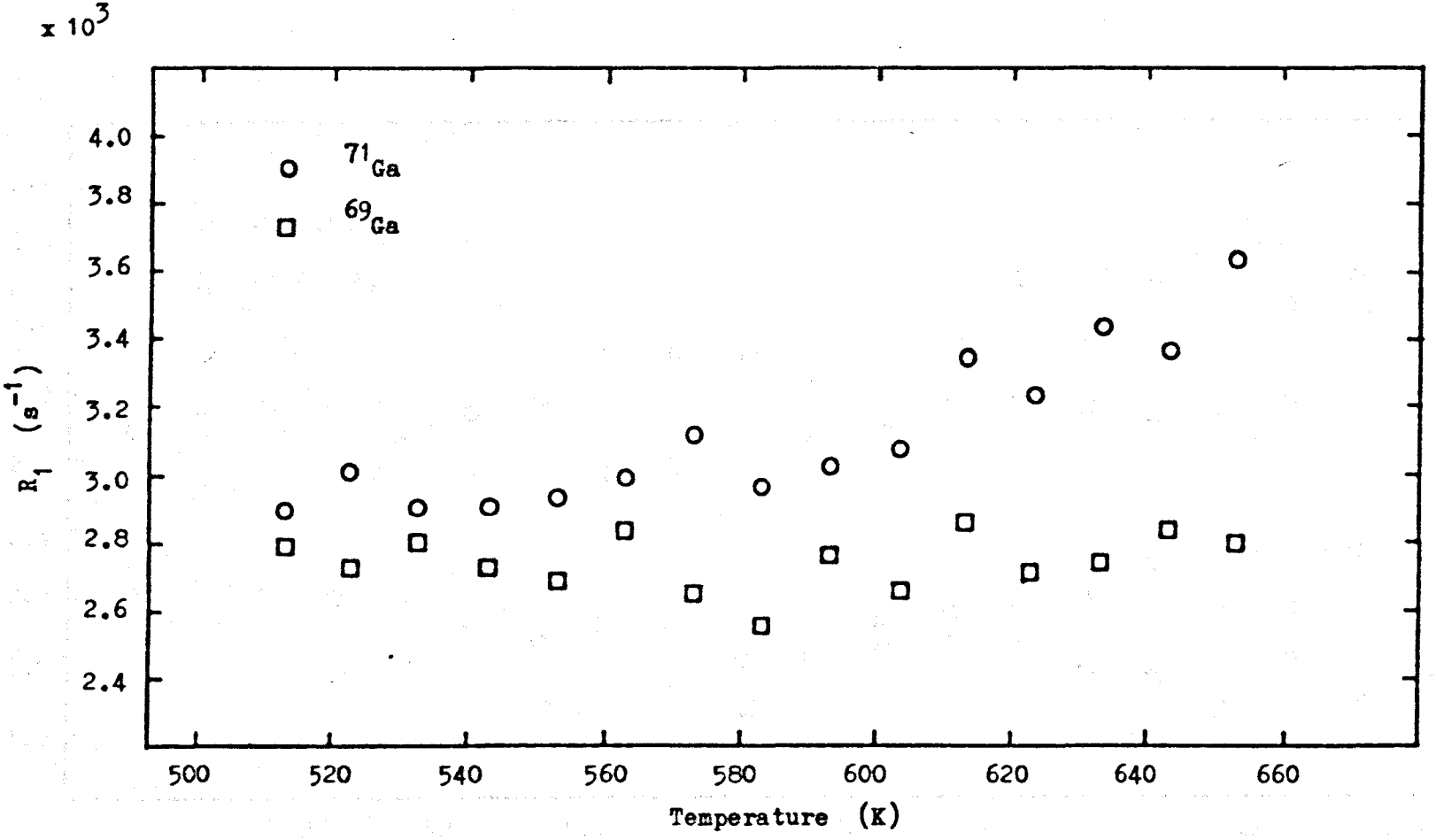

Figure 4.10 Variation of R_1 with temperature for the ^{69}Ga and ^{71}Ga spins in Ga61.5at%Bi.

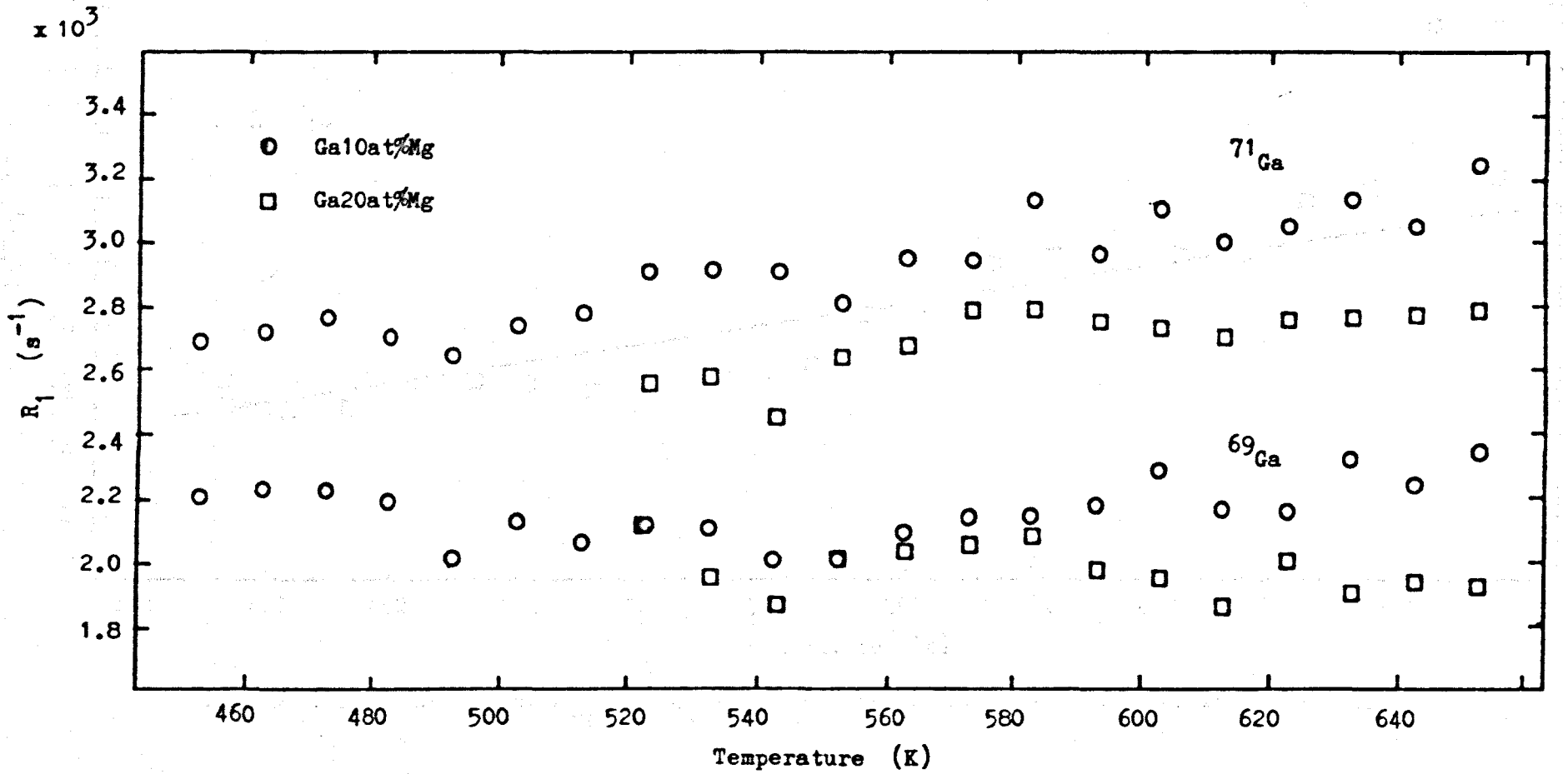

Figure 4.11 Variation of R_1 with temperature for the ^{69}Ga and ^{71}Ga spins in Ga10at%Mg and Ga20at%Mg.

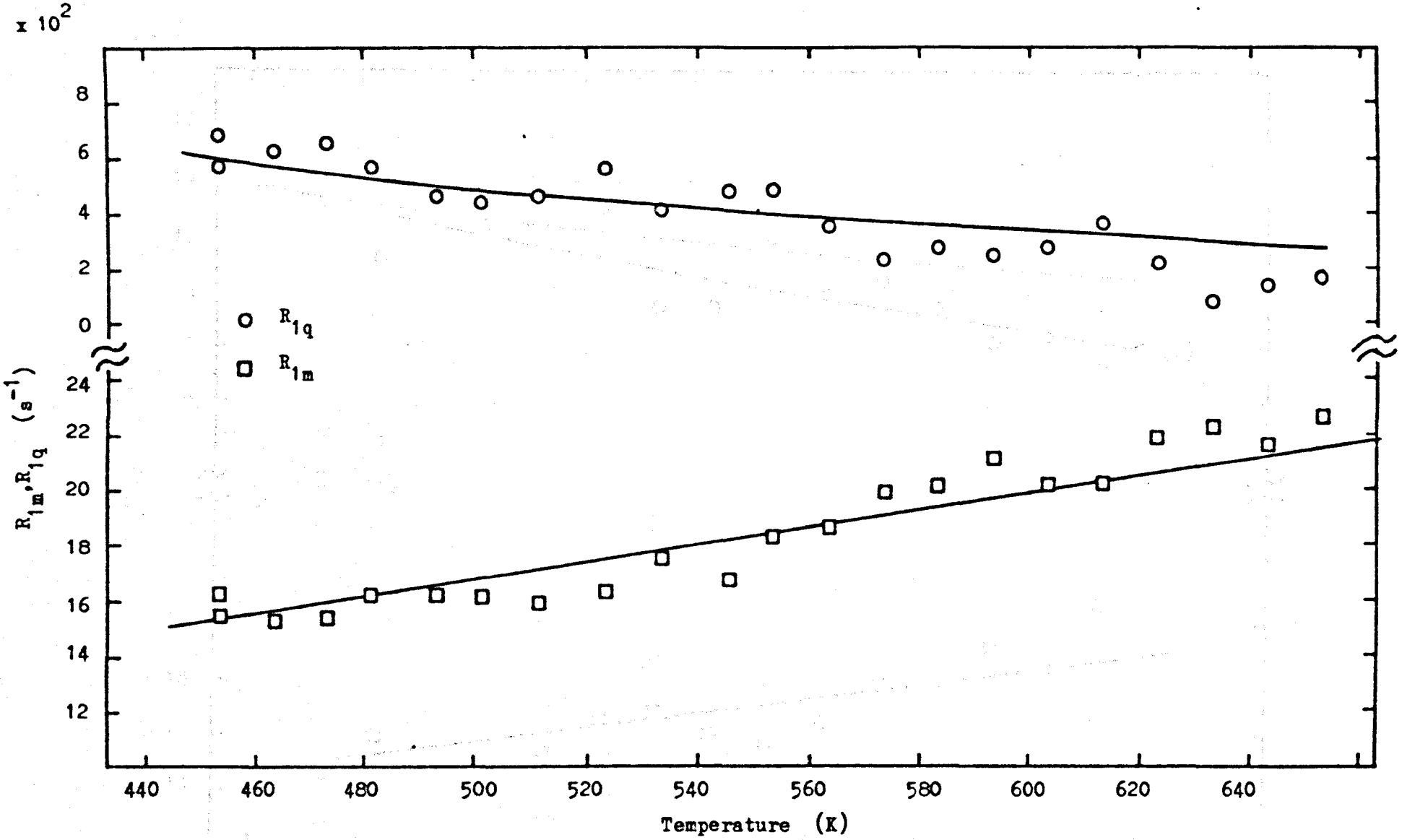

Figure 4.12 Variation of R_{1q} and R_{1m} with temperature for the ^{69}Ga spins in Ga20at%Al.

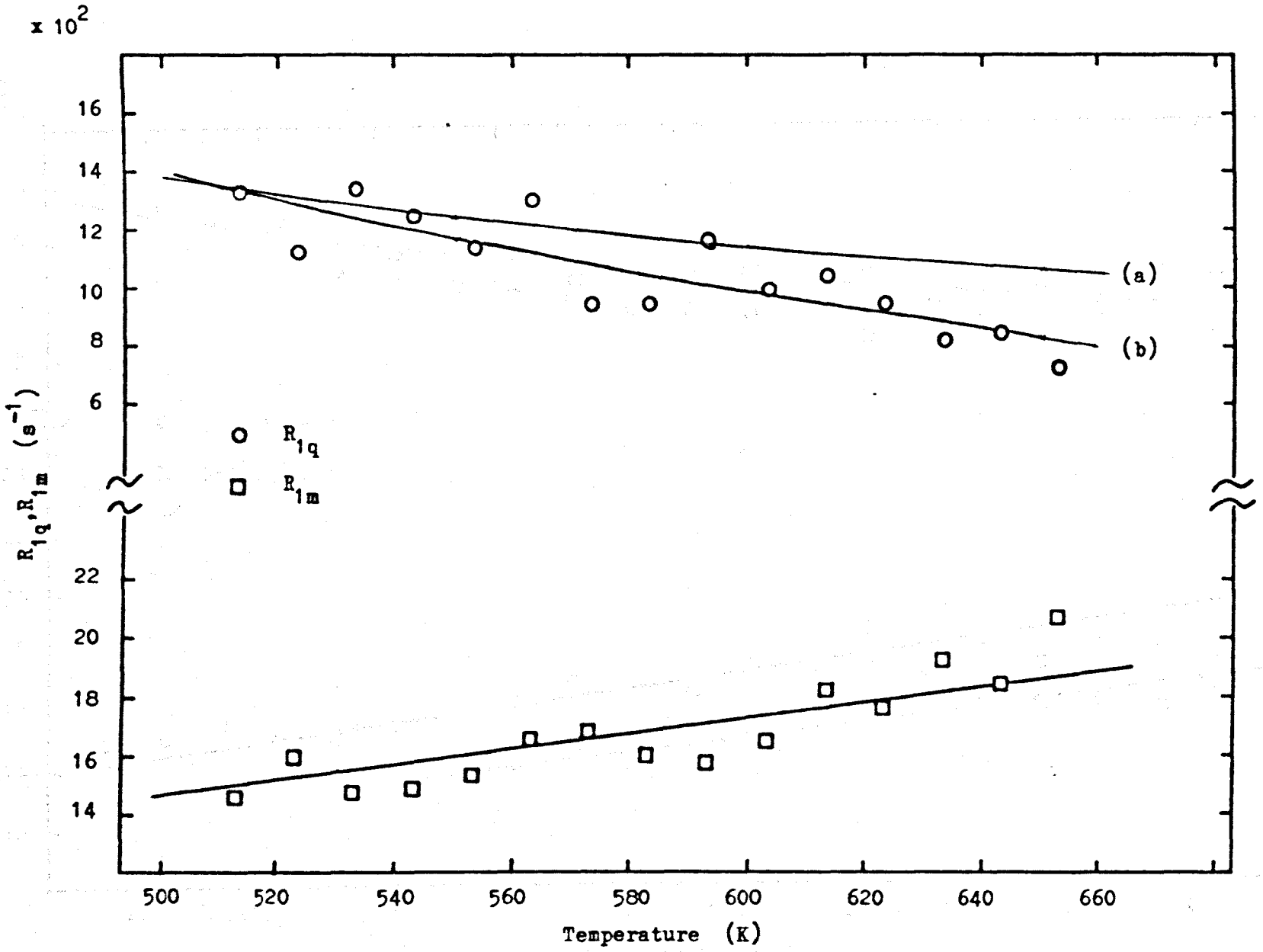

Figure 4.13 Variation of R_{1q} and R_{1m} with temperature for the ^{69}Ga spins in Ga61.5at%Bi.

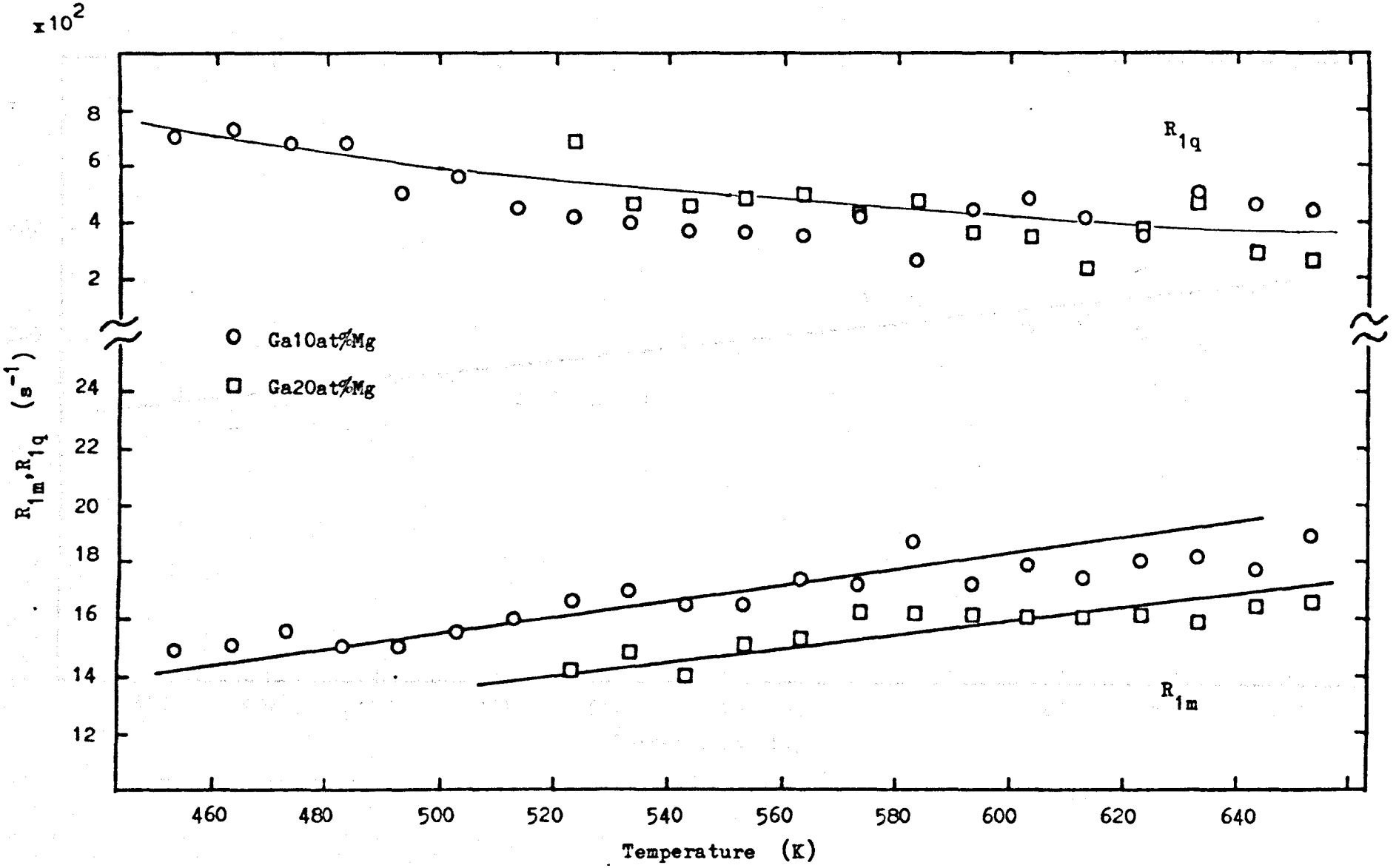

Figure 4.14 Variation of R_{1q} and R_{1m} with temperature for the ^{69}Ga spins in Ga10at%Mg and Ga20at%Mg.

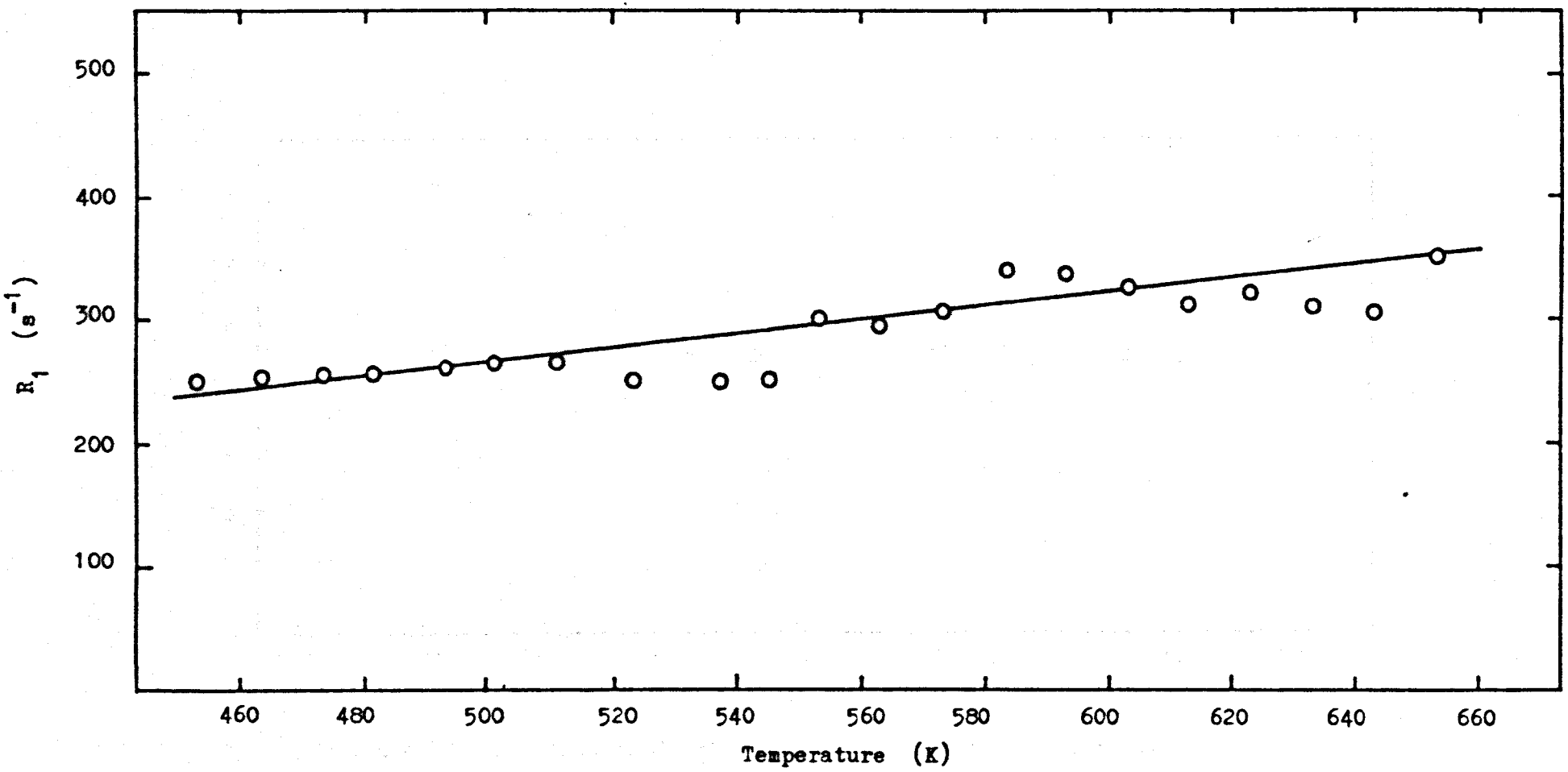

Figure 4.15 Variation of R_1 with temperature for the ^{27}Al spins in Ga20at%Al.

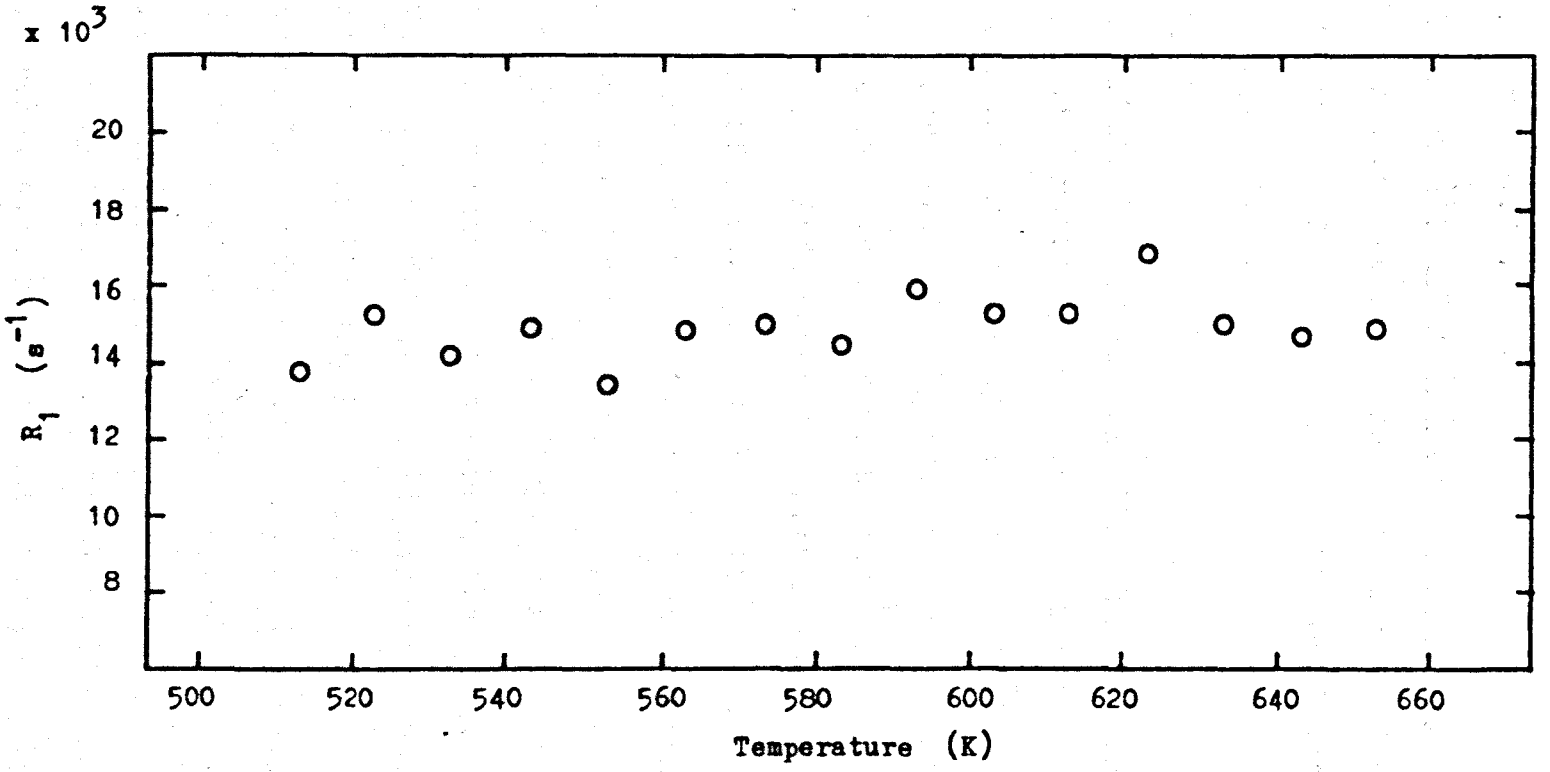

Figure 4.16 Variation of R_1 with temperature for the ^{209}Bi spins in Ga61.5at%Bi.

4.3.2.2 Aluminium Results in the Ga20at%Al Alloy

The variation of the spin-lattice relaxation rate as a function of temperature for the ^{27}Al spins in Ga20at%Al is shown in figure 4.15.

4.3.2.3 Bismuth Results in the Ga61.5at%Bi Alloy

The observed spin-lattice relaxation rate for the ^{209}Bi spins as a function of temperature in the Ga61.5at%Bi alloy is shown in figure 4.16.

4.4 Discussion

4.4.1 Results obtained in Pure Rb and the Rb/Na Alloy

Holcomb and Norberg (5) measured T_1 for the ^{85}Rb and ^{87}Rb spins over the temperature range 253°K to 413°K. Above the melting point our values for R_1 for ^{85}Rb are about 20% smaller than theirs whereas our values of R_1 for ^{87}Rb are approximately 10% higher. These differences lie within the joint error bars of the two sets of data. Below the melting point we do not observe the sharp discontinuity in R_1 that is seen in their data. This latter difference may be explained by the presence of impurities in their sample. They, in fact, state that the purity of the Rb sample was not especially good. Furthermore they find $T_2 < T_1$ for ^{85}Rb in the liquid phase which tends to suggest impurities in the sample. Although we did not check the equality of T_1 and T_2 in our samples they were, as stated in 4.2.2.1, prepared from Rb which was 99.9% pure.

4.4.1.1 Hyperfine Contribution to R_1 for ^{85}Rb

Assuming only s-like contributions to the Knight shift and magnetic relaxation rate our data may be analysed using the modified Korringa relationship given in Chapter 1, equation 1.11, which is

$$R_{1s} = 4\pi k_B \gamma_n^2 K_s^2 TK(\alpha)(\hbar\gamma_e^2)^{-1} \qquad 4.36$$

The solid line (a) on figure 4.7 shows a fit of this equation to our pure metal data using the Knight shift measurements of Gutowsky and McGarvey (10) (11) who give the Knight shift at the melting point $K_L = 0.662\%$ and $\frac{1}{K_L} \cdot \frac{\partial K_L}{\partial T} = 14.10^{-5}$. The fitted line assumes $K(\alpha) = 0.60$ and is independent of temperature. In a similar analysis of Holcomb and Norberg's data Rossini and Knight (6) find $K(\alpha) = 0.75$ in the pure metal.

The Knight shifts of both components of the Rb/Na alloy system have been measured over a wide range of composition by Rimai and Bloembergen (12) and van Hemmen et al. Both authors find the familiar linear dependence of Knight shift on concentration but differ on the magnitude of $K_o^{-1}\frac{\partial K}{\partial c}$ where K_o represents the shift of the resonant nucleus in the absence of the non-resonant nucleus whose concentration in the alloy is given by c. Rimai and Bloembergen find $K_o^{-1}\frac{\partial K}{\partial c} = 0.518$ and 0.270 for Na and Rb in Na/Rb whereas van Hemmen et al give values of 0.54 and 0.45. Now it is a general rule (14) that $K_o^{-1}\frac{\partial K}{\partial c}$ is approximately the same for each atomic species in a binary alloy. Therefore we shall use the data given by van Hemmen et al . We shall assume that $\frac{\partial K_L}{\partial T}$ is the same as in the pure metal. Then, again, assuming that K and R_{1m} have only s-like contributions line (b) on figure 4.7 shows a fit of equation 4.36 to our data which gives a value of $K(\alpha) = 0.74$. The difference

between this and the value of K(α) obtained for the pure metal is probably not significant and merely reflects experimental error. However, the fact that values of K(α) lying in the range 0.60 to 0.75 have been obtained in the pure metal and alloy indicates the relative unimportance of non-s terms.

4.4.1.2 Quadrupolar Contribution to R_1 for ^{85}Rb

In the pure metal our R_{1q} values of ^{85}Rb are about four times larger than those obtained by Rossini and Knight. This is due to the differences in the original R_1 data. Owing to the large error bars on our R_{1q} data it is difficult to say with any degree of certainty how R_{1q} varies with temperature although it does appear to increase slowly with temperature. Rossini and Knight concluded from their analysis that R_{1q} was constant with increasing temperature although, once again, their error bars were quite large. It may be instructive to note how these relatively large error bars arise. The average error in our measurements of R_1 for ^{87}Rb was about 20% and that in ^{85}Rb about 10%. However, when equation 4.33 is used to calculate R_{1q} for ^{85}Rb, because of the close cancellation between the terms in the numerator the nett error is about 60%. This close cancellation arises because of the relative magnitudes of the total relaxation rates of the two isotopes and the value of Φ, the ratio of the gyromagnetic ratios. Thus, although the two isotopes of Rb have quite different gyromagnetic ratios and the hyperfine and quadrupolar contributions to R_1 for ^{85}Rb are both

significant Rb turns out not to be such a good candidate for separating the relaxation components as one would expect.

Again, owing to the large error it is difficult to say how R_{1q} varies in the alloy.

4.4.1.3 Analysis of the ^{23}Na Data

The variation of R_1 with temperature in pure liquid Na has been measured by Holcomb and Norberg (5), Narath and Weaver (15) and Jolly and Titman (16). No evidence for a quadrupole contribution to R_1 has been found and all the authors agree that the contact term determines the magnetic relaxation in the liquid phase.

The variation of R_1 with temperature for the ^{23}Na spins in Na/Tl alloys has been determined by Hanabusa and Bloembergen (17) and Jolly and Titman (16) who also investigated Na/Hg alloys. The latter authors found that in the alloys Na7at% Tl, Na10at%Hg and Na15at%Hg a substantial quadrupolar contribution to R_1 was present which varied with temperature approximately as D^{-1}.

The straight line on figure 4.8 indicates the variation of R_{1s} calculated from equation 4.36. K_s was calculated from the value of the Knight shift at the m.p. for pure Na, $K_L = 0.116\%$ (10) (11) and $\frac{1}{K_o}.\frac{\partial K}{\partial c} = 0.54$ (13). We have assumed that $\frac{1}{K_L}\frac{\partial K_L}{\partial T} = 18.10^{-5}$, the same as in the pure metal (18). This is not unreasonable as Kellington and Titman (19) found that $\frac{\partial K_L}{\partial T}$ is unaffected by the addition of Tl to Na.

Finally, we assumed that K(α) is unchanged from the pure metal value 0.62 given by Jolly and Titman. It will be seen from Figure 4.8 that the trend of the data suggests the presence of a quadrupole contribution to R_1 which is relatively very small compared to the hyperfine contribution. This result is similar to that obtained by Kaeck who studied Rb/Cs alloys (7). Unfortunately, since R_{1q} is only of the same order of magnitude as the experimental error it is impossible to accurately determine its temperature dependence.

4.4.2 Results Obtained in Ga Alloys

Cartledge et al (4) (9) have measured the variation of R_1 with temperature for the ^{69}Ga and ^{71}Ga spins in pure liquid Gallium over a temperature range of 240°K to 570°K. They found that the magnetic contribution, R_{1m}, to the relaxation rate of ^{69}Ga fitted the modified Korringa relationship given by equation 4.36 with K(α) independent of temperature and equal to 0.694. It was therefore concluded that non-s contributions to the relaxation and Knight shift were not significant. Their data for R_{1q} for ^{69}Ga showed a variation with temperature approximately proportional to $T^{-\frac{1}{2}}$. This data is, in fact, shown in chapter 2, Figure 2.9. Similar results to these have also been obtained by Kerlin (20).

4.4.2.1 The Hyperfine Contribution to R_1 for ^{69}Ga in the Alloys

Since the analysis of the temperature variation of the

hyperfine contribution to R_1 is not the main point of this thesis only a brief discussion will be given.

As far as the author is aware there have been no reported measurements of the Knight shift of Ga in Ga/Al, Ga/Bi or Ga/Mg alloys. Therefore, in order to proceed we shall assume that the Ga Knight shift is the same as in the pure metal i.e. K_s = 0.4528% and also that its variation with temperature is given by $\frac{1}{K_L}.\frac{\partial K_L}{\partial T} = -7.2.10^{-5}$ as in the pure liquid metal.

Again, assuming only s-like contributions, and a K(a) that is independent of temperature, the straight lines on Figures 4.12, 4.13 and 4.14 indicate a fit of equation 4.36 to the R_{1m} data obtained in the Ga20at%Al, Ga61.5at%Bi, Ga10at%Mg and Ga20at%Mg alloys. There seems little point in deriving values of K(a) from these lines due to our lack of knowledge of the true Knight shift. However, the goodness of fit probably indicates that the hyperfine interaction in these alloys is adequately described by the modified Korringa relationship. It is interesting to note that Cartledge et al (4) (9) found that equation 4.36 described the R_{1m} data in Ga/In, Ga/Sn and Ga/Zn alloys where the Ga Knight shift is known and found no evidence of substantial non-s contributions.

4.4.2.2 Analysis of R_1 data for ^{27}Al in Ga20at% Al

El-Hanany and Zamir (21) have shown that in pure Al R_1 is entirely due to the hyperfine interaction. The straight line on Figure 4.15 shows a fit of equation 4.36

to the ^{27}Al R_1 results obtained in the Ga20at%Al alloy using $K_L = 0.162\%$ and $\frac{1}{K_L}.\frac{\partial K_L}{\partial T} = 0.84.10^{-5}\ ^{o}K^{-1}$, the values appropriate to pure Al.

Although we have not used the true Knight shift for the alloy the fitted line indicates that R_1 can be accounted for by the hyperfine interaction. This conclusion agrees with that of Cartledge (9) who measured R_1 for ^{27}Al in Ga8at%Al and Claridge et al (22) who studied Al 11 at%Si. The probable explanation for the unobservable R_{1q} in Al and its alloys is the small value of the Sternheimer antishielding factor.

4.4.2.3 Analysis of R_1 data for ^{209}Bi in Ga61.5at%Bi.

The variation of R_1 with temperature in pure Bi has been studied by Rossini and Knight (6) and Heighway and Seymour (23) using nmr techniques. Both groups agree that the data is best interpreted by assuming a substantial contribution to the Knight shift from non-s electrons, the contribution from the orbital term and from core-polarisation due to p-type electrons being of the order of $-0.25K_s$. Taking this into account and using 4.36 to estimate R_{1s} Heighway and Seymour found a small quadrupolar contribution which varied with temperature as D^{-1}. However, as mentioned in chapter 2, recent pac measurements (24) on trace amounts of ^{207}Po in liquid Bi have shown unequivocally that R_{1q} varies approximately as $T^{-\frac{1}{2}}$. This clearly shows the danger in attempting to separate the hyperfine and quadrupolar contributions using the Korringa relationship.

We have the further difficulty in attempting to analyse our data in the Ga61.5at%Bi alloy in that we do not know the Bi Knight shift in this alloy. It is possible to fit equation 4.36 to the data shown in Figure 4.16 using the value of K_s for pure Bi. However, the general trend of the data is found to be flatter than that given by this analysis and, bearing in mind the experimental error, it is tentatively concluded that there is a small quadrupolar contribution present. It should be noted that Claridge et al (22) examined the alloys Bi50at%In, Bi50at%Pb, Bi50at%Sb and Bi50at%Sn using nmr and found, in each alloy, a quadrupolar contribution to R_1 for ^{209}Bi which had a fairly rapid variation with temperature. However, once again, these authors used the Korringa relationship to estimate the hyperfine contribution.

4.4.2.4 Quadrupolar Contribution to R_1 for ^{69}Ga in the Alloys

As a preliminary exercise we shall attempt to fit the theoretical expression for R_{1q} in a substitutional alloy given by equations 4.22, 4.23 and 4.24 to the data obtained with the Ga61.5at%Bi alloy. We choose this alloy because its concentration is nearest to the 50at% value where, theoretically, the largest diffusion like contribution is present.

The Schirmacher formula for $v_2(r)$ given by equation 3.59 gives a proportional to the ionic charge, Z, and hence the valency. Claridge et al (22) have found no evidence for this. However, this is probably due to the fact that the proportionality only holds for substitutional alloys. For the Ga/Bi alloy we have $a = 5/3$. We shall take B = 10A

from the difference between the two and three particle terms found in the calculations of Chapter 3. Larsson et al (25) have measured D for Ga between 303°K and 500°K. Their results show that D is approximately proportional to T^2 over this temperature range and we shall assume a similar proportionality occurs above 500°K. Then the curve (a) on Figure 4.13 represents the variation of R_{1q} predicted by equation 4.22 assuming $A \propto T^{-\frac{1}{2}}$ and $B \propto D^{-1}$.

It will be seen that the trend of the data is much faster than that predicted by the substitutional theory. In fact a better fit to the data is obtained by putting $R_{1q} \propto D^{-1}$ as shown by curve (b). The data for R_{1q} in the Ga10at%Mg, Ga20at%Mg and Ga20at%Al alloys also fit a variation of this form as shown by the curves on Figures 4.12 and 4.14.

The fact that R_{1q} in these alloys is found to vary with temperature more rapidly than the theory predicts must be due to the fact that the alloys are non-substitutional and related to the "size effect" described by Cartledge et al (4). Consider the relaxing nucleus surrounded by a shell of atoms. The presence of a bigger or smaller atom in the shell will cause a large distortion in the electric field gradient. Should this atom leave the shell via a diffusive step then the effect will be a large 1/D contribution to R_{1q}.

During the course of the present work an expression for R_{1q} in a binary alloy has been published by von Hartrott et al (2). Their treatment is based upon the extension of

Warren's theory to binary alloys by Gabriel (26). Gabriel's expression forthe relaxation rate in a binary alloy may be written as

$$R_{1q} \propto \int \Big[c_a^2 u_a(q)^2 a_{aa}(q) + c_b^2 u_b(q)^2 a_{bb}(q) + 2c_a c_b u_a(q) u_b(q) a_{ab}(q) + \Big[u_a(q) - u_b(q)\Big]^2 c_a c_b \Big] S_s(q,o) d^3q \qquad 4.37$$

where $a_{aa}(q)$, $a_{bb}(q)$ and $a_{ab}(q)$ are partial interference functions and $u_a(q)$ and $u_b(q)$ are the Fourier transforms of the effective field gradients caused at the probe atom by the two atomic species constituting the alloy.

Using the mean interference function $\bar{a}(q)$ defined by

$$\bar{a}(q) = \frac{c_a^2 a_{aa} u_a^2 + c_b^2 u_b^2 a_{bb} + c_a c_b u_a u_b a_{ab}}{c_a^2 u_a^2 + c_b^2 u_b^2 + c_a c_b u_a u_b} \qquad 4.38$$

equation 4.37 can be rearranged in a form that is analagous to the cross section for scattering of neutrons from an ensemble of nuclei containing two nuclear species with different scattering length; here the total cross section consists of a coherent and an incoherent part.

$$R_{1q} \propto \int_0^\infty \Big[u_{coh}(q)^2 \bar{a}(q) + u_{inc}(q)^2 \Big] S_s(q,o) d^3q$$

where $$u_{coh}(q)^2 = \Big[c_a u_a(q) + c_b u_b(q) \Big]^2$$

and $$u_{inc}(q)^2 = c_a c_b \Big[u_a(q) - u_b(q) \Big]^2 \qquad 4.39$$

Finally, using the Vineyard approximation, $S(q,\omega) = a(q)S_s(q,\omega)$, equation 4.39 gives

$$R_{1q} \propto \int \left[u_{coh}(q)^2 S(q,\omega) + u_{inc}(q)^2 S_s(q,\omega) \right] d^3q \qquad 4.40$$

It is then argued by the authors that R_{1q} consists of two distinct terms, the first of which does not change appreciably with temperature but the second of which varies approximately as D^{-1}. However, this is not at all apparent from the form of equation 4.40. The first term is similar to the formulae given by Sholl and Warren for the pure metal case and therefore gives an approximately 1/D dependence. Also $u_{inc}(q)^2$ in the second term is a series of small peaks extending up to large q values and therefore this term does not give a 1/D dependence. Thus we dispute von Hartrott's interpretation of equation 4.40 and point out that it does not correctly describe the variation with temperature of R_{1q} in a binary alloy as he suggests.

4.4.3 Summary

In this chapter our new version of the theory of quadrupole relaxation in liquid metals has been extended to cover the case of liquid binary alloys. It was found that the theory predicted an increase in the rate of variation of R_{1q} with temperature with increase in alloy concentration.

Unfortunately, the experiments on the Rb50at%Na alloy gave results for R_{1q} that were not accurate enough to compare with the theory. However, an increase in the rate of variation of R_{1q} for the ^{69}Ga spins was found in the alloys

Ga10at%Mg, Ga20at%Mg, Ga20at%Al and Ga61.5at%Bi in qualitative agreement with the theory. Similar results have been obtained by Cartledge et al (3) in Ga/In alloys and von Hartrott et al (2) in InSb.

Thus the theory appears to give a reasonable description of quadrupolar relaxation in liquid metals and alloys. Furthermore, it is likely to be applicable to the liquid inert gases, with the use of the appropriate interatomic potentials, and it also appears to explain recent unpublished data on molten alkyl halides (27)

4.5 References

1) W.W. Warren Jn. and W.G. Clark, Phys Rev., 177, 600 (1969)

2) M. von Hartrott, K. Nishiyama, J. Rossbach, E. Weihreter and D. Quitmann, J. Phys. F: Metal Phys., 7, 713 (1977)

3) G. Cartledge, R.L. Havill and J.M. Titman, J. Phys. C: Solid State Phys., 6, L23 (1973)

4) G Cartledge, R.L. Havill and J.M. Titman, J. Phys. F: Metal Phys., 6, 639 (1976)

5) D.F. Holcomb and R.E. Norberg, Phys. Rev., 98, 1074 (1955)

6) F.A. Rossini and W.D. Knight, Phys. Rev., 178, 641 (1969)

7) J.A. Kaeck, Phys. Rev. B. 5, 1659 (1972)

8) R.I. Jolly, Thesis 1973, Sheffield University

9) G. Cartledge, Thesis 1976, Sheffield University

10) H.S. Gutowsky and B.R. McGarvey, J. Chem Phys., 20, 1472 (1952)

11) B.R. McGarvey and H.S. Gutowsky, J. Chem Phys., 21, 2114 (1953)

12) L. Rimai and N. Bloembergen, J. Phys. Chem. Solids, 13, 257 (1960)

13) J.L. van Hemmen, S.B. van der Molen and W. van der Lugt, Phil. Mag., 29, 493 (1974)

14) J.M. Titman in Nuclear Magnetic Resonance in Liquid Metals and Alloys, Physics Reports, 33 (1977) p.26

15) A. Narath and H.T. Weaver, Phys. Rev., 175, 373 (1968)

16) R.I. Jolly and J.M. Titman, J. Phys. F: Metal Phys., 3, 1071 (1973)

17) M. Hanabusa and N. Bloembergen, J. Phys. Chem. Solids, 27, 363 (1966)

18) M. Watabe, M. Tanaka, H. Endo and B.K. Jones, Phil. Mag., 12, 347 (1965)

19) S.H. Kellington and J.M. Titman, Phil. Mag., 15, 1045 (1967)

20) A.L. Kerlin, Thesis 1972, University of California

21) V. El-Hanany and D. Zamir, Phys. Rev., B5, 30 (1972)

22) E. Claridge, D.S. Moore, E.F.W. Seymour and C.A. Sholl J. Phys. F., 2, 1162 (1972)

23) J. Heighway and E.F.W. Seymour, J. Phys. F., 1, 138 (1971)

24) F. Dimmling, M. von Hartrott, Th Kornrumpf, K. Nishiyama and D. Riegel, Proc. 4th Int. Conf. on Hyperfine Interactions, U.S.A. (1977)

25) S.J. Larsson, L. Broman, C. Roxbergh and A Lodding, Z. Naturf, 259, 1472 (1970)

26) H. Gabriel, Phys. Stat. Sol (b), 64, 63 (1974)

27) J.M. Titman, private communication.

APPENDIX I MODULATION BROADENING OF LORENTZIAN LINES

1 THEORY

The theory presented below is an outline of the analysis given by Wahlquist (1).

Let $H_a(t)$ be the homogeneous applied magnetic field whose time dependence involves only the slow linear sweep across an absorption line. Let H_o be the field at which resonance occurs, $H_{\frac{1}{2}}$ the half-width (distance between half-intensity points) of the true line, and H_ω the amplitude of the sinusoidal modulation with circular frequency ω. The normalised unsaturated Lorentzian absorption line may be written

$$g(H) = \pi^{-1} \frac{\frac{1}{2}H_{\frac{1}{2}}}{(\frac{1}{2}H_{\frac{1}{2}})^2+(H-H_o)^2} \qquad 1$$

and under modulation a signal will be generated which is proportional to

$$g\left[H(t)\right] = \pi^{-1} \frac{\frac{1}{2}H_{\frac{1}{2}}}{(\frac{1}{2}H_{\frac{1}{2}})^2+\left[H_a(t)+H_\omega \cos\omega t-H_o\right]^2} \qquad 2$$

The sweep rate is assumed to be very small so that $H_a(t)$ remains essentially constant over a time interval $2\pi/\omega$.

Writing $H_a-H_o = H_\delta$ and Fourier analyzing $g(t)$

$$g(t) = \pi^{-1} \frac{\frac{1}{2}H_{\frac{1}{2}}}{(\frac{1}{2}H_{\frac{1}{2}})^2+(H_\delta+H_\omega\cos\omega t)^2}$$

$$= \frac{H_{\frac{1}{2}}}{2\pi} \sum_{n=o}^{\infty} a_n(H_{\frac{1}{2}},H_\omega, H_\delta)\cos n\omega t \qquad 3$$

where the integrals for the Fourier amplitudes

$$a_n(H_{\frac{1}{2}},H_\omega,H_\delta) = (\omega/\pi) \int_{-\frac{\pi}{\omega}}^{\frac{\pi}{\omega}} \frac{\cos n\omega t}{(\frac{1}{2}H_{\frac{1}{2}})^2+(H_\delta+H_\omega\cos\omega t)^2}\, dt \qquad 4$$

may be performed by a standard technique of contour integration. Using phase detection of the fundamental the recorded signal will be proportional to the Fourier coefficient a_1.

Define dimensionless parameters α and β where

$$\alpha = (H_\delta/H_\omega) \quad -\infty < \alpha < \infty \quad , \beta = (\tfrac{1}{2}H_{\frac{1}{2}}/H_\omega) \quad 0 < \beta < \infty \qquad 5$$

and the auxiliary variables γ and u where

$$\gamma = 1+\beta^2+\alpha^2$$

$$u = \gamma + \left[\gamma^2-4\alpha^2\right]^{\frac{1}{2}} \qquad 2 < u < \infty \qquad 6$$

Then the result of the integration for n = 1 may be expressed as

$$a_1 = \pm\left(\frac{2}{H_\omega}\right)^2 \frac{(2\gamma-u)^{\frac{1}{2}}}{2(u-2)^{\frac{1}{2}}(u-\gamma)} \qquad 7$$

The detected signal, $a_1\left[H_{\frac{1}{2}},H_\omega,H_\delta(t)\right]$, is obtained by restoring the linear time variation of H_a, or equivalently, H_δ.

The pertinent properties of the resultant curve, which is similar in shape to the derivative of the Lorentzian curve, may be obtained by taking the derivative

$$(da_1/dH_\delta) = -\frac{(2/H_\omega^3)u^{\frac{1}{2}}(u^2-u-2\gamma u+3\gamma)}{(u-2)^{\frac{1}{2}}(u-\gamma)^3} \qquad 8$$

Setting the factor $(u^2-u-2\gamma u+3\gamma)$ to zero generates relationships giving the location and amplitude of the two antisymmetric peaks of a_1 for any modulation amplitude. Letting the symbol for any quantity with a suffix p attached denote that quantity evaluated at the peaks, these relations are

$$(H_\delta)_p = a_p H_\omega = (a_p/2\beta)H_{\frac{1}{2}} \qquad 9$$

$$(a_1)_p = \pm \tfrac{3}{2}(2/H_{\frac{1}{2}})^2\left[\frac{(u_p-2)}{u_p(2u_p-3)}\right]^{\frac{1}{2}} \qquad 10$$

$$a_p = \pm\left[1+\tfrac{5}{3}\beta^2-\tfrac{4}{3}\beta(\beta^2+\tfrac{3}{4})^{\frac{1}{2}}\right]^{\frac{1}{2}} \qquad 11$$

$$u_p = 2+\tfrac{4}{3}\beta^2+\tfrac{4}{3}\beta(\beta^2+\tfrac{3}{4})^{\frac{1}{2}} \qquad 12$$

2. CALIBRATION OF MODULATION

It is required to show that, if $\delta H_{meas.}$ represents the measured linewidth and δH the true linewidth measured between points of maximum and minimum slope,

$$\delta H_{meas} = 2H_\omega - \delta H \qquad 13$$

provided $H_\omega \gg \delta H$.

From 9 and 11 we have

$$(H_\delta)_p = \pm \left[1+\tfrac{5}{3}\beta^2-\tfrac{4}{3}\beta\,(\beta^2+\tfrac{3}{4})^{\frac{1}{2}}\right]^{\frac{1}{2}} H_\omega$$

$$\simeq \pm \left[1+\tfrac{5}{3}\beta^2-\tfrac{4}{3}\beta(\tfrac{3}{4})^{\frac{1}{2}}(1+\tfrac{1}{2}\,\tfrac{4}{3}\beta^2)\right]^{\frac{1}{2}} H_\omega$$

using the binomial expansion.

If $H_\omega \gg H_{\frac{1}{2}}$ then $\beta \ll 1$ and ignoring terms of higher than first order in β,

$$(H_\delta)_p = \pm \left[1-\tfrac{4}{3}\beta(\tfrac{3}{4})^{\frac{1}{2}}\right]^{\frac{1}{2}} H_\omega$$

$$= \pm \left[1-\tfrac{4}{3}\beta(\tfrac{3}{4})^{\frac{1}{2}}\tfrac{1}{2}\right] H_\omega$$

$$= \pm \left[1-\frac{\beta}{\sqrt{3}}\right] H_\omega$$

Putting $\beta = \frac{1}{2}\, H_{\frac{1}{2}}/H_\omega$ and $H_{\frac{1}{2}} = \sqrt{3}\delta H$ we obtain

$$(H_\delta)_p = \pm\left[H_\omega - \frac{\delta H}{2}\right]$$

But $\quad \delta H_{meas} = 2\left|(H_\delta)_p\right|$

Hence $\quad \delta H_{meas} = 2H_\omega - \delta H.$

3 THE COMPUTER PROGRAM

The program uses the subroutine E04GAF written by the Numerical Algorithms Group. The subroutine finds the minimum of the sum of squares of m non-linear functions, or residuals, each of n variables,

$$S(\underline{x}) = \underline{f}^T\underline{f} = \sum_{i=1}^{m} [f_i(x_1,x_2,.....,x_n)]^2, \qquad (m \geq n) \qquad 14$$

The user must supply subroutines to calculate the values of the functions and the Jacobian matrix, J, of first partial derivatives of the functions where $J_{ij} = \partial f_i/\partial x_j$.

The method used is based on an iterative technique due to Marquardt (2), (3), where, at the point $\underline{x}$, given a parameter $\lambda > 0$, the correction $\underline{\delta}$ required to give an improved estimate of the minimum is obtained by solving for $\underline{\delta}$ the equations,

$$(J^TJ+\lambda D)\underline{\delta} = -J^T\underline{f} \qquad 15$$

D is a diagonal matrix and $D_{ii} > 0$, i = 1(1)n. If the sum of squares $S(\underline{x}+\underline{\delta})$ is less than $S(\underline{x})$ then $\underline{x}+\underline{\delta}$ is accepted as the starting point for the next iteration, otherwise λ is increased and the process is repeated. When $\lambda = 0$ the equations 15 are the same as in the Gauss Newton method for which convergence is quadratic, but which may diverge. The effect of including λ is to introduce an adjustable bias towards the steepest descent vector of the sum of squares, $2J^Tf$, where progress is assured but may be slow, whenever the method appears to be diverging.

Further details of the subroutine and its implementation can be found in document no. 427 of the NAG library manual. (ICL 1900 system).

In the present case the subroutine is used to fit to the experimental data a function of the form,

$$f(H_a) = \pm \frac{C(2\gamma - u)^{\frac{1}{2}}}{(u-2)^{\frac{1}{2}}(u-\gamma)} + A\,H_a + B \qquad 16$$

by adjusting the values of $H_{\frac{1}{2}}$, H_o, A, B and C. The first term in 16 is the expression 7 given by Wahlquist for a modulation broadened line including an arbitrary constant C representing the amplitude of the signal. The second and third terms represent a linear baseline of slope A and intercept B.

The program is listed below together with the output obtained from the analysis of a typical ^{201}Hg signal. The five variables are stored in the array X where

$$X(1) = H_o \quad X(2) = C \quad X(3) = H_{\frac{1}{2}} \quad X(4) = A \quad X(5) = B \qquad 17$$

The program automatically calculates initial estimates of the variables before entry into E04 GAF. After each iteration the sum of squares and the current values contained in X are printed out. Following the final exit from the subroutine the fitted curve is calculated and the graph plotter used to display this together with the original signal. The graphical output obtained from a ^{199}Hg signal is also shown.

```
      LIBRARY(SUBGROUPSRF7)
      LIBRARY(SUBGROUPSRGP)
      LIBRARY(SUBGROUPNAGF)
      LIBRARY(SUBGROUPNAGG)
      PROGRAM(HUGO)
      INPUT 1=CRO
      OUTPUT 2=LPO
      COMPACT
      COMPRESS INTEGER AND LOGICAL
      MASTER HUGO

      DIMENSION X(5),E(5),D(5),F(510),U(555),SA(512),TITLE(9),GNAME(32),
     #HNAME(11),SNAME(16),CHARS(12)
      DATA GNAME(1)/32HGRAPH OF SIGNAL AND FITTED CURVE/,HNAME(1)/11HCHA
     #NNEL NO./,SNAME(1)/16HSIGNAL AMPLITUDE/,CHARS(1)/12HWIDTH      G/
      COMMON SC(510),HA(510),AV(6,5),HOMEG,BETA,HDELT(510),ALPHA(510),GA
     #MMA(510),U(510),A1(510)
      EXTERNAL FUNCT,LSQ,MONIT
      ICOUNT=0
      READ(1,100)MCOUNT
100   FORMAT(I2)
      CALL GPHGRAPH(7,7HP01HUGO,6)
      CALL MOVEORIG(2.0,-16.0)
500   CONTINUE
      IFAIL=0
      MODE=1
      IPRINT=1
      MAXFUN=50
      N=5
      READ(1,110)TITLE
110   FORMAT(9A8)
      READ(1,120)HOMEG,GPCM
120   FORMAT(F7.2)
      HOMEG=(HOMEG*511.0)/(GPCM*17.82)
      READ(1,130)IS1,IS2
130   FORMAT(2I4)
      READ(1,140) (SA(I),I=1,512)
140   FORMAT(8F7.0)
      L=0
      DO 1 I=1,510
      L=I+1
 1    SA(I)=SA(L)
      WRITE(2,150)TITLE
150   FORMAT(/////1H ,9A8)
      WRITE(2,160)
160   FORMAT(//1H ,16HDATA INPUT CHECK)
      WRITE(2,170) (SA(I),I=1,510)
170   FORMAT(1H ,16F7.0)
      M=0
      DO 2 I=IS1,IS2
      M=M+1
      HA(M)=I
 2    SC(M)=SA(I)
      IW=(N+4)*N+M
      SCMAX=1.0
      SCMIN=1.0E5
      DO 3 I=1,M
      IF(SC(I).GT.SCMAX) SCMAX=SC(I)
 3    IF(SC(I).LT.SCMIN) SCMIN=SC(I)
```

```
      K=1
      L=2
      DO 4 I=1,M
      IF(SC(I).EQ.SCMAX) K=I
    4 IF(SC(I).EQ.SCMIN) L=I
      BASE=(SCMAX-SCMIN)/2.0+SCMIN
      X(5)=BASE
      A1P=SCMAX-X(5)
      DO 5 I=K,L
      IF(SC(I)-X(5).GT.0.0) GOTO 5
      X(1)=I-1+IS1
      X(1)=X(1)-0.5
      GOTO 6
    5 CONTINUE
    6 HDELP=(K-L)/2.0
      ALPHP=HDELP/HOMEG
      UP=4.0*ALPHP*ALPHP-2.0*ALPHP*SQRT(4.0*ALPHP*ALPHP-3.0)
      X(2)=A1P/(SQRT(2.0*UP-3.0)/(SQRT(UP)*SQRT(UP-2.0)*(UP-2.0)))
      X(3)=HOMEG*(UP-2.0)*SQRT(3.0/(2.0*UP-3.0))
      X(4)=0.0
      WRITE(2,180)K,L,SCMAX,SCMIN
  180 FORMAT(//1H ,1HK,I4//1H ,1HL,I4//1H ,5HSCMAX,F7.0//1H ,5HSCMIN,F7.
     #0)
      E(1)=1.0E-5
      E(2)=1.0E-5
      E(3)=1.0E-5
      E(4)=1.0E-5
      E(5)=1.0E-5
      CALL E04GAF(M,N,X,F,S,E,MODE,D,W,IW,FUNCT,LSQ,MONIT,IPRINT,MAXFUN,
     1IFAIL)
      WRITE(2,190)IFAIL
  190 FORMAT(//1H ,6HIFAIL=,I1)
      CALL MONIT(M,N,X,F,S,E,-1)
      IFAIL=1
      IA=N+1
      CALL F01ADF(N,AV,IA,IFAIL)
      WRITE(2,200)IFAIL
  200 FORMAT(//1H ,6HIFAIL=,I1)
      WRITE(2,210)
  210 FORMAT(//1H ,9HVARIANCES)
      FAC=S/(M-N)
      WRITE(2,220)
  220 FORMAT(//1H ,11X,4HX(1),11X,4HX(2),11X,4HX(3),11X,4HX(4),11X,4HX(5)
     #)
      DO 7 I=1,N
      I1=I+1
      DO 8 J=1,I
    8 D(J)=FAC*AV(I1,J)
      IF(I.EQ.3) X3VAR=D(3)
  230 FORMAT(4E15.4)
    7 WRITE(2,230) (D(J),J=1,I)
      WCH=X(3)/1.7321
      WG=(WCH*17.82*GPCM)/511.0
      X3MD=SQRT(X3VAR)
      DWCH=WCH*X3MD/X(3)
      DWG=DWCH*WG/WCH
      WRITE(2,240)WCH,DWCH,WG,DWG,X3MD
  240 FORMAT(////1H ,3HWCH,F8.2//1H ,4HDWCH,F8.2//1H ,2HWG,F8.2//1H ,3HD
     #WG,F8.4//1H ,4HX3MD,F8.4)
      BETA=0.5*X(3)/HOMEG
      DO 9 I=1,510
      HA(I)=I
      HDELT(I)=HA(I)-X(1)
      ALPHA(I)=HDELT(I)/HOMEG
      GAMMA(I)=1.0+BETA*BETA+ALPHA(I)*ALPHA(I)
      U(I)=GAMMA(I)+SQRT(GAMMA(I)*GAMMA(I)-4.0*ALPHA(I)*ALPHA(I))
```

```
      A1(I)=X(2)*SQRT(2.0*GAMMA(I)-U(I))/(SQRT(U(I)-2.0)*(U(I)-GAMMA(I))
     #)
      IF(HA(I).GT.X(1)) A1(I)=-A1(I)
      A1(I)=A1(I)+X(4)*HA(I)+X(5)
      SA(I)=SA(I)-BASE
    9 A1(I)=A1(I)-BASE
      CALL MOVEORIG(25.0,0.0)
      CALL HGPSYMBL(0.0,12.0,0.8,TITLE,0.0,72)
      CALL HGPSYMBL(0.0,8.5,0.6,GNAME,0.0,32)
      SFH=16.0/509.0
      DO 10 I=1,510
   10 HA(I)=(HA(I)-1.0)*SFH
      SAMAX=SCMAX-BASE
      A1MAX=-1.0
      DO 11 I=1,510
   11 IF(A1(I).GT.A1MAX) A1MAX=A1(I)
      SPMAX=SAMAX
      IF(A1MAX.GT.SAMAX) SPMAX=A1MAX
      SPAMP=4.0
      IF(WG.GT.10.0) SPAMP=2.0
      SFS=SPAMP/SPMAX
      DO 12 I=1,510
      SA(I)=SA(I)*SFS
   12 A1(I)=A1(I)*SFS
      CALL HGPAXISV(0.0,0.0,HNAME,-11,16.0,0.0,1.0,509.0,16.0,-4)
      AL=2.0*SPAMP
      NH=4
      IF(WG.GT.10.0) NH=3
      CALL HGPAXISV(0.0,-SPAMP,SNAME,16,AL,90.0,-SPMAX,SPMAX,SPAMP,NH)
      CALL HGPLINE(HA,SA,510,1)
      CALL HGPLINE(HA,A1,510,1)
      CALL HGPSYMBL(5.5,-8.0,0.6,CHARS,0.0,12)
      CALL HGPNUMBER(8.5,-8.0,0.6,WG,0.0,0.2,1)
      ICOUNT=ICOUNT+1
      IF(ICOUNT.LT.MCOUNT) GOTO 500
      CALL GPHENDPLOT(25.0)
      STOP
      END


      SUBROUTINE FUNCT(M,N,X,F,IFL)
      LOGICAL IFL
      DIMENSION X(N),F(M)
      COMMON SC(510),HA(510),AV(6,5),HOMEG,BETA,HDELT(510),ALPHA(510),GA
     #MMA(510),U(510),A1(510)
      BETA=0.5*X(3)/HOMEG
      DO 1 I=1,M
      HDELT(I)=HA(I)-X(1)
      ALPHA(I)=HDELT(I)/HOMEG
      GAMMA(I)=1.0+BETA*BETA+ALPHA(I)*ALPHA(I)
      U(I)=GAMMA(I)+SQRT(GAMMA(I)*GAMMA(I)-4.0*ALPHA(I)*ALPHA(I))
      A1(I)=X(2)*SQRT(2.0*GAMMA(I)-U(I))/(SQRT(U(I)-2.0)*(U(I)-GAMMA(I))
     #)
      IF(HA(I).GT.X(1)) A1(I)=-A1(I)
    1 F(I)=A1(I)+X(4)*HA(I)+X(5)-SC(I)
      RETURN
      END
```

```
      SUBROUTINE LSQ(M,N,X,F,A,V)
      DIMENSION X(N),F(M),A(N,N),V(N),AJAC(510,5)
      COMMON SC(510),HA(510),AV(6,5),HOMEG,BETA,HDELT(510),ALPHA(510),GA
     #MMA(510),U(510),A1(510)
      DO 1 I=1,M
      AJAC(I,1)=X(2)*(1.0/HOMEG)*SQRT(U(I))*(U(I)*U(I)-U(I)-2.0*GAMMA(I)
     #*U(I)+3.0*GAMMA(I))/(SQRT(U(I)-2.0)*(U(I)-GAMMA(I))*(U(I)-GAMMA(I)
     #)*(U(I)-GAMMA(I)))
      AJAC(I,2)=SQRT(2.0*GAMMA(I)-U(I))/(SQRT(U(I)-2.0)*(U(I)-GAMMA(I)))
      AJAC(I,3)=X(2)*(1.0/HOMEG)*BETA*SQRT(2.0*GAMMA(I)-U(I))*(GAMMA(I)+
     #U(I)-U(I)*U(I))/(SQRT(U(I)-2.0)*(U(I)-2.0)*(U(I)-GAMMA(I))*(U(I)-G
     #AMMA(I))*(U(I)-GAMMA(I)))
      AJAC(I,4)=HA(I)
      AJAC(I,5)=1.0
      IF(HA(I).LE.X(1)) GOTO 1
      AJAC(I,2)=-AJAC(I,2)
      AJAC(I,3)=-AJAC(I,3)
    1 CONTINUE
      DO 3 J=1,N
      DO 3 I=1,J
      SUM=0.0
      DO 2 K=1,M
    2 SUM=SUM+AJAC(K,I)*AJAC(K,J)
      AV(I,J)=2.0*SUM
    3 A(I,J)=SUM
      DO 5 I=1,N
      SUM=0.0
      DO 4 K=1,M
    4 SUM=SUM+F(K)*AJAC(K,I)
    5 V(I)=SUM
      RETURN
      END
```

```
      SUBROUTINE MONIT(M,N,X,F,S,V,IR)
      DIMENSION X(N),F(M),V(N)
      COMMON SC(510),HA(510),AV(6,5),HOMEG,BETA,HDELT(510),ALPHA(510),GA
     #MMA(510),U(510),A1(510)
      IF(IR.GE.0) GOTO 1
      WRITE(2,100)
  100 FORMAT(////1H ,45HFIT TO A MODULATION BROADENED LORENTZIAN LINE)
    1 CONTINUE
      IF(IR.LT.0) GOTO 2
      WRITE(2,110)IR
  110 FORMAT(//1H ,I6,25H EVALUATIONS OF RESIDUALS)
    2 CONTINUE
      WRITE(2,120)S
  120 FORMAT(/1H ,17HSUM OF SQUARES = ,E17.9)
      WRITE(2,130) (X(I),I=1,N)
  130 FORMAT(1H ,6H X(1)=,E17.9,6H X(2)=,E17.9,6H X(3)=,E17.9,6H X(4)=,E
     #17.9,6H X(5)=,E17.9)
      IF(IR.LT.0) GOTO 3
      WRITE(2,140) (V(I),I=1,N)
  140 FORMAT(1H ,17HPRESENT GRADIENTS/1H ,6X,E17.9,6X,E17.9,6X,E17.9,6X,
     #E17.9,6X,E17.9)
    3 CONTINUE
      RETURN
      END
```

31.5.76 HG201 ROOM TEMP 4HRS

DATA INPUT CHECK

35664. 35656. 35644. 35620. 35611. 35551. 35533. 35507. 35484. 35513. 35463. 35461. 35456. 35461. 35454. 35479.
35397. 35411. 35437. 35400. 35433. 35490. 35505. 35540. 35585. 35612. 35584. 35585. 35547. 35504. 35431. 35390.
35343. 35325. 35298. 35294. 35309. 35319. 35348. 35362. 35407. 35418. 35426. 35418. 35419. 35411. 35396. 35393.
35369. 35354. 35347. 35338. 35323. 35357. 35364. 35396. 35432. 35487. 35523. 35612. 35623. 35723. 35753. 35812.
35818. 35853. 35853. 35867. 35870. 35879. 35862. 35882. 35818. 35854. 35824. 35859. 35847. 35865. 35880. 35925.
35949. 35992. 36029. 36030. 36008. 36036. 36005. 36008. 35971. 35959. 35876. 35849. 35810. 35772. 35732. 35707.
35634. 35656. 35604. 35579. 35577. 35593. 35573. 35623. 35627. 35652. 35660. 35702. 35740. 35805. 35875. 35914.
35941. 35958. 35986. 36015. 35991. 35991. 36004. 36022. 35998. 35984. 35961. 35939. 35916. 35902. 35881. 35852.
35852. 35845. 35838. 35812. 35851. 35843. 35843. 35897. 35889. 35912. 35912. 35938. 35935. 35929. 35915. 35896.
35867. 35916. 35929. 35904. 35916. 35976. 35988. 36012. 35964. 35934. 35936. 35914. 35941. 35935. 35969. 35971.
35981. 36004. 35992. 35981. 35962. 35944. 35930. 35947. 35956. 35971. 36013. 36019. 36020. 36063. 36080. 36105.
36092. 36131. 36183. 36249. 36264. 36332. 36363. 36394. 36387. 36403. 36410. 36457. 36476. 36510. 36518. 36518.
36440. 36453. 36405. 36393. 36380. 36424. 36458. 36492. 36523. 36572. 36567. 36609. 36653. 36658. 36661. 36697.
36729. 36737. 36751. 36735. 36722. 36723. 36739. 36731. 36701. 36703. 36688. 36721. 36679. 36682. 36684. 36663.
36672. 36618. 36586. 36553. 36492. 36461. 36416. 36382. 36315. 36260. 36236. 36159. 36142. 36118. 36050. 35975.
35881. 35797. 35689. 35658. 35585. 35512. 35435. 35399. 35311. 35257. 35168. 35105. 35017. 34959. 34876. 34784.
34710. 34639. 34551. 34483. 34454. 34422. 34350. 34341. 34291. 34221. 34189. 34158. 34135. 34104. 34083. 34094.
34050. 34039. 34012. 34016. 34001. 34031. 34037. 34076. 34096. 34103. 34091. 34068. 34077. 34013. 34017. 33996.
33986. 33985. 34003. 34015. 34006. 34071. 34123. 34156. 34247. 34281. 34340. 34390. 34431. 34444. 34518. 34527.
34577. 34615. 34663. 34679. 34690. 34720. 34720. 34711. 34701. 34649. 34647. 34601. 34573. 34567. 34599. 34621.
34626. 34645. 34656. 34655. 34702. 34678. 34719. 34747. 34749. 34775. 34818. 34836. 34828. 34832. 34802. 34831.
34862. 34866. 34898. 34952. 34966. 35034. 35107. 35172. 35227. 35313. 35344. 35345. 35363. 35376. 35398. 35405.
35385. 35366. 35351. 35304. 35313. 35263. 35249. 35176. 35139. 35093. 35073. 35059. 35082. 35067. 35057. 35057.
35038. 35050. 35091. 35091. 35102. 35063. 35091. 35083. 35112. 35104. 35104. 35105. 35101. 35099. 35104. 35139.
35152. 35188. 35232. 35240. 35256. 35268. 35288. 35301. 35309. 35282. 35277. 35256. 35249. 35204. 35173. 35142.
35124. 35143. 35154. 35145. 35194. 35193. 35194. 35178. 35157. 35158. 35182. 35175. 35169. 35188. 35203. 35233.
35237. 35303. 35313. 35335. 35280. 35286. 35217. 35182. 35156. 35132. 35111. 35121. 35117. 35115. 35110. 35130.
35104. 35128. 35175. 35178. 35230. 35249. 35287. 35286. 35281. 35339. 35342. 35315. 35334. 35320. 35320. 35326.
35317. 35311. 35281. 35248. 35258. 35240. 35238. 35262. 35248. 35264. 35273. 35281. 35269. 35291. 35282. 35309.
35299. 35335. 35348. 35386. 35385. 35382. 35364. 35375. 35341. 35292. 35278. 35253. 35208. 35224. 35208. 35192.
35199. 35211. 35236. 35256. 35270. 35274. 35260. 35265. 35255. 35286. 35279. 35286. 35285. 35265. 35255. 35217.
35190. 35167. 35099. 35052. 34978. 34951. 34890. 34838. 34823. 34815. 34800. 34793. 34829. 34829.

```
L 290

SCMAX 36751.

SCMIN 33985.

      1 EVALUATIONS OF RESIDUALS

 SUM OF SQUARES =   0.220158493E 08
  X(1)=  0.248500000E 03 X(2)=  0.368942279E 06 X(3)=  0.131737852E 03 X(4)=  0.000000000E 00 X(5)=  0.353680000E 05
 PRESENT GRADIENTS
        0.340399013E 06        0.706718128E 02       -0.336321352E 06       -0.726674299E 07       -0.287213665E 05

      3 EVALUATIONS OF RESIDUALS

 SUM OF SQUARES =   0.137894779E 08
  X(1)=  0.246362051E 03 X(2)=  0.255043299E 06 X(3)=  0.121605145E 03 X(4)= -0.268925327E 00 X(5)=  0.354879369E 05
 PRESENT GRADIENTS
       -0.265297028E 05       -0.270397999E 02        0.246548804E 04        0.108774711E 07       -0.252142532E 04

      4 EVALUATIONS OF RESIDUALS

 SUM OF SQUARES =   0.122775132E 08
  X(1)=  0.246555850E 03 X(2)=  0.145029828E 06 X(3)=  0.100223374E 03 X(4)= -0.693699793E 00 X(5)=  0.356007120E 05
 PRESENT GRADIENTS
       -0.542452518E 05       -0.105115312E 03        0.357850202E 06        0.118203334E 07        0.783705235E 01

      5 EVALUATIONS OF RESIDUALS

 SUM OF SQUARES =   0.105914915E 08
  X(1)=  0.246910367E 03 X(2)=  0.167724934E 06 X(3)=  0.102101320E 03 X(4)= -0.661281935E 00 X(5)=  0.355925245E 05
 PRESENT GRADIENTS
        0.114594190E 05       -0.526831366E 01        0.238212088E 05        0.392522833E 05        0.324737501E 01
```

```
    13 EVALUATIONS OF RESIDUALS

SUM OF SQUARES =    0.105856412E 08
 X(1)=  0.246851700E 03 X(2)=  0.167600283E 06 X(3)=  0.101858333E 03 X(4)= -0.661924243E 00 X(5)=  0.355926892E 05
PRESENT GRADIENTS
        0.760745555E-01         0.263072889E-05         0.353392991E-01         0.100212097E-01        -0.149726868E-03

    15 EVALUATIONS OF RESIDUALS

SUM OF SQUARES =    0.105856412E 08
 X(1)=  0.246851700E 03 X(2)=  0.167600283E 06 X(3)=  0.101858333E 03 X(4)= -0.661924243E 00 X(5)=  0.355926892E 05
PRESENT GRADIENTS
        0.624117469E-01         0.260686193E-05         0.345602860E-01         0.142021179E-01        -0.167846680E-03

    18 EVALUATIONS OF RESIDUALS

SUM OF SQUARES =    0.105856412E 08
 X(1)=  0.246851700E 03 X(2)=  0.167600283E 06 X(3)=  0.101858333E 03 X(4)= -0.661924243E 00 X(5)=  0.355926892E 05
PRESENT GRADIENTS
        0.610497342E-01         0.261128935E-05         0.344508199E-01         0.144462585E-01        -0.172138214E-03

IFAIL=0
```

FIT TO A MODULATION BROADENED LORENTZIAN LINE

SUM OF SQUARES = 0.105856412E 08

X(1)= 0.246851700E 03 X(2)= 0.167600283E 06 X(3)= 0.101858333E 03 X(4)= -0.661924243E 00 X(5)= 0.355926892E 05

IFAIL=0

VARIANCES

X(1)	X(2)	X(3)	X(4)	X(5)
0.5713E-01				
0.7972E 00	0.2252E 08			
0.1571E-03	0.4920E 04	0.1172E 01		
0.1427E-04	0.8457E 02	0.1699E-01	0.1289E-02	
-0.1083E-01	-0.2147E 05	-0.4310E 01	-0.3287E 00	
0.1044E 03				

WCH 58.81

DWCH 0.62

WG 24.26

DWG 0.2578

X3MD 1.0824

19.10.76. HG199 40C

GRAPH OF SIGNAL AND FITTED CURVE

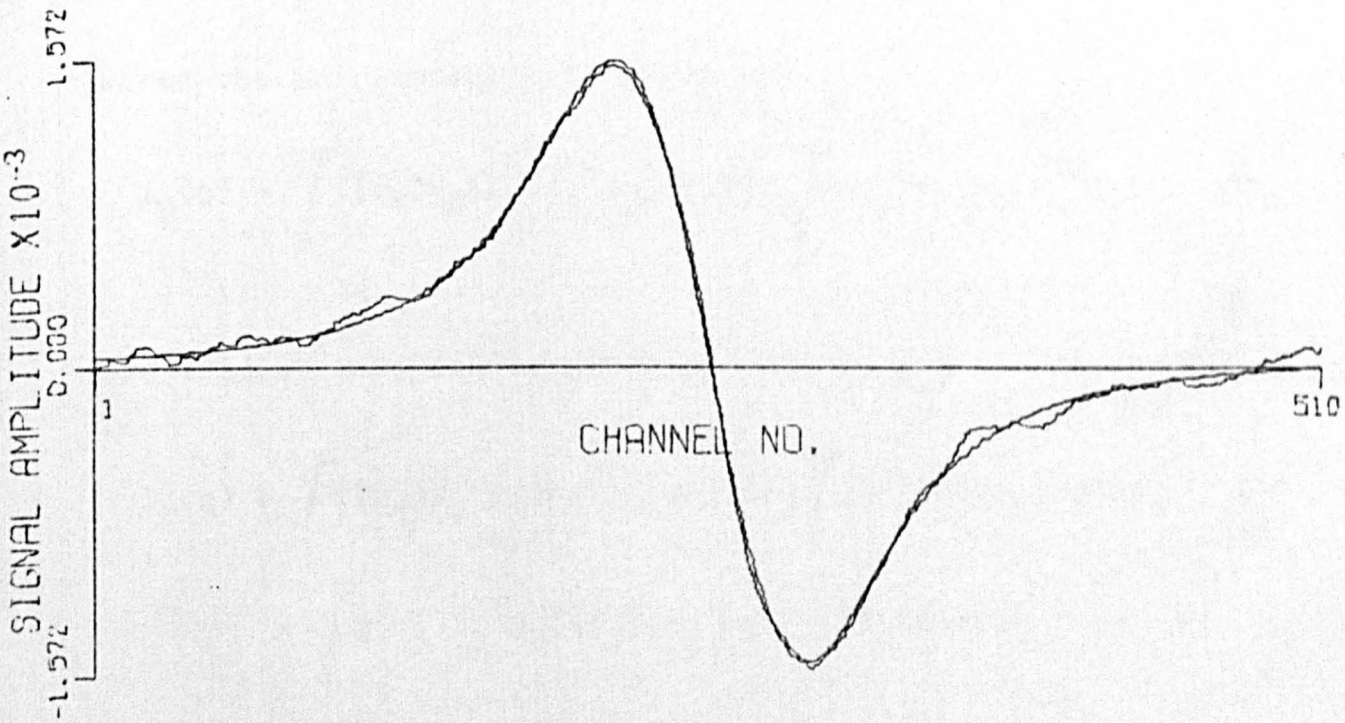

WIDTH 4.8G

4 REFERENCES

1) H.Wahlquist, J. Chem Phys., 35, 1708 (1961)

2) D.W. Marquardt, J. Soc. Industrial and Applied Mathematics, 2, 431 (1963)

3) R. Fletcher, UKAEA Research Group Report No. AERE-R 6799 Published by HMSO (1971)

APPENDIX II CALCULATION OF THE TEMPERATURE DEPENDENCE OF R_{1Q}

1 THEORY

As shown in Chapter 3 the quadrupole relaxation rate is given by the following expression,

$$R_{1q} = 2\beta \int_0^\infty q^2 \left[I_p(q) + 2n\rho I_t(q) \right] dq \int_{-\infty}^{\infty} S_s^{\,2}(q,\omega)\, d\omega \qquad 1$$

where the pair integral is given by

$$I_p(q) = \int_0^\infty f(r_1) v_2(r_1) r_1^{\,2} j_2(qr_1)\, dr_1 \int_0^\infty g(r_o) v_2(r_o) r_o^{\,2} j_2(qr_o)\, dr_o \qquad 2$$

the triplet integral is given by

$$I_t(q) = \int_0^\infty f(r_1) v_2(r_1) r_1^{\,2} j_2(qr_1)\, dr_1 \int_0^\infty g(r_o) v_2(r_o) r_o^{\,2}\, dr_o \times \int_0^\infty g(r_3) r_3^{\,3} j_2(qr_3)\, dr_3 \int_{-1}^{1} g(r_{o3}) P_2(z)\, dz \qquad 3$$

and

$$\beta = \frac{2n(2I+3)}{15I^2(2I-1)} \left[\frac{eQ(1-\gamma_{eff})}{\hbar} \right]^2 \rho, \qquad 4$$

$$r_{o3}^{\,2} = r_o^{\,2} + r_3^{\,2} - 2 r_o r_3 \cos\theta \qquad 5$$

$$z = \cos\theta \qquad 6$$

1.1 THE PAIR INTEGRAL

As explained in Chapter 3 we treat $f(r_1)v_2(r_1)r_1^{\,2}$ and $g(r_o)v_2(r_o)r_o^{\,2}$ as delta functions giving

$$I_p(q) = j_2(qr_1)j_2(qr_o) \qquad 7$$

For a delta function at a this gives $I_p(q) = \left[j_2(qa)\right]^2$ 8
and if q is expressed in units of $^1/a$ this simply becomes

$$I_p(q) = \left[j_2(q)\right]^2 \qquad 9$$

For a delta function at $b \neq a$, for example $b = 1.05a$ then

$$I_p(q) = \left[j_2(q\ 1.05)\right]^2 \qquad 10$$

1.2 THE TRIPLET INTEGRAL

Treating $f(r_1)v_2(r_1)r_1^2$ as a delta function reduces the first integral to $j_2(qr_1)$. In the second integral $g(r_o)v_2(r_o)r_o^2$, is also treated as a delta function which picks out some particular value of r_o, say b, so that $r_{o3}^2 = r_3^2+b^2-2r_3\,b\cos\theta$ in the final integral. To integrate requires a form of $g(r_{o3})$. In our calculations we used simplified forms of $g(r_{o3})$ for the hard sphere model of a liquid and for liquid mercury. We shall describe first the calculations based upon the hard sphere model.

1.2.1 CALCULATIONS USING THE HARD SPHERE MODEL

We chose the hard sphere form for packing fraction $n = 0.445$ (1). This was simplified using straight line approximations as shown in figure II 1.

For clarity we shall consider the case b = a initially and then extend the results for the general delta function position. We therefore put $r_o = a$ and, letting $r_3 = r$, $r_{o3} = \rho$ we have from 5 and 6

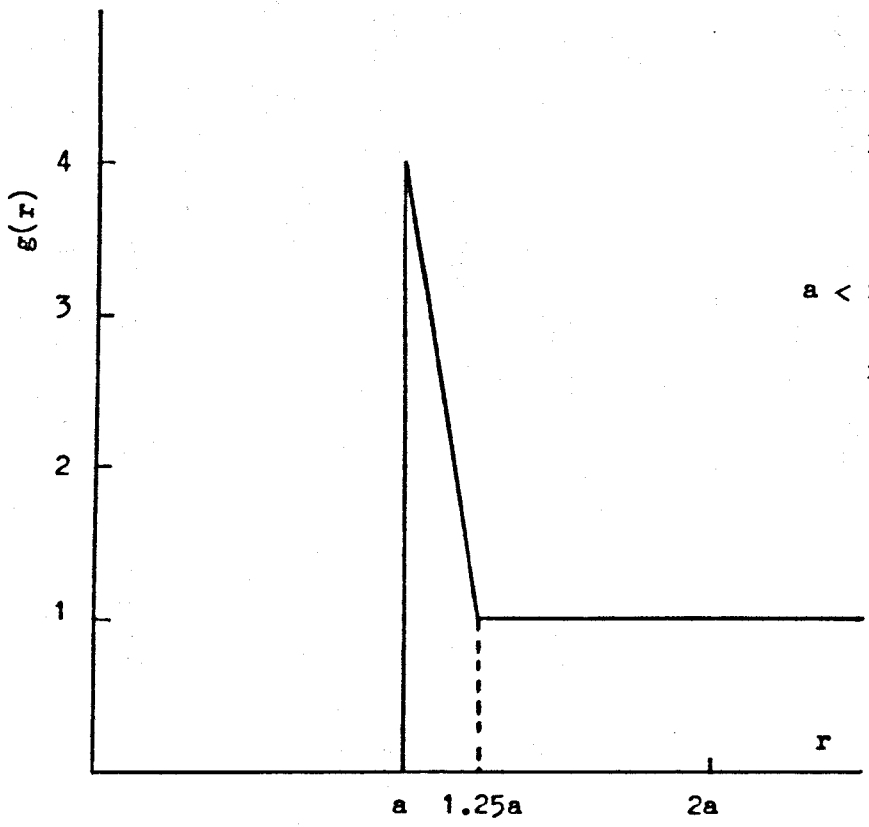

For,

$r < a$, $g(r) = 0$

$a < r < 1.25a$, $g(r) = -12\frac{r}{a} + 16$

$r > 1.25a$, $g(r) = 1$

Figure 11.1 Simplified form of the hard sphere g(r) used in the calculations.

$$\rho^2 = a^2+r^2-2arz \qquad 11$$

Also, in order for the integral to converge we write

$$\int_{-1}^{1} g(\rho)P_2(z)dz = \int_{-1}^{1} \left[g(\rho)-1\right]P_2(z)dz \qquad 12$$

Considering first the region $o < \rho < a$, we have

$$\int_{-1}^{1} \left[g(\rho)-1\right]P_2(z)dz = -\tfrac{1}{2}\int_{r/2a}^{1}(3z^2-1)dz$$

$$= -\frac{r}{16a^3}(4a^2-r^2)$$

$$= -\frac{x}{16}(4-x^2) \text{ putting } x = \frac{r}{a} \qquad 13$$

The limits in equation 13 should be noted. When $\rho = o$, $z = \frac{a^2+r^2}{2ar} \geqslant 1$, setting the upper limit at 1. When $\rho = a$, $z = \frac{r^2}{2ar} = \frac{r}{2a}$ giving the lower limit. Thus when $r = 2a$ the integral is zero.

Now considering the region $a \leqslant \rho \leqslant \frac{5a}{4}$. we have at $\rho = a$, $z = r/2a$ and at $\rho = \frac{5a}{4}$,

$\frac{25}{16}a^2 = a^2+r^2-2arz'$ where z' is the required limit.

i.e. $z' = \frac{16r^2-9a^2}{32ar} = \frac{r}{2a} - \frac{9a}{32r}$

Then

$$\int_{-1}^{1}\left[g(\rho)-1\right]P_2(z)dz = \tfrac{1}{2}\int_{\frac{r}{2a}-\frac{9a}{32r}}^{r/2a}\left[15-\frac{12}{a}(a^2+r^2-2arz)^{\frac{1}{2}}\right](3z^2-1)dz$$

$$= \tfrac{1}{2}\int_{\frac{r}{2a}-\frac{9a}{32r}}^{r/2a}\left[15-12(1+(\tfrac{r}{a})^2-2(\tfrac{r}{a})z)^{\frac{1}{2}}\right](3z^2-1)dz$$

$$= \tfrac{1}{2}\int_{\frac{x}{2}-\frac{9}{32x}}^{x/2}\left[15-12(1+x^2-2xz)^{\frac{1}{2}}\right](3z^2-1)dz \qquad 14$$

Expression 14 is correct for $r \leqslant 2a$. However when $r = 2a$ the upper limit equals 1. Now z is integrated only between -1 an 1 so that for $r > 2a$ we must cut off the integral at the upper limit of 1.

Thus for $r > 2a$ we use

$$\int_{-1}^{1}\left[g(\rho)-1\right]P_2(z)dz = \tfrac{1}{2}\int_{\frac{x}{2}-\frac{9}{32x}}^{1}\left[15-12(1+x^2-2xz)^{\frac{1}{2}}\right](3z^2-1)dz \qquad 15$$

To summarise, for $r \leqslant 2a$ we use expressions 13 and 14 to evaluate the integral but for $r > 2a$ expression 15 must be used.

We shall now consider the general case $b \neq a$ where

$$\rho^2 = b^2+r^2-2brz \qquad 16$$

For the region $0 \leqslant \rho \leqslant a$ we have

$$\int_{-1}^{1}\left[g(\rho)-1\right]P_2(z)dz = -\tfrac{1}{2}\int_{n}^{1}(3z^2-1)dz$$

where n is the limit of z when $\rho = a$ i.e. $a^2 = b^2+r^2-2brz$

$$n = \frac{b^2+r^2-a^2}{2br} \qquad 17$$

Then $$\int_{-1}^{1}\left[g(\rho)-1\right]P_2(z)dz = -\tfrac{1}{2}\left[z^3-z\right]_n^1$$

$$= -\tfrac{1}{2}\,(1-n^3-1+n)$$

$$= \tfrac{1}{2}n(n^2-1) \qquad 18$$

It should be noted that this integral equals zero when n equals 1 i.e. at

$$a^2 = b^2+r^2-2br = (b-r)^2$$

$$a = \pm\,(b-r)$$

The positive sign gives r = o which is below the cut-off at r = a. The negative sign gives r = a+b which is equivalent to r = 2a for the delta function at a.

For the region $a \leqslant \rho \leqslant \frac{5a}{4}$, at $\rho = a$, $z = n$ as above, at $\rho = \frac{5a}{4}$, we have

$\frac{25a^2}{16} = b^2+r^2-2br\zeta$ where ζ is the required limit

$$\zeta = \frac{16(b^2+r^2)-25a^2}{32br}$$

Then

$$\int_{-1}^{1}\left[g(\rho)-1\right]P_2(z)dz = \tfrac{1}{2}\int_{\zeta}^{n}\left[15-\frac{12}{a}(b^2+r^2-2brz)^{\frac{1}{2}}\right](3z^2-1)dz$$

$$= \tfrac{1}{2}\int_{\zeta}^{n}\left[15-12\left(\frac{b^2}{a^2}+\frac{r^2}{a^2}-\frac{2brz}{a^2}\right)^{\frac{1}{2}}\right](3z^2-1)dz \qquad 20$$

Again when $r > a+b$ we must cut off the top limit at 1 and in this region

$$\int_{-1}^{1}\left[g(\rho)-1\right]P_2(z)dz = \tfrac{1}{2}\int_{\xi}^{1}\left[15-12\left(\frac{b^2}{a^2}+\frac{r^2}{a^2}+\frac{2brz}{a^2}\right)^{\frac{1}{2}}\right](3z^2-1)dz \qquad 21$$

Writing $x = r/a$ as before 17 and 18 become

$$\int_{-1}^{1}\left[g(\rho)-1\right]P_2(z)dz = \tfrac{1}{2}n(n^2-1) \qquad 22$$

$$\text{where } n = \frac{\frac{b^2}{a^2}+x^2-1}{2(\frac{b}{a})x} = \frac{y^2+x^2-1}{2yx} \quad \text{with } y = \frac{b}{a} \qquad 23$$

Equations 20 and 21 become

$$\int_{-1}^{1}\left[g(\rho)-1\right]P_2(z)dz = \tfrac{1}{2}\int_{\xi}^{n}\left[15-12(y^2+x^2-2xyz)^{\frac{1}{2}}\right](3z^2-1)dz \qquad 24$$

and

$$\int_{-1}^{1}\left[g(\rho)-1\right]P_2(z)dz = \tfrac{1}{2}\int_{\xi}^{n}\left[15-12(y^2+x^2-2xyz)^{\frac{1}{2}}\right](3z^2-1)dz \qquad 25$$

$$\text{with} \quad \xi = \frac{16(y^2+x^2)-25}{32xy} \qquad 26$$

The condition $r = a+b$ becomes $x = 1+y$.

Thus to summarise for the general delta function position $b \neq a$, for $x \leq 1+y$ we use expressions 22 and 24 to evaluate the integral with n and ξ given by 23 and 26. For $x > 1+y$ we use only expression 25.

1.2.2 CALCULATIONS USING g(r) FOR LIQUID MERCURY

The simplified form of the radial distribution function used for mercury is shown in Figure II.2. It is based upon that given by Kaplow et al (2).

Again for clarity we shall first consider the case b = a. For the region $o < \rho < a$, we have

$$\int_{-1}^{1}\left[g(\rho)-1\right]P_2(z)dz = -\tfrac{1}{2}\int_{r/2a}^{1}(3z^2-1)dz$$

$$= -\frac{x}{16}(4-x^2) \quad \text{with } x = r/a \qquad 27$$

which is the same as the result for the hard sphere model. Again when r = 2a the integral is zero.

Considering now the region $a \leqslant \rho \leqslant 1.18a$, when $\rho = a$, $z = r/2a = \frac{x}{2}$, when $\rho = 1.18a$, the required limit z' is given by

$$z' = \frac{a^2+r^2-\rho^2}{2ar} = \frac{r^2+(1-1.18^2)a^2}{2ar} = \frac{r}{2a}-\frac{0.392a}{2r} = \frac{x}{2}-\frac{0.196}{a}$$

Hence

$$\int_{-1}^{1}\left[g(\rho)-1\right]P_2(z)dz = \tfrac{1}{2}\int_{z'}^{r/2a}\left[\frac{9.17\rho}{a}-9.17\right](3z^2-1)dz$$

$$= \tfrac{1}{2}\int_{z'}^{r/2a}\left[\frac{9.17(a^2+r^2-2arz)^{\frac{1}{2}}}{a}-9.17\right](3z^2-1)dz$$

$$= \tfrac{1}{2}\int_{\frac{x}{2}-\frac{0.196}{x}}^{x/2}\left[9.17(1+x^2-2xz)^{\frac{1}{2}}-9.17\right](3z^2-1)dz \qquad 28$$

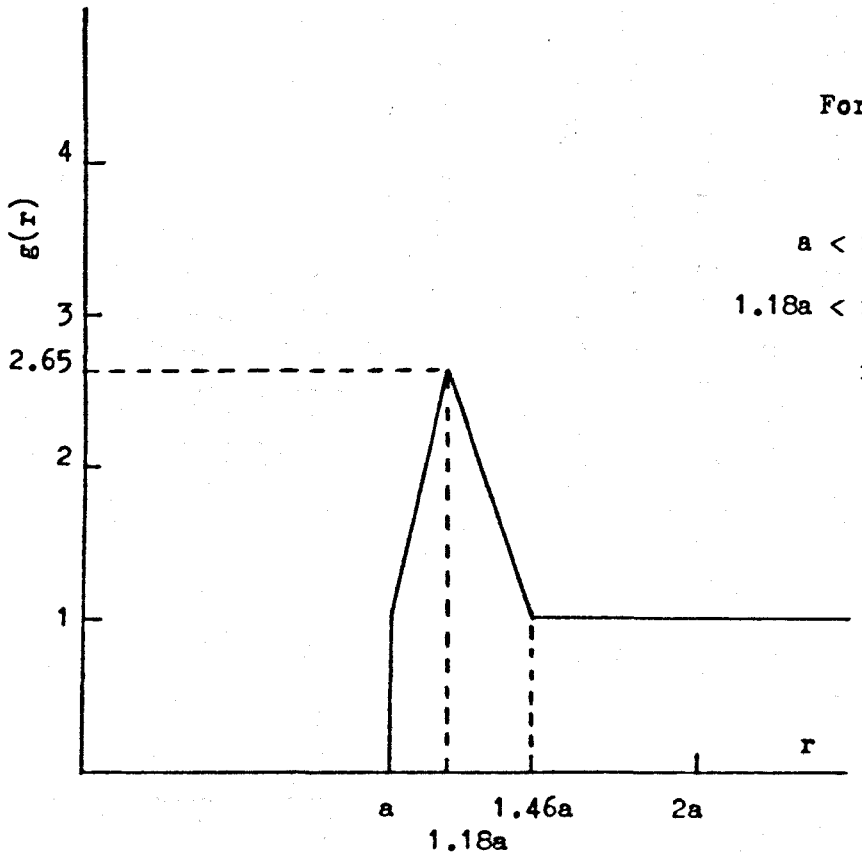

For,

$r < a$, $g(r) = 0$

$a < r < 1.18a$, $g(r) = 9.17\frac{r}{a} - 8.17$

$1.18a < r < 1.46a$, $g(r) = -5.89\frac{r}{a} + 9.6$

$r > 1.46a$, $g(r) = 1$

Figure 11.2 Simplified form of g(r) for liquid mercury.

For the region $1.18a \leqslant \rho \leqslant 1.46a$, when $\rho = 1.18a$, $z = \frac{x}{2} - \frac{0.196}{x}$, when $\rho = 1.46a$, the required limit z" is given by

$$z'' = \frac{r^2+a^2-1.46^2a^2}{2ar} = \frac{r}{2a} + \frac{(1-1.46^2)a}{r} = \frac{x}{2} - \frac{0.566}{x}$$

Then

$$\int_{-1}^{1} \left[g(\rho)-1\right] P_2(z)\,dz = \tfrac{1}{2} \int_{\frac{x}{2}-\frac{0.196}{x}}^{\frac{x}{2}-\frac{0.566}{x}} \left[8.60-5.89(1+x^2-2xz)^{\frac{1}{2}}\right](3z^2-1)\,dz \qquad 29$$

As before the upper limit of z for any integral must not exceed 1 and so we replace the upper limit of the integral by 1 in expression 28 when $x>2$ and in expression 29 when $\frac{x}{2} - \frac{0.196}{x} > 1$, i.e. $x > 2.18$.

To summarise, for $1 \leqslant x \leqslant 2$,

$$\begin{aligned}\int_{-1}^{1} \left[g(\rho)-1\right] P_2(z)\,dz = &-\frac{x}{16}(4-x^2) \\ &+ \tfrac{1}{2} \int_{x/2-0.196/x}^{x/2} \left[9.17(1+x^2-2xz)^{\frac{1}{2}}-9.17\right](3z^2-1)\,dz \\ &+ \tfrac{1}{2} \int_{x/2-0.566/x}^{x/2-0.196/x} \left[8.60-5.89(1+x^2-2xz)^{\frac{1}{2}}\right](3z^2-1)\,dz \qquad 30\end{aligned}$$

For $2 \leqslant x \leqslant 2.18$,

$$\begin{aligned}\int_{-1}^{1} \left[g(\rho)-1\right] P_2(z)\,dz = &\tfrac{1}{2} \int_{x/2-0.196/x}^{1} \left[9.17(1+x^2-2xz)^{\frac{1}{2}}-9.17\right](3z^2-1)\,dz \\ &+ \tfrac{1}{2} \int_{x/2-0.566/x}^{x/2-0.196/x} \left[8.60-5.89(1+x^2-2xz)^{\frac{1}{2}}\right](3z^2-1)\,dz \qquad 31\end{aligned}$$

and for $x \geqslant 2.18$,

$$\int_{-1}^{1}\left[g(\rho)-1\right]P_2(z)dz = \tfrac{1}{2}\int_{x/2-0.566/x}^{1}\left[8.60-5.89(1+x^2-2xz)^{\frac{1}{2}}\right](3z^2-1)dz \qquad 32$$

We shall now extend the results as before for the general case $b \neq a$.

As with the hard sphere model, for the region $o \leqslant \rho \leqslant a$,

$$\int_{-1}^{1}\left[g(\rho)-1\right]P_2(z)dz = \tfrac{1}{2}n(n^2-1) \qquad 33$$

where $n = \dfrac{b^2+r^2-a^2}{2br}$

For the region $a \leqslant \rho \leqslant 1.18a$, when $\rho = a$, $z = n$. When $\rho = 1.18a$ then

$(1.18)^2a^2 = b^2+r^2-2br\xi$ where ξ is the required limit

$$\xi = \frac{b^2+r^2-(1.18)^2a^2}{2br} = \frac{(\frac{b}{a})^2+(\frac{r}{a})^2-(1.18)^2}{2(\frac{b}{a})(\frac{r}{a})} \qquad 34$$

Then

$$\int_{-1}^{1}\left[g(\rho)-1\right]P_2(z)dz = \tfrac{1}{2}\int_{\xi}^{n}\left[\frac{9.17}{a}(b^2+r^2-2brz)^{\frac{1}{2}}-9.17\right](3z^2-1)dz \qquad 35$$

Again expression 34 is correct up to $r = a+b$, beyond which the top limit is 1.

Finally, for the region $1.18a \leqslant \rho \leqslant 1.46a$,

$$\int_{-1}^{1}\left[g(\rho)-1\right]P_2(z)dz = \tfrac{1}{2}\int_{\lambda}^{\xi}\left[8.60-\frac{5.89}{a}(b^2+r^2-2brz)^{\frac{1}{2}}\right](3z^2-1)dz \qquad 36$$

where ξ is given by expression 34 and $\lambda = \dfrac{(\frac{b}{a})^2+(\frac{r}{a})^2-(1.46)^2}{2(\frac{b}{a})(\frac{r}{a})}$

Once again expression 36 is alright up to $\xi = 1$, beyond which the upper limit is 1.

Writing $x = \frac{r}{a}$ and $y = \frac{b}{a}$ as before we can summarise the results as follows.

For the region $1 \leqslant x \leqslant 1+y$,

$$\int_{-1}^{1}\left[g(\rho)-1\right]P_2(z)dz = \tfrac{1}{2}n(n^2-1) + \tfrac{1}{2}\int_{\xi}^{n}\left[9.17(y^2+x^2-2xyz)^{\frac{1}{2}}-9.17\right](3z^2-1)dz + \tfrac{1}{2}\int_{\lambda}^{\xi}\left[8.60-5.89(y^2+x^2-2xyz)^{\frac{1}{2}}\right](3z^2-1)dz \qquad 37$$

with
$$n = \frac{y^2+x^2-1}{2xy} \qquad 38$$

$$\xi = \frac{y^2+x^2-(1.18)^2}{2xy} \qquad 39$$

$$\lambda = \frac{y^2+x^2-(1.46)^2}{2xy} \qquad 40$$

For the region $1+y \leqslant x \leqslant x'$ where x' is given by $\dfrac{y^2+x'^2-(1.18)^2}{2x'y} = 1$

$$\int_{-1}^{1}\left[g(\rho)-1\right]P_2(z)dz = \tfrac{1}{2}\int_{\xi}^{1}\left[9.17(y^2+x^2-2xyz)^{\frac{1}{2}}-9.17\right](3z^2-1)dz + \tfrac{1}{2}\int_{\lambda}^{\xi}\left[8.60-5.89(y^2+x^2-2xyz)^{\frac{1}{2}}\right](3z^2-1)dz \qquad 41$$

and for the region $x > x'$,

$$\int_{-1}^{1}\left[g(\rho)-1\right]P_2(z)dz = \tfrac{1}{2}\int_{\lambda}^{1}\left[8.60-5.89(y^2+x^2-2xyz)^{\frac{1}{2}}\right](3z^2-1)dz \qquad 42$$

Returning to the expression for the triplet integral given by equation 3, having calculated the integral over $g(r_{03})$ for a given value of r_o i.e. b we now require to integrate over $r_3^2 g(r_3) j_2(qr_3)$. i.e. we now require

$$2n\rho\int_0^{\infty} g(r_3)r_3^2 j_2(qr_3)F(r_3)dr_3$$

where $F(r_3) = \int_{-1}^{1} g(r_{03})P_2(z)dz$

Now the packing fraction $n = \dfrac{\text{volume of the atomic sphere}}{\text{volume allowed for each sphere}} = \dfrac{\omega}{\Omega}$

where $\omega = \dfrac{na^3}{6}$, a being the sphere diameter

and the number density $\Omega = \dfrac{1}{\rho}$. Hence $2n\rho = \dfrac{12n}{a^3}$.

We therefore require to evaluate

$$I(r_3) = 12n\int_0^{\infty} g(r_3)\left(\frac{r_3}{a}\right)^2 j_2(qr_3)F(r_3)\frac{dr_3}{a} \qquad 43$$

Writing $r_3 = r$ and changing variable to $x = \dfrac{r}{a}$ with $dx = \dfrac{dr}{a}$

$$I(x) = 12n\int_0^{\infty} g(x)x^2 j_2(qx)F(x)dx \qquad 44$$

In the actual calculations F(x) is the weighted sum of integrals for different delta function positions.

2. THE COMPUTER PROGRAMS

Calculations were carried out using two programs, INT1 and INT2.

Using the expressions developed in section 1.2 INT2 first calculated the value of the final integral in equation 3 for various delta function positions and found the weighted sum of these integrals corresponding to F(x) in equation 44. The product

$$F5(x) = 12ng(x)x^2F(x) \qquad 45$$

was then calculated. As mentioned previously the value taken for n for the hard sphere model was 0.445. For mercury a value of 0.375 was used. The simplified forms of g(x) as shown in Figures II.1 and II.2 were also used.

The graph plotter was used to plot F5(x) and a straight line approximation of this function was made. This approximation to F5(x) was fed into the second program INT1 which initially calculated the integral given by 44, i.e.,

$$I(x) = \int_0^\infty F5(x)j_2(qx)dx \qquad 46$$

Using a weighted sum of appropriate Bessel functions INT1 then proceeded to calculate $q^2I_p(q)$ and $q^2 2n\rho I_t(q)$ and then the sum $q^2\left[I_p(q)+2n\rho I_t(q)\right]$ and each of these functions were output to the graph plotter.

Next the final integral in expression 1 for R_{1q} was calculated using the Egelstaff-Schofield expression for $S_s(q,\omega)$ together with the result given by Sholl (3) i.e.

$$\int_{-\infty}^{\infty} S_s^2(q,\omega)d\omega = \frac{mDe^x K_1(x)}{k_B T \ 2\pi}\left[\frac{0.582+x\sqrt{2}}{0.582+x}\right] \qquad 47$$

where $x = \frac{mD^2q^2}{k_B T}$. Expression 47 was calculated as a function of q with q again in units of $\frac{1}{a}$. The value of m used was $333.66.\ 10^{-27}$kg and a was taken as $2.6.\ 10^{-10}$m. this being obtained from the cut off in g(r) as quoted by Sholl (3).

The product

$$F(q) = q^2\left[I_p(q)+2\pi\rho I_t(q)\right]\int_{-\infty}^{\infty} S_s^2(q,\omega)d\omega \qquad 48$$

was then calculated and output to the graph plotter. Expression 48 was finally integrated over all q to give a result for R_{1q} in arbitrary units.

The above steps were repeated for four temperatures the lowest of which, 233°K, being the melting point of mercury. The values used for the diffusion coefficient, D, at each temperature were taken from the data of Meyer (4).

The programs utilised the following three scientific subroutines provided by the Numerical Algorithms Group.

(i) Subroutine DOIACF

This routine evaluates a definite integral to a specified accuracy using the method described by Patterson (5) of the optimum addition of points to Gauss quadrature formulae.

(ii) Subroutine DOIGAF

This routine integrates a function which is specified numerically at four or more points, over the whole of its specified range, using third order finite - difference formulae with error estimates, according to a method due to Gill and Miller (6)

(iii) Subroutine S18ADF

The routine calculates an approximate value for the modified Bessel function $K_1(x)$ using a method based on three Chebyshev expansions (7).

Further details of the subroutines and their implementation may be found in the NAG library manual.

As an example the programs used to calculate the variation of R_{1q} with temperature for liquid mercury using the mercury g(r) and a range of interaction $\Delta = 0.1$ a are listed below together with their relevant output. The positions of the delta functions used for this range together with their relative weightings are shown diagrammatically in Figure II.3.

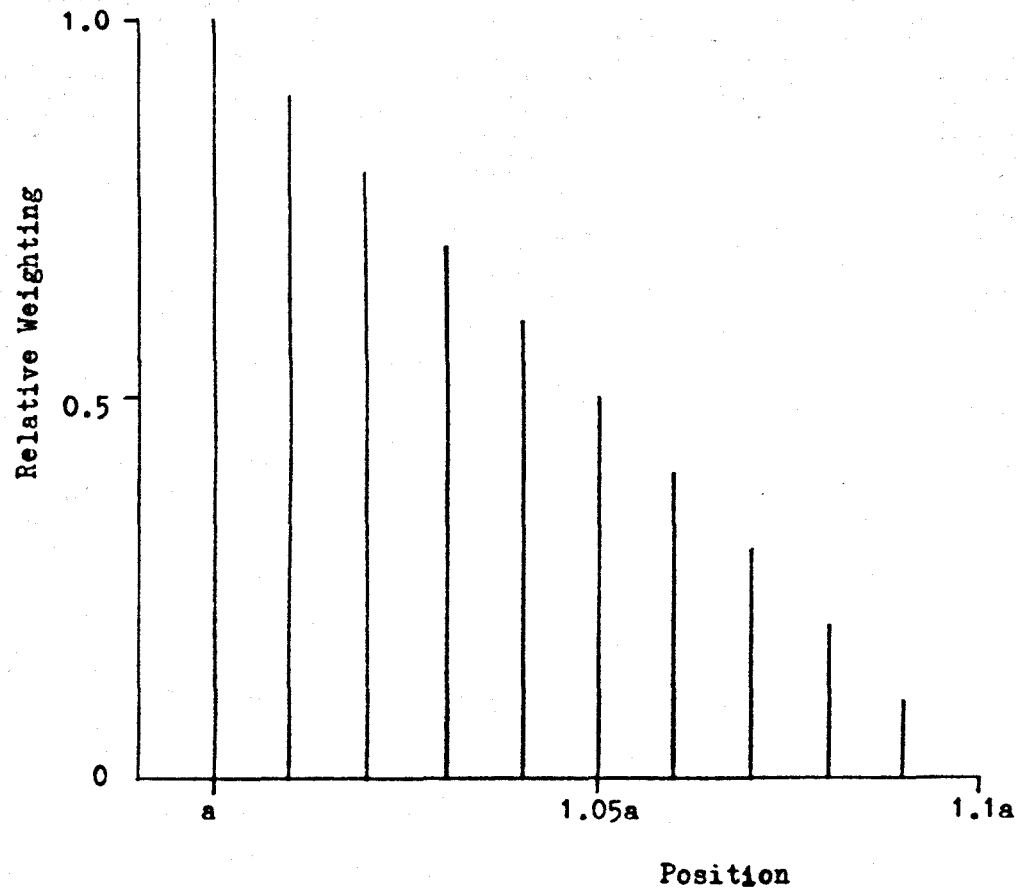

Figure 11.3 Diagrammatic representation of the delta functions used for a range of interaction $\Delta = 0.1a$.

```
      LIBRARY(SUBGROUPSRF7)
      LIBRARY(SUBGROUPSRGP)
      LIBRARY(SUBGROUPNAGF)
      LIBRARY(SUBGROUPNAGG)
      PROGRAM(INT2)
      INPUT 1=CRO
      OUTPUT 2=LPO
      COMPACT
      TRACE 2
      MASTER INT2

      DIMENSION TOTAL(201),Y(201),SMFNC(201),F5(201)
      COMMON J,Y,BOA
      EXTERNAL FUN1,FUN2
      CALL GPHGRAPH(7,7HP01INT2,6)
      CALL MOVEORIG(2.0,-14.0)
      CALL GPHSLINE(0.0,0.0,20.0,0.0)
      CALL GPHSLINE(0.0,-5.0,10.0,90.0)
      DO 500 I=1,201
      SMFNC(I)=0.0
  500 CONTINUE
      DO 1 I=1,10
      R=I-1
      BOA=1.0+R*0.01
      AMP=1.0-R*0.1
      DO 2 J=1,201
      S=J-1
      S=S/100.0
      Y(J)=1.0+S
      SIGMA=(BOA*BOA+Y(J)*Y(J)-1.0)/(2.0*BOA*Y(J))
      ONE=0.5*SIGMA*(SIGMA*SIGMA-1.0)
      IF(SIGMA.GT.1.0) ONE=0.0
      IF(SIGMA.GT.1.0) SIGMA=1.0
      EPSIL=(BOA*BOA+Y(J)*Y(J)-1.18*1.18)/(2.0*Y(J)*BOA)
      A=EPSIL
      B=SIGMA
      RELACC=1.0E-4
      ABSACC=0.0
      IFAIL=1
      CALL D01ACF(A,B,FUN1,RELACC,ABSACC,ACC,ANS,NPTS,IFAIL)
      IF(IFAIL)9,10,9
    9 WRITE(2,102)
  102 FORMAT(1H ,45H INTEGRAL DID NOT REACH THE REQUIRED ACCURACY)
   10 CONTINUE
      TWO=0.5*ANS
      IF(EPSIL.GT.1.0) TWO=0.0
      IF(EPSIL.GT.1.0) EPSIL=1.0
      RLAMB=(BOA*BOA+Y(J)*Y(J)-1.46*1.46)/(2.0*Y(J)*BOA)
      A=RLAMB
      B=EPSIL
      IFAIL=1
      CALL D01ACF(A,B,FUN2,RELACC,ABSACC,ACC,ANS,NPTS,IFAIL)
      IF(IFAIL)11,12,11
   11 WRITE(2,102)
   12 CONTINUE
      THREE=0.5*ANS
      IF(RLAMB.GT.1.0) THREE=0.0
      TOTAL(J)=ONE+TWO+THREE
```

```
2   CONTINUE
    M=201
    DO 15 J=1,M
    TOTAL(J)=TOTAL(J)*AMP
15  CONTINUE
    DO 16 J=1,M
    SMFNC(J)=SMFNC(J)+TOTAL(J)
16  CONTINUE
    DO 17 J=1,M
    Y(J)=Y(J)-1.0
    Y(J)=Y(J)*10.0
17  CONTINUE
    TOTMN=1.0
    DO 18 J=1,M
    IF(TOTAL(J).LT.TOTMN) TOTMN=TOTAL(J)
18  CONTINUE
    IF(I.GT.1) GOTO 19
    SF=5.0/TOTMN
    SF=-SF
19  DO 20 J=1,M
    TOTAL(J)=TOTAL(J)*SF
20  CONTINUE
    CALL HGPLINE(Y,TOTAL,M,1)
1   CONTINUE
    DO 21 J=1,M
    Y(J)=Y(J)/10.0
    Y(J)=Y(J)+1.0
21  CONTINUE
    DO 22 J=1,M
    F1=9.17*Y(J)-8.17
    F11=9.60-5.89*Y(J)
    F12=1.0
    IF(Y(J).GT.1.18) F1=F11
    IF(Y(J).GT.1.46) F1=F12
    F2=Y(J)**2
    F5(J)=SMFNC(J)*F1*F2*12.0*0.375
22  CONTINUE
    DO 23 J=1,M
    Y(J)=Y(J)-1.0
    Y(J)=Y(J)*10.0
23  CONTINUE
    SHMIN=1.0
    DO 24 J=1,M
    IF(SMFNC(J).LT.SHMIN) SHMIN=SMFNC(J)
24  CONTINUE
    SF=5.0/SHMIN
    SF=-SF
    DO 25 J=1,M
    SMFNC(J)=SMFNC(J)*SF
25  CONTINUE
    CALL MOVEORIG(30.0,0.0)
    CALL GPHSLINE(0.0,0.0,20.0,0.0)
    CALL GPHSLINE(0.0,-5.0,10.0,90.0)
    CALL HGPLINE(Y,SMFNC,M,1)
    SF=0.2
    DO 26 J=1,M
    F5(J)=F5(J)*SF
26  CONTINUE
    CALL MOVEORIG(30.0,0.0)
    CALL GPHSLINE(0.0,0.0,20.0,0.0)
    CALL GPHSLINE(0.0,-5.0,10.0,90.0)
    CALL HGPLINE(Y,F5,M,1)
    CALL GPHENDPLOT(25.0)
    PAUSE 99
    END
```

```
      FUNCTION FUN1(X)
      DIMENSION Y(201)
      COMMON J,Y,BOA
      FUN1=(9.17*SQRT(BOA*BOA+Y(J)*Y(J)-2.0*BOA*Y(J)*X)-9.17)*(3.0*X*X-1
     #.0)
      RETURN
      END
```

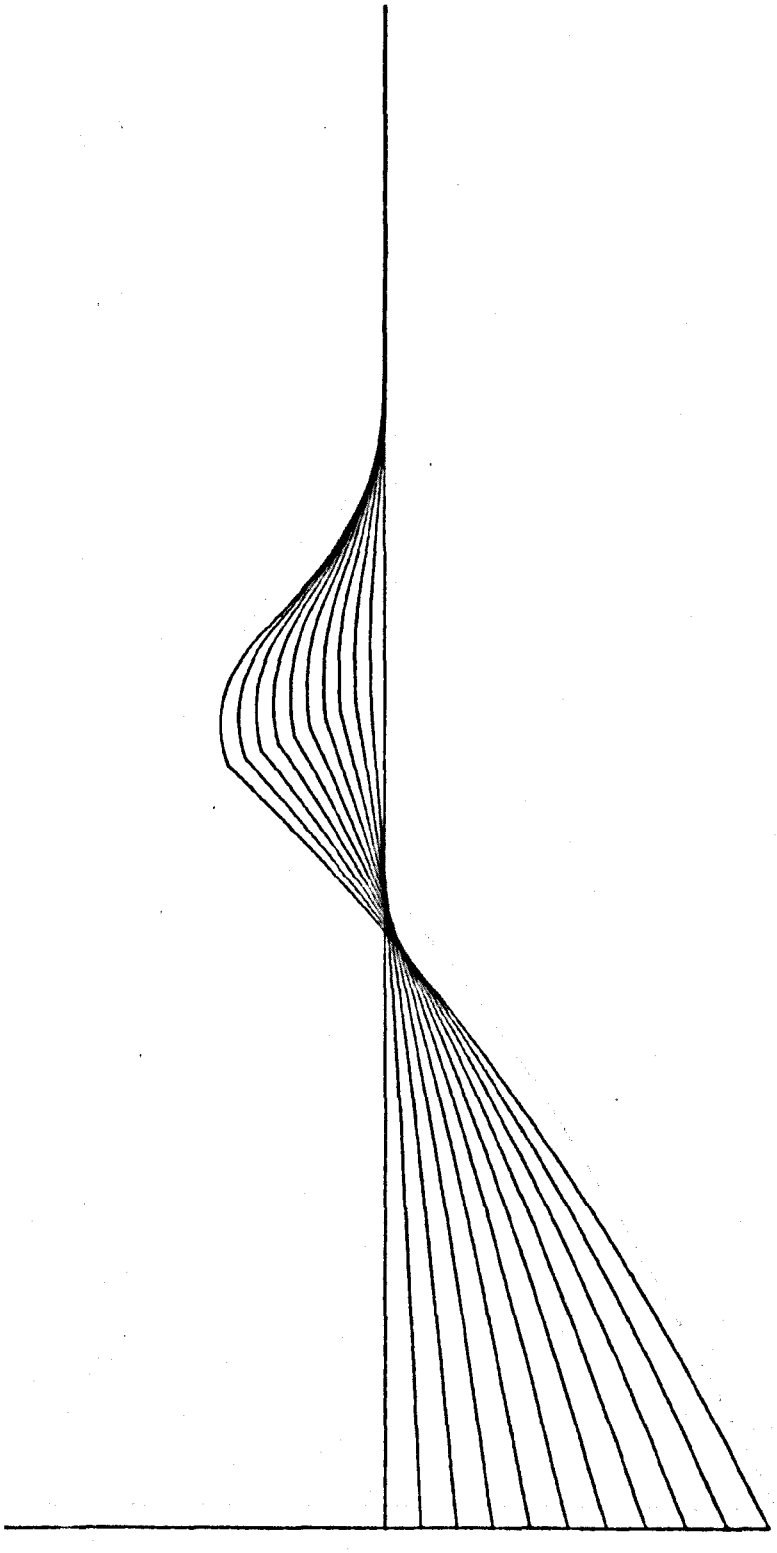

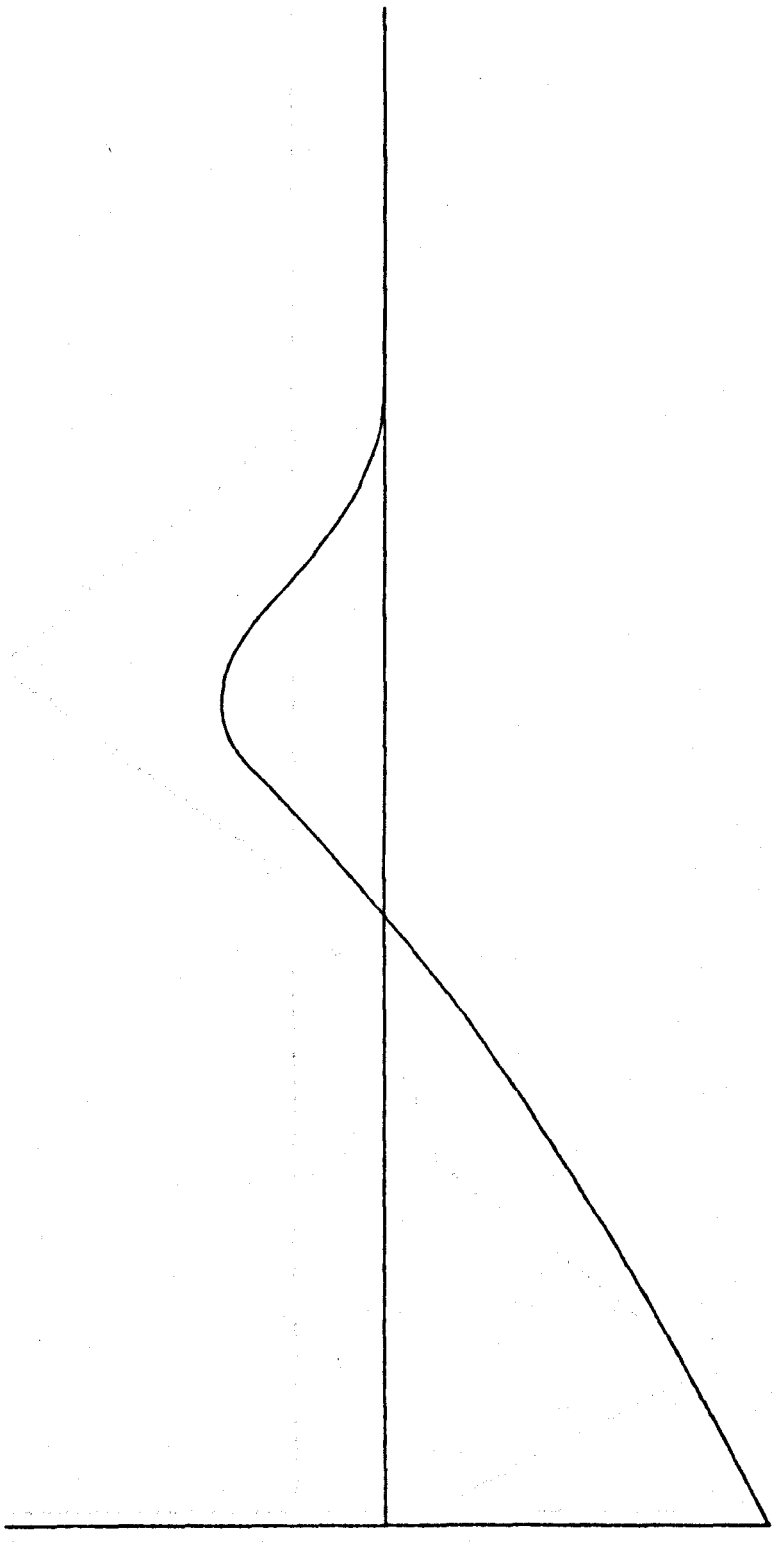

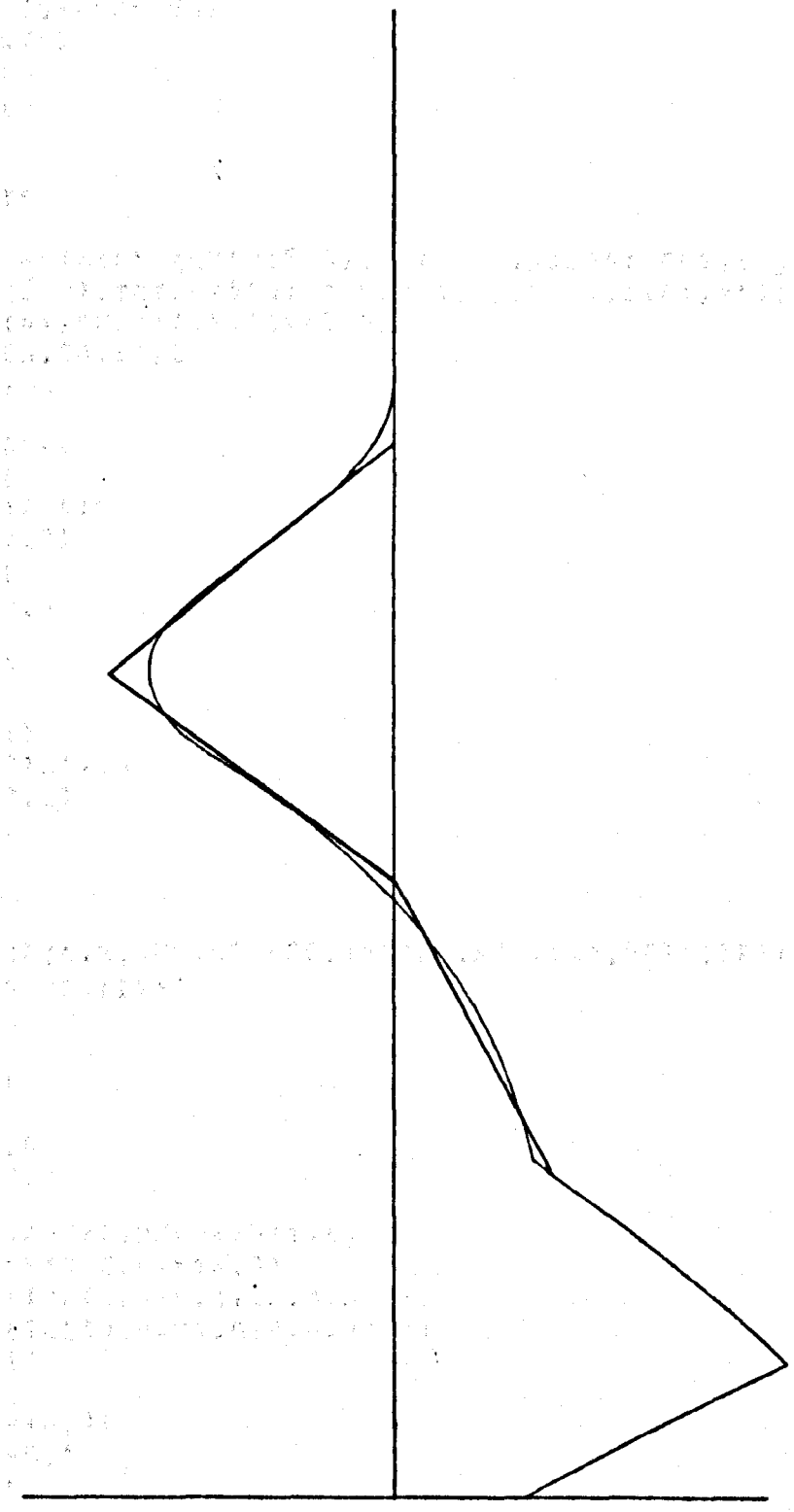

```
      LIBRARY(SUBGROUPSRF7)
      LIBRARY(SUBGROUPSRGP)
      LIBRARY(SUBGROUPNAGF)
      LIBRARY(SUBGROUPNAGG)
      PROGRAM(INT1)
      INPUT 1=CRO
      OUTPUT 2=LPO
      COMPACT
      TRACE 2
      MASTER INT1

      DIMENSION RLIM(6),SUMFQ(500),Q1(500),RJ2Q1(500),SMRJ2(500),PTERM(5
     #00),TTERM(500),TOTFQ(500),TOTFN(500),T(4),D(4),R1Q(4),XQ(500),ESA(
     #500),REDT(4),REDR1(4),F4X(500)
      COMMON Q,CA,CB,SF,L
      EXTERNAL FUN
      L=500
      RELACC=1.0E-4
      ABSACC=0.0
      READ(1,101)RLIM
  101 FORMAT(6F5.2)
      DO 1 I=1,L
      SUMFQ(I)=0.0
    1 CONTINUE
      DO 2 N=1,5
      A=RLIM(N)
      B=RLIM(N+1)
      READ(1,102)CA,CB
  102 FORMAT(2F7.2)
      DO 3 I=1,L
      R=I
      Q=R/5.0
      IFAIL=1
      CALL D01ACF(A,B,FUN,RELACC,ABSACC,ACC,ANS,NPTS,IFAIL)
      SUMFQ(I)=SUMFQ(I)*ANS
    3 CONTINUE
    2 CONTINUE
      DO 4 I=1,L
      R=I
      Q1(I)=R/5.0
      SMRJ2(I)=0.0
    4 CONTINUE
      CALL GPHGRAPH(7,7HP01INT1,6)
      CALL MOVEORIG(2.0,-14.0)
      CALL GPHSLINE(0.0,0.0,20.0,0.0)
      CALL GPHSLINE(0.0,-4.0,8.0,90.0)
      DO 5 I=1,10
      R=I-1
      DFPN=1.0+R*0.01
      AMP=1.0-R*0.1
      DO 6 J=1,L
      X=Q1(J)
      X=X*DFPN
      RJ2Q1(J)=(3.0/X**3-1.0/X)*SIN(X)-(3.0/X**2)*COS(X)
      RJ2Q1(J)=RJ2Q1(J)*AMP
    6 CONTINUE
      DO 7 J=1,L
      SMRJ2(J)=SMRJ2(J)+RJ2Q1(J)
    7 CONTINUE
```

```
      IF(I.GT.1) GOTO 9
      RJMAX=-1.0
      DO 8 J=1,L
      IF(RJ2Q1(J).GT.RJMAX) RJMAX=RJ2Q1(J)
    8 CONTINUE
      SF=4.0/RJMAX
    9 CALL DEGAS(Q1,RJ2Q1)
    5 CONTINUE
      DO 10 I=1,L
      PTERM(I)=SMRJ2(I)*SMRJ2(I)*Q1(I)*Q1(I)
      TTERM(I)=SMRJ2(I)*SUMFQ(I)*Q1(I)*Q1(I)
      TOTFQ(I)=PTERM(I)+TTERM(I)
   10 CONTINUE
      CALL MOVEORIG(25.0,0.0)
      CALL GPHSLINE(0.0,0.0,20.0,0.0)
      CALL GPHSLINE(0.0,-4.0,8.0,90.0)
      SMMAX=-1.0
      DO 11 I=1,L
      IF(SMRJ2(I).GT.SMMAX) SMMAX=SMRJ2(I)
   11 CONTINUE
      SF=4.0/SMMAX
      CALL DEGAS(Q1,SMRJ2)
      CALL MOVEORIG(25.0,0.0)
      CALL GPHSLINE(0.0,0.0,20.0,0.0)
      CALL GPHSLINE(0.0,-4.0,8.0,90.0)
      TMAX=-1.0
      DO 12 I=1,L
      IF(PTERM(I).GT.TMAX) TMAX=PTERM(I)
   12 CONTINUE
      WRITE(2,109) TMAX,SF
      SF=4.0/TMAX
      CALL DEGAS(Q1,PTERM)
      CALL NEWPEN(3)
      CALL DEGAS(Q1,TTERM)
      CALL NEWPEN(2)
      CALL DEGAS(Q1,TOTFQ)
      CALL NEWPEN(1)
      CALL MOVEORIG(25.0,0.0)
      CALL GPHSLINE(0.0,0.0,20.0,0.0)
      CALL GPHSLINE(0.0,0.0,4.0,90.0)
      CALL MOVEORIG(25.0,0.0)
      CALL GPHSLINE(0.0,0.0,20.0,0.0)
      CALL GPHSLINE(0.0,0.0,4.0,90.0)
      CALL MOVEORIG(25.0,0.0)
      CALL GPHSLINE(0.0,0.0,20.0,0.0)
      CALL GPHSLINE(0.0,-4.0,8.0,90.0)
      CALL MOVEORIG(-50.0,0.0)
      RKB=1.38E-23
      READ(1,103)A,RM
  103 FORMAT(F5.2,F7.2)
      A=A*1.0E-10
      RM=RM*1.0E-27
      READ(1,104)T,D
  104 FORMAT(4F6.1/4F5.2)
      DO 14 I=1,4
      D(I)=D(I)*1.0E-9
      DO 15 J=1,L
      QOA=Q1(J)/A
      XQ(J)=(RM*D(I)*D(I)*QOA*QOA)/(RKB*T(I))
      F1X=EXP(XQ(J))
      IFAIL=0
      F2X=S18ADF(XQ(J),IFAIL)
      F3X=(0.582+XQ(J)*1.4142)/(0.582+XQ(J))
      F4X(J)=F1X*F2X
      ESA(J)=(D(I)*F1X*F2X*F3X)/T(I)
      TOTFN(J)=TOTFQ(J)*ESA(J)
```

```
      IF(I.GT.1) GOTO 15
      WRITE(2,110) Q1(J),QOA,XQ(J),F4X(J),ESA(J),TOTFQ(J),TOTFN(J)
  110 FORMAT(1H ,7E11.4)
   15 CONTINUE
      IF(I.GT.1) GOTO 16
      F4XMX=-1.0
      XQMAX=-1.0
      DO 17 J=1,L
      IF(F4X(J).GT.F4XMX) F4XMX=F4X(J)
      IF(XQ(J).GT.XQMAX) XQMAX=XQ(J)
   17 CONTINUE
      SFF4X=4.0/F4XMX
      SFXQ=20.0/XQMAX
      WRITE(2,109) F4XMX,XQMAX,SFF4X,SFXQ
  109 FORMAT(1H ,E11.4)
   16 DO 18 J=1,L
      F4X(J)=F4X(J)*SFF4X
      XQ(J)=XQ(J)*SFXQ
   18 CONTINUE
      CALL NEWPEN(2)
      CALL HGPSCURVE(XQ,F4X,L,0,0.0,0.0)
      CALL MOVEORIG(25.0,0.0)
      IF(I.GT.1) GOTO 23
      ESAMX=-1.0
      DO 22 J=1,L
      IF(ESA(J).GT.ESAMX) ESAMX=ESA(J)
   22 CONTINUE
      SFESA=4.0/ESAMX
      WRITE(2,109) ESAMX,SFESA
   23 SF=SFESA
      CALL NEWPEN(3)
      CALL DEGAS(Q1,ESA)
      CALL MOVEORIG(25.0,0.0)
      IF(I.GT.1) GOTO 20
      TOTFNM=-1.0
      DO 19 J=1,L
      IF(TOTFN(J).GT.TOTFNM) TOTFNM=TOTFN(J)
   19 CONTINUE
      SFTOTF=4.0/TOTFNM
      WRITE(2,109) TOTFNM,SFTOTF
   20 SF=SFTOTF
      CALL NEWPEN(1)
      CALL DEGAS(Q1,TOTFN)
      CALL MOVEORIG(-50.0,0.0)
      N=L
      IFAIL=0
      CALL D01GAF(Q1,TOTFN,N,ANS,ER,IFAIL)
      WRITE(2,105)
  105 FORMAT(/1H ,37H TEMP(K)  INTEGRAL     ERROR      IFAIL)
      WRITE(2,106)T(I),ANS,ER,IFAIL
  106 FORMAT(1H ,F7.1,2X,E11.4,2X,E11.4,2X,I2)
      R1Q(I)=ANS
   14 CONTINUE
      WRITE(2,107)
  107 FORMAT(//1H ,23H T/TM     R1Q(T)/R1Q(TM))
      DO 21 I=1,4
      REDT(I)=T(I)/T(1)
      REDR1(I)=R1Q(I)/R1Q(1)
      WRITE(2,108) REDT(I),REDR1(I)
  108 FORMAT(1H ,F6.2,7X,F5.2)
   21 CONTINUE
      CALL GPHENDPLOT(25.0)
      PAUSE 99
      END
```

```
      FUNCTION FUN(X)
      COMMON Q,CA,CB,SF,L
      FX=CA*X+CB
      FQX=((3.0/(Q*X)**3-1.0/(Q*X))*SIN(Q*X)-3.0*COS(Q*X)/(Q*X)**2)
      FUN=FX*FQX
      RETURN
      END


      SUBROUTINE DEGAS(X,Y)
      DIMENSION X(500),Y(500)
      COMMON Q,CA,CB,SF,L
      Z=L
      Z=Z*0.01
      DO 1 I=1,L
      X(I)=X(I)/Z
      Y(I)=Y(I)*SF
    1 CONTINUE
      CALL HGPLINE(X,Y,L,1)
      DO 2 I=1,L
      X(I)=X(I)*Z
    2 CONTINUE
      RETURN
      END

      FINISH
```

```
0.9820E 02 0.3777E 12 0.1958E 02 0.2886E 00 0.1997E-11 0.1538E 00 0.3072E-12
0.9840E 02 0.3785E 12 0.1966E 02 0.2880E 00 0.1993E-11 0.1364E 00 0.2719E-12
0.9860E 02 0.3792E 12 0.1974E 02 0.2874E 00 0.1989E-11 0.1099E 00 0.2187E-12
0.9880E 02 0.3800E 12 0.1982E 02 0.2868E 00 0.1985E-11 0.7871E-01 0.1563E-12
0.9900E 02 0.3808E 12 0.1990E 02 0.2862E 00 0.1981E-11 0.4770E-01 0.9449E-13
0.9920E 02 0.3815E 12 0.1998E 02 0.2856E 00 0.1977E-11 0.2180E-01 0.4309E-13
0.9940E 02 0.3823E 12 0.2006E 02 0.2850E 00 0.1973E-11 0.5045E-02 0.9954E-14
0.9960E 02 0.3831E 12 0.2014E 02 0.2844E 00 0.1969E-11-0.1982E-05-0.3902E-17
0.9980E 02 0.3838E 12 0.2022E 02 0.2838E 00 0.1965E-11 0.7311E-02 0.1436E-13
0.1000E 03 0.3846E 12 0.2030E 02 0.2832E 00 0.1961E-11 0.2567E-01 0.5033E-13
0.1232E 05
0.2030E 02
0.3248E-03
0.9852E 00
0.6079E-07
0.6580E 08
0.3666E-09
0.1091E 11

TEMP(K)   INTEGRAL     ERROR      IFAIL
 233.0    0.3679E 01    0.3050E-04    0

TEMP(K)   INTEGRAL     ERROR      IFAIL
 300.0    0.3403E 01    0.1962E-04    0

TEMP(K)   INTEGRAL     ERROR      IFAIL
 400.0    0.3193E 01    0.9864E-05    0

TEMP(K)   INTEGRAL     ERROR      IFAIL
 500.0    0.3000E 01    0.5347E-05    0


T/TH     R1Q(T)/R1Q(TH)
 1.00          1.00
 1.29          0.93
 1.72          0.87
 2.15          0.82
```

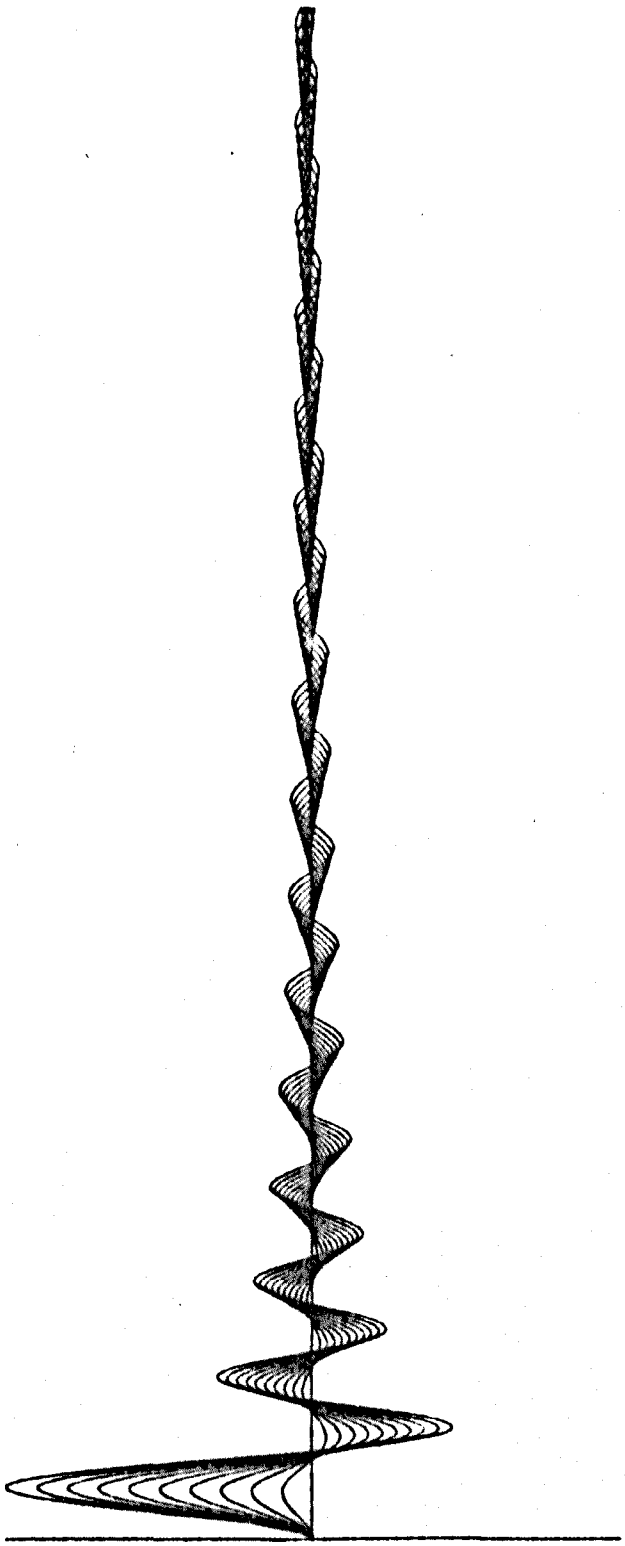

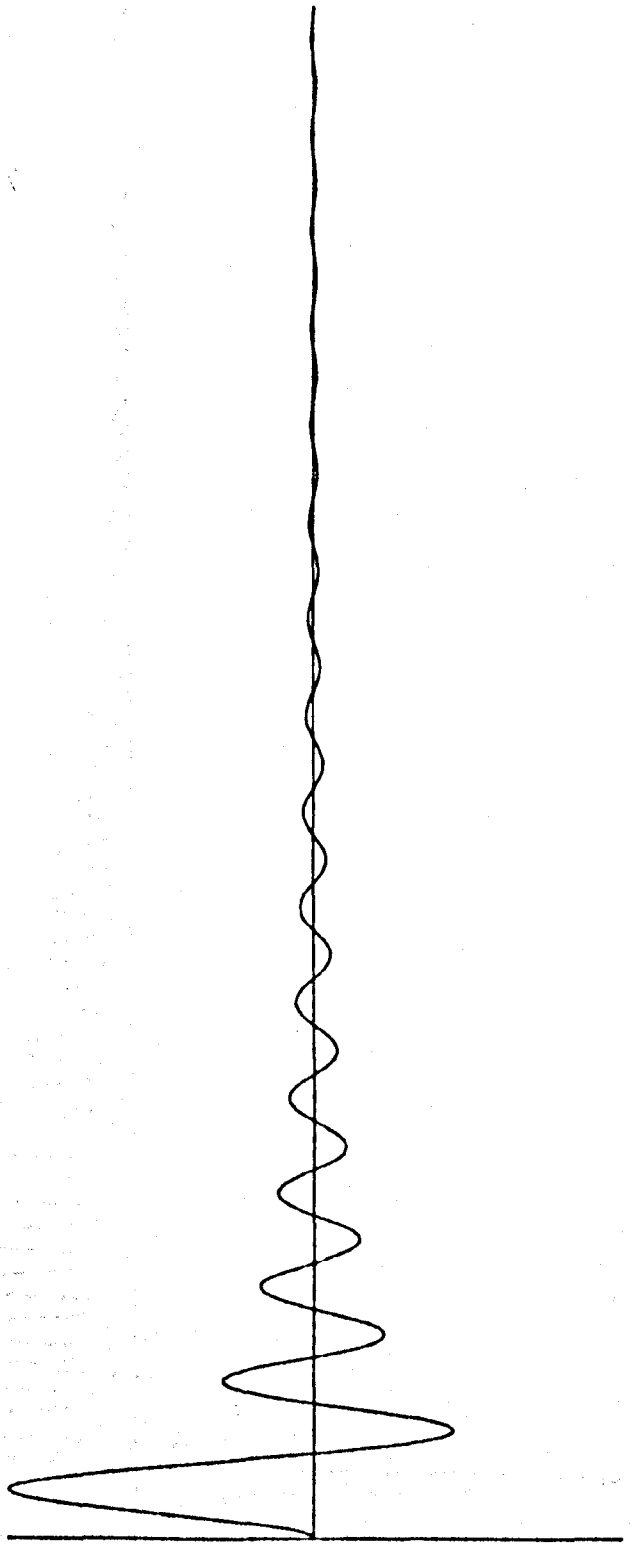

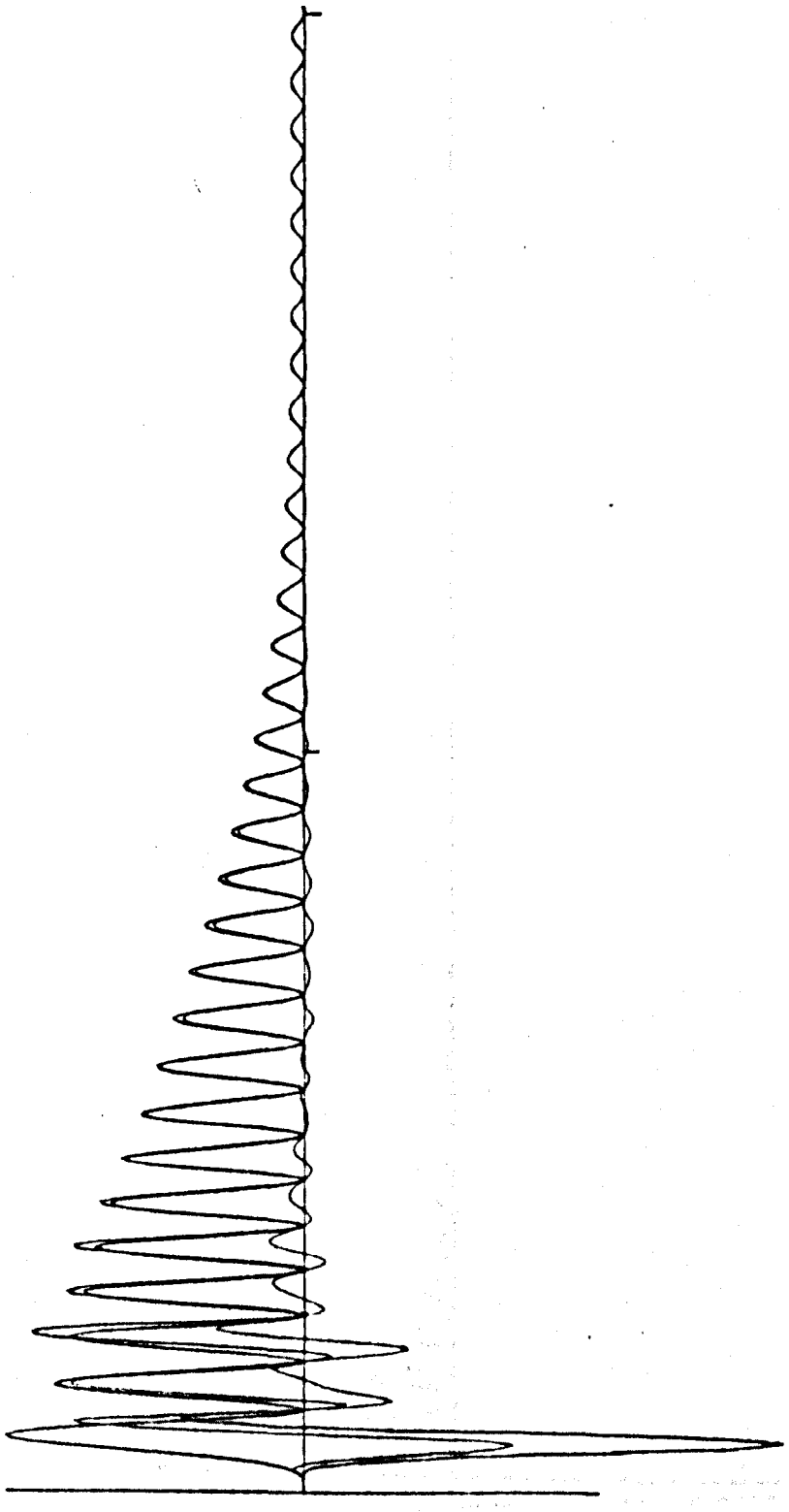

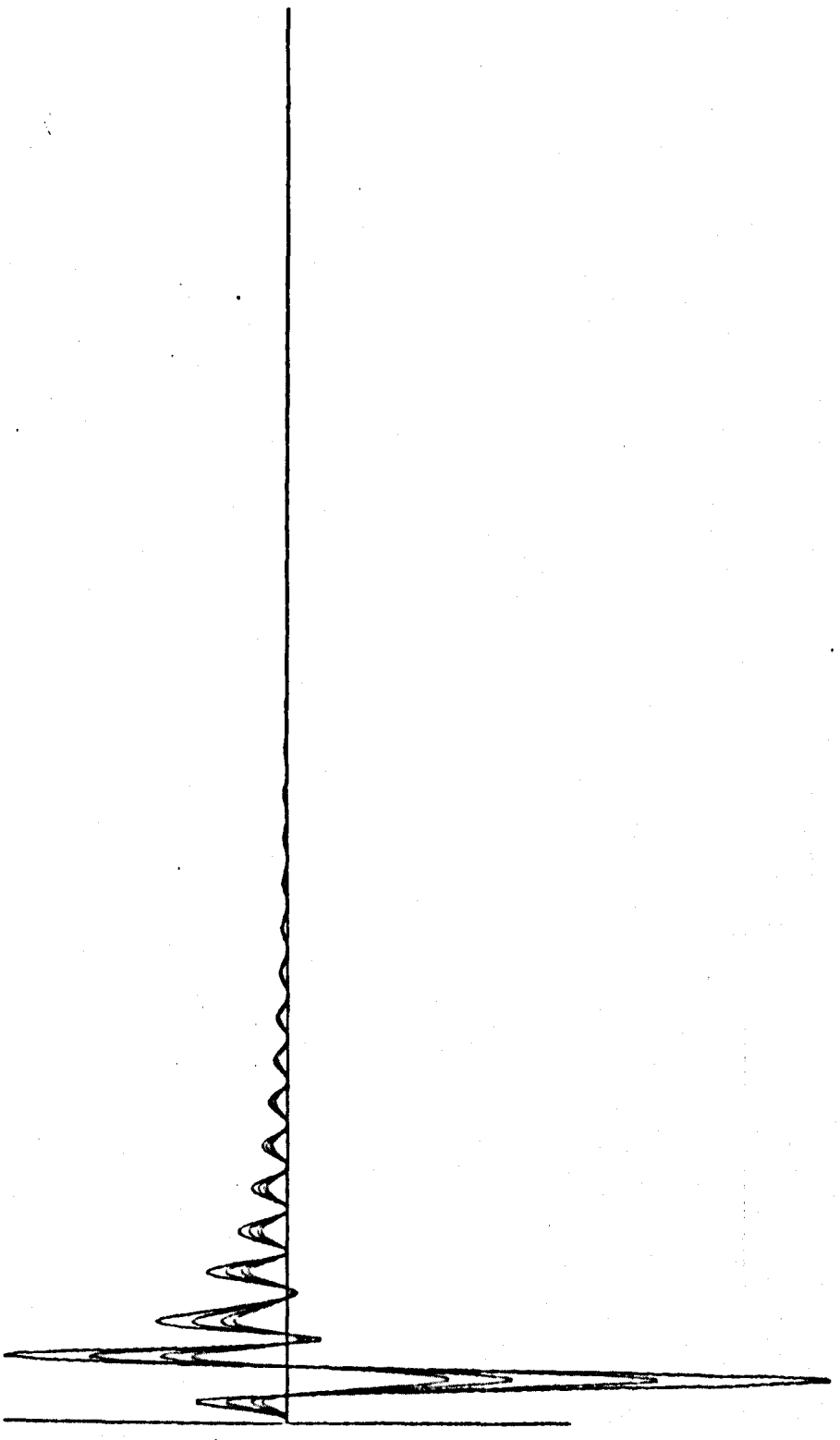

3 REFERENCES

1) W.H. Young, Proc. 3rd. Int. Conf. Liquid Metals, Bristol, 1977 Inst. Phys. Conf. Ser. No 30 (1976)

2) R. Kaplow, S.L. Strong and B.L. Averbach, Phys. Rev., 138A, 1336 (1965)

3) C.A. Sholl, J. Phys. F: Metal Phys., 4, 1556 (1974)

4) R.E. Meyer, J. Phys. Chem.,65, 567 (1961)

5) T.N.L. Patterson, Maths. Comp., 22, 847 (1968)

6) P.E. Gill and G.F. Miller, Comp. Journal, 15, 80 (1972)

7) M. Abramowitz and I.A.Stegun, Handbook of Mathematical Functions, Chap. 9.6, p.374. Dover Publications, 1968.